Aus dem Centre for Transdisciplinary Neurosciences Rostock (CTNR)

mit der

Klinik für Psychosomatische Medizin und Psychotherapie
– Sektion Gerontopsychosomatik und demenzielle Erkrankungen
Leitung: Prof. Dr. med. Stefan Teipel

in Kooperation mit dem

Rudolf-Zenker-Institut für Experimentelle Chirurgie
Leitung: Prof. Dr. med. Brigitte Vollmar

Ernährung, Neuroinflammation und Amyloid-Pathologie im Mausmodell – Ausblick auf Clearance-Messungen

Kumulative Dissertation zur Erlangung des akademischen Grades

Doktorin der Medizinwissenschaften (Dr. rer. hum.)

der Universitätsmedizin Rostock

Vorgelegt von:

Luisa Müller,

geboren am 10.04.1994 in Schlema

https://doi.org/10.18453/rosdok_id00005030

Gutachter:

Prof. Dr. Stefan Teipel
Universitätsmedizin Rostock, Klinik und Poliklinik für Psychosomatik und Psychotherapeutische Medizin, Sektion für Gerontopsychosomatik und demenzielle Erkrankungen sowie Leiter der klinischen Forschung des Deutschen Zentrums für Neurodegenerative Erkrankungen e.V. (DZNE) am Standort Rostock/Greifswald

Prof. Dr. Angela Kuhla
Universitätsmedizin Rostock, Rudolf-Zenker-Institut für Experimentelle Chirurgie

Prof. Dr. Reiner Ulrich, PhD
Universität Leipzig, Veterinärmedizinische Fakultät, Institut für Veterinär-Pathologie

Jahr der Einreichung: 2023

Jahr der Verteidigung: 2024

„To the scientist there is the joy in pursuing truth which nearly counteracts the depressing revelations of truth."

H. P. Lovecraft

1. Inhaltsverzeichnis

2. Der kumulativen Arbeit zugrundeliegende Studien

Studie 1[#]: Power Guerra N, **Müller L**, Pilz K, Glatzel A, Jenderny D, Janowitz D, Vollmar B, Kuhla A. Dietary-Induced Low-Grade Inflammation in the Liver. Biomedicines. 2020 Dec 9;8(12):587. doi: 10.3390/biomedicines8120587 *(IF: 4,757)*

Studie 2: **Müller L***, Power Guerra N*, Schildt A, Lindner T, Stenzel J, Behrangi N, Bergner C, Alberts T, Bühler D, Kurth J, Krause B.J, Janowitz D, Teipel S, Vollmar B, Kuhla A. (*equal contribution) [18F]GE-180-PET and Post Mortem Marker Characteristics of Long-Term High-Fat-Diet-Induced Chronic Neuroinflammation in Mice. Biomolecules 2023, 13, 769. https://doi.org/10.3390/biom13050769 *(IF: 6,064)*

Studie 3: Bühler D, Power Guerra N, **Müller L**, Wolkenhauer O, Düffer M, Vollmar B, Kuhla A* and Wolfien M* (*equal contributions) Leptin deficiency-caused behavioral change–A comparative analysis using EthoVision and DeepLabCut. Front. Neurosci. 2023 17:1052079. doi: 10.3389/fnins.2023.1052079 *(IF: 5,152)*

Studie 4: Power Guerra N, Leyens K, **Müller L**, Brauer D, Janowitz D, Schlick S, Pilz K, Grabe HJ, Vollmar B, Kuhla A. The effect of different weight loss strategies to treat non-alcoholic fatty liver disease focusing on fibroblast growth factor 21. Front Nutr. 2022 Aug 10;9:935805. doi: 10.3389/fnut.2022.935805 *(IF: 6.010)*

Studie 5[#]: **Müller L**, Power Guerra N, Stenzel J, Rühlmann C, Lindner T, Krause BJ, Vollmar B, Teipel S, Kuhla A. Long-Term Caloric Restriction Attenuates β-Amyloid Neuropathology and Is Accompanied by Autophagy in APPswe/PS1delta9 Mice. Nutrients. 2021 Mar 18;13(3):985. doi: 10.3390/nu13030985 *(IF: 6,706)*

Studie 6: (in Vorbereitung): **Müller L**, Lindner T, Polei S, Vollmar B, Weber M-A, Teipel S, Radbruch A, Kuhla A, Deike-Hofmann K. Intravenously administered gadolinium contrast agent as a novel approach to measure brain clearance with magnetic resonance imaging in an Alzheimer´s disease model of transgenic APPswe/PS1dE9 mice

[#] Die gekennzeichneten Studien 1 und 5 wurden bereits in der kumulativen Dissertation von Frau Dr. rer. hum. Nicole Power Guerra unter dem Aspekt „Die Rolle von FGF21 in der hepatisch-zerebralen Kommunikation“ thematisiert.

Die veröffentlichten Originalarbeiten sind unter Abschnitt 10 im Anhang ab Seite 43 zu finden

3. Zusammenfassung

Adipositas ist mit vielen Begleit- und Folgeerkrankungen assoziiert und gilt als Risikofaktor neurodegenerativer Erkrankungen wie der Alzheimerschen Erkrankung (AD). Ein wesentlicher Pathomechanismus, der sowohl bei Adipositas als auch bei AD feststellbar ist, ist die Neuroinflammation. Diese kann zur pro-inflammatorischen Aktivierung von Mikroglia und Astroglia führen, charakterisiert durch erhöhte Expressionslevel pro-inflammatorisch wirksamer Mediatoren wie Interleukin (IL) -1β, IL-6 und Tumornekrosefaktor-α (TNF-α). Daraus resultieren Störungen physiologischer Funktionen wie z. B. der effizienten Beseitigung von metabolischen Abbauprodukten aus dem zentralen Nervensystem (ZNS). In diesem Zusammenhang wird der Begriff „Clearance“ verwendet, um allgemein die Entfernung von Substanzen aus dem Gehirn entweder durch Degradation im Hirngewebe selbst oder durch Abtransport aus dem ZNS zu beschreiben. Eine Störung der Hirn-Clearance kann die Bildung von Amyloid-β (Aβ) -Plaques begünstigen und über nachgelagerte Mechanismen wie z. B. die Induktion neuroinflammatorischer Prozesse zur Progression von AD beitragen.

Basierend auf Mausmodellen der Neuroinflammation, ausgelöst durch Adipositas (Hochfett-Diät (HFD) -Modell und Leptin-Defizienz (ob/ob) -Modell) oder modelliertem AD-Phänotyp (APPswe/PS1dE9 (tg) -Modell), wurde in dieser Arbeit das Zusammenspiel zwischen Ernährung, inflammatorischen Prozessen, Aβ-Pathologie und Neurodegeneration untersucht. Zunächst wurde analysiert, ob Fehlernährung im Rahmen einer langzeitigen, fettreichen Diät (HFD, 60 % Fett) zu einer persistierenden niedrigschwelligen Inflammation, manifestiert in der Leber (Studie 1) sowie im Gehirn (Studie 2), führen kann. Während die entzündliche Infiltration mit Granulozyten und Makrophagen zwischen HFD- und fettarmer, aber kohlenhydratreicher Diät (KD) keine Unterschiede zeigte, konnte hinsichtlich der Expression pro-inflammatorischer Mediatoren in der HFD-Gruppe die Induktion hepatischer TNF-α-Expression gezeigt werden, welche gegenüber der KD tendenziell und gegenüber einer weiteren Kontrollgruppe mit standardisiert-ausgewogene Makronährstoffdiät (SD) signifikant war. Im Gehirn führte die HFD nicht zu erhöhtem TNF-α-Level, sondern zu erhöhter zerebraler IL-1β-Expression. Im HFD-Modell zeigten sich keine kognitiven Unterschiede im Morris-Water-Maze-Test (MWM). Um zu untersuchen, ob Adipositas generell zu Verhaltensänderungen führen kann, wurde zusätzlich im ob/ob-Modell der genetisch-induzierten Adipositas gearbeitet (Studie 3). Hier zeigten ob/ob-Mäuse geschlechtsunabhängig bereits im Alter von acht Wochen eine Reduktion der Bewegung und des explorativen Verhaltens, was generell als ängstlicher Habitus interpretiert werden kann. Die Ernährung wurde anschließend als modulierbarer Faktor zur Reduktion inflammatorischer Prozesse untersucht (Studie 4). Hier zeigte sich im Vergleich zu fortgesetzter HFD ein positiver Effekt eines Diätwechsels von HFD zu KD auf die Reduktion des Körpergewichts. Eine Kombination aus KD und Laufbandtraining (LBT) oder KD, LBT und Intervallfasten (IF) führte zu signifikant reduzierter hepatischer TNF-α-Expression. Im Gehirn scheint insbesondere die Kombination aus LBT und IF sowohl in Kombination mit HFD als auch mit KD, für eine verringerte zerebrale IL-1β- und IL-6-Expression verantwortlich zu sein. Zusätzlich wurde Ernährung als modulierbarer Faktor der Aβ-Pathologie untersucht (Studie 5). Hier zeigte eine langfristige Kalorienrestriktion (KR) bei tg-Mäusen eine Besserung des Glukose-Stoffwechsels im ZNS und eine verbesserte kognitive Leistung im MWM. Außerdem zeigte diese Studie zum ersten Mal, dass eine KR-induzierte Autophagie als Mechanismus der Hirn-Clearance in tg-Mäusen mit Abschwächung der Aβ-Pathologie und Neuroinflammation einhergeht. Um die Hirn-Clearance weiter untersuchen zu können, wurde ein Verfahren zur Gadoliniumkontrastmittel-basierten MRT-Bildgebung etabliert (Studie 6). Die hierbei in einem longitudinalen Ansatz gemessene Hirn-Clearance-Kapazität konnte zunächst keine statistisch signifikanten Unterschiede zwischen tg-Mäusen und Wildtyp-Geschwistertieren zeigen. Möglicherweise ist die erwartete Effektstärke des Alters und Genotyps auf die Hirn-Clearance kleiner als erwartet und die gewählte Tieranzahl auch aufgrund hoher interindividueller Variabilität zu niedrig, um die Unterschiede adäquat abbilden zu können. Hier erfolgt daher aktuell noch eine Optimierung des Versuchs.

Ob und in welchem Ausmaß sich Störungen der Hirn-Clearance-Kapazität auch in den genetischen oder Diät-induzierten Modellen der Adipositas wiederfinden, ist künftig ein Forschungsfeld, das in der Arbeitsgruppe mit der neu etablierten MRT-Methode untersucht werden soll, um möglicherweise eine weitere pathomechanistische Verbindung zwischen Adipositas, Neuroinflammation und Aβ-Pathologie aufzudecken.

4. Einleitung

4.1 Ernährung, Adipositas und Neuroinflammation

Die Prävalenz von Übergewicht (BMI ≥25) und starkem Übergewicht bzw. Adipositas (BMI ≥30) nimmt seit Jahren kontinuierlich zu [1]. Bei beiden Krankheitsbildern kommt es zur Gewichtszunahme, die vor allem durch eine übermäßige Akkumulation von Fettgewebe entsteht. Neben soziokulturellen Einflüssen und mangelnder Bewegung ist Fehlernährung mit einem ständigen Überangebot an kalorien- und damit häufig auch fett- sowie zuckerreicher Nahrung einer der Hauptgründe für die Gewichtszunahme bei Adipositas [1].
Eine Fehlernährung hat im Kontext von Adipositas häufig schwerwiegende gesundheitliche Konsequenzen, darunter eine Reihe nachgewiesener Begleit- und Folgeerkrankungen z. B. des kardiovaskulären Systems (zusammengefasst in der Übersichtsarbeit von Ciumărnean et al. [2]), des muskuloskeletalen Systems (zusammengefasst in der Übersichtsarbeit von Anandacoomarasamy et al. [3]) und des (Auto-)Immunsystems (zusammengefasst in der Übersichtsarbeit von Hotamisligil [4]). Adipositas ist zusätzlich bereits seit Jahren als Risikofaktor für die Entstehung neurodegenerativer Erkrankungen wie der Alzheimerschen Erkrankungen (AD) anerkannt [5–8]. Ein wesentlicher Pathomechanismus, der sowohl bei Adipositas als auch bei AD feststellbar ist, ist die Neuroinflammation.
Es wird angenommen, dass die durch Adipositas ausgelöste Neuroinflammation aus einer persistierenden chronisch-niedrigschwelligen Entzündung der Körperperipherie resultiert.
Der Begriff Entzündung wird in der Medizin nicht immer einheitlich verwendet [9], ist aber im Allgemeinen als Reaktion des Körpers auf einen schädigenden internen oder externen Reiz definiert, deren Ziel es ist diesen Reiz zu beseitigen, die entstandenen Schäden zu reparieren und die Homöostase wiederherzustellen. Beteiligt dabei sind neben dem lymphatischen System eine Vielzahl mobiler Zellen und Moleküle die dem angeborenen/unspezifischen oder dem erworbenen/spezifischen Immunsystem zugeordnet werden können. Eine strikte Abgrenzung zwischen angeborenem und erworbenen Immunsystem ist jedoch nicht immer möglich [10]. Dem angeborenen Immunsystem werden beispielsweise Makrophagen und Granulozyten als zelluläre Immunabwehrmechanismen zugeordnet, während auf humoraler Ebene vor allem Interferone und das Komplement-System wirken können (zusammengefasst von Koenderman et al. [11]). Das erworbene Immunsystem ist funktionell vor allem durch Lymphozyten charakterisiert. Auf zellulärer Ebene sind vor allem T- und B-Zellen an der spezifischen Immunantwort beteiligt, während auf humoraler Ebene die von B-Zellen gebildeten Antikörper eine entscheidende Rolle einnehmen (zusammengefasst von Bonilla und Oettgen [12]). Humorale und zelluläre Immunantwort arbeiten für gewöhnlich eng orchestriert miteinander zusammen, wichtige Signalmediatoren hierbei sind Chemokine und Zytokine [13].
Die persistierende chronisch-niedrigschwellige Entzündung bei Adipositas ist durch eine Erhöhung von Mediatoren mit pro-inflammatorischem Potenzial wie gesättigten Fettsäuren und Zytokinen gekennzeichnet [4]. Diese Mediatoren können die myeloiden Zellen des Gehirns, dazu zählen u. a. parenchymale Mikroglia, perivaskuläre Zellen, meningeale Makrophagen und aus dem Blut eingewanderte Monozyten [14], über verschiedene Wege beeinflussen [15, 16]. Bei Adipositas sind neuroinflammatorische Prozesse vor allem im Hypothalamus nachweisbar, was zu Dysregulationen der Hypothalamus-Hypophysen-Achse führt, die weitere Störungen der Regulierung des Körpergewichts und der Nahrungsaufnahme begünstigen [17] und somit zu einen Teufelskreis aus Fehlernährung, Übergewicht und Neuroinflammation führen können.

4.2 Neuroinflammation, Amyloidpathologie und Neurodegeneration

Im Allgemeinen wird Neuroinflammation als Oberbegriff für alle pro-inflammatorischen Immunantworten im zentralen Nervensystem (ZNS) genutzt. Die Bezeichnung Neuroinflammation wird dabei meist unabhängig vom auslösenden Ereignis, z. B. Infektionen, Traumata, Ischämie oder Toxinen, verwendet [18] und umfasst deshalb ein sehr heterogenes Krankheitsgeschehen hinsichtlich Kontext, Verlauf und Dauer [19]. Im Rahmen dieser Arbeit sollen daher nur die wichtigsten Charakteristika näher betrachtet werden, die für das

Verständnis von Neuroinflammation im Rahmen neurodegenerativer Erkrankungen, im speziellen bei AD, nötig sind.
Obwohl die zugrundeliegenden Ursachen vieler neurodegenerativer Erkrankungen noch nicht im Detail verstanden sind, finden sich neuroinflammatorische Prozesse immer wieder als gemeinsamer Pathomechanismus [20]. Neuroinflammatorische Prozesse werden daher als wichtiger kausaler Prozess für die Abnahme kognitiver Fähigkeiten [21, 22] sowie Verhaltensänderungen angesehen [23, 24]. Dies trifft auch auf AD als prominenten Vertreter neurodegenerativer Erkrankungen zu. Nach der weithin anerkannten Amyloid-Kaskaden-Hypothese ist die Ablagerung von Amyloid-β (Aβ) im Gehirn das auslösende Ereignis für weitere pathologische Veränderungen bei AD [25, 26]. Dennoch gibt es mittlerweile zahlreiche Hinweise, dass diese Hypothese allein nicht ausreicht, um viele Aspekte der AD-Pathogenese zu erklären [27]. Die Entdeckung erhöhter Konzentrationen von Entzündungsmarkern bei Patienten mit AD und die Identifikation von AD-Risikogenen, die mit dem Immunsystem vernetzt sind, legen nahe, dass Neuroinflammation eine wichtige Rolle in der Entstehung und Progression von AD einnimmt [18, 28]. Neuroinflammation kann dabei durch Aβ-Ablagerungen induziert werden, was zu weiteren krankhaften Veränderungen im ZNS bis hin zum Untergang von Neuronen führen kann [29, 30]. Weitere Publikationen zeigen zusätzlich einen kausalen Zusammenhang zwischen Neuroinflammation und verstärkter Aβ-Akkumulation [31].
Verschiedene Grade mikroglialer und astroglialer Aktivierung werden häufig bei AD und anderen neurodegenerativen Erkrankungen beobachtet [32, 33]. Dabei sind Mikroglia die prominentesten im ZNS-ansässigen Immunzellen, die an der Neuroinflammation beteiligt sind [34]. Die inflammatorische Aktivierung von Mikroglia führt zu charakteristischen morphologischen Veränderungen, bei denen diese ihre feinen Fortsätze zurückziehen und sowohl die Zellkörper als auch die Fortsätze hypertroph werden [35]. Der Wechsel vom homöostatischen zum pro-inflammatorischen Phänotyp ist außerdem durch eine erhöhte Expression von Zytokinen wie Interleukin (IL) -1β, IL-6 und Tumornekrosefaktor-α (TNF-α) sowie pro-inflammatorischen Chemokinen und reaktiven Sauerstoffspezies gekennzeichnet [36].
Neben der pro-inflammatorischen Aktivierung von Mikroglia können auch Astroglia eine solche Aktivierung erfahren. Dabei konnte bereits gezeigt werden, dass Mikroglia die Aktivierung von Astroglia auslösen können [37]. In den so aktivierten Astroglia kommt es anschließend zu einer erhöhten Expression von pro-inflammatorischen Mediatoren wie IL-1β, TNF-α und Stickoxiden (NO) sowie Genen des Komplement-Systems [33]. Daraus resultierend werden homöostatische Funktionen, welche Astroglia physiologisch übernehmen, wie z. B. die Aufrechterhaltung der Blut-Hirn-Schranke (BHS) [38, 39], aber auch die effiziente Beseitigung metabolischer Abbauprodukte aus dem ZNS [40], gestört.

4.3 Hirn-Clearance und Amyloidpathologie

Speziell im ZNS ist aufgrund der hohen metabolischen Aktivität neuronaler Zellen [41] die Homöostase des empfindlichen Gleichgewichtes aus Produktion und Abbau bzw. Abtransport von potentiell toxischen Molekülen von besonderer Relevanz. In diesem Zusammenhang wird der Begriff „Clearance“ verwendet, um allgemein die Entfernung von Substanzen aus dem Gehirn über eine Vielzahl möglicher, zum Teil überlappender Systeme zu beschreiben [42].
Die Degradations-Clearance findet lokal im Gehirn statt. Hier kommt es extrazellulär zu enzymatischem Abbau z. B. durch Proteasen, welche von Astroglia sezerniert werden [43, 44]. Nach Aufnahme der abzubauenden Moleküle sowohl in Neurone als auch in Gliazellen findet zudem ein intrazellulärer Abbau u. a. über Autophagie-Mechanismen statt. Autophagie ist ein hochkonservierter kataboler Prozess, bei dem beschädigte Organellen und fehlerhafte Proteine mit Hilfe von Lysosomen abgebaut und anschließend recycelt werden können, um die Proteinhomöostase aufrechtzuerhalten [45].
Es konnten mittlerweile auch zahlreiche ineinandergreifende Mechanismen nachgewiesen werden, bei denen die Clearance durch Abtransport aus dem ZNS über das Blut, die Lymphe oder durch Rezirkulation in die cerebrospinale Flüssigkeit (CSF) gewährleistet wird [42]. Die Möglichkeit zum Transport von Proteinen über die BHS hängt dabei von Molekulargewicht, Größe und Löslichkeit dieser ab [46]. Frühe Studien konnten die Relevanz spezieller

Transportsysteme durch die BHS aus dem ZNS für die Aβ-Clearance bestätigen [47]. Neben dem Transport über die BHS wurde in den letzten Jahren jedoch auch die Relevanz des gerichteten Austauschs von interstitieller Flüssigkeit (ISF) und CSF für die Drainage extrazellulärer Flüssigkeiten und die Beseitigung interstitieller Abfallstoffe im Rahmen der Hirn-Clearance bestätigt [40, 48]. Da das Parenchym selbst über kein Lymphgefäßsystem verfügt, haben sich dazu Gliazell-vermittelte perivaskuläre Netzwerke gebildet, die als sogenanntes glymphatisches System die Funktion des Lymphsystems im ZNS übernehmen (kürzlich zusammengefasst in der Übersichtsarbeit von Hablitz und Nedergaard [49]). Nichtsdestotrotz konnte auch die Existenz meningealer Lymphgefäße im Gehirn nachgewiesen werden, die womöglich eine zentrale Schnittstelle für die Clearance der mit der CSF zirkulierenden Proteine darstellt [50]. Weitere Orte der CSF-Absorptionsclearance finden sich in den Arachnoidalzotten [51] und über paraneurale Routen der optischen [52, 53] und olfaktorischen Nerven [54, 55], welche schließlich in das periphere Lymphsystem dränieren.
Störungen insbesondere bei der Hirn-Clearance wurden als pathogene Faktoren bei verschiedenen neurodegenerativen Erkrankungen mit Proteinaggregationen identifiziert, z. B. die Ablagerung von Aβ bei AD [56]. Der Akkumulation von Aβ liegt ein Ungleichgewicht zwischen dessen Produktion und Clearance zugrunde [57]. Insbesondere bei der wesentlich häufiger auftretenden sporadischen AD wird spekuliert, dass eine verminderte Clearance maßgeblich zur AD-Pathogenese beiträgt [58]. Hierbei wird angenommen, dass Störungen der Hirn-Clearance die Bildung von Aβ-Plaques begünstigen und so über nachgelagerte Pathomechanismen wie z. B. die Induktion neuroinflammatorischer Prozesse zur Progression von AD beitragen [59]. Darüber hinaus ist Aβ selbst in der Lage, den Abtransport über die beschriebenen Hirn-Clearance-Routen zu beeinträchtigen [60, 61]. Aufgrund dieses Kausalitäts-Dilemmas steht in der aktuellen Grundlagenforschung weiterhin die Frage nach der genauen zeitlichen Abfolge der einzelnen pathologischen Veränderungen im Raum.

4.4 Mausmodelle in der Grundlagenforschung für die Erforschung des Zusammenhangs zwischen Ernährung, Neuroinflammation und Amyloidpathologie

Tiermodelle spielen in der Erforschung von neurologischen und verhaltensbezogenen, jedoch auch entzündlichen Korrelaten des menschlichen Alterns eine entscheidende Rolle. Insbesondere murine Modelle werden aufgrund ihrer vergleichsweise günstigen Unterhaltung und einfachen Handhabbarkeit, der guten genetischen Charakterisierung sowie verhältnismäßig einfachen Manipulierbarkeit häufig zur Klärung experimenteller Fragestellungen in der Grundlagenforschung genutzt [62]. Zusätzlich weisen die durchschnittlichen Lebenserwartungskurven von Mäusen vergleichbare Muster in der Abnahme des Allgemeinzustandes in Verbindung mit normalen und pathologischen Alterungsprozessen wie beim Menschen auf [62].
Aufgrund des bereits beschriebenen Zusammenhangs zwischen metabolischen Störungen und Neurodegeneration eignen sich murine Adipositas-Modelle zur Erforschung neuroinflammatorischer und neurodegenerativer Prozesse. Es gibt eine Vielzahl von Modellen, die auf veränderten Diäten wie der Cafeteria-Diät oder einer Hoch-Fett-Diät (HFD) beruhen [63, 64]. In diesen Modellen entsteht der Phänotyp über einen längeren Zeitraum, wobei die authentischere Darstellung der humanen Adipositas-Pathologie hervorgehoben wird [65]. Daneben kann die Adipositas im Mausmodell auch genetisch induziert werden. Ein häufig genutztes Modell sind Leptin-defiziente (ob/ob) -Mäuse, die aufgrund abnormaler Leptin-Signalübertragung übermäßig viel Nahrung zu sich nehmen [66]. Durch die stetige Nahrungsaufnahme kommt es in diesem genetischen Modell bereits in sehr jungem Alter zur Ausprägung einer Adipositas [67].
Zur Abbildung neuroinflammatorischer Prozesse bei neurodegenerativen Erkrankungen wie AD wurde ebenfalls eine Vielzahl genetisch veränderter Phänokopien der humanen AD-Pathologie in Mausmodellen etabliert [68]. Basierend auf der Amyloid-Kaskaden-Hypothese [25, 26] konzentriert sich die Mehrheit der Modelle auf bekannte Mutationen in den Genen für das Amyloid-Precursor-Protein (APP) und/oder den Presenilinen (PS), die aus hereditären AD-

Formen bekannt sind. Hier zählen z. B. 5xFAD-Mäuse [69], ARTE10-Mäuse [70] oder APPswe/PS1dE9-Mäuse [71] zu den häufig genutzten Modellen. Die Mauslinien unterscheiden sich meist in den spezifischen Mutationen, aber auch in verwendeten Promotoren und genetischen Hintergründen. In der aktuellen Forschung sind doppelt transgene APP/PS1-Mäuse weit verbreitet, da der synergistische Effekt von mutiertem APP und PS1 im Vergleich zu monogenen Linien ein früheres Auftreten der nachweisbaren Aβ-Pathologie und einen schnelleren Krankheitsverlauf ermöglicht [72].
Bisher spiegeln die verschiedenen Mausmodelle für Neuroinflammation und Neurodegeneration jeweils nur gewisse Teilaspekte dieser hochkomplexen Pathomechanismen wider. Daher ist die Auswahl des am besten geeigneten Modells für die jeweilige Forschungshypothese von entscheidender Bedeutung [73–75].

4.5 Wissenschaftliche Hypothesenableitung

Basierend auf Mausmodellen für die Untersuchung der Neuroinflammation, ausgelöst durch Adipositas (HFD- und ob/ob-Modell) oder modelliertem AD-Phänotyp (APPswe/PS1dE9 Modell), und auf Grundlage des dargestellten aktuellen Standes der Wissenschaft soll in dieser Arbeit das Zusammenspiel zwischen Ernährung, inflammatorischen Prozessen, Aβ-Pathologie und Neurodegeneration untersucht werden. Zusätzlich soll beleuchtet werden, ob es einen möglichen Zusammenhang zwischen den genannten pathologischen Veränderungen und Störungen der Hirn-Clearance-Funktion gibt. Dazu wurden nachfolgende Hypothesen abgeleitet:

I. Fehlernährung im Rahmen einer langzeitigen, fettreichen Diät führt zu einer persistierenden niedrigschwelligen systemischen Inflammation, manifestiert als organständige Inflammation in der Leber (Studie 1), sowie zu Neuroinflammation (Studie 2).

II. Adipositas führt zu Verhaltensänderungen (Studie 3).

III. Ernährungsintervention (Diätwechsel) kann als therapeutischer Ansatz der Adipositas angesehen werden und mindert die persistierende niedrigschwellige Inflammation (Studie 4).

IV. Ernährungsintervention (Kalorienrestriktion) kann zu einer Steigerung der Hirn-Clearance über Autophagie-Mechanismen und damit zu einer Reduktion der Belastung durch Aβ-Plaques sowie zu einer reduzierten Neuroinflammation führen (Studie 5).

V. Kontrastmittelbasierte Bildgebung kann *in vivo* genutzt werden, um die Hirn-Clearance-Kapazität einschätzen zu können (Studie 6).

5. Material und Methoden

Die detaillierte Beschreibung der angewandten Methodik und der verwendeten Materialien der bereits publizierten Studien 1–5 ist den jeweiligen Originalarbeiten im Anhang zu entnehmen. Im nachfolgenden Text werden daher nur die für das Verständnis dieser Dissertation wichtigen Methoden der bisher noch nicht veröffentlichten Studie 6 näher erläutert.

5.1 Tierexperimentelle Arbeiten

Die in dieser Arbeit genutzten Mausmodelle (HFD, ob/ob und APPswe/PS1dE9) sind detailliert in den jeweiligen Publikationen (im Anhang: Veröffentlichte Originalarbeiten ab Seite 43) zu finden. Alle tierexperimentellen Arbeiten erfolgten mit Genehmigung des örtlichen Tierversuchsausschusses Landesamt für Landwirtschaft, Lebensmittelsicherheit und Fischerei (LALLF) des Landes Mecklenburg-Vorpommern (LALLF M-V/TSD/7221.3-2-002/14, genehmigt am 07.03.2014; LALLF M-V/TSD/7221.3-2-001/18, genehmigt am 01.03.2018; sowie LALLF M-V/TSD/7221.3-2-009/20, genehmigt am 11.05.2020)] und unter Beachtung der ARRIVE-Richtlinien. Alle Tiere erhielten eine Betreuung gemäß der EU-Richtlinie 2010/63/EU.

5.2 Gadoliniumkontrastmittel (GBCA) -basierte Bildgebungs-untersuchungen zur Evaluation der Hirn-Clearance-Kapazität

In Studie 6 wurden longitudinale Untersuchungen im Alter von sechs, neun und zwölf Monaten bei n = 9 APPswe/PS1dE9 (tg) -Mäusen und n = 9 Wildtyp (wt) -Geschwistertieren mit einem Scan-Protokoll durchgeführt, das aus einer hoch-T2w Inv. Rec. RARE (FLAIR)-Sequenz bestand: *T2w RARE Inv. Rec. transversal: TE/TR/TI: 37 ms/10000 ms/1800 ms, Echo-Abstand: 12,333 ms, Rare-Faktor: 8, FoV: 20 x 21 mm, Bildmatrix: 234 x 246, Auflösung: 85 x 85 µm, Schichtdicke: 500 µm, Schichten: 16, TA: 3:50 min/s.* Für eine Untergruppe aus n = 6 tg-Tieren und n=6 wt-Tieren im Alter von neun und zwölf Monaten wurde abwechselnd eine T1w-RARE-Sequenz und eine hoch-T2w FLAIR-Sequenz verwendet, so dass T1w-Bilder zusätzlich zur Beurteilung von parenchymalen Veränderungen verwendet werden konnten: *T1w RARE transversal: TE/TR: 16ms/1160ms, Rare-Faktor: 8, FoV: 20 x 21 mm, Bildmatrix: 234 x 246, Auflösung: 85 x 85 µm, Schichtdicke: 500 µm, Schichten: 16, TA: 2:40 min/s.*
Beide Verfahren wurden einmal vor (=Baseline) und wiederkehrend für 180–182 min nach GBCA-Applikation durchgeführt. Nach den Baseline-Scans mit beiden Sequenzen erhielten die Mäuse das GBCA Gadotersäure (DOTAREM® 0,5 mmol/l, Guerbert) in einer Dosierung von 0,025 ml/g Körpergewicht als Bolus über einen Schwanzvenenkatheter. Im Rahmen der bildgebenden Untersuchung wurden Mäuse mit 1,5–2,5 % Isofluran (Baxter, Unterschleißheim, Deutschland) und Sauerstoff (Air Liquide, Hamburg, Deutschland) anästhesiert. Die Mäuse wurden in Bauchlage in einen 7-Tesla-Kleintier-Scanner für Magnetresonanztomographie (MRT) (Bruker BioSpin GmbH, Ettlingen, Deutschland) gelegt, der mit einer ^{1}H-Kryo-Sende-/Empfangsspulenanordnung mit zwei Elementen ausgestattet war. Die Körperkerntemperatur der Tiere wurde mit Hilfe eines temperaturgesteuerten Heizkissens auf 37 °C gehalten.
Die T2w-Aufnahmen zeigen CSF hypointens gegenüber dem Hirnparenchym [76]. Nach Injektion des GBCA sorgt dies für eine größtmögliche Signalintensitätsänderung zur Begutachtung der ventrikulären Clearance in den CSF-gefüllten Räumen. Demgegenüber eignen sich T1w-Aufnahmen vor allem zur Untersuchung der GBCA-induzierten Signalintensitätsänderungen im Hirnparenchym selbst [77, 78], welche ein Anhaltspunkt für die Effizienz des Austauschs von CSF und ISF im Rahmen der glymphatischen Clearance sein kann.
Voxelwerte wurden in manuell eingegrenzten Bereichen von Interesse (engl. Volumes of Interest, VOI) in den Ventrikeln (in T2w-Bildern) und im Hirnparenchym (T1w-Bilder) bestimmt (Abbildung 1 A und B). Die anschließende Datenanalyse wurde mit PMOD-Software (Version 3.7; PMOD Technologies) durchgeführt. Mit der eingebauten Funktion „calculate selected VOI statistics“ wurden mittlere Voxelwerte als Maß für die Helligkeit/Signalintensität im

ausgewählten VOI berechnet. Auf Grundlage dieser Werte wurden Intensitäts-Zeit-Kurven erstellt, welche die relative Veränderung der mittleren Voxelwerte der VOIs als Prozentsatz ausgehend vom Ausgangsniveau (=0 %) zeigen. Die weitere Analyse dieser Intensitäts-Zeit-Kurven wurde mit der Software IgorPro (V6.37, WaveMetrics) durchgeführt. Der Anstieg der Signalintensität nach GBCA-Injektion und der anschließende Abfall des Signals während der Auswaschphase wurden mit einer Modellfunktion beschrieben, die aus einer Exponentialfunktion für den Anstieg, addiert mit einer Exponentialfunktion für den Abfall, besteht. Dieses Modell wurde aufgrund der Annahme gewählt, dass die GBCA-Anreicherung und -Ausschwemmung in den Ventrikeln zu einem großen Teil diffusionsgetriebene Prozesse sind, die sich typischerweise gut mit einem exponentiellen Ansatz beschreiben lassen. Werden alle experimentellen Daten an diese Modellfunktion angepasst, ergeben sich die exponentiellen Konstanten für den ansteigenden bzw. den abfallenden Teil jeder Intensitäts-Zeit-Kurve (schematisch dargestellt in Abbildung 1 C). Da diese Konstanten für die Anflutungs- und die Auswaschphase unabhängig von der Signalintensität sind, können sie direkt für den Vergleich zwischen den Tieren verwendet werden, ohne dass eine weitere Normalisierung der Daten erforderlich ist.

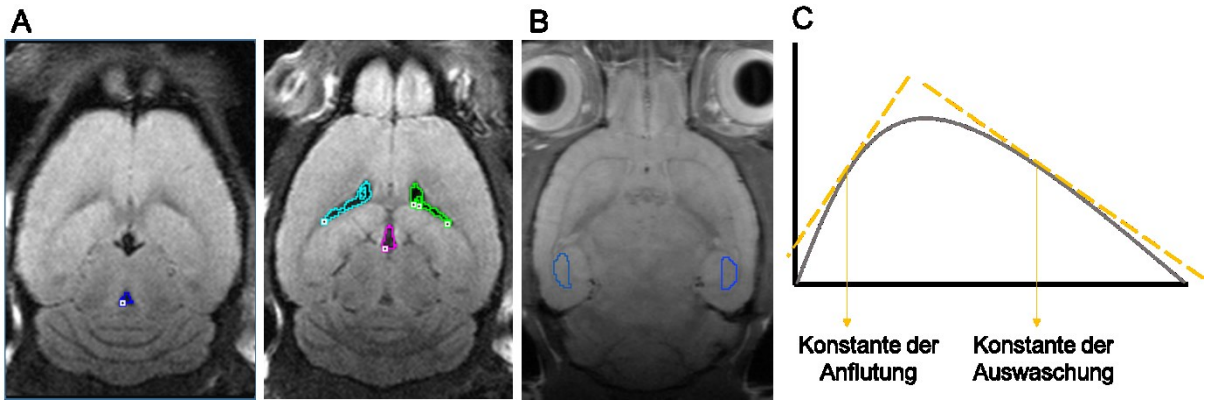

Abbildung 1: Schematische Abbildung zur Auswertung von MRT-Bildern. A) Volumes of Interest (VOI) in T2-gewichteten Bildern im vierten (dunkelblau, linkes Bild) und im dritten Ventrikel (pink) sowie den beiden lateralen (türkis und grün) Ventrikeln (rechtes Bild). B) VOI im Hippocampus (blau) in einem T1-gewichteten Bild. C) Schematische Darstellung der Intensitäts-Zeit-Kurven, an denen die Konstanten für Anflutung und Auswaschung mit Hilfe des Anstiegs (gestrichelte gelbe Linien) ermittelt wurden. Der Anstieg wurde mit einer Modellfunktion errechnet, die aus einer Exponentialfunktion für den Anstieg, addiert mit einer Exponentialfunktion für den Abfall, besteht.

6. Ergebnisse

6.1 Studie 1

In der vorliegenden Studie [79] wurde mit Hilfe einer 24-wöchigen HFD ein Adipositas-Mausmodell generiert, das mit zwei Kontrollgruppen verglichen wurde. Die erste Kontrollgruppe erhielt eine fettarme, aber kohlenhydratreiche Diät (KD), die zweite Gruppe eine standardisiert-ausgewogene Makronährstoffdiät (SD). Die Arbeit zielte darauf ab, das pro-inflammatorische Potenzial der Diät-induzierten Adipositas (von engl. diet-induced obesity, DIO) auf die Leber zu charakterisieren.
Sowohl im äußeren Erscheinungsbild (Abbildung 2 A) als auch im Körpergewicht (Abbildung 2 B) unterschieden sich die Mäuse der HFD-Gruppe deutlich von denen der KD- und SD-Gruppe ($p < 0,0001$). *In situ* zeigte sich eine Aufhellung der Lebern sowohl in der HFD- als auch in der KD-Gruppe im Vergleich zur SD-Gruppe, was auf Fetteinlagerungen hindeutete (Abbildung 2 C). Die Analyse der Lebergewichte ergab signifikant erhöhte Werte in der HFD-Gruppe ($p < 0,0001$ vs. KD-Gruppe; $p = 0,013$ vs. SD-Gruppe; Abbildung 2 D). Mikroskopisch zeigte sich zudem in HE-gefärbten Präparaten der HFD-Gruppe eine Steatose mit einem signifikant erhöhten Leberfettanteil in der HFD-Gruppe ($p < 0,0001$ vs. KD und SD, Abbildung 2 E und F). Als zusätzlicher Befund zeigte sich in Mäusen der KD-Gruppe ein signifikant erhöhter hepatischer Cholesterolgehalt gegenüber der HFD-Gruppe ($p = 0,0240$, Abbildung 2 K).
Erste Ergebnisse aus HE-gefärbten Präparaten zeigten zudem erhöhte lobuläre Entzündungsherde in der HFD-Gruppe im Vergleich zur SD- ($p = 0,0030$), nicht aber zur KD-Gruppe. Zum spezifischeren Nachweis der organischen Manifestation einer niedrigschwelligen Entzündung in der Leber wurden die entzündlichen Infiltrate der CAE^+ (Granulozyten) und $F4/80^+$ (Makrophagen) in der Leber relativ zur Gesamtzahl der Hepatozyten quantifiziert (Abbildung 2 G-J). Es zeigten sich signifikante Unterschiede zwischen der HFD- und SD-Gruppe (CAE^+: $p = 0,0003$; $F4/80^+$: $p = 0,0002$), nicht jedoch zwischen HFD- und KD-Gruppe. Außerdem gab es bei beiden Analysen einen signifikanten Unterschied zwischen beiden Kontrollen (CAE^+: $p < 0,0001$; $F4/80^+$: $p = 0,006$).
Neben der entzündlichen Infiltration mit Granulozyten und Makrophagen wurde auch die Expression pro-inflammatorischer Mediatoren in der Leber untersucht. Dabei wurde insbesondere die hepatische mRNA-Expression der pro-inflammatorischen Zytokine *il-1β*, *il-6* und *tnf-α* quantifiziert (Abbildung 2 L). Die Ergebnisse zeigen insgesamt einen heterogenen Effekt der verschiedenen Diäten auf die Zytokin-Expression. Die *il-1β*-mRNA-Expression in der KD-Gruppe war signifikant niedriger als in der HFD- und SD-Gruppe ($p < 0,0001$ vs. HFD-Gruppe; $p = 0,0021$ vs. SD-Gruppe). Erstaunlicherweise war dies bei der *il-6*-mRNA-Expression genau umgekehrt, und die KD-Gruppe zeigte im Vergleich zur HFD- und SD-Gruppe eine signifikant höhere Expression ($p = 0,0106$ vs. HFD-Gruppe; $p = 0,0124$ vs. SD-Gruppe). Nur die *tnf-α*-mRNA-Expression war erwartungsgemäß in der HFD-Gruppe am höchsten, was im Vergleich zur SD-Gruppe signifikant war ($p = 0,0052$), nicht aber gegenüber der KD-Gruppe. Darüber hinaus wurde eine signifikante Erhöhung der *tnf-α*-mRNA-Expression in der KD-Gruppe im Vergleich zur SD-Gruppe ($p = 0,005$) festgestellt.

Zusammenfassend wurden in der vorliegenden Studie die Auswirkungen einer HFD im Vergleich zu zwei verschiedenen Kontrolldiäten untersucht. Dabei zeigte sich nur im Vergleich zwischen HFD und SD ein signifikanter Effekt auf die entzündliche Infiltration mit Granulozyten und Makrophagen, nicht jedoch im Vergleich zur KD. Bei Begutachtung der Expression pro-inflammatorischer Mediatoren konnte jedoch sowohl tendentiell gegenüber KD als auch signifikant gegenüber SD die Induktion der mRNA-Expression des pro-inflammatorisch wirksamen TNF-α durch HFD gezeigt werden.

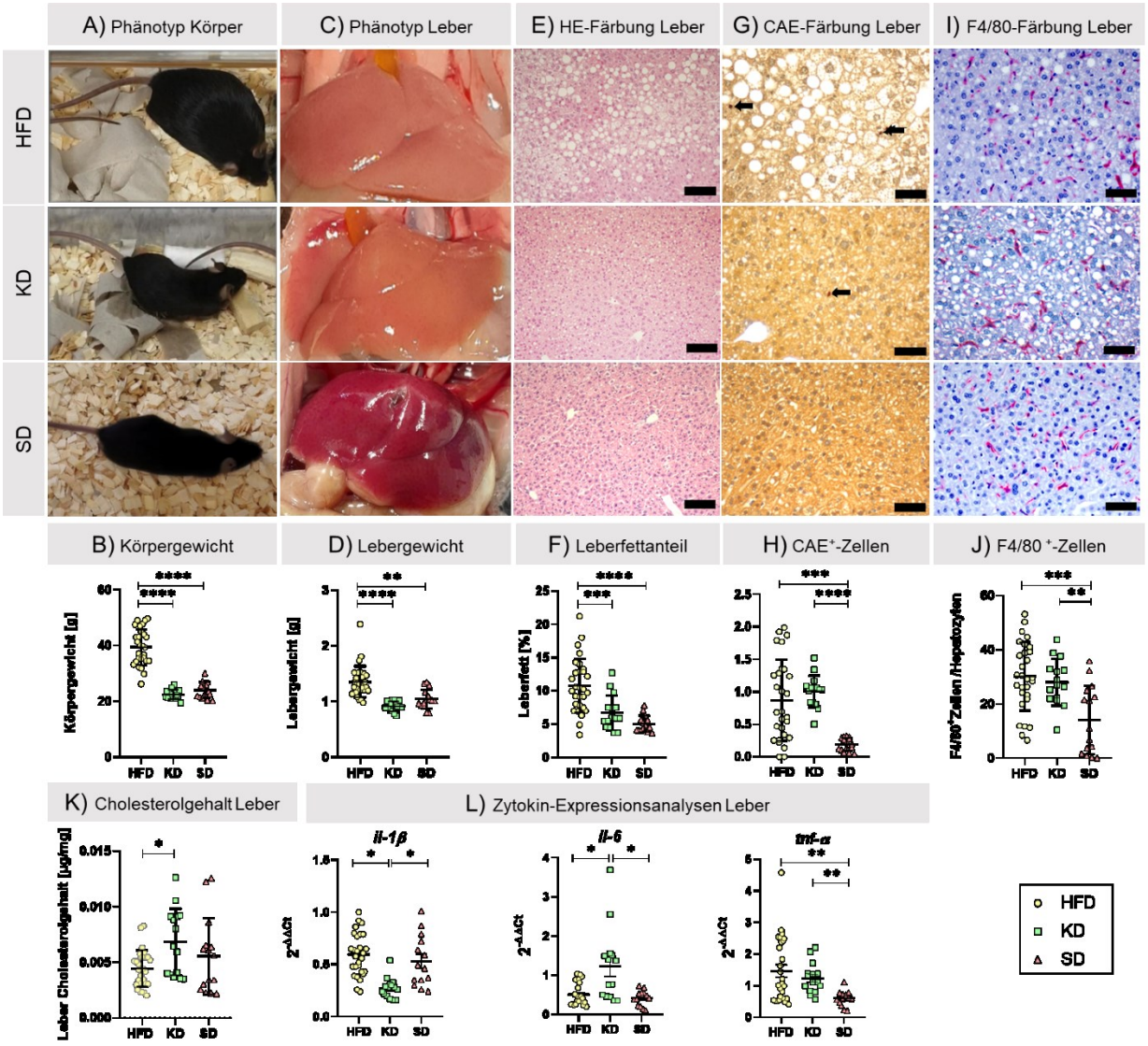

*Abbildung 2: Übersicht zum Vergleich der Mäuse der Hoch-Fett-Diät (HFD, n = 29) mit Mäusen auf kohlenhydratreicher Diät (KD, n = 15) oder standardisiert-ausgewogener Makronährstoffdiät (SD, n = 15). Alle Werte dargestellt als Mittelwert±Standardabweichung. A) Repräsentative Bilder des Phänotyps von Mäusen der HFD-, KD- und SD-Gruppe. B) Körpergewicht der Mäuse. Die Signifikanz der Unterschiede zwischen den Gruppen wurde mittels Brown-Forsythe und Welch-ANOVA mit angeschlossenem Tukey Post-hoc-Test geprüft, **** p < 0,0001. C) Repräsentative in situ-Bilder der Lebern von Mäusen der HFD-, KD- und SD-Gruppe. D) Lebergewicht der verschiedenen Gruppen. Signifikanz der Unterschiede zwischen den Gruppen wurde mittels einfacher ANOVA nach Rängen (Kruskal-Wallis) und anschließendem Tukey Post-hoc-Test geprüft; **** p < 0,0001, ** p < 0,01. E) Repräsentative HE-gefärbte Leberpräparate (200-fache Vergrößerung, Maßstabsbalken 50 µm). F) Prozentualer Anteil des vesikulären Fettgehalts in der Leber. Signifikanz der Unterschiede zwischen den Gruppen wurde mittels Brown-Forsythe und Welch-ANOVA sowie anschließendem Tukey Post-hoc-Test geprüft, **** p < 0,0001, *** p < 0,001. G) Repräsentative Bilder CAE-gefärbter Leberpräparate (CAE+-Zellen durch Pfeile gekennzeichnet, 400-fache Vergrößerung, Maßstabsbalken 20 µm). H) Relative Anzahl der Granulozyten (CAE+) im Verhältnis zur Anzahl der Hepatozyten. Signifikanz der Unterschiede zwischen den Gruppen wurde mittels einfacher ANOVA nach Rängen (Kruskal-Wallis) und anschließendem Tukey Post-hoc-Test geprüft, **** p < 0,0001, *** p < 0,001. I) Repräsentative F4/80-gefärbte Leberpräparate mit (F4/80+-Zellen rot, 400-fache Vergrößerung, Maßstabsbalken von 20 µm). J) Relative Anzahl der Makrophagen (F4/80+) im Verhältnis zur Anzahl der Hepatozyten. Signifikanz der Unterschiede zwischen den Gruppen wurde mittels einfacher ANOVA und anschließendem Tukey Post-hoc-Test geprüft, *** p< 0,001, ** p < 0,01. K) Cholesterolgehalt [µg/mg] in der Leber. Signifikanz der Unterschiede zwischen den Gruppen wurde mittels einfacher ANOVA nach Rängen (Kruskal-Wallis) und anschließendem Tukey Post-hoc-Test geprüft, * p < 0,05. L) mRNA-Expression der Zytokine il-1β, il-6 und tnf-α in der Leber. Signifikanz der Unterschiede zwischen den Gruppen wurde mittels einfacher ANOVA (il-1β) oder einfacher ANOVA nach Rängen (Kruskal-Wallis) (il-6 und tnf-α) und anschließendem Tukey Post-hoc-Test geprüft, ** p < 0,01, * p < 0,05.*

6.2 Studie 2

In der vorliegenden Studie 2 [80] wurde ebenfalls in dem 24-wöchigen HFD-Mausmodell im Vergleich zu einer KD gearbeitet, um das pro-inflammatorische Potenzial der DIO auf das Gehirn durch eine Kombination aus *In-vivo*-PET-Analysen mit 2-[^{18}F]fluoro-2-deoxy-D-glucose ([^{18}F]FDG) und (4S)-N,N-Diethyl-9-[2-[^{18}F]fluoroethyl]-5-methoxy-2,3,4,9-tetrahydro-1H-carbazole-4-carboxamide (flutriciclamide, [^{18}F]GE-180) und *Ex-vivo*-histologischen und -biochemischen Analysen von Gehirngewebe zu untersuchen.
In Übereinstimmung mit Studie 1 konnte auch hier die Ausprägung eines DIO-Phänotyps in der HFD-Gruppe gezeigt werden. Die Auswirkungen des DIO-Phänotyps auf den Glucose-Stoffwechsel im ZNS wurden *in vivo* mittels [^{18}F]FDG-PET analysiert. Es zeigte sich ein statistisch signifikanter Unterschied im korrigierten standardisierten Aufnahmewert (engl. standardized Uptakevalue, $SUV_{glc,c}$) zwischen beiden Diäten ($F_{(1,24)} = 14,5,\ p = 0,0009$) im Kortex ($p = 0,0042$), Hippocampus ($p = 0.0004$) und Hypothalamus ($p = 0,0006$) als ausgewertete Zielregionen.
Um die Auswirkungen des DIO-Phänotyps auf die Entzündung im ZNS *in vivo* zu beobachten, wurde eine [^{18}F]GE-180-PET-Bildgebung durchgeführt. Während der Analyse wurde aufgrund bisher nicht beschriebener Referenzmöglichkeiten bei dem genutzten Analyseansatz auf weitere Normalisierungsschritte verzichtet und das Messergebnis als prozentuale injizierte Dosis pro ml (%ID/ml) dargestellt. Für alle drei Zielregionen (Kortex, Hippocampus und Hypothalamus) waren die %ID-Werte in der HFD-Gruppe tendenziell erhöht, zeigten jedoch keinen statistisch signifikanten Effekt der entsprechenden Ernährung zwischen KD und HFD ($F_{(1,21)} = 1,691,\ p = 0,2075$). Als Parameter zur Evaluation des möglichen Einflusses einer Neuroinflammation auf die kognitive Leistung wurde der MWM-Test durchgeführt. Hier zeigte die HFD lediglich einen Einfluss auf die Schwimmgeschwindigkeit ($p = 0,0042$). Es gab jedoch keine statistisch signifikanten Unterschiede zwischen HFD und KD hinsichtlich der Latenzzeit zum Auffinden der Plattform, der Zeit, die im korrekten Quadranten verbracht wurde oder der Frequenz, mit der die Plattformfläche gekreuzt wurde.
Zur Analyse einer organständigen Manifestation der persistierenden systemischen niedrigschwelligen Inflammation der DIO im Gehirn wurden anschließend weitere Ex-vivo-Analysen durchgeführt. Zunächst erfolgten histologische Analysen, um eine pro-inflammatorische zelluläre Immunreaktion im Gehirn bewerten zu können. Dazu wurden Präparate mit immunhistochemischen Reaktionen auf häufig verwendete Marker für Mikroglia-Aktivierung (TSPO, Iba1 und TMEM119) und Astroglia-Aktivierung (GFAP) quantifiziert. In dem mit Iba1 reagierten Gewebe wurde die morphologische Aktivierung der Mikroglia außerdem als Ramifikations-Index (Ri) bewertet. Darüber hinaus wurde für *tspo*, *iba1* und *gfap* eine mRNA-Expressionsanalyse durchgeführt, um die immunhistochemischen Reaktionen zu ergänzen. Keine der beschriebenen Analysen zeigte einen statistisch signifikanten Unterschied zwischen der HFD- und der KD-Gruppe.
Zusätzlich wurde auch die mRNA-Expression der Zytokine *il-1β*, *il-6* und *tnfα* als Indikatoren für eine Neuroinflammation bei langfristiger HFD analysiert (Abbildung *3* E). Die PCR-Analyse des Hirngewebes ergab statistisch signifikant erhöhte Werte von pro-inflammatorischem *il-1β* ($p = 0,0224$) sowie eine Tendenz zu erhöhtem *il-6* ($p = 0,0763$), aber keinen statistisch signifikanten Unterschied der *tnf-α* mRNA-Expression ($p = 0,8261$).

Zusammenfassend stellen sich in dieser Arbeit die Auswirkungen einer HFD im Vergleich zu einer KD auf die organständige niedrigschwellige Inflammation im Gehirn ähnlich wie in der Leber (Studie 1) dar. Hinsichtlich der Beteiligung von Mikro- und Astroglia an der Entzündungsreaktion unterschieden sich beide Gruppen nicht signifikant, jedoch zeigte die HFD die Induktion einer erhöhten mRNA-Expression des pro-inflammatorischen Zytokins *il-1β*.

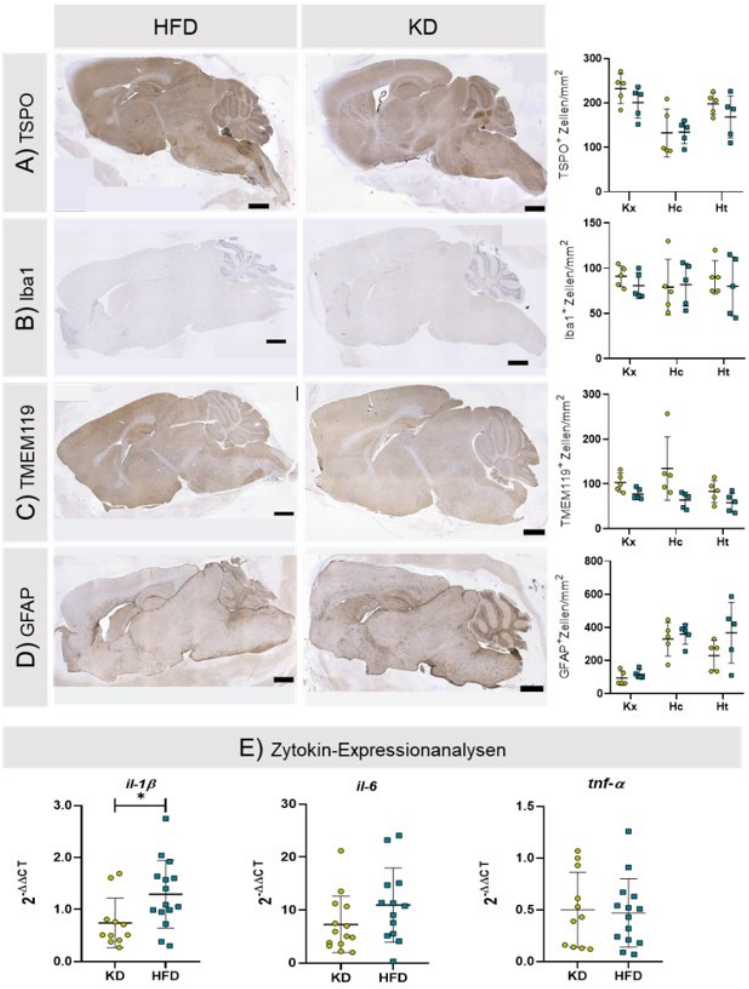

*Abbildung 3: Übersicht zum Vergleich der Mäuse mit Hoch-Fett-Diät (HFD) mit Mäusen fettarmer aber kohlenhydrat-reicher Kontroll-Diät (KD) hinsichtlich Immunreaktionen im Gehirn. Repräsentative Abbildungen für immun-histochemische Reaktionen auf Marker für zelluläre Immunantwort durch Mikroglia-Aktivierung A) TSPO, B) Iba1, C) TMEM119, sowie Astroglia-Aktivierung D) GFAP mit den dazugehörigen Quantifizierungen, dargestellt als Mittelwert±Standardabweichung in den Zielgebieten Kortex (Kx), Hippocampus (Hc) und Hypothalamus (Ht) (HFD n = 5; KD n = 5). Signifikanz der Unterschiede zwischen den Gruppen wurde mittels einfacher ANOVA mit wiederholten Messungen ohne weitere Post-hoc-Korrektur getestet. E) mRNA-Expressionsanalyse der pro-inflammatorischen Zytokine il-1β (HFD n = 15; KD n = 11), il-6 (HFD n = 13; KD n = 14) und tnf-α (HFD n = 14; KD n = 11). Signifikanz der Unterschiede zwischen den Gruppen wurde mittels ungepaartem t-Test (il-1β und tnf-α) bzw. Mann-Whitney-Test (il-6) geprüft, * p < 0,05.*

6.3 Studie 3

In der vorliegenden Studie 3 [81] wurde im genetischen ob/ob-Modell der Adipositas gearbeitet und die durch Adipositas ausgelösten Verhaltensänderungen näher untersucht. Dazu wurden sowohl weibliche als auch männliche ob/ob-Mäuse im Alter von acht, 24 und 40 Wochen mit ihren zugehörigen wt-Geschwistertieren zwei gängigen Verhaltenstests, dem offenen-Feld-Test (OF, Abbildung 4 A) und dem erhöhten Plus-Labyrinth (engl. Elevated Plus Maze, EPM, Abbildung 4 B), unterzogen, um geschlechts- und altersabhängig Adipositas-bedingte Verhaltensänderungen zu untersuchen.

Dabei wurde zunächst die Etablierung eines adipösen Phänotyps in den ob/ob-Mäusen abgesichert. Sowohl das Körpergewicht (i) als auch das viszerale (ii) und subkutane Fett (iii) war bei ob/ob-Mäusen im Vergleich zu den wt-Geschwistertieren signifikant erhöht. Die Analyse mittels dreifacher ANOVA ergab einen starken Effekt des Genotyps (i: $p < 0{,}0001$, $F_{(1,78)} = 360{,}5$; ii: $p < 0{,}0001$, $F_{(1,69)} = 184{,}3$; iii: $p < 0{,}0001$, $F_{(1,58)} = 483{,}1$). Darüber hinaus zeigen die Daten einen starken Effekt des Alters (i: $p < 0{,}0001$, $F_{(2,78)} = 63{,}98$; ii: $p < 0{,}0001$, $F_{(2,69)} = 13{,}54$; iii: $p < 0{,}0001$, $F_{(2,58)} = 46{,}70$), aber keinen geschlechtsspezifischen Effekt.

In Bezug auf die Verhaltensänderungen mit Fokus auf Bewegungsparameter zeigte die statistische Analyse, dass der Genotyp für die Verhaltensänderung bei ob/ob-Mäusen im Vergleich zu ihren wt-Geschwistertieren maßgeblich verantwortlich war ($p < 0{,}0001$ für alle, OF: Geschwindigkeit $F_{(1,64)} = 198{,}6$; Eintritt ins Zentrum $F_{(1,63)} = 80{,}41$; Eintritt in Peripherie $F_{(1,64)} = 90{,}87$; EPM: Geschwindigkeit $F_{(1,77)} = 132{,}2$; Eintritt in offene Arme $F_{(1,78)} = 21{,}5$; Eintritt in geschlossene Arme $F_{(1,77)} = 105{,}5$). Hierbei wurden alle korrelierenden Parameter von weiblichen und männlichen ob/ob- und wt-Mäusen im Alter von acht, 24 und 40 Wochen zur Analyse genutzt. Die ob/ob-Mäuse zeigten bereits im Alter von acht Wochen signifikante

Veränderungen im Vergleich zu den wt-Mäusen, daher scheint das Alter bei den Adipositas-bedingten Verhaltensänderungen der ob/ob-Mäuse eine untergeordnete Rolle zu spielen. Aus diesem Grund wurden für die weiteren Post-hoc-Analysen die Datensätze für Geschlecht und Alter zusammengeführt. Dabei zeigte sich, dass die in OF gesammelten Daten zur Gesamtdistanz und Geschwindigkeit bei ob/ob-Mäusen im Vergleich zu wt-Geschwistertieren signifikant reduziert waren ($p < 0{,}0001$, Abbildung 4 C). Ebenso waren die Zeiten, die im Zentrum und in der peripheren Zone verbracht wurden, bei ob/ob-Mäusen im Vergleich zu wt-Geschwistertieren signifikant reduziert ($p < 0{,}0001$, Abbildung 4 C). Auch im EPM zeigten sich signifikante Unterschiede in der zurückgelegten Strecke und der Geschwindigkeit ($p < 0{,}0001$, Abbildung 4 D) zwischen beiden Gruppen. Die ob/ob-Mäuse besuchten im Vergleich zu wt-Geschwistertieren signifikant weniger offene und geschlossene Arme ($p < 0{,}0001$, Abbildung 4 D). Außerdem zeigten ob/ob-Mäuse im Vergleich zu wt- Geschwistertieren ein signifikant reduziertes exploratives Verhalten, charakterisiert durch reduziertes Aufrichten ($p = 0{,}0020$), Strecken nach vorne ($p = 0{,}0020$) und durch das Lehnen über den Rand hinaus nach unten ($p < 0{,}0001$) (Abbildung 4 E).

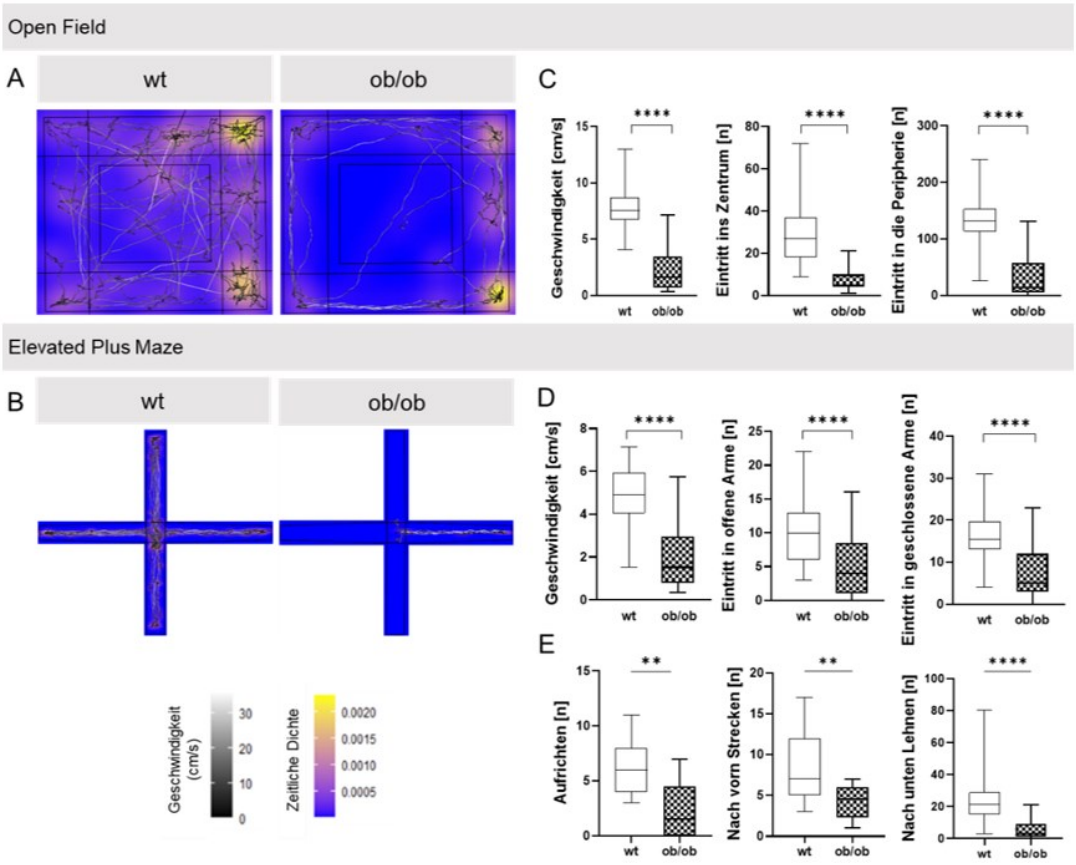

*Abbildung 4: Übersicht zum Vergleich des Verhaltens von Leptin-defizienten (ob/ob) -Mäusen und Wildtyp (wt) Geschwistertieren im offenes-Feld-Test (OF) und Elevated Plus Maze (EPM). A) Repräsentative Heatmap eines Durchlaufs für wt und ob/ob im OF. B) Repräsentative Heatmap eines Durchlaufs für wt und ob/ob im EPM. C) Auswertung der Bewegungsparameter Geschwindigkeit [cm/s] sowie Eintritt in das Zentrum und die Peripherie im OF (wt: n = 46; ob/ob: n = 40). D) Auswertung der Bewegungsparameter Geschwindigkeit [cm/s] sowie Eintritt in offene und geschlossene Arme im EPM (wt: n = 45; ob/ob: n = 45). E) Auswertung der Verhaltensparameter „Aufrichten", „Nach vorn Strecken" und „Nach unten Lehnen" im EPM (wt: n = 11, ob/ob: n = 12). Signifikanz der Unterschiede zwischen den Gruppen wurde mittels ungepaartem t-Test geprüft, ** p < 0,01 **** p < 0,0001.*

Zusammenfassend konnte diese Studie zeigen, dass eine genetisch-induzierte Adipositas im ob/ob-Modell geschlechtsunabhängig bereits im Alter von acht Wochen zu robusten Veränderungen im Verhalten führt. Hier zeigten die ob/ob-Mäuse im Vergleich zu ihren wt-Geschwistertieren ein reduziertes Bewegungsmuster und ein reduziertes exploratives Verhalten, was generell als Anzeichen eines ängstlichen Habitus interpretiert werden kann.

6.4 Studie 4

In Studie 4 [82] wurde erneut im Modell der DIO gearbeitet. Im Anschluss an die Etablierung einer DIO durch 24-wöchige HFD-Fütterung wurde die therapeutische Wirkung von Interventionen auf die persistierende niedrigschwellige Inflammation evaluiert. Die genutzten Interventionen waren Diätwechsel auf KD, Intervallfasten (IF) oder Laufbandtraining (LBT) und diese wurden, wie in Abbildung 5 A dargestellt, allein oder in Kombination für insgesamt weitere sechs Monate durchgeführt.

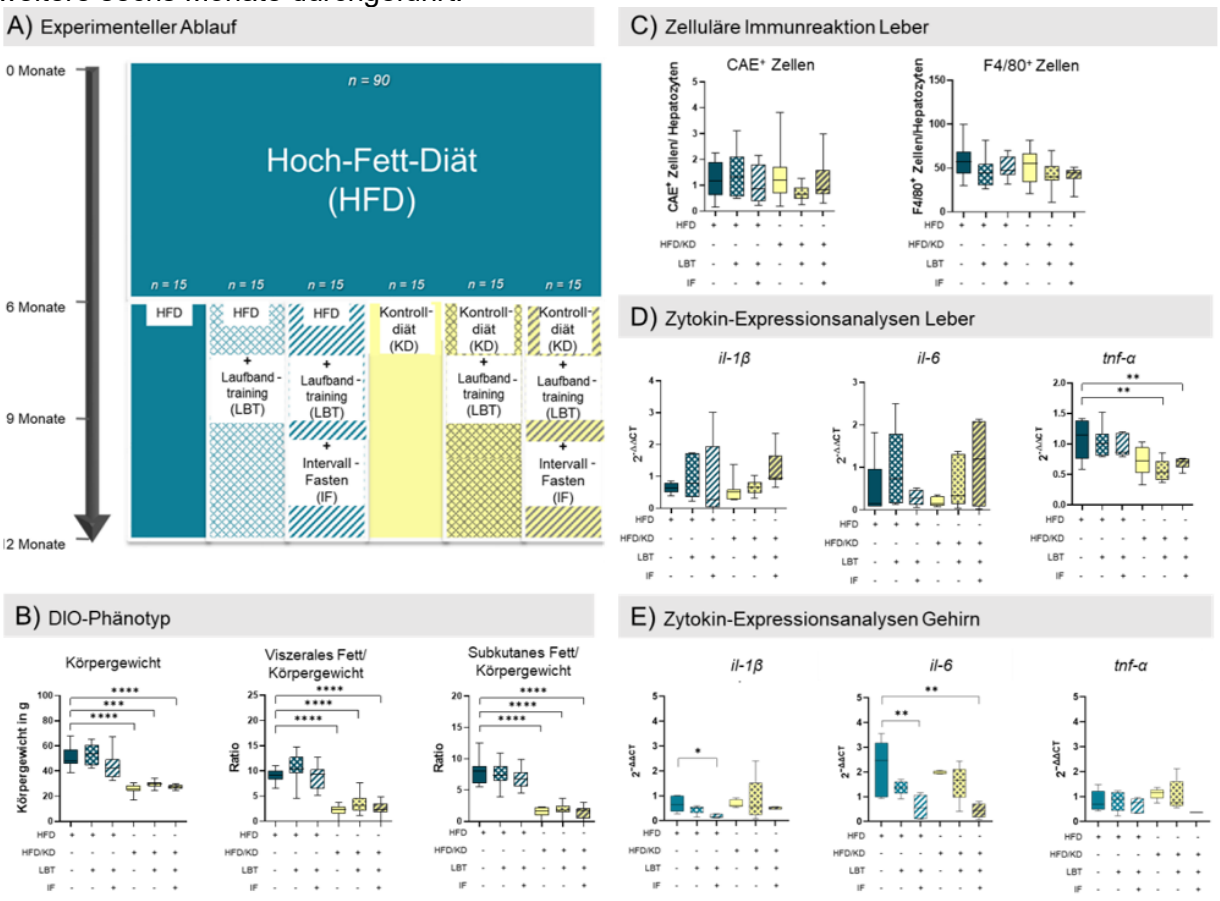

*Abbildung 5: A) Experimenteller Ablauf und B-E) Ergebnisse der Untersuchung zur therapeutischen Wirkung der Interventionen Diätwechsel zu kohlenhydratreicher Kontroll-Diät (HFD/KD), Laufbandtraining (LBT) und Intervallfasten (IF) auf Mäuse, die durch Hoch-Fett-Diät (HFD) einen Phänotyp der Diät-induzierten Adipositas (DIO) entwickelt haben. B) Quantifizierung von Körpergewicht und dem Verhältnis aus viszeralem und subkutanem Fett zum Körpergewicht dargestellt als Mittelwert±Standardabweichung. Signifikanz der Unterschiede zwischen den Gruppen wurde mittels einfacher ANOVA und anschließendem Tukey Post-hoc-Test getestet, *** $p < 0{,}001$, **** $p < 0{,}0001$. C) Relative Anzahl der Granulozyten (CAE⁺) und Makrophagen (F4/80⁺) im Verhältnis zur Anzahl der Hepatozyten dargestellt als Mittelwert±Standardabweichung. Signifikanz der Unterschiede zwischen den Gruppen wurde mittels einfacher ANOVA und anschließendem Tukey Post-hoc-Test getestet. D) mRNA Expressionsanalyse der pro-inflammatorischen Zytokine il-1β, il-6 und tnf-α in der Leber, dargestellt als Mittelwert±Standardabweichung. Signifikanz der Unterschiede zwischen den Gruppen wurde mittels Brown–Forsythe und Welch-ANOVA mit anschließendem Tamhane-T2 Post-hoc-Test getestet ** $p \leq 0{,}01$, * $p < 0{,}05$. E) mRNA-Expressionsanalyse der pro-inflammatorischen Zytokine iL-1β, iL-6 und tnfα im Gehirn, dargestellt als Mittelwert±Standardabweichung. Signifikanz der Unterschiede zwischen den Gruppen wurde mittels einfacher ANOVA und anschließendem Tukey Post-hoc-Test getestet ** $p \leq 0{,}01$, * $p < 0{,}05$.*

Nach Einführung der Interventionen führte nur die Ernährungsumstellung auf KD allein ($p < 0{,}0001$) oder in Kombination mit LBT ($p < 0{,}0001$) oder IF und LBT ($p = 0{,}0010$) innerhalb weniger Wochen zu einem signifikanten Gewichtsverlust im Vergleich zur Referenzgruppe, die weiterhin HFD ohne Interventionen (HFD/HFD) erhielt. Dieser Effekt der Ernährungsumstellung zeigte sich auch am Anteil von viszeralem und subkutanem Fett zum Gesamtkörpergewicht ($p < 0{,}0001$; KD, KD+LBT und KD+IF+LBT vs. HFD/HFD, Abbildung 5 B). Bei weiterer Analyse des Effekts der Interventionen auf die Anzahl entzündlicher Infiltrate

in der Leber (CAE$^+$ und F4/80$^+$, Abbildung 5 C) konnten keine signifikanten Effekte durch Diätwechsel auf KD gezeigt werden. Im Einklang damit waren die mRNA-Expressionen der pro-inflammatorischen Zytokine *il-1β* und *il-6* ebenfalls nahezu unverändert (Abbildung 5 D). Bemerkenswert ist, dass die mRNA-Expression von *tnf-α* in der KD-Gruppe tendenziell ($p = 0,0550$ *vs. HFD/HFD*) sowie in der KD+LBT-Gruppe ($p = 0,0028$ vs. HFD/HFD) und der KD+IF+LBT-Gruppe ($p = 0,0296$ vs. HFD/HFD) signifikant gesenkt wurde (Abbildung 5 D). Außerdem zeigte die mRNA-Expression des anti-inflammatorischen Zytokins il-*10* eine Tendenz zum Anstieg bei Ernährungsumstellung, insbesondere bei der Kombination KD+IF+LBT (p = 0,0866 vs. HFD/HFD). Durch anschließende Korrelationsanalysen konnte gezeigt werden, dass die mRNA-Expression von *tnf-α* direkt Parameter wie Körpergewicht, Anteil von Fettgewebe und Leberfettgehalt widerspiegelt (durchschnittlich r = 0,6; alle $p < 0,05$).
Erste bisher unveröffentlichte Ergebnisse zur Auswirkung der Interventionen auf die inflammatorischen Prozesse im Gehirn lassen darauf schließen, dass ebenfalls die Expression pro-inflammatorischer Mediatoren durch Interventionen beeinflusst werden kann (Abbildung 5 E). Hier zeigt sich ein positiver Effekt der Kombination aus IF+LBT, der selbst in Kombination mit HFD zu einer Verringerung der zerebralen mRNA-Expression von *il-1β* führte ($p = 0,0353$). Zusätzlich führte HFD+IF+LBT ($p = 0,0086$ vs. HFD/HFD) und KD+IF+LBT ($p = 0,0068$ vs. HFD/HFD) zu einer signifikant verringerten zerebralen mRNA-Expression von *il-6*.

Zusammenfassend konnte diese Studie einen positiven Effekt eines Diätwechsels auf die Reduktion des Körpergewichts sowie des viszeralen und subkutanen Fettanteils zeigen. Allerdings zeigte der Diätwechsel allein oder in Kombination mit IF oder LBT keinen Effekt auf die entzündlichen Infiltrate in der Leber. Eine Kombination aus KD+LBT und KD+IF+LBT führte dennoch zu signifikant verringerter mRNA-Expression von *tnf-α* in der Leber. Erste Daten, welche die Zytokin-mRNA-Expression im Gehirn evaluieren, zeigen ein ähnliches Bild. Hier scheint jedoch insbesondere die Kombination aus IF+LBT sowohl in der HFD- als auch in der KD-Gruppe für eine verringerte mRNA-Expression der pro-inflammatorischen Zytokine *il-1β* und *il-6* verantwortlich zu sein.

6.5 Studie 5

Als Modell für Amyloid-induzierte Neuroinflammation wurde in der vorliegenden Studie [83] das transgene AD-Modell der APPswe/PS1dE9-Maus genutzt und evaluiert, inwieweit eine Ernährungsintervention am Beispiel der Kalorienrestriktion (KR) zu einer Milderung des AD-Phänotyps, insbesondere der Neuroinflammation, führt. Es ist allgemein anerkannt, dass KR die Neuropathologie in AD-Modellen durch bisher unbekannte Mechanismen abschwächt. Ein vielversprechender Prozess, der durch KR ausgelöst wird, ist Autophagie, von der bekannt ist, dass sie aggregierte Proteine abbaut. Darüber hinaus kann Autophagie die Glukoseaufnahme beeinflussen und somit den zerebralen Hypometabolismus bei AD mildern. Um diese Hypothese zu überprüfen, wurden tg-Mäuse und ihre wt-Geschwistertiere entweder 16 oder 68 Wochen lang einer KR unterzogen. Während eine kurzzeitige KR über 16 Wochen keine deutlichen Veränderungen des AD-Phänotyps bei tg-Mäusen ergab, zeigte eine langfristige KR über 68 Wochen positive Auswirkungen auf die Pathophysiologie. So waren der zerebrale Glukosestoffwechsel und die neuronale Integrität nach 68 Wochen KR bei tg-Mäusen deutlich verbessert, was im Vergleich zu *ad libitum* (AL) gefütterten tg-Mäusen durch eine erhöhte [^{18}F]FDG-Aufnahme im Kortex ($p = 0,0161$) und Hippocampus ($p = 0,0035$) deutlich wurde. Als weiterer Parameter des zerebralen Metabolismus zeigte sich ein erhöhtes Verhältnis aus N-Acetylaspartat zu Kreatin im Gesamtgehirn ($p = 0.0272$) unter Verwendung von PET-Bildgebung und Magnetresonanz-Spektroskopie (MRS). Zusätzlich konnte durch die 68-wöchige KR eine Verbesserung der kognitiven Leistungsfähigkeit gezeigt werden. Im MWM zeigten tg-Mäuse, die KR erhielten, signifikant häufigere N-Quadrant- ($p = 0,0018$) und Plattformkreuzungen ($p = 0,0161$) sowie eine geringere Latenzzeit zur ersten Plattformkreuzung ($p = 0,0069$) im Vergleich zu AL gefütterten tg-Mäusen und unterschieden sich somit nicht mehr von den wt-Kontrollen (mit und ohne KR) (Abbildung 6 A und B).

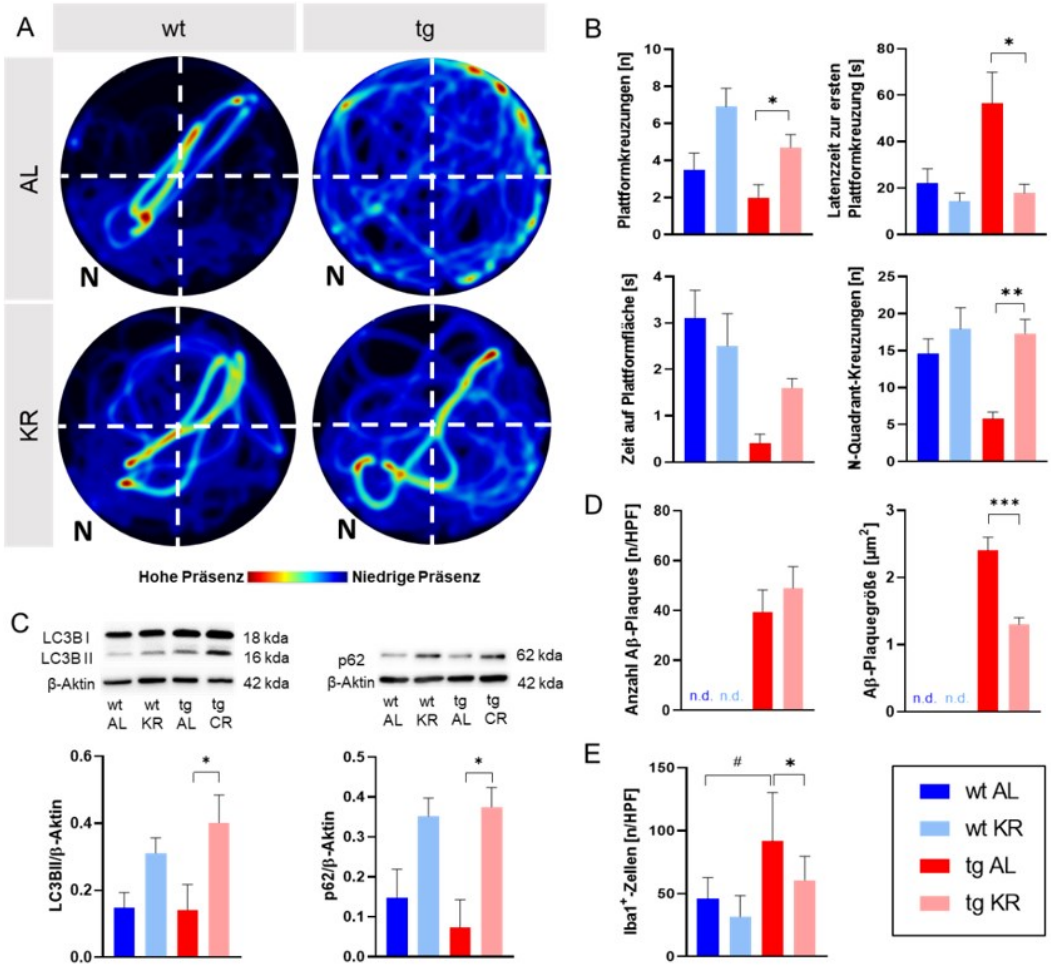

*Abbildung 6: Übersicht über die Auswirkung einer 68-wöchigen Kalorienrestriktion (KR) im Modell der APPswe/PS1dE9-Maus (tg) im Vergleich zu den Wildtyp (wt) -Geschwistertieren und ad libitum (AL) -Fütterung. A) Repräsentative Heatmaps der Bewegungsmuster der Mäuse im Morris Water Maze (MWM). Der N-Quadrant, der die Plattform beinhaltete, befand sich jeweils im unteren linken Quadranten. B) Auswertung des MWM nach Anzahl der Plattformkreuzungen [n], Latenzzeit zur ersten Plattformkreuzung [s], Zeit auf der Plattformfläche [s] und N-Quadrat-Kreuzungen [n]. Werte dargestellt als Mittelwert±Standardfehler. Signifikanz der Unterschiede zwischen den Gruppen (wt AL n = 11; wt KR n = 17; tg AL n = 4; tg KR n = 6) wurde mittels ungepaartem t-Test und anschließender Bonferroni-Korrektur geprüft, * p < 0,05, ** p < 0,005. C) Repräsentative Western-Blots für die densitometrische Analyse der Proteinexpression der Autophagie-assoziierten Proteine LC3BII und p62 im Gehirn (wt AL n = 10; wt KR n = 11; tg AL n = 7; tg KR n = 8). Die Signale wurden auf die von β-Aktin korrigiert. Werte dargestellt als Mittelwert±Standardfehler. Signifikanz der Unterschiede zwischen den Gruppen (wt AL n = 11; wt KR n = 10; tg AL n = 4; tg KR n = 6) wurde mittels einfacher ANOVA nach Rängen (Kruskal-Wallis) und anschließendem Dunns Post-hoc-Test geprüft, * p < 0,05. D) Quantifizierung der Anzahl (pro Gesichtsfeld) und Größe der Amyloid β (Aβ)-Plaques im Hippocampus. Werte dargestellt als Mittelwert±Standardfehler. Signifikanz der Unterschiede zwischen den Gruppen (wt AL n = 11; wt KR n = 10; tg AL n = 12; tg KR n = 8) wurde mittels ungepaartem t-Test und anschließender Bonferroni-Korrektur geprüft, n. d.= nicht detektiert, *** p < 0,0001. E) Quantifizierung der Anzahl der Iba1-positiven Zellen (pro Gesichtsfeld) im Hippocampus. Werte dargestellt als Mittelwert±Standardfehler. Signifikanz der Unterschiede zwischen den Gruppen (wt AL n = 11; wt KR n = 10; tg AL n = 12; tg KR n = 8) wurde mittels einfacher ANOVA und anschließendem Sidak Post-hoc-Test geprüft, * p < 0,05 vs. AL, # p < 0,05 vs. wt.*

Um eine Erklärung für den positiven Effekt der KR auf den AD-Phänotyp zu finden, wurden Autophagie-Mechanismen untersucht (Abbildung 6 C). Hier führte die 68-wöchige KR zu einem signifikanten Anstieg der LC3BII- ($p = 0,0392$) und p62-Proteinexpression ($p = 0,0176$), was auf eine Induktion der Autophagie hinweist. Dies zeigte sich bei den tg-Mäusen mit KR durch einen signifikanten Rückgang der Aβ-Plaques im Kortex ($p < 0,0001$) sowie einer Reduktion der Größe der Aβ-Plaques im Hippocampus ($p < 0,0001$, Abbildung 6 D) im Vergleich mit den Werten der tg-Mäuse mit AL-Fütterung. Begleitet wurde dies durch eine Verminderung der Neuroinflammation, gemessen an der verringerten Mikrogliose, die durch

eine signifikant verringerte Anzahl von Iba1$^+$-Zellen im Hippocampus ($p = 0,0329$, Abbildung 6 E), nicht jedoch im Kortex ($p = 0,5096$) angezeigt wurde.

Zusammenfassend lässt sich sagen, dass eine langfristige KR eine allgemeine neuroprotektive Wirkung bei tg-Mäusen entfaltet. Dies wurde durch eine Besserung des Glukosestoffwechsels im ZNS und eine verbesserte kognitive Leistung im MWM gezeigt. Außerdem zeigt diese Studie zum ersten Mal, dass eine KR-induzierte Autophagie als Mechanismus der Hirn-Clearance in tg-Mäusen mit der beobachteten Abschwächung der Aβ-Pathologie und Neuroinflammation einhergeht.

6.6 Studie 6

Neben dem Befund aus Studie 5 zur Aktivierung der organständigen Hirn-Clearance mittels Autophagie-Induktion wurde im selben tg-Modell die Hirn-Clearance-Kapazität, im speziellen von den Mechanismen, welche zu einem Abtransport von Aβ aus dem Gehirn beitragen, untersucht. Dazu wurde ein neuer longitudinaler *In-vivo*-Ansatz mittels GBCA-MRT-Bildgebung etabliert, der sowohl die ventrikuläre Hirn-Clearance-Kapazität in T2-gewichteten MRT-Aufnahmen (Abbildung 7 A) als auch die parenchymale/glymphatische Hirn-Clearance Kapazität in T1-gewichteten MRT-Aufnahmen (Abbildung 7 E) untersucht. Als Zielregion wurde zur Evaluation der parenchymalen Hirn-Clearance der Hippocampus ausgewählt, da dieser in der zuvor präsentierten Studie 5 stärker von der zellulären Clearance über Autophagie profitierte als z. B. der Kortex [83].
Zur Auswertung der ventrikulären Clearance wurden Intensitäts-Zeit-Kurven erstellt (beispielhafte Darstellung der gemittelten Werte aller Ventrikel im Alter von sechs, neun und zwölf Monaten in Abbildung 7 B). Da die reinen Signalintensitäts-Änderungen technischen Schwankungen unterliegen könnten, wurden aus den vorliegenden Kurven der Anstieg der Signalintensität nach der GBCA-Injektion und der anschließende Abfall des Signals während der Auswaschphase mit einer Modellfunktion beschrieben, aus der sich Konstanten für die Anflutungs- (Abbildung 7 C) und die Auswaschphase unabhängig von den Intensitätswerten ergeben (Abbildung 7 D). Lediglich in der Anflutungsphase im vierten Ventrikel konnte durch einfache ANOVA mit wiederholten Messungen ein Alterseffekt gezeigt werden ($p = 0,0420, F_{(1,951.29,26)} = 3,570$), Post-hoc-Vergleiche ergaben jedoch keine signifikanten Unterschiede zwischen tg-Mäusen und wt-Mäusen der verschiedenen Altersgruppen. Weitere Analysen der Konstanten ergaben weder im dritten, vierten noch in den beiden lateralen Ventrikeln weitere Effekte.
Zur Auswertung der parenchymalen Hirn-Clearance-Kapazität im Hippocampus wurde ähnlich vorgegangen. Auch hierfür wurden zunächst Intensitäts-Zeit-Kurven erstellt (Abbildung 7 F), aus denen Konstanten für das Ausmaß der Anflutungs- (Abbildung 7 G) und der Auswaschphase (Abbildung 7 H) des GBCA ermittelt wurden. Hier ergab sich für die Anflutungskonstante ein statistisch signifikanter Alterseffekt ($p = 0,0156, F_{(1,8)} = 9,370$), der auf ein vermehrtes Anfluten im Alter von zwölf Monaten hindeutet. Dieser Alterseffekt ergab in der Gruppe der tg-Mäuse einen signifikanten Unterschied zwischen neun und zwölf Monaten ($p = 0,0251$) nicht jedoch bei den wt-Mäusen ($p = 0,4973$). Für die Abflutungskonstante konnte kein solcher Effekt beschrieben werden, allerdings zeichnete sich ein tendentieller Effekt des Genotyps ($p = 0,0825, F_{(1,8)} = 3,939$) ab.

Zusammenfassend muss betont werden, dass die hier dargestellten Ergebnisse der Studie 6 aktuell noch weiterer Auswertung und Revision in enger Zusammenarbeit mit der kooperierenden Arbeitsgruppe von Prof. Radbruch und Dr. Deike-Hofmann (DZNE Bonn) unterliegen. Die vorläufige Ergebnisinterpretation lässt vermuten, dass die hier vorgestellte Methodik bislang nur in Bezug auf die Anflutungskonstanten (im vierten Ventrikel und Hippocampus) einen Alterseffekt aufdecken konnte. Die Abbildung der Hirn-Clearance-Kapazität durch die Auswaschungskonstante konnte hingegen keine statistisch signifikanten Unterschiede zeigen. Möglicherweise ist die erwartete Effektstärke des Alters und Genotyps auf die Hirn-Clearance kleiner als erwartet und die gewählte Tieranzahl auch aufgrund hoher interindividueller Variabilität zu niedrig, um die Unterschiede abbilden zu können.

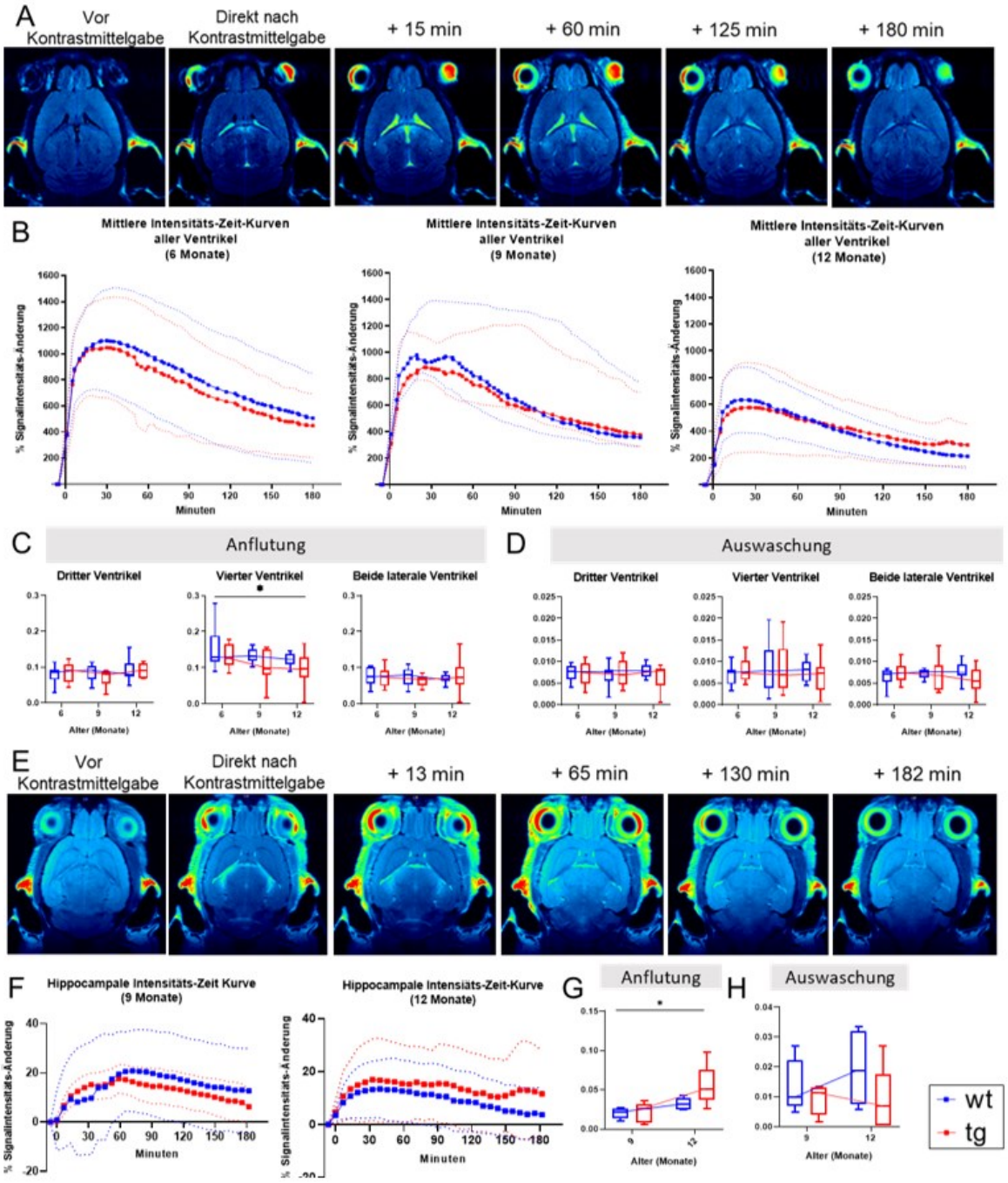

*Abbildung 7: Übersicht der Messergebnisse der Gadoliniumkontrastmittel-basierten (GBCA) Bildgebung zur Einschätzung der Hirn-Clearance-Kapazität. A) Repräsentative T2-gewichtete MRT-Aufnahmen unmittelbar vor und zu ausgewählten Messzeitpunkten nach Verabreichung des GBCA. B) Gemittelte Intensitäts-Zeit-Kurven aller Ventrikel von transgenen APPswe/PS1dE9 (tg) -Mäusen (rot, n = 9) und den zugehörigen Wildtyp (wt) -Geschwistertieren (blau, n = 9) im Alter von sechs, neun und zwölf Monaten, Werte dargestellt als Mittelwert±Standardabweichung (fein gepunktete Linien). C) Konstanten der Anflutungs- und D) der Auswaschphase (einheitenlos) im dritten, vierten und in beiden lateralen Ventrikeln, dargestellt als Median mit 10.-90. Perzentile. Signifikanz der Unterschiede zwischen den Gruppen wurde mittels zweifacher ANOVA mit wiederholten Messungen und anschließendem Sidak Post-hoc-Test geprüft, * Alterseffekt $p < 0,05$. E) Repräsentative T1-gewichtete MRT-Aufnahmen unmittelbar vor und zu ausgewählten Messzeitpunkten nach Verabreichung des GBCA. F) Gemittelte Intensitäts-Zeit-Kurven im Hippocampus von tg-Mäusen (rot, n = 5) und den zugehörigen wt-Geschwistertieren (blau, n = 5) im Alter von neun und zwölf Monaten, Werte dargestellt als Mittelwert±Standardabweichung (fein gepunktete Linien). G) Konstanten der Anflutungs- und H) der Auswaschphase (einheitenlos) im Hippocampus dargestellt als Median mit 10.-90. Perzentile. Signifikanz der Unterschiede zwischen den Gruppen wurde mittels zweifacher ANOVA mit wiederholten Messungen und anschließendem Sidak Post-hoc-Test geprüft * Alterseffekt $p < 0,05$.*

7. Diskussion

In der vorliegenden Arbeit wurde in drei verschiedenen Mausmodellen das Zusammenspiel von Ernährung, Neuroinflammation und Amyloidpathologie untersucht. Insbesondere wurde gezeigt, wie die Ernährung als modulierbarer Faktor sowohl bei Adipositas als auch bei AD die Pathophysiologie beeinflussen kann. Hier zeigte sich, dass bei einer Ernährung mit übermäßiger Kalorienzufuhr ein adipöser Phänotyp entsteht, bei dem es organständig sowohl in der Leber als auch im ZNS zur Aktivierung eines pro-inflammatorischen Zytokinprofils kommt. Außerdem konnte gezeigt werden, dass Adipositas das Verhalten beeinflussen und insbesondere ängstliches Verhalten begünstigen kann. Darüber hinaus wurde die Modulation der Ernährung als therapeutischer Ansatz genutzt. Ein Diätwechsel sowie IF konnte (allein und in Verbindung mit körperlicher Aktivität bei LBT) die mRNA-Expression pro-inflamatorischer Zytokine senken. Im Kontext der AD führte KR als Ernährungsmodulation zusätzlich zu einer Abmilderung der Neuroinflammation und Aβ-Pathologie auf Basis der Induktion von Autophagie als zellulärer Mechanismus der Hirn-Clearance. Die Analyse der parenchymalen Hirn-Clearance konnte einen Interaktionseffekt aus Alter und Genotyp zeigen. Eine Störung der ventrikulären Hirn-Clearance konnte im genutzten AD-Modell mit der neu vorgestellten Methodik hingegen nicht gezeigt werden.

Im Modell der DIO mittels HFD-Fütterung konnte in den beschriebenen Studien 1 und 2 in weiblichen Mäusen gezeigt werden, dass, obwohl es im Vergleich zur KD keine signifikanten Unterschiede in entzündlichen Infiltration der Granulozyten und Makrophagen in der Leber bzw. der Mikroglia und Astroglia im Gehirn zu geben scheint, die DIO dennoch die mRNA-Expressionssteigerung pro-inflammatorischer Zytokine bewirken kann. Damit konnte die Hypothese, dass Fehlernährung im Rahmen einer langzeitigen, fettreichen Diät zu einer persistierenden niedrigschwelligen systemischen Inflammation führt, die sich als organständige Entzündungsreaktion in der Leber (Studie 1) sowie Neuroinflammation (Studie 2) manifestiert, im Hinblick auf eine Expressionssteigerung pro-inflammatorischer Mediatoren bestätigt werden.
Hier zeigte sich für die Leber insbesondere eine erhöhte mRNA-Expression von *tnf-α* als Zeichen einer niedrigschwelligen organständigen Inflammation. Eine erhöhte gewebsständige mRNA-Expression von *tnf-α* in der Leber infolge einer HFD wurde bereits von anderen Arbeitsgruppen beschrieben. So fanden Tanaka et al. bereits nach 16- bis 18-wöchiger HFD eine erhöhte hepatische Expression von *tnf-α* [84]. Demgegenüber konnte die Arbeitsgruppe von van der Heijden et al. diese erhöhte hepatische Expression von *tnf-α* erst nach 40-wöchiger HFD-Fütterung zeigen [85].
Um die generelle Ausprägung einer DIO mit Fokus auf pro-inflammatorische Prozesse in der Leber in Studie 1 zu bewerten, wurden zunächst das Körper- und Lebergewicht der Tiere bestimmt. Als Hauptursache für die erhöhten Körper- und Lebergewichte in der HFD-Gruppe wurde eine diätbedingte Fettakkumulation in der Leber identifiziert. Mäuse der HFD-Gruppe wiesen einen signifikant erhöhten Leberfettgehalt von mehr als 10 % auf, während die beiden Kontrollgruppen einen normalen Leberfettgehalt gesunder Mäuse von 5-8 % [86, 87] aufzeigten. Im Gegensatz zu diesem Befund zeigte der durchgeführte Cholesterol-Assay einen signifikant erhöhten hepatischen Cholesterolgehalt in der KD-Gruppe. Cholesterol kann ein lipotoxisches Wirkprofil haben, welches hauptsächlich durch die Induktion von oxidativem Stress vermittelt wird, was wiederum zur Induktion pro-inflammatorischer Signalwege führen kann [88]. Dies bietet eine mögliche Erklärung für die makroskopisch beobachteten pathologischen Veränderungen in den Lebern der KD-Gruppe, verglichen mit den Lebern der SD-Gruppe. Dennoch ist hervorzuheben, dass nach Herstellerangaben der HFD die von unserer Arbeitsgruppe genutzte KD empfohlen wird [89]. Hier wird seitens des Futtermittelherstellers insbesondere auf die Unterschiede zwischen aufgereinigtem Futter (HFD und KD) und „normalem“ Futter (SD) hingewiesen, bei denen es in der Art und Menge der Ballaststoffe, der Kohlenhydratquelle und dem Vorhandensein oder Fehlen von Phytoöstrogenen zu nicht unerheblichen Unterschieden kommen kann, die als Variablen die Ergebnisinterpretation erschweren [89]. Aus diesem Grund wurde auf die in Studie 1 zusätzlich

genutzte SD-Gruppe für alle weiteren präsentierten Studien zur DIO verzichtet und ausschließlich KD als Kontrollgruppe beibehalten.

In Studie 2 wurde analog zu Studie 1 ein DIO-Phänotyp etabliert und durch Messungen des Körpergewichts bestätigt. Zusätzlich konnten *in vivo* durch Plasmaanalyse erhöhte Triglycerid- und Leptinwerte als Marker für eine DIO in der HFD-Gruppe gemessen werden. In dieser Studie lag der Fokus auf der PET-Bildgebung, um die Auswirkungen der DIO auf den Glukosestoffwechsel ([^{18}F]FDG) bzw. auf Entzündungsprozesse im Gehirn ([^{18}F]GE-180) *in vivo* zu evaluieren. Dabei stellt diese Methodik ein Refinement im Sinne der 3R des Tierschutzes dar [90, 91] und sorgt zusätzlich möglicherweise auch für ein erhöhtes Translationspotenzial, da sowohl [^{18}F]FDG, wie in der Übersichtsarbeit von Minoshima et al. [92] dargestellt, als auch [^{18}F]GE-180 [93] bereits Anwendung in der Klinik finden.
Durch *In-vivo*-[^{18}F]FDG-PET-Bildgebung konnte ein zerebraler Glukose-Hypermetabolismus bei den weiblichen HFD-Mäusen im Vergleich zur KD-Gruppe gemessen werden. Dieser pathologische Zustand wurde bereits für männliche Mäuse beschrieben, die HFD erhielten [94], sowie für männliche und weibliche Patienten mit krankhafter Adipositas [95]. Als mögliche Verbindung zwischen Ernährung und AD konnte ein solcher Glukose-Hypermetabolismus insbesondere im Hippocampus auch bereits bei leichten kognitiven Beeinträchtigungen (engl. Mild Cognitive Impairment, MCI) als Vorstufe der AD gezeigt werden [96].
Bei der *In-vivo*-Untersuchung der Neuroinflammation mittels [^{18}F]GE-180 deuten die Ergebnisse auf eine tendenziell erhöhte zerebrale Aufnahme von [^{18}F]GE-180 in der HFD-Gruppe im Vergleich zur KD-Gruppe hin, die jedoch keine statistische Signifikanz erreichte. Im Allgemeinen sind große Unterschiede im Körpergewicht ein Hindernis für die korrekte Analyse der [^{18}F]GE-180-Aufnahme. Da keine relevante [^{18}F]GE-180-Aufnahme in das Fettgewebe festgestellt werden konnten, wurden die Messergebnisse in der Einheit %ID/ml angegeben. Dies steht ebenfalls im Einklang zur vorhergehenden Arbeit von Barron et al. in Mäusen mit zwölfwöchiger HFD, die über eine gute Übereinstimmung zwischen *In-vivo*-TSPO-Signalen in %ID/ml und TSPO-Immunoreaktivität berichteten [97], jedoch auch zeigen konnten, dass Adipositas allein [^{18}F]GE-180-Signale und TSPO-Immunoreaktivität nicht erhöht [97]. Um die Ergebnisse der [^{18}F]GE-180-PET-Bildgebung bei Mäusen nach 24-wöchiger HFD weiter aufzuklären, wurden die Gehirne *post mortem* mit molekularbiologischen und immunhistochemischen Methoden weiter analysiert. Als Hauptbefund einer humoralen Immunreaktion konnten in der HFD-Gruppe erhöhte mRNA-Expressionswerte von *il-1β* gemessen werden. Die mRNA-Expression von pro-inflammatorischem *il-1β* wird in der Literatur als Schlüsselmerkmal des metabolisch aktivierten Phänotyps von Makrophagen beschrieben [98] und gilt als Schlüsselmediator bei Neuroinflammation [99, 100]. Daher könnte die erhöhte mRNA-Expression von *il-1β* in dem vorliegenden Experiment ein Indikator für einen chronischen, metabolisch-aktivierten Zustand der Mikroglia sein, der sich aus langfristiger HFD ergibt. Hinsichtlich der relativen mRNA-Expression von *tspo* im gesamten Gehirn sowie TSPO-positiver Zellen in immunhistochemischen Analysen der drei Hauptzielregionen (Kortex, Hippocampus und Hypothalamus) konnte in Einklang mit der Arbeit von Barron et al. [97] kein signifikanter Unterschied zwischen der HFD- und der KD-Gruppe gezeigt werden.
An dieser Stelle unterscheiden sich die hier gezeigten Ergebnisse in weiblichen Mäusen mit 24-wöchiger HFD stark von den bisher zumeist an männlichen Mäusen gewonnenen und veröffentlichten Ergebnissen. So konnte bereits gezeigt werden, dass die gleiche HFD, die auch in der hier vorgestellten Studie verwendet wurde, bereits nach kurzfristiger HFD-Verabreichung für einige Tage zu einer akuten Neuroinflammation führt [101]. Bei den wenigen Studien mit weiblichen Mäusen wird in der Literatur ebenfalls ein pro-inflammatorischer Phänotyp nach kurzzeitiger (12-wöchiger) HFD mit ca. 60 % Fettgehalt beschrieben, dieser liegt jedoch in einer wesentlich schwächeren Ausprägung als bei männlichen Mäusen vor [102]. Die Verwendung weiblicher Mäuse war jedoch im vorliegenden Versuchsansatz insofern notwendig, da für den genutzten Verhaltenstest mögliche Verhaltensänderungen durch Probleme im Sozialverhalten männlicher Mäuse ausgeschlossen werden sollten. Eine

intensivere Betrachtung geschlechtsspezifischer Unterschiede bei Verhaltenstests findet sich in der Diskussion zu Studie 3 in diesem Kapitel.
Auch im experimentellen Ablauf gibt es insbesondere hinsichtlich der Dauer und Zusammensetzung der HFD erhebliche Unterschiede. Die Dauer der HFD-Gabe zur Untersuchung der Neuroinflammation bei Mäusen reicht von einigen Tagen [101, 103, 104] bis zu mehreren Wochen [101, 105, 106] oder wenigen Monaten [97, 101, 106]. Daten zur langzeitigen HFD-Fütterung (sechs Monate und mehr), die eine validere Darstellung der langen pathologischen Spanne bei menschlicher Adipositas und deren Komorbiditäten ermöglichen, sind mit Ausnahme dieser Studie bisher nicht verfügbar. Hinsichtlich der Einordnung und des Vergleichs der eigenen Ergebnisse mit anderen Publikationen ist auch zu beachten, dass der Begriff HFD in der Literatur uneinheitlich verwendet wird. So beschreiben einige Studien HFD mit ca. 20 % Fettgehalt [107], während andere den Begriff HFD für Futter mit rund 50 % [63, 108] oder 60 % Fett [101, 104, 105] verwenden.

Da die Etablierung einer DIO in diesem HFD-Modell sehr langwierig ist und in der präsentierten Studie 2 kein Einfluss auf die Kognition festgestellt werden konnte, wurden die Auswirkungen von Adipositas auf das Verhalten im genetischen Modell der ob/ob-Maus untersucht. Die Adipositas in diesem Modell beruht auch auf einer erhöhten Kalorienzufuhr, die sich jedoch auf einer Hyperphagie durch ein fehlendes Sättigungsgefühl begründet [109]. Das ob/ob-Modell entwickelt schnell einen adipösen Phänotyp [110, 111] und zeigt charakteristische Verhaltensänderungen [112], die unter anderem auch durch pro-inflammatorische Stimuli ausgelöst werden können [113]. Die ob/ob-Mäuse können Adipositas-bedingte Verhaltensänderungen modellieren und besitzen daher Relevanz für die Verhaltensforschung, um weitere Forschungsfragen zum Einfluss von Adipositas auf die psychischen Gesundheit zu beantworten [114, 115].
In der vorliegenden Arbeit wurde die Hypothese überprüft, ob Adipositas (ausgelöst durch eine Leptin-Defizienz) generell zu Verhaltensänderungen führt. Dazu wurden zwei gängige Verhaltenstest genutzt. Der OF-Test dient dazu, die generelle Bewegungsaktivität und das explorative Verhalten zu untersuchen, welche z. B. durch den Stimmungszustand und im speziellen durch Angst-assoziierte Veränderungen beeinflusst werden können [116]. Das EPM wird im Spezielleren zur Abschätzung von ängstlichen Verhaltensweisen genutzt, jedoch können auch weitere ethologische Parameter wie das Aufrichten, Strecken nach vorn oder Lehnen nach unten abgelesen werden, um eine Einschätzung zum explorativen Verhalten zu ermöglichen [117]. Im Einklang mit mehreren anderen Studien konnte ein reduziertes Bewegungsmuster in ob/ob-Mäusen gezeigt werden [118, 119]. Zusätzlich konnte in Übereinstimmung mit anderen Arbeiten eine Reduktion des explorativen Verhaltens beobachtet werden, was häufig als ängstliches Verhalten interpretiert wird [120, 121].
Die Ergebnisse der vorliegenden Studie weisen zudem darauf hin, dass hinsichtlich Adipositas-bedingter ängstlicher Verhaltensänderung das Geschlecht der Mäuse keine Rolle zu spielen scheint. Ähnliche Ergebnisse zur geschlechtsunabhängigen Verhaltensänderung sind bereits in der Literatur zu finden [122]. Dennoch wurde in der Verhaltensforschung mit Nagetieren althergebracht häufig nur ein Geschlecht für Verhaltenstests verwendet. Hier wurde sich etwa sechsmal häufiger auf rein männliche Versuchsgruppen bezogen, um z. B. einen möglichen Einfluss des hormonellen Zyklus ausschließen zu können [123]. In anderen Versuchsanordnungen wird hingegen auf Verwendung von rein weiblichen Gruppen zurückgegriffen, da männliche Mäuse ein ausgeprägtes Territorialverhalten zeigen [124]. In der Labortierhaltung werden männliche Mäuse in der Regel in eingeschlechtlichen Gruppen oder einzeln untergebracht. Bei beiden Ansätzen kann es jedoch zu Problemen kommen, z. B. zu einem Mangel an sozialen Kontakten bei Einzelhaltung oder zu aggressiven Veränderungen des Verhaltens zwischen Männchen bei Gruppenhaltung [125]. Wie in der Übersichtsarbeit von Shansky diskutiert, gilt daher ein monosexueller Versuchsansatz seit wenigen Jahren als überholt [126]. Die hier gezeigte Geschlechtsunabhängigkeit im OF und EPM kann in künftigen Studien Beachtung finden und durch den Einschluss beider Geschlechter die benötigte Tieranzahl reduzieren und somit zur Reduktion im Rahmen der 3R des Tierschutzes beitragen [127].

Bemerkenswert ist außerdem, dass es im experimentellen Ansatz der präsentierten Studie 3 bereits nach sehr kurzer Zeit (acht Wochen) zu hochsignifikanten Änderungen dieser Verhaltensparameter bei ob/ob-Mäusen im Vergleich zu ihren wt-Geschwistertieren kam und daher das Alter (trotz eines statistisch signifikanten Alterseffektes) nur eine untergeordnete Rolle im Hinblick auf die Verhaltensänderung einzunehmen scheint. Aufgrund der hier beschriebenen Veränderungen, die sich bereits im sehr jungen Alter von acht Wochen geschlechtsunabhängig zeigen, wäre es möglich und denkbar, einige der anderen präsentierten Studien auf dieses Modell zu übertragen. Dies wäre insbesondere für die im nachfolgenden Absatz näher diskutierte Studie 4 interessant, da die Durchführung im DIO-Modell sehr langwierig war (12 Monate) und zunächst nur Ergebnisse für ein Geschlecht (weibliche Mäuse) generiert wurden.

In Studie 4 wurde im Rahmen einer Interventionsstudie untersucht, ob sich die genutzten Interventionen als therapeutischer Ansatz eignen, um die persistierende niedrigschwellige Inflammation in der Peripherie und dem ZNS abzumildern. Hierbei wurden als Interventionen ein Diätwechsel auf KD oder Nahrungsaufnahmeregulation durch IF, allein oder in Kombination im Modell eingeführt. Diese sind besonders hervorzuheben, da sie auch klinische Anwendung in der Therapie von Adipositas und davon abgeleiteten Erkrankungen wie z. B. nicht-alkoholische Fettlebererkrankung finden [128–130]. Neben der Ernährungsumstellung ist körperliche Aktivität eine weitere Erfolg versprechende Intervention zur Gewichtsreduktion [131] und wurde deshalb auch allein oder in Kombination mit KD und IF in der vorliegenden Studie 4 durchgeführt. Hier konnte jedoch unabhängig von KD oder HFD kein zusätzlicher Nutzen durch Laufbandtraining erzielt werden. Dies wurde auch in der Arbeit von Ringseis et al. beschrieben [132] und ist möglicherweise auf die Häufigkeit des LBT zurückzuführen, da tägliches Training für eine Reduktion des Körpergewichts empfohlen wird [129], dies war so im präsentierten experimentellen Ansatz allerdings nicht durchführbar.
Wie bereits in Studie 1 und 2 dargelegt wurde, hatte die HFD im verwendeten Mausmodell keinen Einfluss auf die Induktion einer zellulären Immunantwort. Somit war zu erwarten, dass auch durch die Interventionen dieser Arbeit keinerlei Unterschiede zwischen den Gruppen auftreten. Allerdings zeigte sich auch in diesem experimentellen Ansatz die Induktion einer pro-inflammatorischen humoralen Immunantwort, ausgelöst durch HFD. Im Rahmen der vorliegenden Studie konnte eine direkte Korrelation zwischen erhöhter mRNA-Expression von *tnf-α* und erhöhtem Körpergewicht als wichtigstes Merkmal von Adipositas gezeigt werden. Dabei ist TNF-α bereits seit Längerem als wichtiger und zwischen den Spezies hochkonservierter Mediator entzündlicher Reaktionen bei Adipositas bekannt [4]. In Studien konnte außerdem belegt werden, dass TNF-α im ob/ob-Modell der Adipositas eine relevante Rolle bei der Vermittlung Adipositas-induzierter inflammatorischer Prozesse einnimmt [133].
Erste präliminäre Daten zum Einfluss der Interventionen auf die zerebrale mRNA-Expression von Zytokinen konnten zeigen, dass die Kombination aus IF+LBT sowohl in der HFD- als auch der KD-Gruppe für eine verringerte mRNA-Expression der pro-inflammatorischen Zytokine *il-1β* und *il-6* verantwortlich zu sein scheint. Die Relevanz von IL-1β als pro-inflammatorisches Zytokin im ZNS ist bereits in der Literatur beschrieben worden [99, 100] und konnte auch in Studie 2 gezeigt werden. IL-6 hingegen ist vor allem im Zusammenhang mit Neurodegeneration beschrieben worden und scheint insbesondere auch bei demenziellen Erkrankungen wie AD verändert zu sein [134]. Ob und inwieweit die gezeigten veränderten Zytokin-Expressionsmuster mit AD-Merkmalen wie der Amyloidpathologie (z. B. Aβ-Plaquegröße) einhergehen, wäre künftig noch eine interessante Ergänzung zur weiteren Analyse und Einordnung der vorliegenden Ergebnisse in den genutzten Adipositasmodellen.

Neben den beiden beschriebenen Adipositas-Modellen für Neuroinflammation ist ein weiteres Modell, was diese Pathologie abbildet, das verwendete tg-Mausmodell des AD-Phänotyps. Dieses ist zusätzlich ein Modell für zerebrale Amyloidose und wird daher häufig in der Erforschung der AD genutzt. Mechanistisch wird davon ausgegangen, dass Aβ die Neuroinflammation auslöst [135]. Im beschriebenen experimentellen Ansatz wurde in diesem Modell untersucht, inwieweit sich eine KR als Ernährungsintervention auf die Progression der

nachgebildeten AD-Pathophysiologie auswirken kann. Das Hauptresultat der beschriebenen Studie 5 war, dass KR die kognitive Funktion durch eine messbare Steigerung der Glukoseaufnahme verbesserte, was auf eine KR-induzierte Steigerung der neuronalen Aktivität hinweist. Dies ging mit einer verringerten Aβ-Ablagerung und einer damit verbundenen verringerten Neuroinflammation (repräsentiert durch Mikroglia-Aktivierung) einher. Insgesamt wird aufgrund der Ergebnisse die Vermutung angestellt, dass der neuroprotektive Effekt der KR auf die Aktivierung von Autophagie als zellulärer Hirn-Clearance-Mechanismus zurückzuführen sein könnte.
Bei der Auswertung der Auswirkung der KR auf den Glukosestoffwechsel mittels [^{18}F]FDG-Bildgebung war im Gegensatz zu Studie 2 nicht mit einer Signalbeeinflussung durch unterschiedliche Fett- und Körpermasse der Mäuse in den jeweiligen Gruppen zu rechnen, so dass analog zu [^{18}F]GE-180 die Ergebnisdarstellung als %ID gewählt wurde. Im Kontrast zum dargestellten pathologischen Glukosehypermetabolismus in Studie 2 ist beim Genotyp und Alter der Mäuse in Studie 5 mit Veränderungen des Glukosestoffwechsels, wie er beim Altern generell und typischerweise in fortgeschrittenen Stadien von AD vorkommt (zusammengefasst von Raut et al. [136]), zu rechnen. Ausgehend von der Grundannahme, dass sich also in allen Versuchsgruppen ein verminderter Glukosestoffwechsel manifestiert hat, deutet das signifikant erhöhte [^{18}F]FDG-Signal in der tg-Gruppe mit KR also auf eine Normalisierung des Glukosestoffwechsels hin. Wieso dieser positive Effekt der KR in der wt-Gruppe nur tendenziell eine Verbesserung des Glukosemetabolismus zeigte, konnte im Rahmen dieser Versuchsreihe jedoch nicht abschließend geklärt werden.
Die KR-vermittelte Abmilderung der Aβ-Neuropathologie in AD-Mausstudien wurde bereits in der Literatur beschrieben. So berichteten z. B. Mouton et al. [137], dass KR das Volumen von Aβ-Plaques bei tg-Mäusen um etwa ein Drittel reduzierte. Außerdem zeigten Patel et al. [138], dass neben der verminderten Anzahl von Aβ-Plaques und Aβ-Plaquegröße auch die immunreaktive Fläche um die Aβ-Plaques im Anschluss an KR im $APP_{swe/ind}$-Mausmodell der AD deutlich reduziert war. Dies zeigte sich in ihren Ergebnissen in einer verringerten Anzahl von Astrozyten ($GFAP^+$-Zellen) [138]. In ähnlicher Weise zeigt die hier präsentierte Studie 5, dass die Anzahl von Aβ-Plaques und die Aβ-Plaquegröße sowie die Anzahl der aktivierten Mikroglia ($Iba1^+$-Zellen) bei tg-Mäusen mit KR deutlich reduziert waren. Dies konnte jedoch erst nach 68 Wochen KR beobachtet werden. Im Gegensatz dazu zeigte eine kurzzeitige 16-wöchige KR keinen Einfluss auf die Aβ-Pathologie, obwohl die Studie von Patel et al. [138] bereits einen anti-amyloidogenen Effekt nach 14 Wochen KR zeigte. Im Gegensatz dazu wurden in weiteren Publikationen im 3xTg AD-Modell von Halagappa et al. auch längere KRs von >20 und >50 Wochen untersucht [139]. Hierbei konnte gezeigt werden, dass nur eine 14-monatige KR die Aβ-Pathologie reduzierte und die kognitive Leistung, analysiert mit MWM, verbessern konnte [139]. Dies deckt sich mit den Ergebnissen der eigenen Studie, in der nur eine langfristige KR das Arbeitsgedächtnis von tg-Mäusen normalisierte. Die Frage, ob die bessere kognitive Leistung durch die KR-induzierte Reduktion des Untergangs von Neuronen vermittelt wird, wurde in der Literatur bereits aufgegriffen. Dong et al. [140] berichteten, dass durch KR eine signifikant höhere Zelldichte in der der CA3-Region des Hippocampus gegenüber hochkalorischen Diäten gemessen werden konnte. Auch in Patienten konnte bereits gezeigt werden, dass eine KR das AD-Risiko senkt, der zugrundeliegende protektive Mechanismus wurde in dieser Arbeit von Luchsinger et al. jedoch nicht aufgeklärt [141].
Neben der Induktion anti-amyloidogener als auch anti-inflammatorischer Effekte ist KR auch in der Lage, Autophagie zu induzieren. Autophagie ist dabei ein bereits detailliert beschriebener kataboler Mechanismus, um aggregierte Proteine wie z. B. Aβ abzubauen [142]. Als üblicher Marker für Autophagie wird die Translokation des Proteins LC3BII zusammen mit Sequestosom-1 (p62) zur Autophagosomenmembran analysiert [143]. In anderen AD-Modellen wurde Autophagie bereits als Mediator der positiven Effekte von KR vermutet, jedoch noch nicht umfassend untersucht und mit zum Teil widersprüchlichen Ergebnissen publiziert (Zusammengefasst von Yang und Zhang [144]). Um die ambivalente Datenlage zu ergänzen, zeigte die aktuelle Studie, dass KR-gefütterte tg-Mäuse eine signifikante Steigerung der Autophagie aufwiesen. Dies wurde durch erhöhte LC3BII- und p62-

Werte belegt, was auf einen neuroprotektiven Mechanismus von KR hindeutet, der schließlich auch eine Wiederherstellung der kognitiven Funktion auf wt-Niveau bewirkte.

Schließlich sollte in Studie 6 die ventrikuläre und parenchymale Hirn-Clearance-Kapazität untersucht werden, die maßgeblich für den Abtransport von potenziell neurotoxischen Metaboliten wie Aβ dient, um sie in der Körperperipherie weiterer Degradation zuzuführen. Zur Messung dieser Hirn-Clearance-Mechanismen gibt es bereits eine Vielzahl von Literatur über die Anwendung von GBCA-gestützter MRT-Bildgebung. Dazu gehören sowohl klinische [145–147] als auch präklinische Studien mit Ratten [148, 149]. Die wenigen Forschungsarbeiten, die GBCA-gestützte MRT-Bildgebung bei Mäusen nutzten, verwendeten invasive intrazisterale Injektionen [150, 151], was zu einem begrenzten translationalen Potenzial führt. Zu AD-Mausmodellen gibt es bislang keine Publikationen. Dennoch sind insbesondere genetisch veränderte Mäuse in der Grundlagenforschung und der Entwicklung von Therapien für AD, aber auch anderer Krankheiten die am häufigsten verwendeten Modelle (zusammengefasst von Kosel et al [152]). Deshalb wurde hier eine neue Methodik der GBCA-gestützten MRT-Bildgebung im selben tg-Mausmodell etabliert. Hierbei wird das GBCA minimalinvasiv über die Schwanzvene verabreicht. Dies ermöglicht neben der Abbildung der Hirn-Clearance auch Aussagen zur Anflutung über die Blutversorgung des ZNS.
Für die Anflutung des GBCA konnte im Hippocampus ein Alterseffekt nachgewiesen werden, der sich insbesondere bei tg-Mäusen in einer verstärkten Anflutung zeigt. Eine Begründung hierfür könnte sich in zerebrovaskulären Läsionen und Störungen der Blut-Hirn-Schranke (BHS) finden, die bei AD auftreten [153], jedoch auch bereits für DIO-Modelle gezeigt werden konnten [154].
Für die Abflutungskonstante als Maß für die Hirn-Clearance-Kapazität konnte kein statistisch signifikanter Effekt des Alters gezeigt werden, auch wenn der Genotyp einen tendenziellen Einfluss haben könnte. Eine mögliche Erklärung für den in diesen preliminären Daten nicht messbaren Unterschied zwischen tg und wt könnte im Modell selbst begründet liegen. Dieses Modell basiert in Anlehnung an familiäre AD-Formen auf einer Aβ-Überproduktion [71]. Diese Überproduktion könnte den pathomechanistischen Einfluss einer veränderten Hirn-Clearance überlagern. Eine andere Erklärung könnte sein, dass die erwartete Effektstärke des Alters und Genotyps auf die Hirn-Clearance kleiner war als erwartet und deshalb die gewählte Tieranzahl in diesem Versuch zur Methodenetablierung auch aufgrund hoher interindividueller Variabilität zu niedrig war, um die Unterschiede abbilden zu können. Dies wird in nachfolgend geplanten Versuchen bei der Ermittlung der benötigten Tieranzahl zu beachten sein. Ob und in welchem Ausmaß sich Störungen dieser Hirn-Clearance-Kapazität auch in den genetischen oder Diät-induzierten Modellen der Adipositas wiederfinden, ist künftig ein weiteres Forschungsfeld, was in der Arbeitsgruppe mit der neu etablierten Methode untersucht werden soll. Dadurch könnte künftig eine weitere pathomechanistische Verbindung zwischen Adipositas, Neuroinflammation und Amyloidpathologie aufgedeckt werden.

Zusammenfassend konnte in der vorliegenden Arbeit an bereits vorhandenes Wissen angeknüpft werden und in drei verschiedenen Mausmodellen der Zusammenhang zwischen Ernährung, Neuroinflammation und Amyloidpathologie näher verstanden werden.
Dabei konnte gezeigt werden, dass Fehlernährung im Rahmen einer langzeitigen, fettreichen Diät zu einer persistierenden niedrigschwelligen Inflammation führt, welche sich nicht zellulär manifestiert, jedoch als erhöhte Expression pro-inflammatorischer humoraler Mediatoren darstellt. In der Leber konnte dies vor allem durch eine erhöhte mRNA-Expression von *tnf-α* veranschaulicht werden, während sich im ZNS die erhöhte mRNA-Expression von *il-1β* als Hauptmediator einer pro-inflammatorischen Antwort herausgestellt hat. Dass ein krankhaftes Übergewicht generell einen Einfluss auf das ZNS zu haben scheint, konnte im genetischen Modell der Adipositas anhand von Verhaltensänderungen mit einer Begünstigung von ängstlichen Verhalten und einem reduzierten explorativen Verhalten gezeigt werden. Als therapeutischer Ansatz der Adipositas konnten Ernährungsinterventionen (Diätwechsel) sowohl in der Leber als auch im ZNS die pro-inflammatorische humorale Immunantwort abmildern. Ernährungsinterventionen im tg-Modell der AD konnten außerdem zu einer

Steigerung der Hirn-Clearance über Autophagie-Mechanismen und damit zu einer Reduktion der Belastung durch Aβ-Plaques sowie zu einer reduzierten Neuroinflammation führen. Um die Hirn-Clearance weiter zu untersuchen, wurde für Mausmodelle außerdem GBCA-gestützte MRT-Bildgebung etabliert. Auch wenn aufgrund der geringen Gruppengröße vorerst keine finalen Schlüsse auf die Clearance-Kapazität in tg- und wt-Mäusen gezogen werden konnten, eröffnet diese Methode eine neue Möglichkeit, um die Hirn-Clearance-Kapazität longitudinal I*n vivo* einschätzen zu können.

8. Literaturverzeichnis

1. WHO (2021) Obesity and overweight. https://www.who.int/news-room/fact-sheets/detail/obesity-and-overweight. Zugegriffen: 04. August 2023
2. Ciumărnean L, Milaciu MV, Negrean V, Orășan OH, Vesa SC, Sălăgean O, Iluţ S, Vlaicu SI (2021) Cardiovascular Risk Factors and Physical Activity for the Prevention of Cardiovascular Diseases in the Elderly. Int J Environ Res Public Health 19(1). doi:10.3390/ijerph19010207
3. Anandacoomarasamy A, Caterson I, Sambrook P, Fransen M, March L (2008) The impact of obesity on the musculoskeletal system. Int J Obes 32(2):211–222. doi:10.1038/sj.ijo.0803715
4. Hotamisligil GS (2017) Inflammation, metaflammation and immunometabolic disorders. Nature 542(7640):177–185. doi:10.1038/nature21363
5. Chuang Y-F, An Y, Bilgel M, Wong DF, Troncoso JC, O'Brien RJ, Breitner J, Ferruci L, Resnick SM, Thambisetty M (2016) Midlife adiposity predicts earlier onset of Alzheimer's dementia, neuropathology and presymptomatic cerebral amyloid accumulation. Mol Psychiatry 21(7):910–915. doi:10.1038/mp.2015.129
6. Morys F, Potvin O, Zeighami Y, Vogel J, Lamontagne-Caron R, Duchesne S, Dagher A (2023) Obesity-Associated Neurodegeneration Pattern Mimics Alzheimer's Disease in an Observational Cohort Study. J Alzheimers Dis 91(3):1059–1071. doi:10.3233/JAD-220535
7. Singh-Manoux A, Czernichow S, Elbaz A, Dugravot A, Sabia S, Hagger-Johnson G, Kaffashian S, Zins M, Brunner EJ, Nabi H, Kivimäki M (2012) Obesity phenotypes in midlife and cognition in early old age: the Whitehall II cohort study. Neurology 79(8):755–762. doi:10.1212/WNL.0b013e3182661f63
8. Xu WL, Atti AR, Gatz M, Pedersen NL, Johansson B, Fratiglioni L (2011) Midlife overweight and obesity increase late-life dementia risk: a population-based twin study. Neurology 76(18):1568–1574. doi:10.1212/WNL.0b013e3182190d09
9. Oronsky B, Caroen S, Reid T (2022) What Exactly Is Inflammation (and What Is It Not?). Int J Mol Sci 23(23). doi:10.3390/ijms232314905
10. Sattler S (2017) The Role of the Immune System Beyond the Fight Against Infection. Adv Exp Med Biol 1003:3–14. doi:10.1007/978-3-319-57613-8_1
11. Koenderman L, Buurman W, Daha MR (2014) The innate immune response. Immunol Lett 162(2 Pt B):95–102. doi:10.1016/j.imlet.2014.10.010
12. Bonilla FA, Oettgen HC (2010) Adaptive immunity. J Allergy Clin Immunol 125(2 Suppl 2):S33-40. doi:10.1016/j.jaci.2009.09.017
13. Borish LC, Steinke JW (2003) 2. Cytokines and chemokines. Journal of Allergy and Clinical Immunology 111(2 Suppl):S460-75. doi:10.1067/mai.2003.108
14. Prinz M, Priller J, Sisodia SS, Ransohoff RM (2011) Heterogeneity of CNS myeloid cells and their roles in neurodegeneration. Nat Neurosci 14(10):1227–1235. doi:10.1038/nn.2923
15. Guillemot-Legris O, Muccioli GG (2017) Obesity-Induced Neuroinflammation: Beyond the Hypothalamus. Trends Neurosci 40(4):237–253. doi:10.1016/j.tins.2017.02.005
16. Kälin S, Heppner FL, Bechmann I, Prinz M, Tschöp MH, Yi C-X (2015) Hypothalamic innate immune reaction in obesity. Nat Rev Endocrinol 11(6):339–351. doi:10.1038/nrendo.2015.48

17. Thaler JP, Guyenet SJ, Dorfman MD, Wisse BE, Schwartz MW (2013) Hypothalamic inflammation: marker or mechanism of obesity pathogenesis? Diabetes 62(8):2629–2634. doi:10.2337/db12-1605

18. Leng F, Edison P (2021) Neuroinflammation and microglial activation in Alzheimer disease: where do we go from here? Nat Rev Neurol 17(3):157–172. doi:10.1038/s41582-020-00435-y

19. DiSabato DJ, Quan N, Godbout JP (2016) Neuroinflammation: the devil is in the details. J Neurochem 139 Suppl 2(Suppl 2):136–153. doi:10.1111/jnc.13607

20. Kempuraj D, Thangavel R, Natteru PA, Selvakumar GP, Saeed D, Zahoor H, Zaheer S, Iyer SS, Zaheer A (2016) Neuroinflammation Induces Neurodegeneration. J Neurol Neurosurg Spine 1(1)

21. Edison P, Archer HA, Gerhard A, Hinz R, Pavese N, Turkheimer FE, Hammers A, Tai YF, Fox N, Kennedy A, Rossor M, Brooks DJ (2008) Microglia, amyloid, and cognition in Alzheimer's disease: An 11C(R)PK11195-PET and 11CPIB-PET study. Neurobiol Dis 32(3):412–419. doi:10.1016/j.nbd.2008.08.001

22. Hashioka S, Wu Z, Klegeris A (2021) Glia-Driven Neuroinflammation and Systemic Inflammation in Alzheimer's Disease. CN 19(7):908–924. doi:10.2174/1570159X18666201111104509

23. Mudgal J, Nampoothiri M, Basu Mallik S, Kinra M, Hall S, Grant G, Anoopkumar-Dukie S, Rao CM, Arora D (2019) Possible involvement of metformin in downregulation of neuroinflammation and associated behavioural changes in mice. Inflammopharmacol 27(5):941–948. doi:10.1007/s10787-019-00638-w

24. Na S, Duan X, Wang R, Fan Y, Xue K, Tian S, Yang Z, Li K, Yue J (2021) Chronic Neuroinflammation Induced by Lipopolysaccharide Injection into the Third Ventricle Induces Behavioral Changes. J Mol Neurosci 71(6):1306–1319. doi:10.1007/s12031-020-01758-7

25. Hardy J, Allsop D (1991) Amyloid deposition as the central event in the aetiology of Alzheimer's disease. Trends in Pharmacological Sciences 12:383–388. doi:10.1016/0165-6147(91)90609-V

26. Selkoe DJ (1991) The molecular pathology of Alzheimer's disease. Neuron 6(4):487–498. doi:10.1016/0896-6273(91)90052-2

27. Herrup K (2015) The case for rejecting the amyloid cascade hypothesis. Nat Neurosci 18(6):794–799. doi:10.1038/nn.4017

28. Akiyama H, Barger S, Barnum S et al (2000) Inflammation and Alzheimer's disease. Neurobiol Aging 21(3):383–421. doi:10.1016/s0197-4580(00)00124-x

29. Giulian D, Haverkamp LJ, Yu JH, Karshin W, Tom D, Li J, Kirkpatrick J, Kuo Y-M, Roher AE (1996) Specific domains of beta-amyloid from Alzheimer plaque elicit neuron killing in human microglia. J Neurosci 16(19):6021–6037. doi:10.1523/JNEUROSCI.16-19-06021.1996

30. McDonald DR, Brunden KR, Landreth GE (1997) Amyloid fibrils activate tyrosine kinase-dependent signaling and superoxide production in microglia. J Neurosci 17(7):2284–2294. doi:10.1523/JNEUROSCI.17-07-02284.1997

31. Yan L-J, Xiao M, Chen R, Cai Z (2013) Metabolic Dysfunction of Astrocyte: An Initiating Factor in Beta-amyloid Pathology? Aging Neurodegener 1(1):7–14. doi:None

32. Bachiller S, Jiménez-Ferrer I, Paulus A, Yang Y, Swanberg M, Deierborg T, Boza-Serrano A (2018) Microglia in Neurological Diseases: A Road Map to Brain-Disease Dependent-Inflammatory Response. Front. Cell. Neurosci. 12:488. doi:10.3389/fncel.2018.00488

33. Kwon HS, Koh S-H (2020) Neuroinflammation in neurodegenerative disorders: the roles of microglia and astrocytes. Transl Neurodegener 9(1):42. doi:10.1186/s40035-020-00221-2

34. Prinz M, Erny D, Hagemeyer N (2017) Ontogeny and homeostasis of CNS myeloid cells. Nat Immunol 18(4):385–392. doi:10.1038/ni.3703

35. Zhan J, Mann T, Joost S, Behrangi N, Frank M, Kipp M (2020) The Cuprizone Model: Dos and Do Nots. Cells 9(4). doi:10.3390/cells9040843

36. Becher B, Spath S, Goverman J (2017) Cytokine networks in neuroinflammation. Nat Rev Immunol 17(1):49–59. doi:10.1038/nri.2016.123

37. Liddelow SA, Guttenplan KA, Clarke LE, Bennett FC, Bohlen CJ, Schirmer L, Bennett ML, Münch AE, Chung W-S, Peterson TC, Wilton DK, Frouin A, Napier BA, Panicker N, Kumar M, Buckwalter MS, Rowitch DH, Dawson VL, Dawson TM, Stevens B, Barres BA (2017) Neurotoxic reactive astrocytes are induced by activated microglia. Nature 541(7638):481–487. doi:10.1038/nature21029

38. Janzer RC, Raff MC (1987) Astrocytes induce blood-brain barrier properties in endothelial cells. Nature 325(6101):253–257. doi:10.1038/325253a0

39. Ramsauer M, Krause D, Dermietzel R (2002) Angiogenesis of the blood-brain barrier in vitro and the function of cerebral pericytes. FASEB J 16(10):1274–1276. doi:10.1096/fj.01-0814fje

40. Iliff JJ, Wang M, Liao Y, Plogg BA, Peng W, Gundersen GA, Benveniste H, Vates GE, Deane R, Goldman SA, Nagelhus EA, Nedergaard M (2012) A paravascular pathway facilitates CSF flow through the brain parenchyma and the clearance of interstitial solutes, including amyloid β. Sci Transl Med 4(147):147ra111. doi:10.1126/scitranslmed.3003748

41. Wang Z, Ying Z, Bosy-Westphal A, Zhang J, Heller M, Later W, Heymsfield SB, Müller MJ (2012) Evaluation of specific metabolic rates of major organs and tissues: comparison between nonobese and obese women. Obesity (Silver Spring) 20(1):95–100. doi:10.1038/oby.2011.256

42. Tarasoff-Conway JM, Carare RO, Osorio RS, Glodzik L, Butler T, Fieremans E, Axel L, Rusinek H, Nicholson C, Zlokovic BV, Frangione B, Blennow K, Ménard J, Zetterberg H, Wisniewski T, Leon MJ de (2015) Clearance systems in the brain-implications for Alzheimer disease. Nat Rev Neurol 11(8):457–470. doi:10.1038/nrneurol.2015.119

43. Wilcock DM, Munireddy SK, Rosenthal A, Ugen KE, Gordon MN, Morgan D (2004) Microglial activation facilitates Abeta plaque removal following intracranial anti-Abeta antibody administration. Neurobiol Dis 15(1):11–20. doi:10.1016/j.nbd.2003.09.015

44. Yin K-J, Cirrito JR, Yan P, Hu X, Xiao Q, Pan X, Bateman R, Song H, Hsu F-F, Turk J, Xu J, Hsu CY, Mills JC, Holtzman DM, Lee J-M (2006) Matrix metalloproteinases expressed by astrocytes mediate extracellular amyloid-beta peptide catabolism. J Neurosci 26(43):10939–10948. doi:10.1523/JNEUROSCI.2085-06.2006

45. Zhang Z, Yang X, Song Y-Q, Tu J (2021) Autophagy in Alzheimer's disease pathogenesis: Therapeutic potential and future perspectives. Ageing Res Rev 72:101464. doi:10.1016/j.arr.2021.101464

46. Zlokovic BV, Begley DJ, Chain-Eliash DG (1985) Blood-brain barrier permeability to leucine-enkephalin, D-alanine2-D-leucine5-enkephalin and their N-terminal amino acid (tyrosine). Brain Res 336(1):125–132. doi:10.1016/0006-8993(85)90423-8

47. Shibata M, Yamada S, Kumar SR, Calero M, Bading J, Frangione B, Holtzman DM, Miller CA, Strickland DK, Ghiso J, Zlokovic BV (2000) Clearance of Alzheimer's amyloid-ss(1-40) peptide from brain by LDL receptor-related protein-1 at the blood-brain barrier. J Clin Invest 106(12):1489–1499. doi:10.1172/JCI10498

48. Abbott NJ (2004) Evidence for bulk flow of brain interstitial fluid: significance for physiology and pathology. Neurochem Int 45(4):545–552. doi:10.1016/j.neuint.2003.11.006

49. Hablitz LM, Nedergaard M (2021) The Glymphatic System: A Novel Component of Fundamental Neurobiology. J Neurosci 41(37):7698–7711. doi:10.1523/JNEUROSCI.0619-21.2021

50. Louveau A, Smirnov I, Keyes TJ, Eccles JD, Rouhani SJ, Peske JD, Derecki NC, Castle D, Mandell JW, Lee KS, Harris TH, Kipnis J (2015) Structural and functional features of central nervous system lymphatic vessels. Nature 523(7560):337–341. doi:10.1038/nature14432

51. Welch K, Pollay M (1961) Perfusion of particles through arachnoid villi of the monkey. Am J Physiol 201:651–654. doi:10.1152/ajplegacy.1961.201.4.651

52. Killer HE, Laeng HR, Groscurth P (1999) Lymphatic capillaries in the meninges of the human optic nerve. J Neuroophthalmol 19(4):222–228

53. Zakharov A, Papaiconomou C, Djenic J, Midha R, Johnston M (2003) Lymphatic cerebrospinal fluid absorption pathways in neonatal sheep revealed by subarachnoid injection of Microfil. Neuropathol Appl Neurobiol 29(6):563–573. doi:10.1046/j.0305-1846.2003.00508.x

54. Kida S, Pantazis A, Weller RO (1993) CSF drains directly from the subarachnoid space into nasal lymphatics in the rat. Anatomy, histology and immunological significance. Neuropathol Appl Neurobiol 19(6):480–488. doi:10.1111/j.1365-2990.1993.tb00476.x

55. Mollanji R, Bozanovic-Sosic R, Silver I, Li B, Kim C, Midha R, Johnston M (2001) Intracranial pressure accommodation is impaired by blocking pathways leading to extracranial lymphatics. Am J Physiol Regul Integr Comp Physiol 280(5):R1573-81. doi:10.1152/ajpregu.2001.280.5.R1573

56. Uchida K (2022) Waste Clearance in the Brain and Neuroinflammation: A Novel Perspective on Biomarker and Drug Target Discovery in Alzheimer's Disease. Cells 11(5). doi:10.3390/cells11050919

57. Selkoe DJ, Hardy J (2016) The amyloid hypothesis of Alzheimer's disease at 25 years. EMBO Mol Med 8(6):595–608. doi:10.15252/emmm.201606210

58. Mawuenyega KG, Sigurdson W, Ovod V, Munsell L, Kasten T, Morris JC, Yarasheski KE, Bateman RJ (2010) Decreased clearance of CNS beta-amyloid in Alzheimer's disease. Science 330(6012):1774. doi:10.1126/science.1197623

59. Wang L, Zhang Y, Zhao Y, Marshall C, Wu T, Xiao M (2019) Deep cervical lymph node ligation aggravates AD-like pathology of APP/PS1 mice. Brain Pathol 29(2):176–192. doi:10.1111/bpa.12656

60. Arbel-Ornath M, Hudry E, Eikermann-Haerter K, Hou S, Gregory JL, Zhao L, Betensky RA, Frosch MP, Greenberg SM, Bacskai BJ (2013) Interstitial fluid drainage is impaired in ischemic stroke and Alzheimer's disease mouse models. Acta Neuropathol 126(3):353–364. doi:10.1007/s00401-013-1145-2

61. Peng W, Achariyar TM, Li B, Liao Y, Mestre H, Hitomi E, Regan S, Kasper T, Peng S, Ding F, Benveniste H, Nedergaard M, Deane R (2016) Suppression of glymphatic fluid transport in a mouse model of Alzheimer's disease. Neurobiol Dis 93:215–225. doi:10.1016/j.nbd.2016.05.015

62. Mitchell SJ, Scheibye-Knudsen M, Longo DL, Cabo R de (2015) Animal models of aging research: implications for human aging and age-related diseases. Annu Rev Anim Biosci 3:283–303. doi:10.1146/annurev-animal-022114-110829

63. Li J, Wu H, Liu Y, Yang L (2020) High fat diet induced obesity model using four strainsof mice: Kunming, C57BL/6, BALB/c and ICR. Exp Anim 69(3):326–335. doi:10.1538/expanim.19-0148

64. Sampey BP, Vanhoose AM, Winfield HM, Freemerman AJ, Muehlbauer MJ, Fueger PT, Newgard CB, Makowski L (2011) Cafeteria diet is a robust model of human metabolic syndrome with liver and adipose inflammation: comparison to high-fat diet. Obesity (Silver Spring) 19(6):1109–1117. doi:10.1038/oby.2011.18

65. Kennedy AJ, Ellacott KLJ, King VL, Hasty AH (2010) Mouse models of the metabolic syndrome. Dis Model Mech 3(3-4):156–166. doi:10.1242/dmm.003467

66. Coleman DL (1978) Obese and diabetes: two mutant genes causing diabetes-obesity syndromes in mice. Diabetologia 14(3):141–148. doi:10.1007/BF00429772

67. Hayakawa J, Wang M, Wang C, Han RH, Jiang ZY, Han X (2018) Lipidomic analysis reveals significant lipogenesis and accumulation of lipotoxic components in ob/ob mouse organs. Prostaglandins Leukot Essent Fatty Acids 136:161–169. doi:10.1016/j.plefa.2017.01.002

68. de Bem AF, Krolow R, Farias HR, Rezende VL de, Gelain DP, Moreira JCF, Duarte JMdN, Oliveira J de (2020) Animal Models of Metabolic Disorders in the Study of Neurodegenerative Diseases: An Overview. Front Neurosci 14:604150. doi:10.3389/fnins.2020.604150

69. Oakley H, Cole SL, Logan S, Maus E, Shao P, Craft J, Guillozet-Bongaarts A, Ohno M, Disterhoft J, van Eldik L, Berry R, Vassar R (2006) Intraneuronal beta-amyloid aggregates, neurodegeneration, and neuron loss in transgenic mice with five familial Alzheimer's disease mutations: potential factors in amyloid plaque formation. J Neurosci 26(40):10129–10140. doi:10.1523/JNEUROSCI.1202-06.2006

70. Willuweit A, Velden J, Godemann R, Manook A, Jetzek F, Tintrup H, Kauselmann G, Zevnik B, Henriksen G, Drzezga A, Pohlner J, Schoor M, Kemp JA, Kammer H von der (2009) Early-onset and robust amyloid pathology in a new homozygous mouse model of Alzheimer's disease. PLoS One 4(11):e7931. doi:10.1371/journal.pone.0007931

71. Jankowsky JL, Slunt HH, Ratovitski T, Jenkins NA, Copeland NG, Borchelt DR (2001) Co-expression of multiple transgenes in mouse CNS: a comparison of strategies. Biomolecular Engineering 17(6):157–165. doi:10.1016/S1389-0344(01)00067-3

72. Esquerda-Canals G, Montoliu-Gaya L, Güell-Bosch J, Villegas S (2017) Mouse Models of Alzheimer's Disease. J Alzheimers Dis 57(4):1171–1183. doi:10.3233/JAD-170045

73. Jankowsky JL, Zheng H (2017) Practical considerations for choosing a mouse model of Alzheimer's disease. Mol Neurodegener 12(1):89. doi:10.1186/s13024-017-0231-7

74. Martins T, Castro-Ribeiro C, Lemos S, Ferreira T, Nascimento-Gonçalves E, Rosa E, Oliveira PA, Antunes LM (2022) Murine Models of Obesity. Obesities 2(2):127–147. doi:10.3390/obesities2020012

75. Webster SJ, Bachstetter AD, Nelson PT, Schmitt FA, van Eldik LJ (2014) Using mice to model Alzheimer's dementia: an overview of the clinical disease and the preclinical behavioral changes in 10 mouse models. Front Genet 5:88. doi:10.3389/fgene.2014.00088

76. Gabr RE, Hasan KM, Haque ME, Nelson FM, Wolinsky JS, Narayana PA (2016) Optimal combination of FLAIR and T2-weighted MRI for improved lesion contrast in multiple sclerosis. J Magn Reson Imaging 44(5):1293–1300. doi:10.1002/jmri.25281

77. Hattingen E, Müller A, Jurcoane A, Mädler B, Ditter P, Schild H, Herrlinger U, Glas M, Kebir S (2017) Value of quantitative magnetic resonance imaging T1-relaxometry in predicting contrast-enhancement in glioblastoma patients. Oncotarget 8(32):53542–53551. doi:10.18632/oncotarget.18612

78. Grahl S, Bussas M, Pongratz V, Kirschke JS, Zimmer C, Berthele A, Hemmer B, Mühlau M (2021) T1-Weighted Intensity Increase After a Single Administration of a Linear Gadolinium-Based Contrast Agent in Multiple Sclerosis. Clin Neuroradiol 31(1):235–243. doi:10.1007/s00062-020-00882-6

79. Power Guerra N, Müller L, Pilz K, Glatzel A, Jenderny D, Janowitz D, Vollmar B, Kuhla A (2020) Dietary-Induced Low-Grade Inflammation in the Liver. Biomedicines 8(12). doi:10.3390/biomedicines8120587

80. Müller L, Power Guerra N, Schildt A, Lindner T, Stenzel J, Behrangi N, Bergner C, Alberts T, Bühler D, Kurth J, Krause BJ, Janowitz D, Teipel S, Vollmar B, Kuhla A (2023) 18FGE-180-PET and Post Mortem Marker Characteristics of Long-Term High-Fat-Diet-Induced Chronic Neuroinflammation in Mice. Biomolecules 13(5). doi:10.3390/biom13050769

81. Bühler D, Power-Guerra N, Müller L, Wolkenhauer O, Düffer M, Vollmar B, Kuhla A, Wolfien M (2023) Leptin deficiency-caused behavioral change -a comparative analysis using EthoVision and DeepLabCut. Front. Neurosci. 17:421. doi:10.3389/fnins.2023.1052079

82. Power Guerra N, Leyens K, Müller L, Brauer D, Janowitz D, Schlick S, Pilz K, Grabe HJ, Vollmar B, Kuhla A (2022) The effect of different weight loss strategies to treat non-alcoholic fatty liver disease focusing on fibroblast growth factor 21. Front Nutr 9:935805. doi:10.3389/fnut.2022.935805

83. Müller L, Power Guerra N, Stenzel J, Rühlmann C, Lindner T, Krause BJ, Vollmar B, Teipel S, Kuhla A (2021) Long-Term Caloric Restriction Attenuates β-Amyloid Neuropathology and Is Accompanied by Autophagy in APPswe/PS1delta9 Mice. Nutrients 13(3). doi:10.3390/nu13030985

84. Tanaka Y, Nagoshi T, Takahashi H, Oi Y, Yoshii A, Kimura H, Ito K, Kashiwagi Y, Tanaka TD, Yoshimura M (2022) URAT1-selective inhibition ameliorates insulin resistance by attenuating diet-induced hepatic steatosis and brown adipose tissue whitening in mice. Mol Metab 55:101411. doi:10.1016/j.molmet.2021.101411

85. van der Heijden RA, Sheedfar F, Morrison MC, Hommelberg PPH, Kor D, Kloosterhuis NJ, Gruben N, Youssef SA, Bruin A de, Hofker MH, Kleemann R, Koonen DPY, Heeringa P (2015) High-fat diet induced obesity primes inflammation in adipose tissue prior to liver in C57BL/6j mice. Aging (Albany NY) 7(4):256–268. doi:10.18632/aging.100738

86. Echeverría F, Valenzuela R, Bustamante A, Álvarez D, Ortiz M, Espinosa A, Illesca P, Gonzalez-Mañan D, Videla LA (2019) High-fat diet induces mouse liver steatosis with a concomitant decline in energy metabolism: attenuation by eicosapentaenoic acid (EPA) or hydroxytyrosol (HT) supplementation and the additive effects upon EPA and HT co-administration. Food Funct 10(9):6170–6183. doi:10.1039/c9fo01373c

87. Liebig M, Hassanzada A, Kämmerling M, Genz B, Vollmar B, Abshagen K (2018) Microcirculatory disturbances and cellular changes during progression of hepatic steatosis to liver tumors. Exp Biol Med (Maywood) 243(1):1–12. doi:10.1177/1535370217738730

88. Tirosh O (2018) Hypoxic Signaling and Cholesterol Lipotoxicity in Fatty Liver Disease Progression. Oxid Med Cell Longev 2018:2548154. doi:10.1155/2018/2548154

89. Ulman E.A. (2011) The “Original” High-Fat Diets for Diet Induced Obesity. https://www.weizmann.ac.il/vet/sites/vet/files/uploads/diet_d12451_d12492.pdf. Zugegriffen: 14. Februar 2023

90. Lauber DT, Fülöp A, Kovács T, Szigeti K, Máthé D, Szijártó A (2017) State of the art in vivo imaging techniques for laboratory animals. Lab Anim 51(5):465–478. doi:10.1177/0023677217695852

91. Tremoleda JL, Kerton A, Gsell W (2012) Anaesthesia and physiological monitoring during in vivo imaging of laboratory rodents: considerations on experimental outcomes and animal welfare. EJNMMI Res 2(1):44. doi:10.1186/2191-219X-2-44

92. Minoshima S, Mosci K, Cross D, Thientunyakit T (2021) Brain F-18FDG PET for Clinical Dementia Workup: Differential Diagnosis of Alzheimer's Disease and Other Types of Dementing Disorders. Semin Nucl Med 51(3):230–240. doi:10.1053/j.semnuclmed.2021.01.002

93. Rauchmann B-S, Brendel M, Franzmeier N et al (2022) Microglial Activation and Connectivity in Alzheimer Disease and Aging. Ann Neurol 92(5):768–781. doi:10.1002/ana.26465

94. Sanguinetti E, Guzzardi MA, Panetta D, Tripodi M, Sena V de, Quaglierini M, Burchielli S, Salvadori PA, Iozzo P (2019) Combined Effect of Fatty Diet and Cognitive Decline on Brain Metabolism, Food Intake, Body Weight, and Counteraction by Intranasal Insulin Therapy in 3×Tg Mice. Front. Cell. Neurosci. 13:188. doi:10.3389/fncel.2019.00188

95. Tuulari JJ, Karlsson HK, Hirvonen J, Hannukainen JC, Bucci M, Helmiö M, Ovaska J, Soinio M, Salminen P, Savisto N, Nummenmaa L, Nuutila P (2013) Weight loss after bariatric surgery reverses insulin-induced increases in brain glucose metabolism of the morbidly obese. Diabetes 62(8):2747–2751. doi:10.2337/db12-1460

96. Apostolova I, Lange C, Mäurer A, Suppa P, Spies L, Grothe MJ, Nierhaus T, Fiebach JB, Steinhagen-Thiessen E, Buchert R (2018) Hypermetabolism in the hippocampal formation of cognitively impaired patients indicates detrimental maladaptation. Neurobiol Aging 65:41–50. doi:10.1016/j.neurobiolaging.2018.01.002

97. Barron AM, Tokunaga M, Zhang M-R, Ji B, Suhara T, Higuchi M (2016) Assessment of neuroinflammation in a mouse model of obesity and β-amyloidosis using PET. J Neuroinflammation 13(1):221. doi:10.1186/s12974-016-0700-x

98. Robblee MM, Kim CC, Porter Abate J, Valdearcos M, Sandlund KLM, Shenoy MK, Volmer R, Iwawaki T, Koliwad SK (2016) Saturated Fatty Acids Engage an IRE1α-Dependent Pathway to Activate the NLRP3 Inflammasome in Myeloid Cells. Cell Rep 14(11):2611–2623. doi:10.1016/j.celrep.2016.02.053

99. Mendiola AS, Cardona AE (2018) The IL-1β phenomena in neuroinflammatory diseases. J Neural Transm (Vienna) 125(5):781–795. doi:10.1007/s00702-017-1732-9

100. Sobesky JL, Barrientos RM, May HS de, Thompson BM, Weber MD, Watkins LR, Maier SF (2014) High-fat diet consumption disrupts memory and primes elevations in hippocampal IL-1β, an effect that can be prevented with dietary reversal or IL-1 receptor antagonism. Brain Behav Immun 42:22–32. doi:10.1016/j.bbi.2014.06.017

101. Thaler JP, Yi C-X, Schur EA, Guyenet SJ, Hwang BH, Dietrich MO, Zhao X, Sarruf DA, Izgur V, Maravilla KR, Nguyen HT, Fischer JD, Matsen ME, Wisse BE, Morton GJ, Horvath TL, Baskin DG, Tschöp MH, Schwartz MW (2012) Obesity is associated with hypothalamic injury in rodents and humans. J Clin Invest 122(1):153–162. doi:10.1172/JCI59660

102. Lainez NM, Jonak CR, Nair MG, Ethell IM, Wilson EH, Carson MJ, Coss D (2018) Diet-Induced Obesity Elicits Macrophage Infiltration and Reduction in Spine Density in the Hypothalami of Male but Not Female Mice. Front Immunol 9:1992. doi:10.3389/fimmu.2018.01992

103. Nakandakari SCBR, Muñoz VR, Kuga GK, Gaspar RC, Sant'Ana MR, Pavan ICB, da Silva LGS, Morelli AP, Simabuco FM, da Silva ASR, Moura LP de, Ropelle ER, Cintra DE, Pauli JR (2019) Short-term high-fat diet modulates several inflammatory, ER stress, and apoptosis markers in the hippocampus of young mice. Brain Behav Immun 79:284–293. doi:10.1016/j.bbi.2019.02.016

104. Waise TMZ, Toshinai K, Naznin F, NamKoong C, Md Moin AS, Sakoda H, Nakazato M (2015) One-day high-fat diet induces inflammation in the nodose ganglion and hypothalamus of mice. Biochem Biophys Res Commun 464(4):1157–1162. doi:10.1016/j.bbrc.2015.07.097

105. Bona Schraiber R de, Mello AH de, Garcez ML, Bem Silveira G de, Zacaron RP, Souza Goldim MP de, Budni J, Silveira PCL, Petronilho F, Ferreira GK, Rezin GT (2019) Diet-induced obesity causes hypothalamic neurochemistry alterations in Swiss mice. Metab Brain Dis 34(2):565–573. doi:10.1007/s11011-018-0337-9

106. Hao S, Dey A, Yu X, Stranahan AM (2016) Dietary obesity reversibly induces synaptic stripping by microglia and impairs hippocampal plasticity. Brain Behav Immun 51:230–239. doi:10.1016/j.bbi.2015.08.023

107. Kim MS, Choi M-S, Han SN (2011) High fat diet-induced obesity leads to proinflammatory response associated with higher expression of NOD2 protein. Nutr Res Pract 5(3):219–223. doi:10.4162/nrp.2011.5.3.219

108. Kim JD, Yoon NA, Jin S, Diano S (2019) Microglial UCP2 Mediates Inflammation and Obesity Induced by High-Fat Feeding. Cell Metab 30(5):952-962.e5. doi:10.1016/j.cmet.2019.08.010

109. Szczypka MS, Rainey MA, Palmiter RD (2000) Dopamine is required for hyperphagia in Lepob/ob mice. Nat Genet 25(1):102–104. doi:10.1038/75484

110. Memon RA, Fuller J, Moser AH, Smith PJ, Grunfeld C, Feingold KR (1999) Regulation of putative fatty acid transporters and Acyl-CoA synthetase in liver and adipose tissue in ob/ob mice. Diabetes 48(1):121–127. doi:10.2337/diabetes.48.1.121

111. Nilsson C, Raun K, Yan F, Larsen MO, Tang-Christensen M (2012) Laboratory animals as surrogate models of human obesity. Acta Pharmacol Sin 33(2):173–181. doi:10.1038/aps.2011.203

112. Schepers J, Gebhardt C, Bracke A, Eiffler I, Bohlen Und Halbach O von (2020) Structural and functional consequences in the amygdala of leptin-deficient mice. Cell Tissue Res 382(2):421–426. doi:10.1007/s00441-020-03266-x

113. Wang Y, Xu J, Liu Y, Li Z, Li X (2018) TLR4-NF-κB Signal Involved in Depressive-Like Behaviors and Cytokine Expression of Frontal Cortex and Hippocampus in Stressed C57BL/6 and ob/ob Mice. Neural Plast 2018:7254016. doi:10.1155/2018/7254016

114. Clark TD, Crean AJ, Senior AM (2022) Obesogenic diets induce anxiety in rodents: A systematic review and meta-analysis. Obesity Reviews 23(3):e13399. doi:10.1111/obr.13399

115. Espinosa-Carrasco J, Burokas A, Fructuoso M, Erb I, Martín-García E, Gutiérrez-Martos M, Notredame C, Maldonado R, Dierssen M (2018) Time-course and dynamics of obesity-related behavioral changes induced by energy-dense foods in mice. Addiction Biology 23(2):531–543. doi:10.1111/adb.12595

116. Gould TD, Dao DT, Kovacsics CE (2009) The Open Field Test Mood and Anxiety Related Phenotypes in Mice. Humana Press, Totowa, NJ, S 1–20

117. Walf AA, Frye CA (2007) The use of the elevated plus maze as an assay of anxiety-related behavior in rodents. Nat Protoc 2(2):322–328. doi:10.1038/nprot.2007.44

118. Qin X, Wang W, Wu H, Liu D, Wang R, Xu J, Jiang H, Pan F (2020) PPARγ-mediated microglial activation phenotype is involved in depressive-like behaviors and neuroinflammation in stressed C57BL/6J and ob/ob mice. Psychoneuroendocrinology 117:104674. doi:10.1016/j.psyneuen.2020.104674

119. Wu H, Wang R, Qin X, Liu D, Wang W, Xu J, Jiang H, Pan F (2021) Effects of chronic stress on depressive-like behaviors and JMJD3 expression in the prefrontal cortex and

hippocampus of C57BL/6 and ob/ob mice. J Psychiatr Res 133:142–155. doi:10.1016/j.jpsychires.2020.12.014

120. Asakawa A, Inui A, Inui T, Katsuura G, Fujino MA, Kasuga M (2003) Leptin treatment ameliorates anxiety in ob/ob obese mice. J Diabetes Complications 17(2):105–107. doi:10.1016/s1056-8727(02)00185-x

121. Finger BC, Dinan TG, Cryan JF (2010) Leptin-deficient mice retain normal appetitive spatial learning yet exhibit marked increases in anxiety-related behaviours. Psychopharmacology (Berl) 210(4):559–568. doi:10.1007/s00213-010-1858-z

122. Fritz A-K, Amrein I, Wolfer DP (2017) Similar reliability and equivalent performance of female and male mice in the open field and water-maze place navigation task. Am J Med Genet C Semin Med Genet 175(3):380–391. doi:10.1002/ajmg.c.31565

123. Beery AK, Zucker I (2011) Sex bias in neuroscience and biomedical research. Neurosci Biobehav Rev 35(3):565–572. doi:10.1016/j.neubiorev.2010.07.002

124. Mackintosh JH (1970) Territory formation by laboratory mice. Animal Behaviour 18:177–183. doi:10.1016/0003-3472(70)90088-6

125. Kappel S, Hawkins P, Mendl MT (2017) To Group or Not to Group? Good Practice for Housing Male Laboratory Mice. Animals (Basel) 7(12). doi:10.3390/ani7120088

126. Shansky RM (2019) Are hormones a "female problem" for animal research? Science 364(6443):825–826. doi:10.1126/science.aaw7570

127. Bie P, Debrabant B (2020) Gonadal sex and animal experimentation: Perfection vs. 3R principle? Basic Clin Pharmacol Toxicol 127(2):111–119. doi:10.1111/bcpt.13411

128. Chaix A, Zarrinpar A, Miu P, Panda S (2014) Time-restricted feeding is a preventative and therapeutic intervention against diverse nutritional challenges. Cell Metab 20(6):991–1005. doi:10.1016/j.cmet.2014.11.001

129. Mantovani A, Dalbeni A (2021) Treatments for NAFLD: State of Art. Int J Mol Sci 22(5). doi:10.3390/ijms22052350

130. Romero-Gómez M, Zelber-Sagi S, Trenell M (2017) Treatment of NAFLD with diet, physical activity and exercise. J Hepatol 67(4):829–846. doi:10.1016/j.jhep.2017.05.016

131. Nseir W, Hellou E, Assy N (2014) Role of diet and lifestyle changes in nonalcoholic fatty liver disease. World J Gastroenterol 20(28):9338–9344. doi:10.3748/wjg.v20.i28.9338

132. Ringseis R, Mooren F-C, Keller J, Couturier A, Wen G, Hirche F, Stangl GI, Eder K, Krüger K (2011) Regular endurance exercise improves the diminished hepatic carnitine status in mice fed a high-fat diet. Mol Nutr Food Res 55 Suppl 2:S193-202. doi:10.1002/mnfr.201100040

133. Uysal KT, Wiesbrock SM, Marino MW, Hotamisligil GS (1997) Protection from obesity-induced insulin resistance in mice lacking TNF-alpha function. Nature 389(6651):610–614. doi:10.1038/39335

134. Dhapola R, Hota SS, Sarma P, Bhattacharyya A, Medhi B, Reddy DH (2021) Recent advances in molecular pathways and therapeutic implications targeting neuroinflammation for Alzheimer's disease. Inflammopharmacol 29(6):1669–1681. doi:10.1007/s10787-021-00889-6

135. Craft JM, Watterson DM, van Eldik LJ (2006) Human amyloid beta-induced neuroinflammation is an early event in neurodegeneration. Glia 53(5):484–490. doi:10.1002/glia.20306

136. Raut S, Bhalerao A, Powers M, Gonzalez M, Mancuso S, Cucullo L (2023) Hypometabolism, Alzheimer's Disease, and Possible Therapeutic Targets: An Overview. Cells 12(16). doi:10.3390/cells12162019

137. Mouton PR, Chachich ME, Quigley C, Spangler E, Ingram DK (2009) Caloric restriction attenuates amyloid deposition in middle-aged dtg APP/PS1 mice. Neurosci Lett 464(3):184–187. doi:10.1016/j.neulet.2009.08.038

138. Patel NV, Gordon MN, Connor KE, Good RA, Engelman RW, Mason J, Morgan DG, Morgan TE, Finch CE (2005) Caloric restriction attenuates Abeta-deposition in Alzheimer transgenic models. Neurobiol Aging 26(7):995–1000. doi:10.1016/j.neurobiolaging.2004.09.014

139. Halagappa VKM, Guo Z, Pearson M, Matsuoka Y, Cutler RG, Laferla FM, Mattson MP (2007) Intermittent fasting and caloric restriction ameliorate age-related behavioral deficits in the triple-transgenic mouse model of Alzheimer's disease. Neurobiol Dis 26(1):212–220. doi:10.1016/j.nbd.2006.12.019

140. Dong W, Wang R, Ma L-N, Xu B-L, Zhang J-S, Zhao Z-W, Wang Y-L, Zhang X (2016) Influence of age-related learning and memory capacity of mice: different effects of a high and low caloric diet. Aging Clin Exp Res 28(2):303–311. doi:10.1007/s40520-015-0398-0

141. Luchsinger JA, Tang M-X, Shea S, Mayeux R (2002) Caloric intake and the risk of Alzheimer disease. Arch Neurol 59(8):1258–1263. doi:10.1001/archneur.59.8.1258

142. Lilienbaum A (2013) Relationship between the proteasomal system and autophagy. Int J Biochem Mol Biol 4(1):1–26

143. Bresciani A, Spiezia MC, Boggio R, Cariulo C, Nordheim A, Altobelli R, Kuhlbrodt K, Dominguez C, Munoz-Sanjuan I, Wityak J, Fodale V, Marchionini DM, Weiss A (2018) Quantifying autophagy using novel LC3B and p62 TR-FRET assays. PLoS One 13(3):e0194423. doi:10.1371/journal.pone.0194423

144. Yang Y, Zhang L (2020) The effects of caloric restriction and its mimetics in Alzheimer's disease through autophagy pathways. Food Funct. 11(2):1211–1224. doi:10.1039/C9FO02611H

145. Eide PK, Vinje V, Pripp AH, Mardal K-A, Ringstad G (2021) Sleep deprivation impairs molecular clearance from the human brain. Brain 144(3):863–874. doi:10.1093/brain/awaa443

146. Naganawa S, Nakane T, Kawai H, Taoka T (2017) Gd-based Contrast Enhancement of the Perivascular Spaces in the Basal Ganglia. Magn Reson Med Sci 16(1):61–65. doi:10.2463/mrms.mp.2016-0039

147. Ringstad G, Valnes LM, Dale AM, Pripp AH, Vatnehol S-AS, Emblem KE, Mardal K-A, Eide PK (2018) Brain-wide glymphatic enhancement and clearance in humans assessed with MRI. JCI Insight 3(13). doi:10.1172/jci.insight.121537

148. Iliff JJ, Lee H, Yu M, Feng T, Logan J, Nedergaard M, Benveniste H (2013) Brain-wide pathway for waste clearance captured by contrast-enhanced MRI. J Clin Invest 123(3):1299–1309. doi:10.1172/JCI67677

149. Jost G, Frenzel T, Lohrke J, Lenhard DC, Naganawa S, Pietsch H (2017) Penetration and distribution of gadolinium-based contrast agents into the cerebrospinal fluid in healthy rats: a potential pathway of entry into the brain tissue. Eur Radiol 27(7):2877–2885. doi:10.1007/s00330-016-4654-2

150. Gaberel T, Gakuba C, Goulay R, Martinez De Lizarrondo S, Hanouz J-L, Emery E, Touze E, Vivien D, Gauberti M (2014) Impaired glymphatic perfusion after strokes revealed by contrast-enhanced MRI: a new target for fibrinolysis? Stroke 45(10):3092–3096. doi:10.1161/STROKEAHA.114.006617

151. Zamani A, Walker AK, Rollo B, Ayers KL, Farah R, O'Brien TJ, Wright DK (2022) Impaired glymphatic function in the early stages of disease in a TDP-43 mouse model of amyotrophic lateral sclerosis. Transl Neurodegener 11(1):17. doi:10.1186/s40035-022-00291-4

152. Kosel F, Pelley JMS, Franklin TB (2020) Behavioural and psychological symptoms of dementia in mouse models of Alzheimer's disease-related pathology. Neurosci Biobehav Rev 112:634–647. doi:10.1016/j.neubiorev.2020.02.012

153. Yamazaki Y, Kanekiyo T (2017) Blood-Brain Barrier Dysfunction and the Pathogenesis of Alzheimer's Disease. Int J Mol Sci 18(9). doi:10.3390/ijms18091965

154. de Paula GC, Brunetta HS, Engel DF, Gaspar JM, Velloso LA, Engblom D, Oliveira J de, Bem AF de (2021) Hippocampal Function Is Impaired by a Short-Term High-Fat Diet in Mice: Increased Blood-Brain Barrier Permeability and Neuroinflammation as Triggering Events. Front Neurosci 15:734158. doi:10.3389/fnins.2021.734158

9. Anhang: Abkürzungsverzeichnis

%ID/ml	prozentuale injizierte Dosis pro ml
AD	Alzheimersche Erkrankungen (von engl. Alzheimer´s disease)
AL	ad libitum
APP	Amyloid-Precursor-Protein
Aβ	Amyloid β
BHS	Blut-Hirn-Schranke
CSF	cerebrospinale Flüssigkeit
DIO	Diät-induzierte Adipositas (engl. diet-induced obesity)
EPM	erhöhtes Plus-Labyrinth (engl. Elevated Plus Maze)
GBCA	Gadoliniumkontrastmittel (engl. gadolinium-based contrast agents)
GFAP	Glia-fibrilläres saures Protein (von engl. glial fibrillary acidic protein)
HFD	Hoch-Fett-Diät
Iba1	ionisiertes kalziumbindendes Adaptermolekül 1
IF	Intervallfasten
IL	Interleukin
ISF	interstitielle Flüssigkeit
KD	fettarme und kohlenhydratreiche Kontrolldiät
KR	Kalorienrestriktion
LALLF	Landesamt für Landwirtschaft, Lebensmittelsicherheit und Fischerei
LBT	Laufbandtraining
MCI	leichte kognitive Beeinträchtigungen (engl. mild cognitive impairment)
MRS	Magnetresonanzspektroskopie
MRT	Magnetresonanztomographie
MWM	Morris-Water-Maze-Test
ob/ob	Leptin-defizient
OF	offenes-Feld Test
PET	Positronen-Emissions-Tomographie
PS	Presenilin
Ri	Ramifikations-Index
SD	standardisiert-ausgewogene Makronährstoffdiät
$SUV_{glc,c}$	korrigierter standardisierter Aufnahmewert (engl. standardized uptake value)
tg	transgen
TMEM119	Transmembranprotein 119
TNF-α	Tumornekrosefaktor-α
VOI	Volume of Interest
wt	Wildtyp
ZNS	zentrales Nervensystem

10. Anhang: Veröffentlichte Originalarbeiten

10.1 Studie 1

biomedicines

MDPI

Article

Dietary-Induced Low-Grade Inflammation in the Liver

Nicole Power Guerra [1], Luisa Müller [1,2], Kristin Pilz [3], Annika Glatzel [1], Daniel Jenderny [1], Deborah Janowitz [3], Brigitte Vollmar [1] and Angela Kuhla [1,*]

1 Rudolf-Zenker-Institute for Experimental Surgery, Medical University Rostock, 18057 Rostock, Germany; nicole.guerra@uni-rostock.de (N.P.G.); luisa.mueller2@uni-rostock.de (L.M.); annika.glatzel@uni-rostock.de (A.G.); daniel.jenderny@uni-rostock.de (D.J.); brigitte.vollmar@med.uni-rostock.de (B.V.)
2 Department of Psychosomatic Medicine and Psychotherapy, University of Rostock, 18147 Rostock, Germany
3 Department of Psychiatry, University of Greifswald, 17489 Greifswald, Germany; kristin.pilz@med.uni-greifswald.de (K.P.); deborah.janowitz@med.uni-greifswald.de (D.J.)
* Correspondence: angela.kuhla@uni-rostock.de; Tel.: +49-381-494-2503

Received: 19 October 2020; Accepted: 7 December 2020; Published: 9 December 2020

check for updates

Abstract: The literature describes a close correlation between metabolic disorders and abnormal immune responses, like low-grade inflammation (LGI), which may be one mechanistic link between obesity and various comorbidities, including non-alcoholic fatty liver disease (NAFLD). In our study, we investigated the influence of dietary composition on obesity-derived LGI in the liver. We used a dietary induced obesity mouse model of C57BL/6J mice fed with high fat diet (HFD, 60% fat, 20% protein, 20% carbohydrates) and two different controls. One was rich in carbohydrates (10% fat, 20% protein, 70% carbohydrates), further referred to as the control diet (CD), and the other one is referred to as the standard diet (SD), with a more balanced macronutrient content (9% fat, 33% protein, 58% carbohydrates). Our results showed a significant increased NAFLD activity score in HFD compared to both controls, but livers of the CD group also differed in their macroscopic appearance from healthy livers. Hepatic fat content showed significantly elevated cholesterol concentrations in the CD group. Histologic analysis of the cellular immune response in the liver showed no difference between HFD and CD and expression analysis of immunologic mediators like interleukin (IL)-1β, IL-6, IL-10 and tumor necrosis factor alpha also point towards a pro-inflammatory response to CD, comparable to LGI in HFD. Therefore, when studying diet-induced obesity with a focus on inflammatory processes, we encourage researchers to carefully select controls and not use a control diet disproportionally rich in carbohydrates.

Keywords: high fat diet; control diet; non-alcoholic fatty liver disease; liver inflammation; low-grade inflammation

1. Introduction

Abnormal and excessive accumulation of adipose tissue in the context of severe overweight and obesity is one of the most challenging diseases of the 21st century. This is primarily due to the steadily increasing number of obese patients who are getting younger and younger [1]. In addition to a wide variety of cultural and social influences and a lack of exercise, a permanent oversupply of food rich in calories, and mostly also in fat, leads to weight gain with serious health issues.

As a consequence, obesity is one of the leading causes of the metabolic syndrome, which was described in 1989 by Kaplan [2]. The metabolic syndrome is associated with many other diseases [3,4] including non-alcoholic fatty liver disease (NAFLD), which is seen as the hepatic manifestation of

it [5]. One assumed reason for the prevalence of NAFLD and many other concomitant and secondary diseases of obesity is the persistence of systemic low-grade inflammation (LGI), starting from adipose tissue. However, there is no strict definition of LGI. In general, dietary-induced LGI is a sterile inflammation, which has also been given the name "metaflammation" (an inflammation of metabolic tissue) [3], which is highly entwined with immunometabolism [6]. Since the LGI differs in its triggering mechanisms from an infectious inflammation, both also likely differ in their consequences. While infectious inflammation in its physiological function triggers an immune response of the organism, sterile inflammation has predominantly pathological consequences, e.g., via the alteration of homeostatic checkpoints and the development of autoinflammatory disorders [7].

Interestingly, a close correlation between metabolic diseases and abnormal immune responses such as LGI is observed [3,8]. White adipose tissue is capable of expressing both, metabolic and immunological mediators [9], whose effects are not only local but can affect other organs like the liver or have a systemic impact. This is also shown by a generalized moderate upregulation of pro-inflammatory signaling cascades in overweight and obesity. Important mediators in this context include interleukin (IL)-1β, IL-6 and tumor necrosis factor alpha (TNFα) [10–12]. Moreover, a downregulation of anti-inflammatory mediators such as IL-10 has been reported [12]. All of the above mentioned mediators take part in well-orchestrated and tightly regulated signaling cascades and derailments of them may be responsible for a LGI-mediated interaction between obesity and NAFLD [13,14]. However, which long-term influences in the diet are present, defined as at least 6 months of corresponding diet, on obesity-derived LGI in the liver has not yet been investigated in detail in mice.

A diet-induced obesity mouse model consisting of a 60% high fat diet (HFD) is used in this project to observe the effects of obesity-derived LGI on the liver. As an additional approach, we wanted to investigate the impact of dietary composition of two different low-fat controls on the liver, with a special focus on LGI. One control group received the HFD-manufacturers recommended control diet (CD), broadly used in research [15–18]. This CD matches the HFD regarding sucrose content (as a percent of calories) and fiber structure but has generally a high carbohydrate content and in particular a high starch content ([19]; Product Data—DIO Series Diets, Research Diets Inc., Lane, NJ, USA). As the literature hints towards the role of carbohydrate-rich diets as promotors of systemic LGI, e.g., by oxidative stress induction [20,21], it would be of high interest to have a closer look if this mechanism affects the liver as well. In contrast, the literature suggests that protein-rich diets have anti-inflammatory effects and also reduce liver fat [22], which is an important note when considering studying dietary-induced effects of LGI on the liver. Therefore, the other control group received the in-house standard diet (SD) with matched calorie content to CD but lower carbohydrate content and increased protein content compared to CD and HFD.

2. Experimental Section

2.1. Animal Models

For the experiments, female C57BL/6J mice at the age of 4 weeks were purchased from Charles River (Sulzfeld, Germany). In compliance with our own previous and ongoing investigations, female mice were used for comparability between different studies. Mice were kept in standard cages with 4 to 5 animals per cage, in a temperature controlled room (21 ± 3 °C) with a 12/12 h day-night cycle (lights on from 06:00 am to 06:00 pm CET) containing a twilight period of 30 minutes. The mice were blindly divided into three groups, which were fed different diets and water supply ad libitum over a period of 6 months. After one week of acclimatization, the food was adjusted to the corresponding diet, with designated compositions shown in Figure 1. One group received an HFD (D12492; Research Diets Inc., Lane, NJ, USA), hereinafter referred to as the HFD group (n = 31). The other group received the recommended CD (D12450J; Research Diets Inc., Lane, NJ, USA), hereinafter referred to as the

CD group (n = 16). The third group received SD (ssniff® R/M-H, ssniff Spezialdiäten GmbH, Soest, Germany) and is hereinafter referred to as the SD group (n = 15).

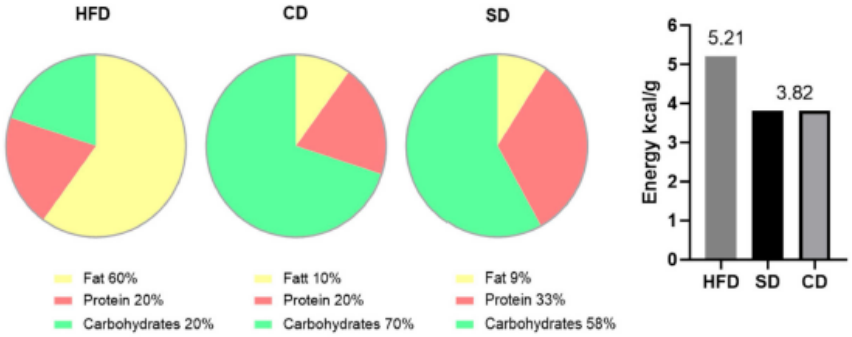

Figure 1. Composition of high fat diet (HFD), control diet (CD) and standard diet (SD) in % of total calories and energy density in kcal/g.

All animal experimental work was carried out with permission of the local Animal Research Committee (Landesamt für Landwirtschaft, Lebensmittelsicherheit und Fischerei (LALLF)) of the state Mecklenburg-Western Pomerania (LALLF M-V/TSD/7221.3-2-001/18, approved on 1 March 2018) and all animals received human care according to the EU Directive 2010/63/EU.

2.2. Blood Sampling and Tissue Preparation

Mice were anaesthetized with 5 vol.% isoflurane (Baxter, Unterschleißheim, Germany), 0.8 L/min O_2 (Air Liquide, Hamburg, Germany) and 1.25 L/min N_2O (Air Liquide, Hamburg, Germany) and blood was taken retrobulbary to exsanguinate the mice. Blood samples were kept at 4 °C until plasma preparation the same day. Therefore, samples were centrifuged at 1200 rpm and 6 °C for 10 min (Centrifuge 5424, Eppendorf, Leipzig, Germany) and supernatant was collected and stored at −80 °C. Then, mice were transcardially perfused with 20–25 mL 0.9% NaCl (Braun, Melsungen Germany) with an estimated flow rate of 2.28–2.83 mL/min. For histological and immunohistochemical analysis, the left lateral liver lobe was dissected and fixed in 4% paraformaldehyde (PFA, ChemCruz, Dallas, TX, USA) solution for five days, embedded in paraffin (Carl Roth, Karlsruhe, Germany) and sectioned in 4 µm thin tissue slices. For molecular analysis, the remaining liver was homogenized and snap frozen in liquid nitrogen and stored at −80 °C.

2.3. Biochemistry

Directly after blood collection, blood sugar concentration in the naive blood sample was assessed with the glucose meter Contour®XT (Bayer, Leverkusen, Germany) according to the manufacturer´s instructions. In the stored plasma samples, aspartate aminotransferase (AST) and alanine aminotransferase (ALT) activities were measured spectrophotometrically as indicators of hepatocellular disintegration and necrosis. The extinction at 340/378 nm was measured with the cobas®c111Analyzer (Roche Diagnostics GmbH, Penzberg, Germany). Measurement of plasma triglycerides was performed using Triglyceride Colorimetric Assay Kit (Nr.: 10010303, Cayman Chemical Company, Hamburg, Germany) according to the manufacturer's instructions. Results are provided in the Supplementary Materials (Table S1).

2.4. Histology, Immunohistochemistry and Image Analysis

Hematoxylin (Merck, Darmstadt, Germany) and eosin (Merck, Darmstadt, Germany) (H&E) staining was performed using standard protocols. Pictures were recorded on a microscope type BX51 with a Color View Soft Imaging System and the corresponding software cellSens Standard 1.14 (all from Olympus, Hamburg, Germany).

From the H&E stained specimens, analyses of tissue content of microvesicular fat was performed using the public domain image analysis software ImageJ (v.1.47) (protocol provided in the supplements as ImageJ Code S1). Furthermore, a NAFLD Activity Score (NAS) was generated to characterize diet-induced liver damage. Following the description by Kleiner et al. [23], the parameters steatosis (score 0–3), hepatocellular ballooning (score 0–2) and lobular inflammation (score 0–3) were used to calculate NAS (total score 0–8). Steatosis was assessed at 50× magnification and ballooning at 100× magnification. Inflammation was assessed by counting inflammatory foci from 20 representative low-power fields (LPF) (200× magnification) with an inflammatory focus characterized as a grouping of at least five inflammatory cells in the tissue, which are not arranged in a row [24]. Examples for the different assigned scores are provided as representative images in the supplements (Figure S1).

For assessment of tissue infiltration of granulocytes as another hallmark of manifestation of LGI in the liver, sectioned paraffin-embedded liver tissue was stained for chloracetate esterase (CAE) with Naphthol AS-D chloroacetate (Sigma-Aldrich, Darmstadt, Germany) and counterstained with hematoxylin (Merck, Darmstadt, Germany). For quantification, the total number of hepatocytes and CAE positive cells (CAE^+) was counted in 20 consecutive high-power fields (HPF) at 400× magnification.

As a second cellular indicator for LGI in the liver, macrophages were stained immunohistochemically. Therefore, overnight incubation (4 °C) with the first antibody (rat anti mouse-F4/80 [MCA497] from Bio-Rad, Hercules, CA, USA) was followed by 1 h incubation at room temperature with the secondary antibody (goat anti rat [MCA497] from Bio-Rad, Hercules, CA, USA) stained with the chromogen Permanent Red (Ref. K0640, DAKO GmbH, Jena, Germany) and counterstained with hematoxylin (Merck, Darmstadt, Germany). For quantification, the total number of hepatocytes was counted in 20 consecutive HPF at 400× magnification and semiautomatic quantification of F4/80 positive cells ($F4/80^+$) was performed via ImageJ (protocol provided in the supplements as ImageJ Code S2).

2.5. Cholesterol Assay

For assessment of hepatic cholesterol content, Cholesterol Quantitation Kit (Calbiochem®, Merck, Darmstadt, Germany) was performed according to manufacturer instructions from 30 µg snap frozen liver tissue.

2.6. Quantitative Real-Time PCR

RNA isolation from snap frozen liver tissue was performed with RNeasy Mini Kit (Qiagen, Venlo, The Netherlands) according to the manufacturer's instructions. RNA integrity was verified by agarose gel electrophoresis and RNA concentration was assessed by absorption measurement with NanoDrop (Thermo Fisher Scientific, Waltham MA, USA). Isolated RNA was transcribed into cDNA with SuperScript™ (Invitrogen, Thermo Fisher Scientific, Waltham MA, USA) and deoxyribonucleosidtriphosphates (Thermo Fisher Scientific, Waltham, MA, USA) were added. Cytokine analyses were performed via quantitative real-time PCR in a BioRad iQ5 Multicolor Real Time PCR Detection System (Conquer Scientific, San Diego, CA, USA) with iQ™ SYBR® Green Supermix (Bio-Rad, Hercules, CA, USA). Primer sequences are shown in Table 1. Measurement results are corrected against the housekeeping gene 40S ribosomal protein S18 (RPS18) and relative quantification was carried out by usage of the $2^{-\Delta\Delta CT}$ method.

2.7. Statistical Analysis

Statistical analysis was performed using GraphPad Prism 8.0.1 (GraphPad Software Inc., San Diego, CA, USA). Data were checked for normality with the Kolmogorov–Smirnov test (for scoring data) or Shapiro–Wilk test and variances of ANOVA were verified by Bartlett's test. If SDs were not significantly different with $p > 0.05$, an ordinary one-way ANOVA was performed followed by Turkey post hoc test, otherwise Brown–Forsythe and Welch ANOVA followed by Tamhane's T2 multiple comparisons test was performed. If data were not normally distributed, the Kruskal–Wallis test with Dunn's post

hoc test for multiple comparisons was conducted. Data are presented as mean ± standard deviation and statistical significance was set at $p < 0.05$. The ROUT method based on the false discovery rate (Q = 0.01) was used to identify and remove outliers if possible and necessary. For further details, see figure legends.

Table 1. Primers used for quantitative real-time PCR.

Primer	Orientation	Sequence
RPS18	Forward	5′-AGGATGTGAAGGATGGGAAG-3′
	Reverse	5′-TTGGATACACCCACAGTTCG-3′
TNFα	Forward	5′-ACATTCGAGGCTCCAGTGAATTCGG-3′
	Reverse	5′-GGCAGGTCTACTTTGGAGTCATTGC-3′
IL-1β	Forward	5′-CCCAAGCAATACCCAAAGAA-3′
	Reverse	5′-TTGTGAGGTGCTGATGTACCA-3′
IL-6	Forward	5′-TCTGACCACAGTGAGGAATGTCCAC-3′
	Reverse	5′-TGGAGTCACAGAAGGAGTGGCTAAG-3′
IL-10	Forward	5′-GCCTTGCAGAAAAGAGAGCT-3′
	Reverse	5′-AAAGAAAGTCTTCACCTGGC-3′

3. Results

3.1. Dietary Impact on Body and Liver Weight

After feeding the mice their respective diet for 6 months, their body weight was measured and liver tissue was collected for further analysis. Animals are shown as representative images (Figure 2a). Analysis of body weight revealed significantly elevated values in the HFD group (Figure 2b, $p < 0.0001$ vs. CD and SD group). Body weight did not differ between the CD and SD group (Figure 2b).

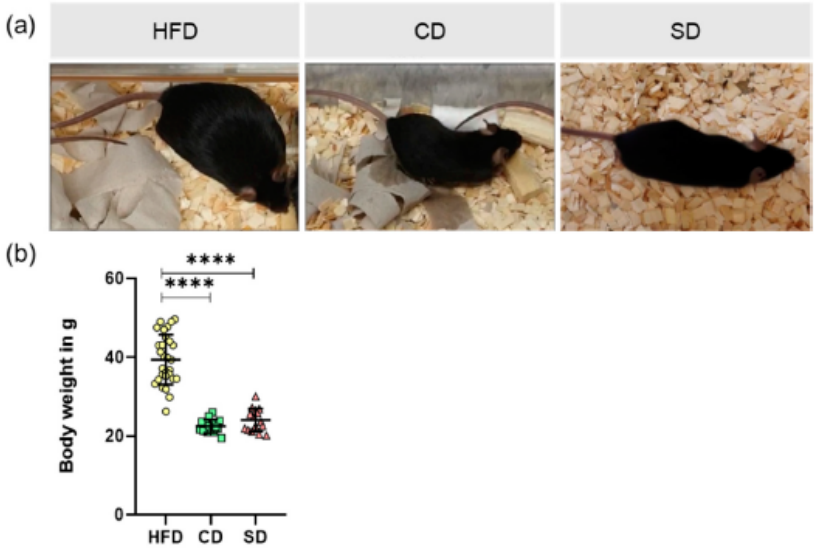

Figure 2. (**a**) Representative images of appearances from mice fed high fat diet (HFD), control diet (CD) or standard diet (SD); (**b**) Body weights of mice in the different groups (HFD: $n = 29$; CD: $n = 15$, SD: $n = 15$), presented as mean ± standard deviation. Significance of differences between the groups was tested by Brown–Forsythe and Welch ANOVA, **** $p < 0.0001$.

Macroscopic appearances of the livers in situ are shown as representative images (Figure 3a). While dissecting the liver, we noticed a visual deviation of both the HFD and CD group to a healthy looking liver as displayed by the SD group. Analysis of liver weight again revealed significantly elevated values in the HFD group (Figure 3b) ($p < 0.0001$ vs. CD group and $p = 0.013$ vs. SD group) and no significant difference between the CD and SD group.

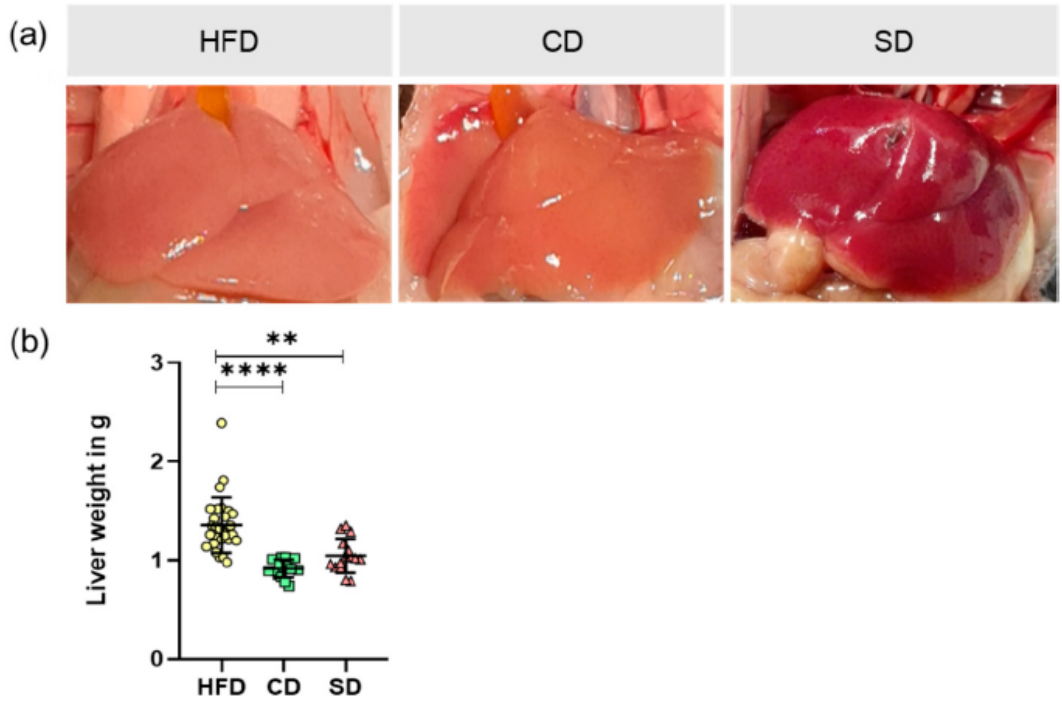

Figure 3. (**a**) Representative in situ images of mice livers from mice fed high fat diet (HFD), control diet (CD) or standard diet (SD); (**b**) Liver weight of the different groups (HFD: $n = 29$; CD: $n = 15$, SD: $n = 15$) presented as mean ± standard deviation. Significance of differences between the groups was tested by one-way ANOVA on Ranks (Kruskal–Wallis); **** $p < 0.0001$, ** $p < 0.01$.

3.2. Dietary Induced Liver Steatosis

The basis for the increased liver weight is probably diet-induced liver steatosis. To analyze this parameter, the microvesicular liver fat content was determined in H&E stained tissue, with representative images shown in Figure 4a. Liver tissue of the HFD group showed excessive macro- and microvesicular fat deposits. In addition, in liver tissue of the CD group, fat depots, mostly microvesicular, were found. Image analysis led to a significantly higher fat quantity in HFD compared to the CD and SD group (Figure 4b, $p = 0.0007$ vs. CD group and $p < 0.0001$ vs. SD group) but not between the SD and CD group. Tissue fat content alone therefore did not serve as an explanation for the macroscopically observed brightening of livers of the CD group. Subsequently we found that in the livers of the CD group, the amount of hepatic cholesterol was significantly higher than in the HFD group ($p = 0.024$) but not in the SD group (Figure 4c).

As an additional parameter to assess the impact of the different diets on the liver, we calculated the NAS for the different groups, according to exemplary scoring in Supplement Figure S1. Fat deposits (representative images shown in Figure 5a) in the HFD group indicated pathological changes in all liver samples. The HFD group, with mostly a score of 2, showed a significantly higher liver steatosis than the CD and SD group (Figure 5b), both $p < 0.0001$) with a score mostly between 0 and 1. The CD group did not differ significantly from the SD group, which is in line with the above shown quantification of liver fat. The SD group constantly showed a score of 0 in all samples, which corresponds to a healthy

liver. As a second parameter for the NAS, ballooning, a form of cell injury and death through fat accumulation, was assessed (Figure 5a). In all our samples, none of the hepatocytes showed ballooning injury to any extent, therefore score 2 was not assigned once. As some samples showed a few ballooned hepatocytes in the HFD group, represented by a score of 1, the scoring was significantly higher than in the CD and SD groups (Figure 5b), $p < 0.0001$) as there were no ballooned cells observed in the livers of the low-fat diets, assigned to score 0. The third parameter to calculate NAS is lobular inflammation (Figure 5a). In all samples, no massive inflammation of liver tissue, assigned to score 3, was found. With 2–4 inflammatory foci per LPF, a stout inflammation, defined as score 2, could be seen in a few livers of the HFD group. Interestingly, when it comes to inflammation, there was only a significant difference between the HFD and SD group (Figure 5b), $p = 0.003$) but not between the HFD and CD group. In the overall result, the examined parameters steatosis, ballooning and inflammation contributed to the NAS result with significantly higher values in the HFD group compared to the CD and SD group (Figure 5b), $p < 0.0001$ vs. CD and SD group). This hints toward a damaging effect of the HFD on the liver.

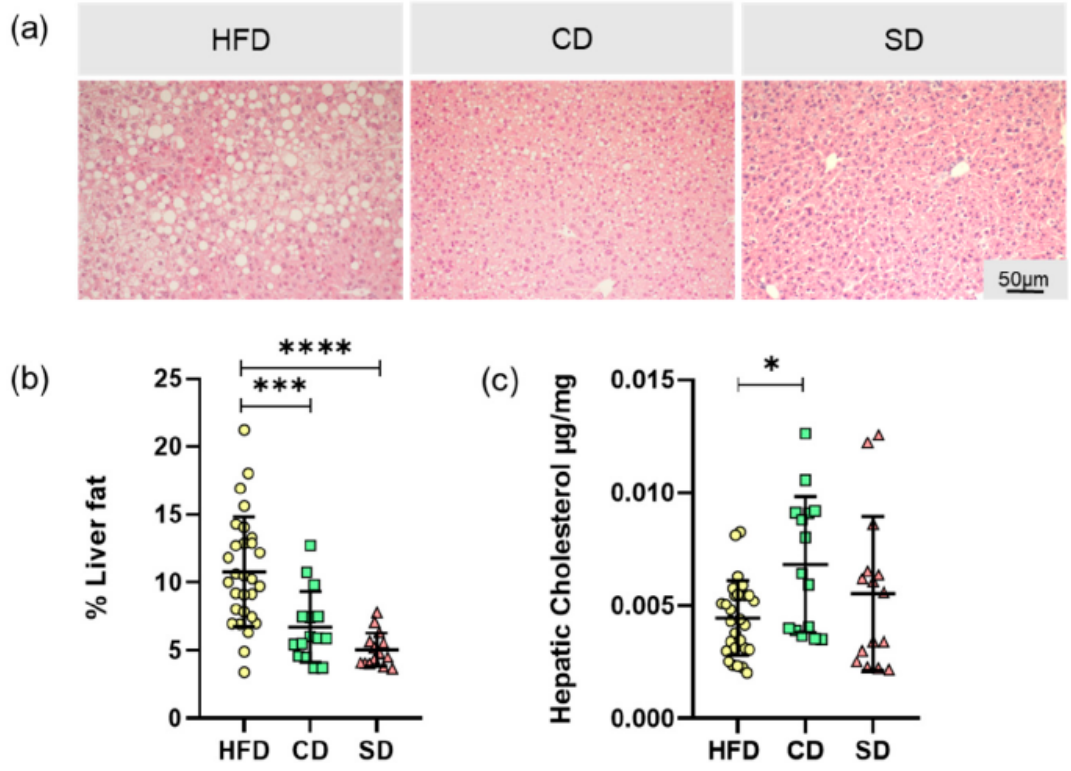

Figure 4. (**a**) Representative LPFs of the livers from mice fed high fat diet (HFD), control diet (CD) or standard diet (SD) (200× magnification, scale bar representing 50 µm valid for all three images); (**b**) Percentage of hepatic vesicular fat content; (**c**) Hepatic cholesterol concentration of the HFD, CD and SD group. Data (HFD: $n = 29$; CD: $n = 15$, SD: $n = 15$) presented as mean ± standard deviation. Significance of differences between the groups was tested by Brown–Forsythe and Welch ANOVA in (**b**) or one-way ANOVA on Ranks (Kruskal–Wallis) in (**c**); **** $p < 0.0001$, *** $p < 0.001$, * $p < 0.05$.

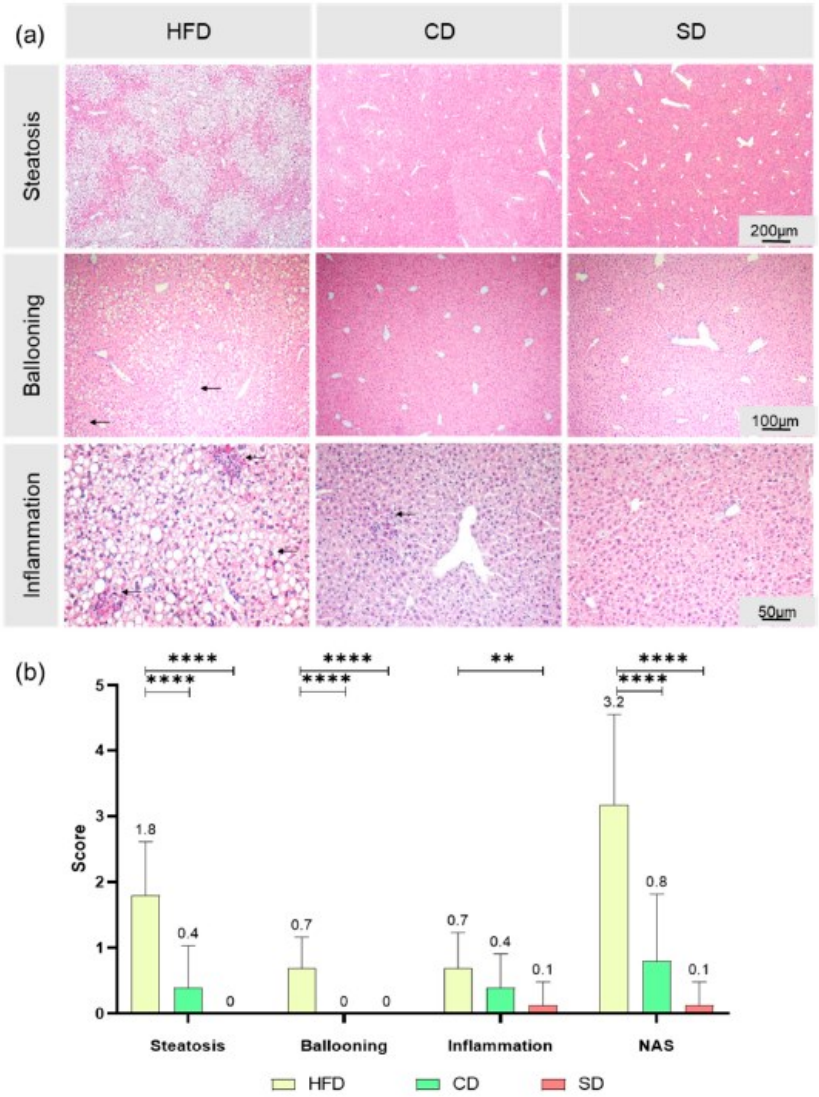

Figure 5. (**a**) Representative images of steatosis (50× magnification, scale bar represents 200 µm valid for all three images), ballooning (100× magnification, scale bar representing 100 µm valid for all three images) with black arrows indicating damaged cells, and inflammation (200× magnification, scale bar representing 50 µm valid for all three images) with black arrows indicating inflammatory foci in livers from mice fed high fat diet (HFD), control diet (CD) or standard diet (SD); (**b**) Assessments of scores for steatosis, ballooning and inflammation as well as calculation of NAS for the groups (HFD: $n = 29$; CD: $n = 15$, SD: $n = 15$). Data presented as mean ± standard deviation. Significance of differences between the groups was tested by one-way ANOVA on Ranks (Kruskal–Wallis); **** $p < 0.0001$, ** $p < 0.01$.

3.3. Dietary-Induced LGI in the Livers of the HFD Group and CD Group

As already indicated by macroscopy changes in the livers of the CD group, potential pathogenic effects of the carbohydrate rich diet emerged, and only a significant difference between the HFD and SD group was observed when scoring lobular inflammation in the NAS assessment. Thus, we chose to gain a more in-depth look into LGI processes in the liver. Therefore, we analyzed the cellular immune reaction by quantification of CAE^+ and $F4/80^+$ cells in the liver, relativized to the total number of

hepatocytes per HPF (Figure 6a). The data we obtained substantiate the results from inflammation scoring in NAS, again showing a significant difference between the HFD and SD group (Figure 6b), CAE$^+$: $p = 0.0003$, Figure 6c), F4/80$^+$: $p = 0.0002$,) but not between the HFD and CD group. Additionally, in both analyses, there was a significant difference between both controls (Figure 6b), CAE$^+$: $p < 0.0001$, Figure 6c), F4/80$^+$: $p = 0.006$). In conclusion, compared to the SD group, the CD group had significantly increased amounts of immune cells in the liver.

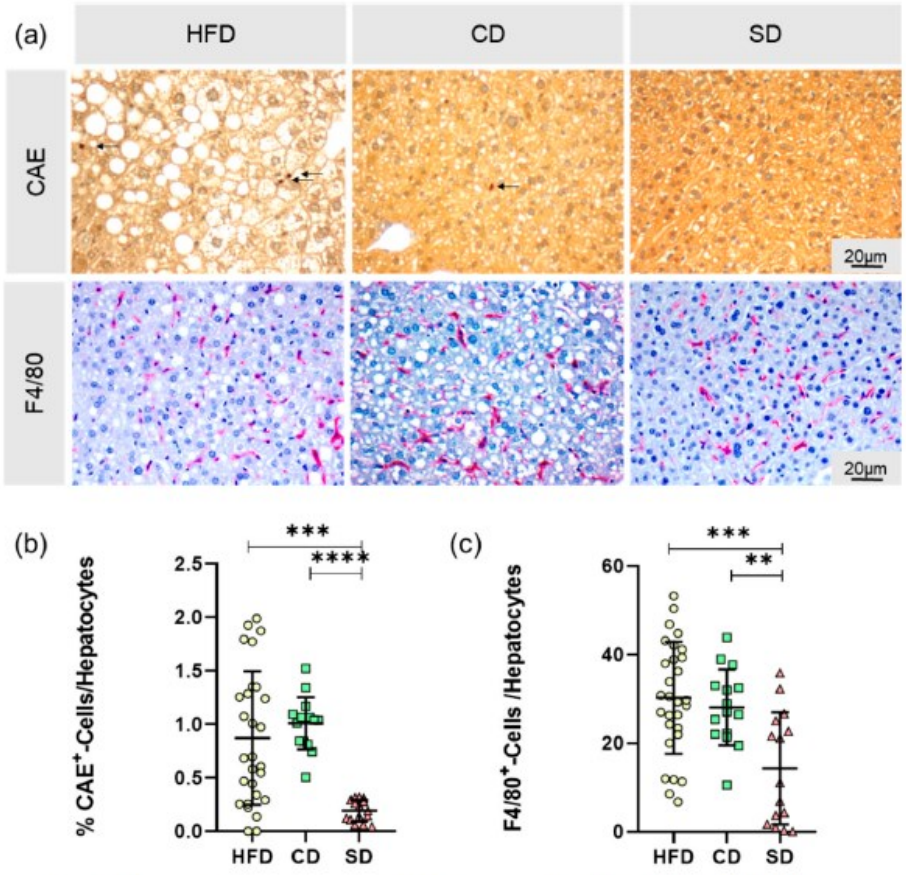

Figure 6. (**a**) Representative images of CAE-staining with CAE$^+$-cells indicated by arrows and F4/80-staining with F4/80$^+$-cells stained in red (both at 400× magnification, scale bar representing 20 µm valid for all images) of livers from mice fed high fat diet (HFD), control diet (CD) or standard diet (SD); (**b**) Relative amount of granulocytes (CAE$^+$) (HFD: $n = 28$; CD: $n = 15$, SD: $n = 15$); (**c**) Relative amount of macrophages (F4/80$^+$) (HFD: $n = 29$; CD: $n = 15$, SD: $n = 15$). Data presented as mean ± standard deviation. Significance of differences between the groups was tested by one-way ANOVA on Ranks (Kruskal–Wallis) in (**b**) or ordinary one-way ANOVA in (**c**); **** $p < 0.0001$, *** $p < 0.001$ ** $p < 0.01$.

In addition to the cellular immune response, we investigated the humoral immune response in liver LGI. As one of the most important synthesis organs, the liver is able to produce many immunogenic mediators. For quantification of the pro-inflammatory cytokines IL-1β, IL-6 and TNFα as well as the anti-inflammatory IL-10, hepatic RNA expression was evaluated by quantitative real-time PCR (Figure 7a–d)). The IL-1β levels in the CD group were significantly lower than in the HFD ($p < 0.0001$) and SD group (Figure 7a), $p < 0.0001$ vs. HFD group, $p = 0.0021$ vs. SD group). This was astonishingly reverted for IL-6 levels where we saw a significant increase in comparison to the HFD and SD group (Figure 7b), $p = 0.0106$ CD vs. HFD group, $p = 0.0124$ CD vs. SD group). Only TNFα values were as expected highest in the HFD group, which was significant compared to SD (Figure 7c), $p = 0.0052$)

but not to the CD group. In addition, a significant elevation of TNFα expression in the CD group compared to the SD group (Figure 7c), $p = 0.005$) was found. For IL-10, we found significantly increased expression when comparing the HFD and CD group with the SD group (Figure 7d), $p = 0.0136$ HFD vs. SD and $p = 0.0275$ CD vs. SD). The results depicting overall a heterogeneous effect of LGI on cytokine expression, but of note, the CD and SD group always differed significantly.

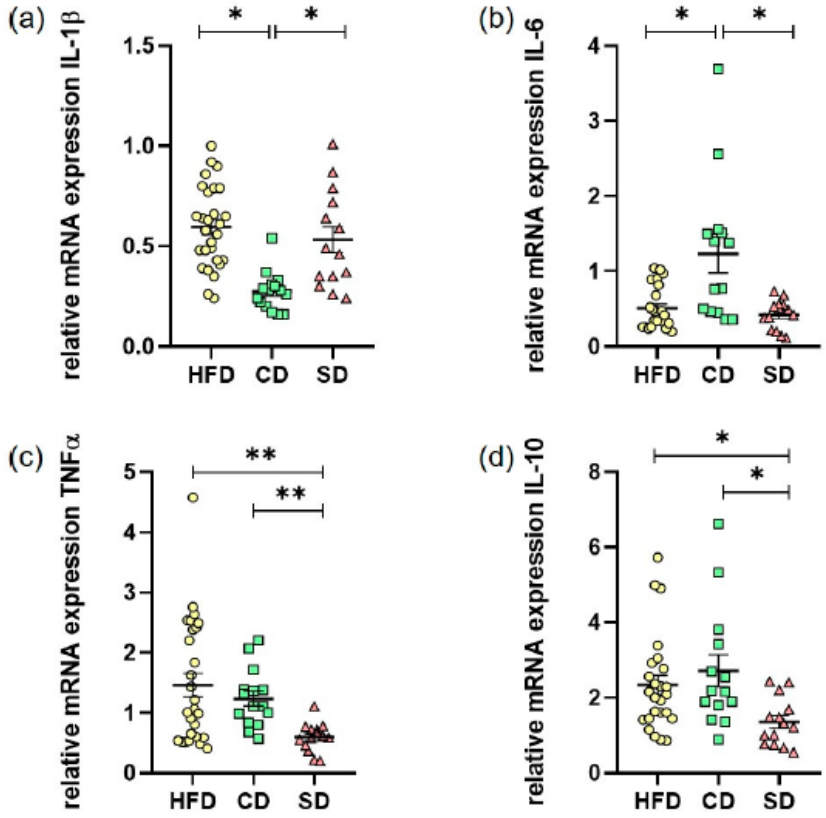

Figure 7. (**a**) Hepatic mRNA expression in the high fat diet (HFD), control diet (CD) or standard diet (SD) group of IL-1β (HFD: $n = 28$, CD: $n = 14$, SD: $n = 14$); (**b**) Hepatic mRNA expression of IL-6 (HFD: $n = 24$, CD: $n = 15$, SD: $n = 14$); (**c**) Hepatic mRNA expression of TNFα (HFD: $n = 28$, CD: $n = 15$, SD: $n = 14$); (**d**) Hepatic mRNA expression of IL-10 (HFD: $n = 25$, CD: $n = 15$, SD: $n = 14$). Data presented as $2^{-\Delta\Delta Ct}$ values determined by quantitative real-time PCR; Data presented as mean ± standard deviation. Significance of differences between the groups was tested by ordinary one-way ANOVA in (**a**) or one-way ANOVA on Ranks (Kruskal–Wallis) in (**b**),(**c**) and(**d**) or; ** $p < 0.01$, * $p < 0.05$.

4. Discussion

Obesity is not merely a health risk itself, but often associated with other concomitant and secondary diseases [3,4,25]. It has become a serious disease of the 21st century due to its steadily increasing prevalence [1], and therefore is of great interest to study underlying disease mechanisms. One mechanism believed to contribute to disease progression is dietary-induced LGI starting from adipose tissue and later also becoming systemic and manifesting in other organs like the liver [26]. This is explainable by the close phylogenetic relationship between the liver and adipose tissue as well as the immune and hematopoietic system, which have evolved from formerly common structures [3]. In humans, as well as in many other mammals, hepatocytes and adipocytes are in close proximity to immune cells and have unhindered access to blood vessels [27–29]. Assuming that within the

framework of the common evolutionary lineage, common signaling molecules and pathways have also been conserved.

To draw more detailed conclusions of dietary effects on liver LGI, a diet-induced obesity mouse model was used in this study. We chose a HFD model to map the development of obesity and especially inflammation. Due to a diet rich in calories and fat, C57BL/6J mice on HFD show a diet-induced obesity phenotype mirroring the situation in obese humans in western industrial countries [30]. The induction of obesity by such a model is usually less artificial and therefore findings are better translatable to humans. This is especially the case because corresponding genotypes of genetically obese mice models like Lep^{ob} /Lep^{ob} mice or mice with tubby gene mutations [31,32] are rarely found in humans.

In our work, we aimed to investigate the dietary impact on effects of obesity-derived LGI in the liver. With our experimental approach, we were able to show an adverse effect of HFD on the liver, represented mainly through an elevated NAS. Surprisingly, when looking especially on LGI processes, the carbohydrate-rich control diet also exacerbated the pro-inflammatory response in the liver.

In terms of assessing dietary effects on mice, body and liver weights of the animals were determined. As expected, mice of the HFD group had significantly increased body and liver weights, whereas the values of the CD and SD group were at the lower limit of the age- and sex-specific normal range [33]. The reason for the increased body and liver weights is diet-induced fat accumulation, examined by analysis of liver fat content as well as determination of hepatic cholesterol. Mice of the HFD group showed significantly increased liver fat content of more than 10%, whereas both the controls were in the same range of liver fat content as healthy mice, which is about 5–8% [24,34].

Contrary to this finding, the hepatic cholesterol assay revealed a significantly increased cholesterol content in the CD group. Cholesterol has lipotoxic effects, mainly mediated by the induction of oxidative stress, which are able to activate pro-inflammatory signaling pathways and thus lead to NAFLD progression, even in lean individuals [35]. This provides a possible explanation for macroscopically observed pathological changes in the livers of the CD group. Therefore, in our experiments, the liver of the CD group with normal liver fat-content but high cholesterol showed a liver LGI equal to mice fed with HFD, which is comparable to previous results of HFD vs. carbohydrate-rich diet [36]. We suggest that starch is the main mediator of the elevated cholesterol content and the pro-inflammatory effects seen in the CD group, which is in line with results of Duwaerts et al. [37], describing a pathogenic effect of diets rich in starch on the liver, independent of calories and nutrient proportions [37]. From a nutritional point of view, CD as well as HFD are rich in lards, contributing to a pro-inflammatory profile [38] in both groups. Additionally, a high carbohydrate amount in the CD also contributes to that [20,21], whilst an elevated protein content, such as in the SD group, exerts more anti-inflammatory effects [22].

To explore the dietary effect on the mice livers in depth, they were histologically processed and analyzed according to aspects that are relevant in NAFLD diagnostics [23,24]. The NAS, created within the scope of evaluation, showed a more than fourfold increase in the HFD group compared to the CD and SD group, mainly due to steatosis. In the HFD group, this indicates the beginning and progression of NAFLD, described in the literature as an organic manifestation of the metabolic syndrome [5]. This damaging effect on the livers also became apparent by significantly increasing ALT and AST plasma values in the HFD group (Supplementary Materials Table S1). A persistent LGI may be a mechanistic link between obesity and the various comorbidities, such as NAFLD. There is strong evidence from the literature that obesity exerts an influence on the immune system and manifests itself as a condition of chronic LGI [11,39]. LGI is triggered or promoted by intrinsic stress factors, tissue dysfunction and changes in homeostatic checkpoints, which commonly occur in obesity [7]. The expression and characterization of a liver manifestation of LGI, triggered by HFD-induced obesity, were therefore another focus of the experiments.

Further characterization of obesity-associated LGI in the liver focused on the local cellular immune response. Cell damage induced in the context of NAFLD can lead to reduced liver function [40] with extensive consequences on the hepatic synthesis performance. In addition to inflammatory foci in the liver, assessed by NAFLD scoring, the number of granulocytes and the number of macrophages was

determined. Due to the heterogeneity of the macrophage population in the liver, we only counted F4/80+ cells, mainly consisting of tissue resident Kupffer cells and macrophages recruited from the bloodstream [41]. In the calculated ratios of both granulocytes and macrophages to the number of hepatocytes, significantly increased values were observed in the HFD group as well as in the CD group. Not only mature macrophages were attracted from the bloodstream, but also myeloid progenitor cells through a closely regulated interaction of genes for chemokines, chemokine receptors, adhesion molecules, myeloid markers and inflammatory cytokines [42]. Therefore, as a further step to characterize diet induced liver LGI, hepatic expression of different cytokines was determined.

In addition to hepatocytes themselves, it is commonly known that immune cells in the liver also play a major role in the expression inflammatory mediators [43]. In our work, determined hepatic expression levels of cytokines do not provide a homogeneous pattern. According to TNFα elevations in obesity shown by other working groups [10,39,44], we were able to show an elevation of hepatic TNFα expression in the HFD group too, but also in the CD group compared to the SD group. Whilst the expression of pro-inflammatory TNFα was in line with the shown cellular immune response, the results of the other three analyzed cytokines differed and were partially contradictory. In contrast to increased IL-6 levels in obesity described in the literature [45], the HFD group only showed a slight increase in hepatic expression compared to the SD group. The hepatic IL-6 expression in the CD group was even higher than in the HFD group, again underpinning the pro-inflammatory potential of the carbohydrate-rich CD. A significantly lower IL-1β and elevated IL-10 level in the CD group may be explainable by an overshooting anti-inflammatory counter-regulation, as IL-10 especially is able to alter the expression of other cytokines [46].

In conclusion, our results show obesity derived liver damage associated with an organic manifestation of a LGI in the livers of the HFD group. Even if not leading to a significant increase of NAS in the CD group over the experimental time, an increased inflammatory potential was shown in the group fed with a diet rich in carbohydrates. Therefore, when studying diet-induced obesity with a focus on inflammatory processes like LGI, we would not suggest using a control diet disproportionately rich in carbohydrates.

Supplementary Materials: The following are available online at http://www.mdpi.com/2227-9059/8/12/587/s1, Table S1: Blood Parameters blood glucose concentration, triglyceride concentration, AST and ALT concentration in the high fat diet (HFD), control diet (CD) and standard diet (SD) group presented as mean ± standard deviation, ImageJ code S1: Code for semiautomatic quantification of liver fat, ImageJ code S2: Code for quantification of F4/80+-cells, Figure S1: Representative images for scoring of steatosis (Score 0-3, 50 x magnification, scale bar represents 200 µm valid for all four), ballooning (Score 0-1, 100x magnification, scale bar represents 100 µm valid for both) with black arrows indicating damaged cells, and inflammation (Score 0-2, 200x magnification, scale bar represents 50 µm valid for all three) with black arrows indicating inflammatory foci

Author Contributions: Conceptualization, A.K. and D.J. (Deborah Janowitz); methodology, A.K. and N.P.G.; validation, N.P.G., A.K., B.V.; formal analysis, N.P.G., L.M., A.G., D.J. (Daniel Jenderny); investigation, N.P.G., L.M., K.P., A.G., D.J. (Daniel Jenderny); resources, A.K., D.J. (Deborah Janowitz), B.V.; data curation, N.P.G., A.K.; writing—original draft preparation, N.P.G. and L.M.; writing—review and editing, A.K. and B.V.; visualization, N.P.G. and L.M.; supervision, A.K., B.V., D.J. (Deborah Janowitz); project administration, A.K. and D.J. (Deborah Janowitz); funding acquisition, A.K. and D.J. (Deborah Janowitz); animal care, N.P.G. and D.J. (Daniel Jenderny). All authors have read and agreed to the published version of the manuscript.

Funding: This research was funded by grant from the Deutsche Forschungsgemeinschaft, Bonn, Germany (KU 3280/1-2 and JA 2872/1-2).

Acknowledgments: The authors cordially thank the technicians of the Rudolf-Zenker Institute for Experimental Surgery and of the Central Animal Care Facility, Rostock University Medical Center for their valuable assistance.

Conflicts of Interest: The authors declare no conflict of interest.

References

1. WHO. Obesity and Overweight. 2018. Available online: https://www.who.int/en/news-room/fact-sheets/detail/obesity-and-overweight (accessed on 19 May 2019).
2. Kaplan, N.M. The Deadly Quartet. *Arch. Intern. Med.* **1989**, *149*, 1514–1520. [CrossRef] [PubMed]

3. Hotamışlıgil, G.S. Inflammation and metabolic disorders. *Nat. Cell Biol.* **2006**, *444*, 860–867. [CrossRef]
4. Schattenberg, J.M.; Schuppan, D. Nonalcoholic steatohepatitis. *Curr. Opin. Lipidol.* **2011**, *22*, 479–488. [CrossRef] [PubMed]
5. Marchesini, G.; Brizi, M.; Bianchi, G.; Tomassetti, S.; Bugianesi, E.; Lenzi, M.; McCullough, A.J.; Natale, S.; Forlani, G.; Melchionda, N. Nonalcoholic Fatty Liver Disease: A Feature of the Metabolic Syndrome. *Diabetes* **2001**, *50*, 1844–1850. [CrossRef] [PubMed]
6. Hotamisligil, G.S. Inflammation, metaflammation and immunometabolic disorders. *Nat. Cell Biol.* **2017**, *542*, 177–185. [CrossRef]
7. Medzhitov, R. Origin and physiological roles of inflammation. *Nat. Cell Biol.* **2008**, *454*, 428–435. [CrossRef]
8. Lumeng, C.N.; Saltiel, A.R. Inflammatory links between obesity and metabolic disease. *J. Clin. Investig.* **2011**, *121*, 2111–2117. [CrossRef]
9. Juge-Aubry, C.E.; Henrichot, E.; Meier, C.A. Adipose tissue: A regulator of inflammation. *Best Pr. Res. Clin. Endocrinol. Metab.* **2005**, *19*, 547–566. [CrossRef]
10. Kim, K.-A.; Gu, W.; Lee, I.-A.; Joh, E.-H.; Kim, D.-H. High Fat Diet-Induced Gut Microbiota Exacerbates Inflammation and Obesity in Mice via the TLR4 Signaling Pathway. *PLoS ONE* **2012**, *7*, e47713. [CrossRef]
11. Wellen, K.E.; Hotamisligil, G.S. Obesity-induced inflammatory changes in adipose tissue. *J. Clin. Investig.* **2003**, *112*, 1785–1788. [CrossRef]
12. Wu, Z.; Xu, J.; Tan, J.; Song, Y.; Liu, L.; Zhang, F.; Zhang, Y.; Li, X.; Chi, Y.; Liu, Y. Mesenteric adipose tissue B lymphocytes promote local and hepatic inflammation in non-alcoholic fatty liver disease mice. *J. Cell. Mol. Med.* **2019**, *23*, 3375–3385. [CrossRef] [PubMed]
13. Koyama, Y.; Brenner, D.A. Liver inflammation and fibrosis. *J. Clin. Investig.* **2017**, *127*, 55–64. [CrossRef]
14. Saltiel, A.R.; Olefsky, J.M. Inflammatory mechanisms linking obesity and metabolic disease. *J. Clin. Investig.* **2017**, *127*, 1–4. [CrossRef] [PubMed]
15. DeGuise, M.; Chehade, L.; Tierney, A.; Beauvais, A.; Kothary, R. Low fat diets increase survival of a mouse model of spinal muscular atrophy. *Ann. Clin. Transl. Neurol.* **2019**, *6*, 2340–2346. [CrossRef]
16. Marei, W.F.A.; Smits, A.; Mohey-Elsaeed, O.; Pintelon, I.; Ginneberge, D.; Bols, P.E.J.; Moerloose, K.; Leroy, J.L.M.R. Differential effects of high fat diet-induced obesity on oocyte mitochondrial functions in inbred and outbred mice. *Sci. Rep.* **2020**, *10*, 1–14. [CrossRef]
17. Penke, M.; Larsen, P.S.; Schuster, S.; Dall, M.; Jensen, B.A.; Gorski, T.; Meusel, A.; Richter, S.; Vienberg, S.G.; Treebak, J.T.; et al. Hepatic NAD salvage pathway is enhanced in mice on a high-fat diet. *Mol. Cell. Endocrinol.* **2015**, *412*, 65–72. [CrossRef]
18. Wang, P.; Shao, X.; Bao, Y.; Zhu, J.; Chen, L.; Zhang, L.; Ma, X.; Zhong, X.-B. Impact of obese levels on the hepatic expression of nuclear receptors and drug-metabolizing enzymes in adult and offspring mice. *Acta Pharm. Sin. B* **2020**, *10*, 171–185. [CrossRef] [PubMed]
19. Ulman, E.A. The "Original" High-Fat Diets for Diet Induced Obesity. 2011. Available online: https://www.weizmann.ac.il/vet/sites/vet/files/uploads/diet_d12451_d12492.pdf (accessed on 9 October 2020).
20. Blaak, E.E.; Antoine, J.; Benton, D.; Björck, I.; Bozzetto, L.; Brouns, F.; Diamant, M.; Dye, L.; Hulshof, T.; Holst, J.J.; et al. Impact of postprandial glycaemia on health and prevention of disease. *Obes. Rev.* **2012**, *13*, 923–984. [CrossRef]
21. Minihane, A.M.; Vinoy, S.; Russell, W.R.; Baka, A.; Roche, H.M.; Tuohy, K.M.; Teeling, J.L.; Blaak, E.E.; Fenech, M.; Vauzour, D.; et al. Low-grade inflammation, diet composition and health: Current research evidence and its translation. *Br. J. Nutr.* **2015**, *114*, 999–1012. [CrossRef]
22. Markova, M.; Pivovarova, O.; Hornemann, S.; Sucher, S.; Frahnow, T.; Wegner, K.; Machann, J.; Petzke, K.J.; Hierholzer, J.; Lichtinghagen, R.; et al. Isocaloric Diets High in Animal or Plant Protein Reduce Liver Fat and Inflammation in Individuals With Type 2 Diabetes. *Gastroenterology* **2017**, *152*, 571–585. [CrossRef]
23. Kleiner, D.E.; Brunt, E.M.; Van Natta, M.; Behling, C.; Contos, M.J.; Cummings, O.W.; Ferrell, L.D.; Liu, Y.-C.; Torbenson, M.S.; Unalp-Arida, A.; et al. Design and validation of a histological scoring system for nonalcoholic fatty liver disease. *Hepatology* **2005**, *41*, 1313–1321. [CrossRef] [PubMed]
24. Liebig, M.; Hassanzada, A.; Kämmerling, M.; Genz, B.; Vollmar, B.; Abshagen, K. Microcirculatory disturbances and cellular changes during progression of hepatic steatosis to liver tumors. *Exp. Biol. Med.* **2017**, *243*, 1–12. [CrossRef]

25. Singh-Manoux, A.; Czernichow, S.; Elbaz, A.; Dugravot, A.; Sabia, S.; Hagger-Johnson, G.; Kaffashian, S.; Zins, M.; Brunner, E.J.; Nabi, H.; et al. Obesity phenotypes in midlife and cognition in early old age: The Whitehall II cohort study. *Neurology* **2012**, *79*, 755–762. [CrossRef] [PubMed]
26. Sikaris, K.A. The Clinical Biochemistry of Obesity. *Clin. Biochem. Rev.* **2004**, *25*, 165–181. [PubMed]
27. Lonardo, A.; Caldwell, S.H.; Loria, P. Clinical physiology of NAFLD: A critical overview of pathogenesis and treatment. *Expert Rev. Endocrinol. Metab.* **2010**, *5*, 403–423. [CrossRef]
28. Milic, S.; Lulić, D.; Štimac, D. Non-alcoholic fatty liver disease and obesity: Biochemical, metabolic and clinical presentations. *World J. Gastroenterol.* **2014**, *20*, 9330–9337.
29. Wree, A.; Kahraman, A.; Gerken, G.; Canbay, A. Obesity Affects the Liver—The Link between Adipocytes and Hepatocytes. *Digestion* **2010**, *83*, 124–133. [CrossRef]
30. Collins, S.; Martin, T.L.; Surwit, R.S.; Robidoux, J. Genetic vulnerability to diet-induced obesity in the C57BL/6J mouse: Physiological and molecular characteristics. *Physiol. Behav.* **2004**, *81*, 243–248. [CrossRef]
31. Kleinendorst, L.; Abawi, O.; Van Der Kamp, H.J.; Alders, M.; Meijers-Heijboer, H.E.; Van Rossum, E.F.; Akker, E.L.V.D.; Van Haelst, M.M. Leptin receptor deficiency: A systematic literature review and prevalence estimation based on population genetics. *Eur. J. Endocrinol.* **2020**, *182*, 47–56. [CrossRef]
32. Tschöp, M.H.; Heiman, M.L. Rodent obesity models: An overview. *Exp. Clin. Endocrinol. Diabetes* **2001**, *109*, 307–319. [CrossRef]
33. Jax.org b6j-data-summary.xlsx. Available online: https://www.jax.org/de/-/media/jaxweb/files/jax-mice-and-services/b6j-data-summary.xlsx (accessed on 14 September 2020).
34. Echeverría, F.; Valenzuela, R.; Bustamante, A.; Álvarez, D.; Ortiz, M.; Espinosa, A.; Illesca, P.; Gonzalez-Mañan, D.; Videla, L.A. High-fat diet induces mouse liver steatosis with a concomitant decline in energy metabolism: Attenuation by eicosapentaenoic acid (EPA) or hydroxytyrosol (HT) supplementation and the additive effects upon EPA and HT co-administration. *Food Funct.* **2019**, *10*, 6170–6183. [CrossRef] [PubMed]
35. Tirosh, O. Hypoxic Signaling and Cholesterol Lipotoxicity in Fatty Liver Disease Progression. *Oxidative Med. Cell. Longev.* **2018**, *2018*, 1–15. [CrossRef] [PubMed]
36. Da Silva-Santi, L.G.; Antunes, M.M.; Caparroz-Assef, S.M.; Carbonera, F.; Masi, L.N.; Curi, R.; Visentainer, J.V.; Bazotte, R.B. Liver Fatty Acid Composition and Inflammation in Mice Fed with High-Carbohydrate Diet or High-Fat Diet. *Nutrients* **2016**, *8*, 682. [CrossRef] [PubMed]
37. Duwaerts, C.C.; Amin, A.M.; Siao, K.; Her, C.; Fitch, M.; Beysen, C.; Turner, S.M.; Goodsell, A.; Baron, J.L.; Grenert, J.P.; et al. Specific Macronutrients Exert Unique Influences on the Adipose-Liver Axis to Promote Hepatic Steatosis in Mice. *Cell. Mol. Gastroenterol. Hepatol.* **2017**, *4*, 223–236. [CrossRef] [PubMed]
38. Wang, X.; Cheng, M.; Zhao, M.; Ge, A.; Guo, F.; Zhang, M.; Yang, Y.; Liu, L.; Yang, N. Differential effects of high-fat-diet rich in lard oil or soybean oil on osteopontin expression and inflammation of adipose tissue in diet-induced obese rats. *Eur. J. Nutr.* **2012**, *52*, 1181–1189. [CrossRef]
39. Van Der Heijden, R.A.; Sheedfar, F.; Morrison, M.C.; Hommelberg, P.P.H.; Kor, D.; Kloosterhuis, N.J.; Gruben, N.; Youssef, S.A.; De Bruin, A.; Hofker, M.H.; et al. High-fat diet induced obesity primes inflammation in adipose tissue prior to liver in C57BL/6j mice. *Aging* **2015**, *7*, 256–268. [CrossRef]
40. Targher, G. Non-alcoholic fatty liver disease, the metabolic syndrome and the risk of cardiovascular disease: The plot thickens. *Diabet. Med.* **2007**, *24*, 1–6. [CrossRef]
41. Morinaga, H.; Mayoral, R.; Heinrichsdorff, J.; Osborn, O.; Franck, N.; Hah, N.; Walenta, E.; Bandyopadhyay, G.; Pessentheiner, A.R.; Chi, T.J.; et al. Characterization of Distinct Subpopulations of Hepatic Macrophages in HFD/Obese Mice. *Diabetes* **2014**, *64*, 1120–1130. [CrossRef]
42. Obstfeld, A.E.; Sugaru, E.; Thearle, M.; Francisco, A.-M.; Gayet, C.; Ginsberg, H.N.; Ables, E.V.; Ferrante, A.W. C-C Chemokine Receptor 2 (CCR2) Regulates the Hepatic Recruitment of Myeloid Cells That Promote Obesity-Induced Hepatic Steatosis. *Diabetes* **2010**, *59*, 916–925. [CrossRef]
43. Robinson, M.W.; Harmon, C.; O'Farrelly, C. Liver immunology and its role in inflammation and homeostasis. *Cell. Mol. Immunol.* **2016**, *13*, 267–276. [CrossRef]
44. Marques, P.; Collado, A.; Martínez-Hervás, S.; Domingo, E.; Benito, E.; Piqueras, L.; Real, J.T.; Ascaso, J.F.; Sanz, M.-J. Systemic Inflammation in Metabolic Syndrome: Increased Platelet and Leukocyte Activation, and Key Role of CX3CL1/CX3CR1 and CCL2/CCR2 Axes in Arterial Platelet-Proinflammatory Monocyte Adhesion. *J. Clin. Med.* **2019**, *8*, 708. [CrossRef] [PubMed]

45. Wieckowska, A.; Papouchado, B.G.; Li, Z.; Lopez, R.; Zein, N.N.; Feldstein, A.E. Increased Hepatic and Circulating Interleukin-6 Levels in Human Nonalcoholic Steatohepatitis. *Am. J. Gastroenterol.* **2008**, *103*, 1372–1379. [CrossRef] [PubMed]
46. Moore, K.W.; Malefyt, R.D.W.; Coffman, R.L.; O'Garra, A. INTERLEUKIN-10AND THEINTERLEUKIN-10 RECEPTOR. *Annu. Rev. Immunol.* **2001**, *19*, 683–765. [CrossRef] [PubMed]

10.2 Studie 2

biomolecules

MDPI

Article

[18F]GE-180-PET and Post Mortem Marker Characteristics of Long-Term High-Fat-Diet-Induced Chronic Neuroinflammation in Mice

Luisa Müller [1,2,3,†], Nicole Power Guerra [1,4,5,†], Anna Schildt [6], Tobias Lindner [6], Jan Stenzel [6], Newshan Behrangi [7], Carina Bergner [8], Teresa Alberts [7], Daniel Bühler [1], Jens Kurth [8], Bernd Joachim Krause [8], Deborah Janowitz [9], Stefan Teipel [2,3,10], Brigitte Vollmar [1,3] and Angela Kuhla [1,3,*]

1 Rudolf-Zenker-Institute for Experimental Surgery, Rostock University Medical Centre, 18057 Rostock, Germany; luisa.mueller2@uni-rostock.de (L.M.)
2 Department of Psychosomatic Medicine and Psychotherapy, Rostock University Medical Centre, 18147 Rostock, Germany
3 Centre for Transdisciplinary Neurosciences Rostock (CTNR), Rostock University Medical Centre, 18147 Rostock, Germany
4 Institute of Anatomy, Rostock University Medical Centre, 18057 Rostock, Germany
5 Smell & Taste Clinic, Department of Otorhinolaryngology, Faculty of Medicine Carl Gustav Carus, Technische Universität Dresden, 01034 Dresden, Germany
6 Core Facility Multimodal Small Animal Imaging, Rostock University Medical Centre, 18057 Rostock, Germany
7 Institute of Anatomy and Cell Biology, Medical University of Bonn, 53115 Bonn, Germany
8 Department of Clinic and Polyclinic for Nuclear Medicine, Rostock University Medical Centre, 18057 Rostock, Germany
9 Department of Psychiatry, University of Greifswald, 17475 Greifswald, Germany
10 Deutsches Zentrum für Neurodegenerative Erkrankungen (DZNE) Rostock/Greifswald, 18147 Rostock, Germany
* Correspondence: angela.kuhla@uni-rostock.de; Tel.: +49-381-494-2503
† These authors contributed equally to this work.

check for updates

Citation: Müller, L.; Power Guerra, N.; Schildt, A.; Lindner, T.; Stenzel, J.; Behrangi, N.; Bergner, C.; Alberts, T.; Bühler, D.; Kurth, J.; et al. [18F]GE-180-PET and Post Mortem Marker Characteristics of Long-Term High-Fat-Diet-Induced Chronic Neuroinflammation in Mice. *Biomolecules* **2023**, *13*, 769. https://doi.org/10.3390/biom13050769

Academic Editors: Anne M. Landau, Francisco R. Lopez-Picon and Nadja Van Camp

Received: 15 March 2023
Revised: 14 April 2023
Accepted: 26 April 2023
Published: 28 April 2023

Abstract: Obesity is characterized by immoderate fat accumulation leading to an elevated risk of neurodegenerative disorders, along with a host of metabolic disturbances. Chronic neuroinflammation is a main factor linking obesity and the propensity for neurodegenerative disorders. To determine the cerebrometabolic effects of diet-induced obesity (DIO) in female mice fed a long-term (24 weeks) high-fat diet (HFD, 60% fat) compared to a group on a control diet (CD, 20% fat), we used in vivo PET imaging with the radiotracer [18F]FDG as a marker for brain glucose metabolism. In addition, we determined the effects of DIO on cerebral neuroinflammation using translocator protein 18 kDa (TSPO)-sensitive PET imaging with [18F]GE-180. Finally, we performed complementary post mortem histological and biochemical analyses of TSPO and further microglial (Iba1, TMEM119) and astroglial (GFAP) markers as well as cerebral expression analyses of cytokines (e.g., Interleukin (IL)-1β). We showed the development of a peripheral DIO phenotype, characterized by increased body weight, visceral fat, free triglycerides and leptin in plasma, as well as increased fasted blood glucose levels. Furthermore, we found obesity-associated hypermetabolic changes in brain glucose metabolism in the HFD group. Our main findings with respect to neuroinflammation were that neither [18F]GE-180 PET nor histological analyses of brain samples seem fit to detect the predicted cerebral inflammation response, despite clear evidence of perturbed brain metabolism along with elevated IL-1β expression. These results could be interpreted as a metabolically activated state in brain-resident immune cells due to a long-term HFD.

Keywords: neuroinflammation; diet-induced obesity; high-fat diet; [18F]FDG PET/CT; [18F]GE-180 PET/CT; TSPO

1. Introduction

Obesity is mainly characterized by the excessive accumulation of adipose tissue [1]. Its prevalence is steadily increasing and reaching pandemic levels, severely burdening patients and health care systems [1,2]. The main contributor inducing a detrimental increase in body weight is a permanent oversupply of food rich in calories and mostly also in fat, forming an imbalance between energy uptake and expenditure [1]. Obesity is associated with a state of chronic systemic low-grade inflammation (LGI) [3,4] affecting adipose tissue, the liver [5,6] and even the central nervous system (CNS) [7]. In this context, a decrease in cognitive abilities has been observed in patients with long-term obesity [8,9]. Additionally, obese patients have an increased risk of developing dementia [10–12].

The main converging mechanism of brain alterations in obesity and neurodegenerative diseases is neuroinflammation [13,14]. In obesity, neuroinflammation is predominantly found in the hypothalamus, leading to dysregulations in the hypothalamus–pituitary axis, thus promoting further disruptions in body mass and food intake regulation [15]. In addition, the literature also suggests neuroinflammatory processes in many other regions of the CNS, for example in the cortex, hippocampus and cerebellum, to be associated with neuronal loss and cognitive changes [16].

Obesity-induced neuroinflammation is thought to result from a persisting peripheral LGI characterized by changes in mediators with pro-inflammatory potential, for example leptin, saturated fatty acids and cytokines. These can affect brain myeloid cells with microglia as the most prominent CNS-resident immune cells [17] as well as astroglia by different pathways [16,18]. Various degrees of microglial and astroglial activation are also commonly observed in different neurodegenerative disorders [19,20]. The pro-inflammatory activation of microglia typically leads to a shift from a homeostatic phenotype to a pro-inflammatory state, characterized by increased expression of pro-inflammatory cytokines, such as interleukin (IL)-1β and tumor necrosis factor α (TNFα), as well as pro-inflammatory chemokines and reactive oxygen species [21]. Furthermore, the pro-inflammatory activation of microglia leads to characteristic morphological changes in which the microglia retract their fine processes, and both the cell bodies and processes become hypertrophic [22].

Besides post mortem histological analyses, neuroinflammation can be assessed in vivo using positron emission tomography (PET). The translocator protein 18 kDa (TSPO), formerly known as the peripheral benzodiazepine receptor, is a prominent biomarker for PET imaging studies [23,24]. For example, (4S)-N,N-Diethyl-9-[2-[^{18}F]fluoroethyl]-5-methoxy-2,3,4,9-tetrahydro-1H-carbazole-4-carboxamide (flutriciclamide, [^{18}F]GE-180 [25]) is a radiotracer with high TSPO affinity [26–28]. TSPO is mainly expressed in glial cells in the brain as a transmembrane protein in the outer mitochondrial membrane. While its biological functions remain largely unclear [29], several studies have shown an upregulation of TSPO expression in activated microglia, and TSPO radiotracers have been used successfully for PET imaging of neuroinflammation in various animal models as reviewed by van Camp et al. [30], including in obese mice [31].

Despite the extensive focus of research on the interconnection between obesity and neurodegeneration that is potentially mediated via neuroinflammatory processes, this is still an open field for research. In particular, publications on the effect of long-term high-caloric malnutrition on neuroinflammation are scarce. Therefore, we used a diet-induced obesity (DIO) mouse model to study the effects of a long-term high-fat diet (HFD) on brain glucose consumption and cerebral neuroinflammation as well as peripheral and cerebral markers of obesity and inflammation. We used a combination of in vivo PET analyses with 2-[^{18}F]fluoro-2-deoxy-D-glucose ([^{18}F]FDG) and [^{18}F]GE-180 and ex vivo histological and biochemical evaluations of brain tissue. Our study aimed to test whether the application of [^{18}F]GE-180 PET could detect potential chronic neuroinflammation induced by long-term HFD in the presented DIO model in vivo. Secondly, we evaluated if post mortem histological and biochemical analyses resemble cellular or humoral immune reactions induced by long-term HFD in line with the in vivo imaging results.

2. Materials and Methods

2.1. Animal Model

For the experiments, female C57BL/6J mice were purchased from Charles River (Sulzfeld, Germany) at the age of 4 weeks. Mice were kept in standard cages with 4 animals per cage in a temperature-controlled room (21 ± 3 °C) with a 12/12 h day/night cycle containing a twilight period of 30 min. After one week of acclimatization, the diet was changed to the corresponding diet. One group received a HFD (D12492; Research Diets, New Brunswick, NJ, USA), hereinafter referred to as the HFD group (16 mice) and the other group received the manufacturers' recommended control diet (CD, D12450J; Research Diets, New Brunswick, NJ, USA), hereinafter referred to as the CD group (16 mice) over a long-term period of 24 weeks. During the experiments, mice had ad libitum access to water.

All animal experimental work was carried out with permission of the local Animal Research Committee (Landesamt für Landwirtschaft, Lebensmittelsicherheit und Fischerei (LALLF)) of the state Mecklenburg-Western Pomerania (LALLF M-V/TSD/7221.3-2-001/18) and all animals received human care according to the EU Directive 2010/63/EU.

2.2. PET/CT Imaging and Image Analysis

Imaging was performed after 24 weeks (=long-term) of the respective diet. For imaging procedures, radiotracers were injected into the tail vein in anesthetized mice (1.5–2.5% isoflurane Baxter, Unterschleißheim, Germany) with oxygen supplement (Air Liquide, Hamburg, Germany). Research conditions during PET imaging were kept identical among animals to ensure accuracy and reliability. These included anesthesia time (<90 min), anesthesia depth (constant breathing frequency, absence of movement) and body temperature (38 °C).

PET imaging using [^{18}F]FDG was performed according to a previously published protocol [32,33]. Briefly, mice were not fasted prior PET imaging. They received 15.38 ± 0.62 MBq of [^{18}F]FDG intravenously (i.v.). 30 min after injection of [^{18}F]FDG, static PET imaging was performed for 30 min in the head-prone position using a small-animal PET/CT scanner (Inveon PET/CT Siemens, Knoxville, TN, USA). PET data were normalized, corrected (for attenuation, decay, scatter, randoms and deadtime) and reconstructed using 2D-ordered subset expectation maximization algorithm (2D-OSEM, 4 iterations, 16 subsets).

To investigate neuroinflammation, the radiotracer [^{18}F]GE-180 was used. Briefly, mice received 15.80 ± 1.45 MBq [^{18}F]GE-180 i.v. PET imaging was performed for a total of 60 min and started simultaneously with the i.v. injection of [^{18}F]GE-180. All 60 min of data were averaged for analysis, and the same corrections and reconstruction algorithm as for [^{18}F]FDG imaging were applied.

PET image analysis was performed with PMOD v.4.0 (PMOD Technologies, Zurich, Switzerland). Detailed procedure of PET data analysis is described by Rühlmann et al. [33]. In short, PET images were co-registered to Mirrione MRI atlas [34] using CT images and anatomical T1-weighted MRI images. The volume of interest (VOI) template of Mirrione was used to extract values in kBq/mL for the following brain regions: cortex, hippocampus and hypothalamus. Additionally, all VOIs of the template were united to obtain a whole-brain VOI. Initially, the % injected dose per mL (%ID/mL) was calculated for standardization.

To address the large difference in weight between CD and HFD mice (see Section 3, Figure 1A), we evaluated the metabolic activity of each radiotracer in the visceral fat tissue and the whole brain (see Figures 1G and 2A). For this, a VOI was placed manually in the visceral fat tissue. For [^{18}F]FDG, the visceral fat was metabolically active to some degree (Figure 1G); therefore, we did not want to overestimate the effect of weight. Thus, we calculated the standardized uptake value using metabolic weight (SUV_c) according to Kleiber et al. [35]. For this, the final blood glucose measurement 24 h post PET imaging

was used. Additionally, SUV_c was corrected using blood glucose concentration ($SUV_{glc,c}$). The following equation was used to calculate $SUV_{glc,c}$ for [^{18}F]FDG:

$$SUV_{glc,c} = \frac{\text{radioactivity concentration}\left[\frac{\text{kBq}}{\text{mL}}\right]}{\text{injected dose [MBq]}} \cdot \text{body weight[g]} \cdot \frac{3}{4} \cdot \text{blood glucose}\left[\frac{\text{mmol}}{\text{L}}\right]$$

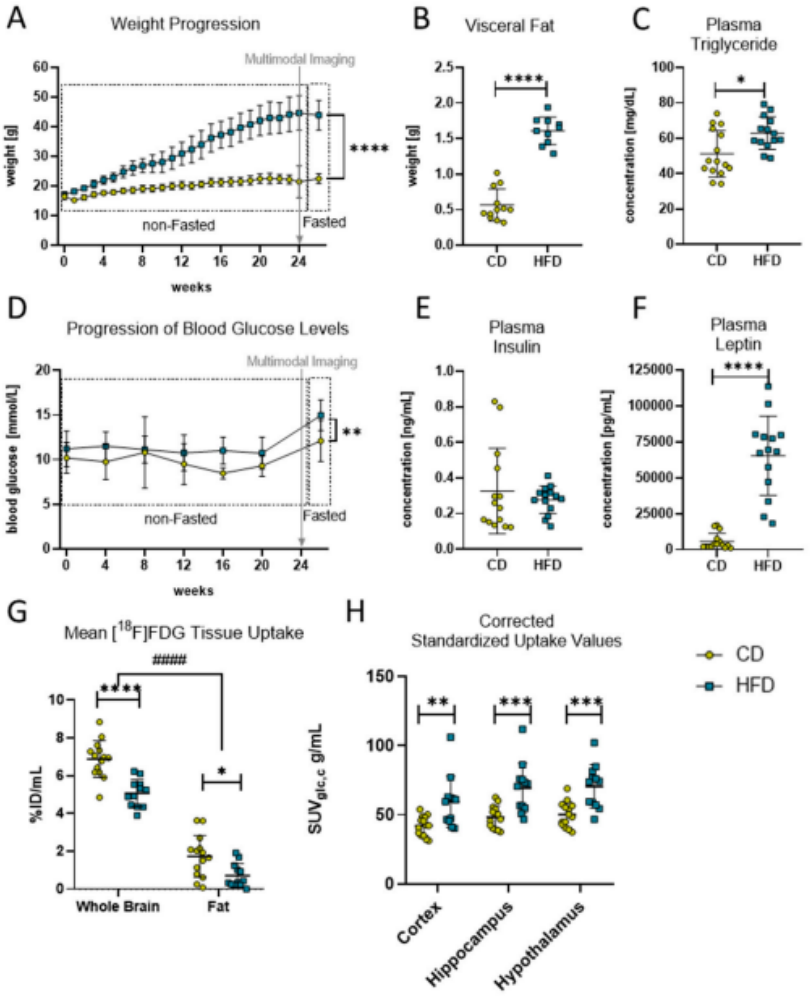

Figure 1. Diet-induced obese phenotype in mice. (**A**) Weekly weight progression (in g) of mice with control diet (CD) and high-fat diet (HFD). Both groups started with n = 16 mice and ended with CD (n = 15) and HFD (n = 14) mice. Last data point was measured after a fasting period of 6–12 h. Time point of multimodal imaging is indicated by the grey arrow. Data presented as group mean ± standard deviation. Statistical analysis by mixed-effects model analysis followed by post hoc tests with Sidak's correction for multiple comparisons, **** $p < 0.0001$. (**B**) Comparison of visceral fat deposition (in g) after 24 weeks in HFD and CD group. Statistical analysis by unpaired *t*-test, **** $p < 0.0001$. (**C**) Comparison of fasted plasma triglyceride concentration (in mg/dL) after 24 weeks in HFD and CD group. Statistical analysis by unpaired *t*-test, * $p < 0.05$. (**D**) Progression of monthly measured blood glucose concentration (in mmol/L) of mice with HFD and CD. Both groups started with n = 16 mice and ended with CD (n = 15) and HFD (n = 14) mice. Last data point measured after a

fasting period of 6–12 h. Time point of multimodal imaging is indicated by the grey arrow. Data presented as group mean ± standard deviation. Statistical analysis by mixed-effects model followed by post hoc tests with Sidak's correction for multiple comparisons, ** $p < 0.01$. (**E**) Comparison of fasted plasma insulin concentration (in mg/mL) after 24 weeks in the HFD and CD group. Statistical analysis by Mann–Whitney test, $p = 0.5409$. (**F**) Comparison of fasted plasma leptin concentration (in pg/mL) after 24 weeks in HFD and CD group. Statistical analysis by Mann–Whitney test, **** $p < 0.0001$. (**G**) Comparison of tracer uptake (%ID/mL) into brain and fat tissue in volumes of interest in mice receiving CD (n = 14) or HFD (n = 12). Statistical analysis by two-way ANOVA followed by post hoc tests with Sidak's correction for multiple comparisons, #### $p < 0.0001$ brain vs. fat, * $p < 0.01$, **** $p < 0.0001$ CD vs. HFD). (**H**) Standardized uptake values corrected for blood glucose concentration and metabolic weight ($SUV_{glc,c}$) in g/mL obtained from [^{18}F]FDG PET imaging. Depicted are cortex, hippocampus and hypothalamus as brain regions of interest of CD (n = 14) or HFD (n = 12). Statistical analysis by repeated measures ANOVA followed by post hoc tests with Sidak's correction for multiple comparisons, ** $p < 0.01$, *** $p < 0.001$.

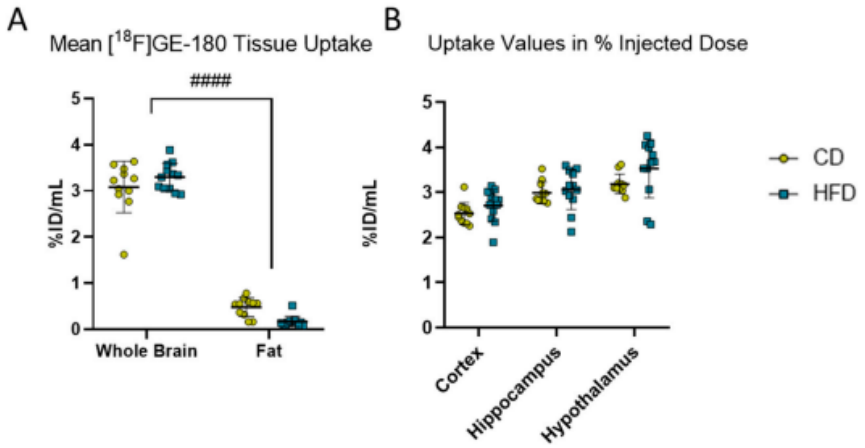

Figure 2. [^{18}F]GE-180 PET imaging. (**A**) Comparison of mean uptake (%ID/mL) into brain and fat tissues in volumes of interest in mice receiving control diet (CD, yellow, n = 12) or high-fat diet (HFD, blue, n = 12). Statistical analysis by two-way ANOVA followed by post hoc tests with Sidak's correction for multiple comparisons, #### $p < 0.0001$ brain vs. fat. (**B**) %ID/mL obtained from [^{18}F]GE-180 PET imaging in cortex, hippocampus and hypothalamus in CD (n = 12) or HFD (n = 12). Statistical analysis by repeated measures ANOVA followed by post hoc tests with Sidak's correction for multiple comparisons.

As for [^{18}F]GE-180, the visceral fat did not show relevant [^{18}F]GE-180 uptake (Figure 2A), no correction for body weight was applied and %ID/mL was used for further analysis.

2.3. Behavioural Test: Morris Water Maze

After 24 weeks of the respective diet, the Morris water maze (MWM) test was performed according to our own previously published work [32,36] as a measure for the mice's spatial reference memory. After four days of acclimatization, on the fifth day (test day), time spent in the north (N) zone, frequency of platform crossing, latency to first platform crossing and velocity were monitored in real time over 180 s. For this, a video camera (15E objective, Computar, CBC Europe, Düsseldorf, Germany with camera CCA1300-60gm, Basler, Ahrensburg, Germany) was used and subsequent digital analysis was applied using Ethovision XT II.5 (Noldus Information Technology, Wageningen, The Netherlands).

2.4. Weight Control, Blood Sampling, Euthanasia and Tissue Preparation

Body weight was measured weekly (Kern PCB, Lübeck, Germany) and monthly retrobulbary blood sampling for glucose measurement was performed under anesthesia (5 vol.% isoflurane (Baxter, Unterschleißheim, Germany), 0.8 L/min O_2 and 1.25 L/min N_2O (both from Air Liquide, Hamburg, Germany)).

After PET imaging, all animals were allowed to fully recover from anesthesia in their home cages for at least 24 h. During the last six to twelve hours, mice were fasted for insulin, glucose, leptin and triglyceride measurements in plasma, followed by final body weight measurement, blood sampling and tissue collection. For this procedure, mice were deeply anesthetized and blood was taken via retrobulbary needles to exsanguinate the mice. Blood samples were kept in EDTA tubes (Microvette® 500, Sarsted, Nümbrecht, Germany) at 4 °C until plasma preparation the same day.

Then, mice were transcardially perfused with 20–25 mL 0.9% NaCl (Braun, Melsungen, Germany) with an estimated flow rate of 2.28–2.83 mL/min. After perfusion, visceral fat and brains were dissected, weighted and naively snap-frozen for molecular analyses or paraffin-fixed for histological analyses.

2.5. Blood and Plasma Analyses

Directly after blood collection, blood glucose concentration in naïve blood samples was assessed with a glucose meter (Contour®XT, Bayer, Leverkusen, Germany). For plasma preparation, blood samples were centrifuged at 1200 rpm and 6 °C for 10 min (Centrifuge 5424, Eppendorf, Leipzig, Germany). Afterwards, the supernatant was collected and stored at −80 °C. From stored plasma samples, measurement of plasma triglycerides was performed using Triglyceride Colorimetric Assay Kit (Nr. 10010303, Cayman Chemical Company, Hamburg, Germany). Additionally, the stored plasma samples were used to perform insulin (Ultra Sensitive Mouse Insulin ELISA, Crystal Chem, Zaandam, The Netherlands) and leptin ELISAs (Mouse/Rat Leptin Quantikine ELISA, R&D Systems, Abingdon, UK) according to the manufacturer's instructions.

2.6. Histology and Immunohistochemistry

Paraffin-embedded specimens (HFD: n = 5, CD: n = 5) were sagittally cut in 4 µm thin sections. To assess TSPO, microgliosis and astrogliosis immunohistochemical reactions were performed with primary antibodies directed against TSPO (polyclonal rabbit anti-TSPO, ab109497, Abcam, Rozenburg, The Netherlands), ionized calcium binding adapter molecule 1 (Iba1; polyclonal rabbit anti-Iba1, 019-19741, FUJIFILM Wako Pure Chemical Corporation, Neuss, Germany), transmembrane protein 119 (TMEM119; monoclonal rabbit anti-TMEM119, Abcam, Cambridge, UK) or glial fibrillary acidic protein (GFAP; monoclonal rabbit anti-GFAP, Abcam, Cambridge, UK). After deparaffination and antigen retrieval in the microwave with citrate buffer (Iba1, GFAP) or Tris-EDTA buffer (TMEM119, TSPO), blocking of endogenous peroxidases was performed with 3 % H_2O_2 solution. Then, slides were exposed to primary antibodies with overnight incubation at 4 °C. After incubation with secondary antibodies for 1 h at room temperature (TSPO, Iba1, GFAP: biotinylated anti-rabbit; Vector Laboratories, Biozol Di-agnostica Vertrieb GmbH, Eching, Germany; TMEM119: biotinylated anti-rabbit, EnVision, Agilent Technologies, Santa Clara, CA, USA), the avidin/biotin-based amplification kit (TSPO, Iba1, GFAP: Vectastain Elite, Biozol Diagnostica Vertrieb GmbH, Eching, Germany; TMEM119: EnVision Kit, Agilent Technologies, Santa Clara, CA, USA) was applied for one hour at room temperature. Visualization was performed with 3,3′-diaminobenzidine tetrahydro-chloride as chromogen for TSPO, Iba1 and GFAP, whereas TMEM119 antibody reactions were visualized with EnVision Kit. In the end, slides were counterstained with hematoxylin, dehydrated, mounted in DePeX (Serva Electrophoresis GmbH, Heidelberg, Germany) and coverslipped.

Recordings of immunohistochemical reactions as well as the corresponding negative controls (Supplementary Materials Figure S1) were performed with Leica DM6 B microscope equipped with a DMC6200 camera (Leica Microsystems CMS GmbH, Wetzlar,

Germany). Quantitative analysis of stained cells was conducted using ImageJ (v 1.53q, Wayne Rasband, National Institutes of Health, Bethesda, MD, USA) with cell counter plugin. In addition to the cell numbers per mm^2, the ramification index according to Zhan et al. [22] was calculated for Iba1-stained tissue as ratio of maximum projection area and maximum cell area, both measured manually.

2.7. Quantitative Real-Time PCR

RNA was isolated with RNeasy Mini (Qiagen, Hilden, Germany) Kit from 100 mg naïvely snap-frozen brain tissue stored at −80 °C. In addition to the manufacturer's instructions, samples were incubated at room temperature for 5 min with 1 mL Qiazol (Qiagen, Hilden, Germany) and for 3 min with 200 µL chloroform (Sigma Aldrich, Taufkirchen, Germany) before 10 min centrifugation at 12,000× *g* at 4 °C (Centrifuge 5804, Eppendorf, Leipzig, Germany).

After isolation, RNA integrity was verified by agarose gel electrophoresis. RNA concentration was assessed by absorption measurement with NanoDrop (Thermo Fisher Scientific, Waltham, MA, USA). A total of 1 µg of the isolated RNA was transcribed into cDNA with added SuperScript™ (Invitrogen, Thermo Fisher Scientific, Waltham, MA, USA) and deoxyribonucleoside triphosphates (Thermo Fisher Scientific, Waltham, MA, USA). For further analysis, cDNA was diluted in a ratio of 1:2.

Analyses of *il-1β*, *il-6* and *tnfα* as well as *gfap* were performed via quantitative real-time PCR in a BioRad iQ5 Multicolor Real-Time PCR Detection System (Conquer Scientific, San Diego, CA, USA) with iQ™ SYBR® Green Supermix (Bio-Rad, Hercules, CA, USA). Measurement results were corrected against the housekeeping gene 40S ribosomal protein S18 (*rps18*), and relative quantification was carried out by usage of the $2^{-\Delta\Delta CT}$ method. Primer sequences are shown in Table 1.

Table 1. Primers used for quantitative real-time PCR.

Primer	Orientation	Sequence
rps18	Forward	*5′-AGGATGTGAAGGATGGGAAG-3′*
	Reverse	*5′-TTGGATACACCCACAGTTCG-3′*
il-1β	Forward	*5′-CCCAAGCAATACCCAAAGAA-3′*
	Reverse	*5′-TTGTGAGGTGCTGATGTACCA-3′*
il-6	Forward	*5′-GTTCTCTGGGAAATCGTGGA-3′*
	Reverse	*5′-GGAAATTGGGGTAGGAAGGA-3′*
tnfα	Forward	*5′-ACATTCGAGGCTCCAGTGAATTCGG-3′*
	Reverse	*5′-GGCAGGTCTACTTTGGAGTCATTGC-3′*
gfap	Forward	*5′-AGAAAACCGCATCACCATTC-3′*
	Reverse	*5′-TCACATCACCACGTCCTTGT-3′*

Furthermore, quantitative real-time PCR of *tspo* and *iba1* expression was performed using TaqMan™ Universal Master Mix II with UNG (Thermo Fisher Scientific GmbH, Dreieich, Germany) with compatible probes for *tspo* (Assay ID: Mm00437828_m1), *iba1* (Assay ID: Mm00479862_g1) and *gapdh* as housekeeping gene (Assay ID: Mm99999915_g1), according to manufacturer's instructions (all from Thermo Fisher Scientific GmbH, Dreieich, Germany).

2.8. Statistical Analysis

Statistical analysis was performed using GraphPad Prism 8.0.1 (GraphPad Software Inc., San Diego, CA, USA). According to Power Guerra et al., prior tests for normal distribution were performed using Shapiro–Wilk test [37]. If necessary, outliers identified with the built-in ROUT method of GraphPad Prism with a maximum desired false discovery rate of 1% (Q = 1%) were removed from the data set. In this case, corrected animal numbers are indicated in the corresponding figure legends. For comparisons between CD and HFD

groups, *t*-test (normally distributed data) or Mann–Whitney test (not normally distributed data) was performed. For evaluation of longitudinal or paired measurements, data were analyzed using either a repeated measure ANOVA or a linear stacked mixed-effects model (which in contrast to ANOVA is able to handle missing values) with diet and experimental time as fixed effects and individual mice as random effect. According to the GraphPad Prism preinstalled packages, the mixed-effects model uses a compound symmetry covariance matrix and is fit using restricted maximum likelihood (REML). Post hoc tests were performed to correct for multiple comparisons using Sidak's method. In general, data are presented as mean ± standard deviation. Differences were deemed statistically significant at $p < 0.05$. For further details, please see figure legends.

3. Results

3.1. Long-Term High-Fat Diet Induces an Obese Phenotype with Brain Glucose Hypermetabolism

To confirm the effects of the HFD and to verify the DIO in the mice, the progression in the mice's body weight was monitored continuously during the experimental time. The linear mixed-effects model analysis revealed a statistically significant effect of experimental time ($F_{(2.30, 66.98)} = 313.0$, $p < 0.0001$), diet ($F_{(1.00, 30.00)} = 196.4$, $p < 0.0001$) and their interaction ($F_{(25.00, 726.00)} = 120.1$, $p < 0.0001$) with statistically significant differences after 24 weeks of the respective diets (Figure 1A, CD: 22.5 ± 1.7 g vs. HFD: 43.9 ± 5.0 g, $p < 0.0001$). Additionally, after 24 weeks post mortem, quantifications of the dissected fat revealed a statistically significant higher mass of visceral fat (Figure 1B, CD: 0.6 ± 0.2 g vs. HFD: 1.6 ± 0.2 g, $p < 0.0001$) and plasma triglyceride concentrations (Figure 1C, CD: 51.2 ± 12.1 mg/dL vs. HFD: 62.9 ± 9.2 mg/dL, $p = 0.013$) in the HFD group compared to the CD group, confirming a DIO phenotype in this group.

Moreover, DIO led to observable derailments in metabolic pathways in the HFD group (Figure 1D–F). The linear mixed-effects model analysis revealed a statistically significant effect of diet ($F_{(1.00, 30.00)} = 20.84$, $p < 0.0001$) but not of experimental time or an interaction effect of both in the non-fasted blood glucose levels of the mice, with a higher average concentration in the HFD group throughout the whole experimental time compared to the CD group (Figure 1D, CD: 9.7 ± 0.8 mmol/L vs. HFD: 11.1 ± 0.3 mmol/L, $p = 0.0026$). Additionally, statistically significant elevated fasting blood glucose levels (Figure 1D, CD: 12.1 ± 2.3 mmol/L vs. HFD: 15.0 ± 1.2 mmol/L, $p = 0.0049$) but not plasma insulin levels (Figure 1E) were measured in the HFD group compared to the CD group after 24 weeks of the diets. Furthermore, the post mortem plasma analyses revealed that the HFD group had statistically significantly elevated plasma concentrations of leptin (Figure 1F, CD: 5714 ± 5596 pg/mL vs. HFD: 65,247 ± 27,496 pg/mL, $p < 0.0001$).

To determine the effects of the DIO phenotype on CNS metabolism in vivo, we performed an [^{18}F]FDG-PET imaging analysis. The analysis of tracer uptake (%ID/mL) in brain tissue and visceral fat for [^{18}F]FDG revealed a statistically significant effect of tissue ($F_{(1, 24)} = 403.1$, $p < 0.0001$) and diet ($F_{(1, 24)} = 29.46$, $p < 0.0001$) but no interaction effect, and post hoc tests showed a statistically significant difference between the CD and HFD in the whole-brain ($p < 0.0001$) and fat VOIs ($p = 0.0119$). Because of the measured differences between the CD and HFD in fat tissue (see methods, Figure 1G), we present SUVs corrected for the metabolic weight according to Kleiber [35] and corrected for blood glucose concentration $SUV_{glc,c}$ when comparing glucose metabolism in the brain VOIs (Figure 1H). In doing so, after 24 weeks, we found a statistically significant effect in $SUV_{glc,c}$ between the two diets ($F_{(1, 24)} = 14.5$, $p = 0.0009$) and significant differences in the cortex (CD: 42.0 ± 7.1 g/mL vs. HFD: 59.3 ± 18.4 g/mL, $p = 0.0042$), hippocampus (CD: 48.3 ± 8.1 g/mL vs. HFD: 69.1 ± 18.1 g/mL, $p = 0.0004$) and hypothalamus (CD: 50.1 ± 9.1 g/mL vs. HFD: 70.5 ± 15.6 g/mL, $p = 0.0006$).

3.2. Long-Term High-Fat Diet Causes Only a Change in Pro-Inflammatory Cytokine Profile

To observe the effects of the DIO phenotype on inflammation in the CNS in vivo, we performed [^{18}F]GE-180 PET imaging. Comparing the activity in whole brain versus fat, the diet did not show a statistically significant effect ($F_{(1, 21)} = 0.1887$, $p = 0.6685$) in the mixed-effects model. However, statistically significant effects of tissue ($F_{(1, 21)} = 1199.0$, $p < 0.0001$) and tissue with diet interaction ($F_{(1, 21)} = 10.240$, $p = 0.0043$) were found, but the post hoc test did not show a statistically significant difference between the CD and HFD in the whole brain ($p = 0.2351$) or fat ($p = 0.0572$). Therefore, we refrained from further normalization steps and presented the results as %ID/mL. We analyzed the VOIs for the cortex, hippocampus and hypothalamus. Although the values of %ID tended to be higher in the HFD group (3.3 ± 0.3 %ID/mL) compared to the CD (3.1 ± 0.6 %ID/mL) group, the repeated measures ANOVA revealed a tissue-dependent ($F_{(1.219, 25.61)} = 80.38$, $p < 0.0001$) effect but no effect of the corresponding diet between the CD and the HFD ($F_{(1, 21)} = 1.691$, $p = 0.2075$).

To further evaluate a pro-inflammatory cellular immune response in the brain, we used post mortem analyses of histological samples with immunohistochemical reactions to three commonly used markers for microglia: TSPO (Figure 3A–H), Iba1 (Figure 4A–H) and TMEM119 (Figure 5A–H). Furthermore, for *tspo* (Figure 3I) and *iba1* (Figure 4I), an mRNA expression analysis was performed to complement these immunohistochemical reactions. In all three reactions of the cortex, hippocampus and hypothalamus, the total number of microglia was counted as TSPO$^+$cells/mm^2 (Figure 3J), Iba1$^+$cells/mm^2 (Figure 4J) and TMEM$^+$cells/mm^2 (Figure 5I), respectively. In the Iba1-reacted tissue, the morphological activation of microglia was further assessed as the ramification index, which is the ratio between the maximum projection area and the maximum cell area (Figure 4K). Neither of the described analyses showed any statistically significant difference between the HFD and CD groups in the TSPO, Iba1 or TMEM119 reactions.

In addition to the three microglia-related immunohistochemical reactions, we also performed a *gfap* mRNA expression analysis and GFAP immunohistochemical reactions to analyze the astroglial cell numbers in the brain tissue (Figure 6). No statistically significantly increased *gfap* expression (Figure 6I) or cell numbers of GFAP$^+$cells/mm^2 (Figure 6J) in either of the presented brain regions, namely the cortex (Figure 6B,F), hippocampus (Figure 6C,G), and hypothalamus (Figure 6D,H), were observed comparing the CD and HFD groups.

Besides cellular immune responses, we also analyzed cytokine expression as an indicator for the DIO-derived humoral reaction of neuroinflammation in long-term HFD mice. The PCR analysis of brain tissue revealed statistically significantly elevated levels of pro-inflammatory *il-1β* (Figure 7A, CD: 0.7 ± 0.5 vs. HFD: 1.3 ± 0.7, $p = 0.0224$) as well as a tendency of increased *il-6* (Figure 7B, CD: 7.3 ± 5.3 vs. HFD: 11.0 ± 7.0, $p = 0.0763$) but no statistically significant difference in *tnfα* expression (Figure 7C).

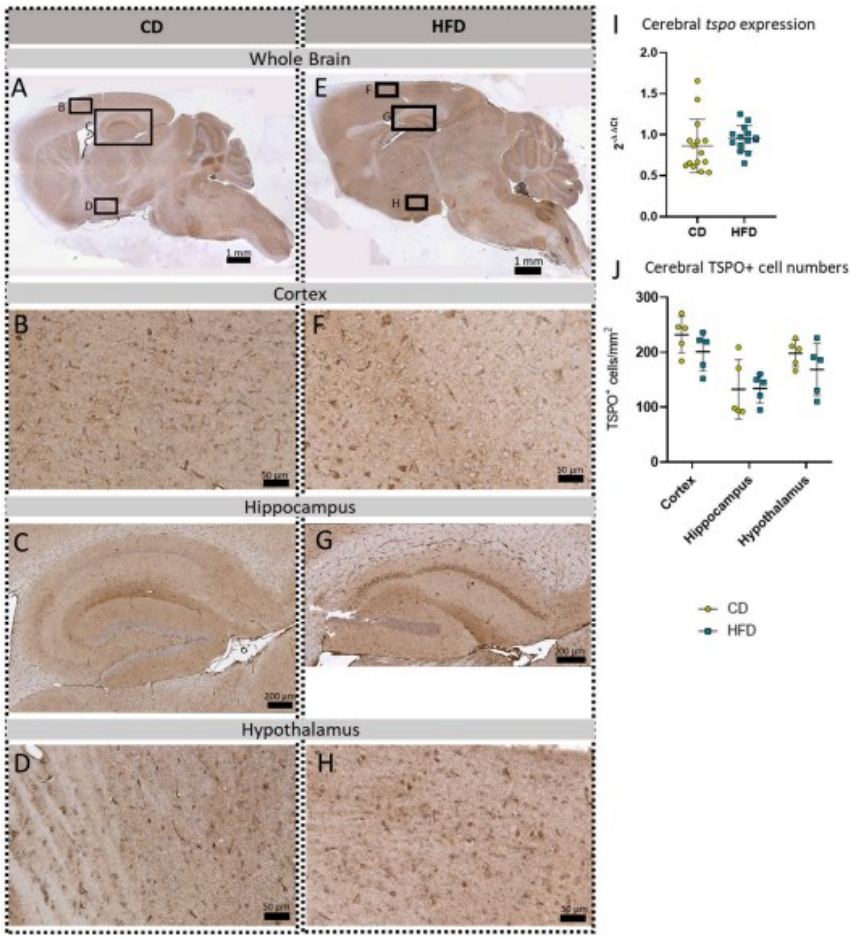

Figure 3. Immunohistochemical TSPO reactions in sagittal brain sections of mice after long-term (24 weeks) control diet (CD, n = 5) or high-fat diet (HFD, n = 5) within designated regions of interest (Figure **B**–**D**,**F**–**H**) defined by black rectangles in overview images (Figure **A**,**E**). (**A**) Overview of a representative sagittal TSPO-reacted brain slice of the CD group with indicated regions for detailed images; scale bar: 1 mm. (**B**) Detailed image of TSPO-reacted cortex of the CD group; scale bar: 50 µm. (**C**) Detailed image of the TSPO-reacted hippocampus of the CD group; scale bar: 200 µm. (**D**) Detailed image of the TSPO-reacted hypothalamus of the CD group; scale bar: 50 µm. (**E**) Overview of a representative sagittal TSPO-reacted brain slice of the HFD group with indicated regions for detailed images; scale bar: 1 mm. (**F**) Detailed image of the TSPO-reacted cortex of the HFD group; scale bar: 50 µm. (**G**) Detailed image of the TSPO-reacted hippocampus of the HFD group; scale bar: 200 µm. (**H**) Detailed image of the TSPO-stained hypothalamus of the HFD group; scale bar: 50 µm. (**I**) $2^{-\Delta\Delta CT}$ values representing relative mRNA expression of *tspo* in the brains of CD (n = 15) vs. HFD (n = 14) group. Data presented as group mean ± standard deviation. Statistical analysis by Mann–Whitney test, $p = 0.267$. (**J**) Mean cell numbers of $TSPO^+$ cells/mm^2 in the cortex, hippocampus and hypothalamus of CD vs. HFD groups. Data presented as group mean ± standard deviation. Statistical analysis by repeated measures ANOVA with post hoc tests without corrections for multiple comparisons; cortex: $p = 0.1905$, hippocampus: $p = 0.9546$, hypothalamus: $p = 0.2638$.

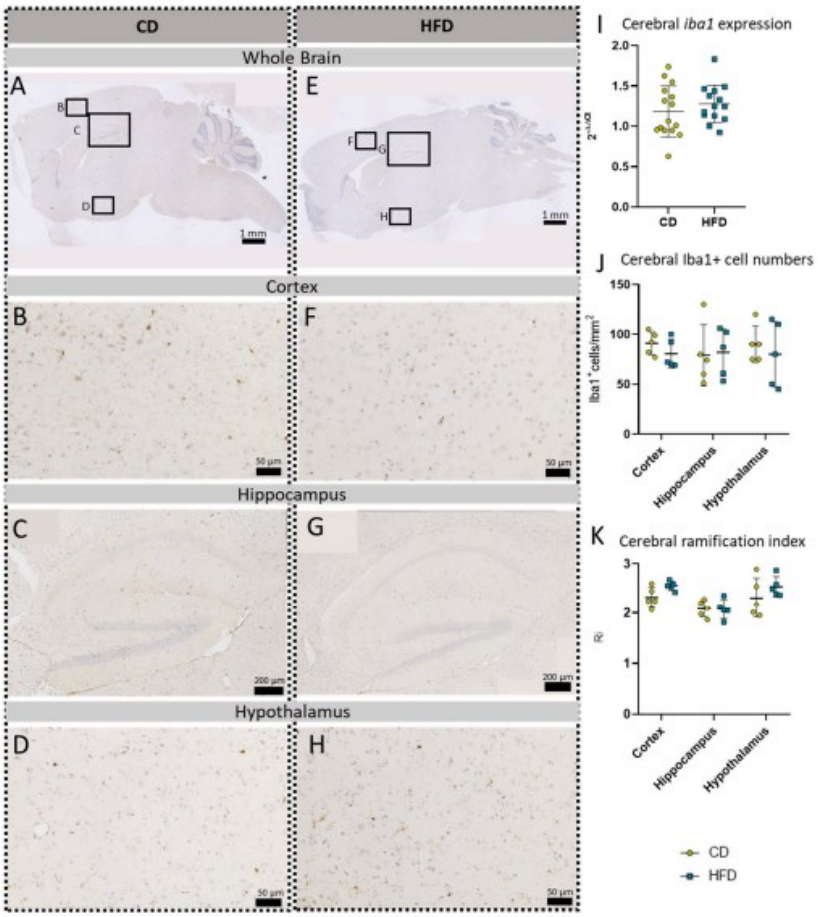

Figure 4. Immunohistochemical Iba1 reactions in sagittal brain sections of mice after long-term (24 weeks) control diet (CD, n = 5) or high-fat diet (HFD, n = 5) within designated regions of interest (Figure **B**–**D**,**F**–**H**) defined by black rectangles in overview images (Figure **A**,**E**). (**A**) Overview of a representative sagittal Iba1-reacted brain slice of CD group with indicated regions for detailed images; scale bar: 1 mm. (**B**) Detailed image of the Iba1-reacted cortex of the CD group; scale bar: 50 µm. (**C**) Detailed image of the Iba1-reacted hippocampus of the CD group; scale bar: 200 µm. (**D**) Detailed image of the Iba1-reacted hypothalamus of the CD group; scale bar: 50 µm. (**E**) Overview of a representative sagittal Iba1-reacted brain slice of the HFD group with indicated regions for detailed images; scale bar: 1 mm. (**F**) Detailed image of the Iba1-reacted cortex of the HFD group; scale bar: 50 µm. (**G**) Detailed image of the Iba1-reacted hippocampus of the HFD group; scale bar: 200 µm. (**H**) Detailed image of the Iba1-reacted hypothalamus of the HFD group; scale bar: 50 µm. (**I**) $2^{-\Delta\Delta CT}$ values representing relative mRNA expression of *iba1* in the brains of CD (n = 15) vs. HFD (n = 14) groups. Data presented as group mean ± standard deviation. Statistical analysis by unpaired *t*-test, $p = 0.9162$. (**J**) Cerebral cell numbers of $Iba1^+$ cells/mm^2 in the cortex, hippocampus and hypothalamus of CD vs. HFD groups. Data presented as group mean ± standard deviation. Statistical analysis by repeated measures ANOVA, with post hoc tests, without corrections for multiple comparisons; cortex: $p = 0.5699$, hippocampus: $p = 0.9981$, hypothalamus: $p = 0.9210$. (**K**) Cerebral mean ramification index of $Iba1^+$ cells in the cortex, hippocampus and hypothalamus of CD vs. HFD groups. Data presented as group mean ± standard deviation. Statistical analysis by repeated measures ANOVA with post hoc tests, without corrections for multiple comparisons; cortex: $p = 0.0611$, hippocampus: $p = 0.9575$, hypothalamus: $p = 0.2951$.

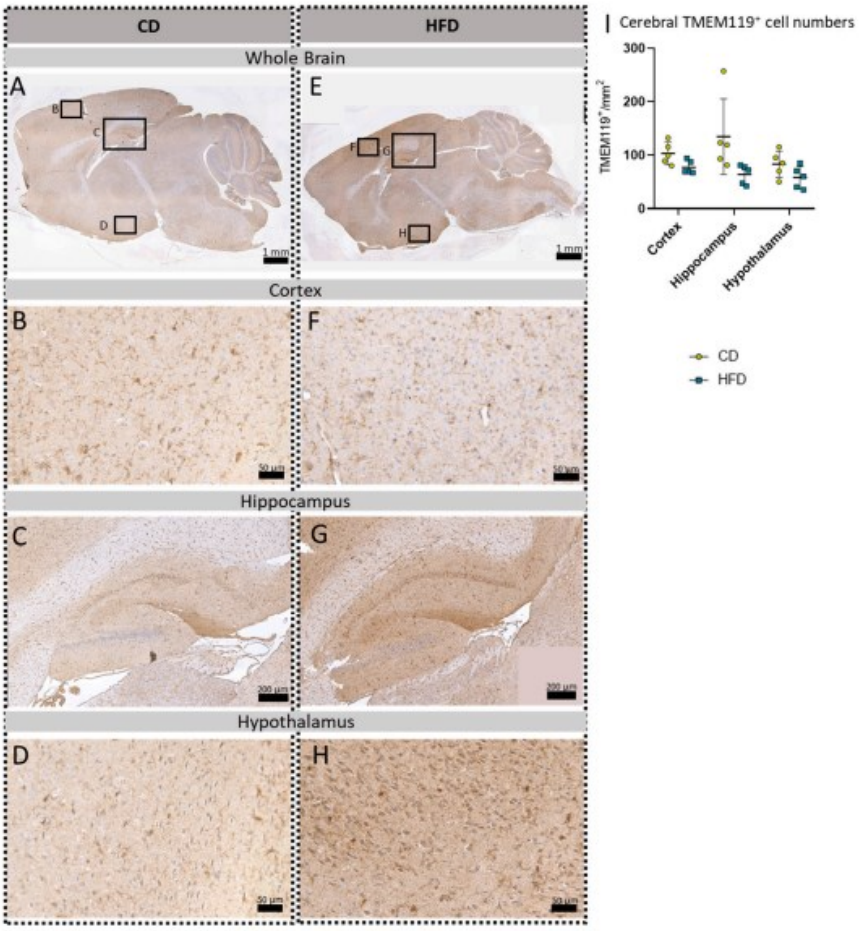

Figure 5. Immunohistochemical TMEM119 reactions in sagittal brain sections of mice after long-term (24 weeks) control diet (CD, n = 5) or high-fat diet (HFD, n = 5) within designated regions of interest (Figure **B**–**D**,**F**–**H**) defined by black rectangles in overview images (Figure **A**,**E**). (**A**) Overview of a representative sagittal TMEM119-reacted brain slice of the CD group with indicated regions for detailed images; scale bar: 1 mm. (**B**) Detailed image of the TMEM119-reacted cortex of the CD group; scale bar: 50 µm. (**C**) Detailed image of the TMEM119-reacted hippocampus of the CD group; scale bar: 200 µm. (**D**) Detailed image of the TMEM119-reacted hypothalamus of the CD group; scale bar: 50 µm. (**E**) Overview of a representative sagittal TMEM119-reacted brain slice of the HFD group with indicated regions for detailed images; scale bar: 1 mm. (**F**) Detailed image of the TMEM119-reacted cortex of the HFD group; scale bar: 50 µm. (**G**) Detailed image of the TMEM119-reacted hippocampus of the HFD group; scale bar: 200 µm. (**H**) Detailed image of the TMEM119-reacted hypothalamus of the HFD group; scale bar: 50 µm. (**I**) Cerebral mean cell numbers of TMEM119⁺ cells/mm^2 in the cortex, hippocampus and hypothalamus of CD vs. HFD groups. Data presented as group mean ± standard deviation. Statistical analysis by repeated measures ANOVA with post hoc tests, without corrections for multiple comparisons; cortex: $p = 0.0511$, hippocampus: $p = 0.0878$, hypothalamus: $p = 0.1223$.

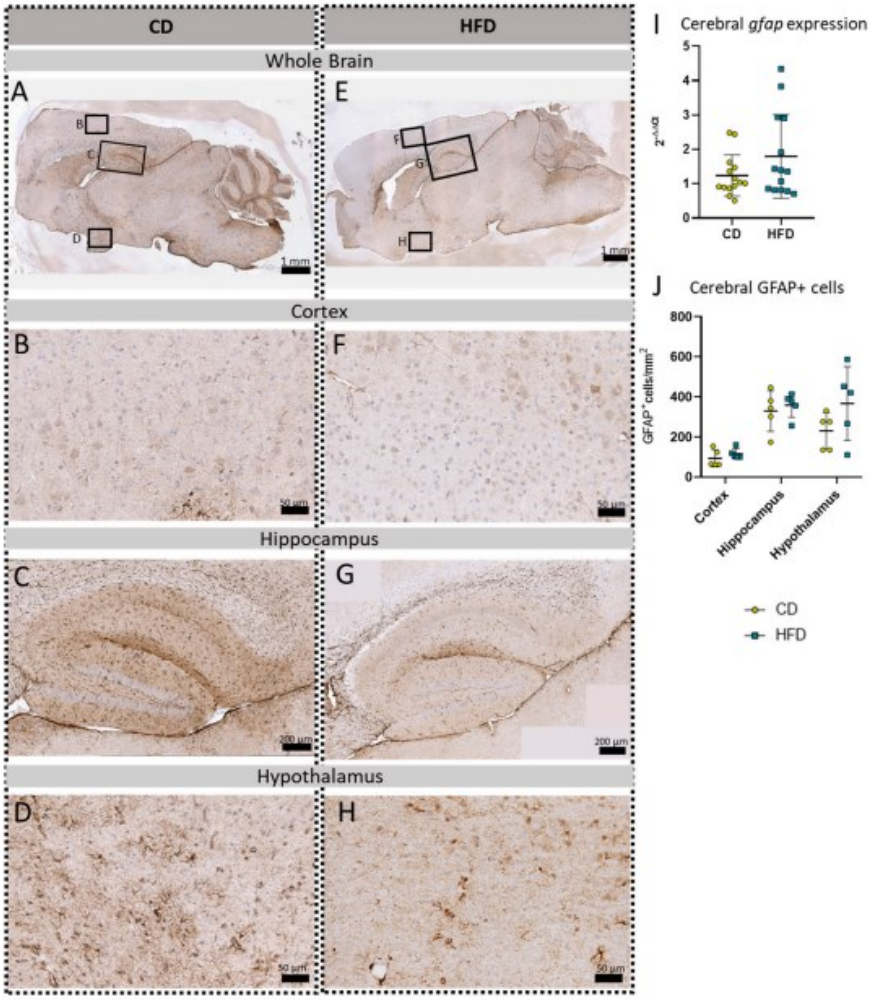

Figure 6. Immunohistochemical GFAP reactions in sagittal brain sections of mice after long-term (24 weeks) control diet (CD, n = 5) or high-fat diet (HFD, n = 5) within designated regions of interest (Figure **B**–**D**,**F**–**H**) defined by black rectangles in overview images (Figure **A**,**E**). (**A**) Overview of a representative sagittal GFAP-reacted brain slice of the CD group with indicated regions for detailed images; scale bar: 1 mm. (**B**) Detailed image of the GFAP-reacted cortex of the CD group; scale bar: 50 µm. (**C**) Detailed image of the GFAP-reacted hippocampus of the CD group; scale bar: 200 µm. (**D**) Detailed image of the GFAP-reacted hypothalamus of the CD group; scale bar: 50 µm. (**E**) Overview of a representative sagittal GFAP-reacted brain slice of the HFD group with indicated regions for detailed images; scale bar: 1 mm. (**F**) Detailed image of the GFAP-reacted cortex of the HFD group; scale bar: 50 µm. (**G**) Detailed image of the GFAP-reacted hippocampus of the HFD group; scale bar: 200 µm. (**H**) Detailed image of the GFAP-reacted hypothalamus of the HFD group; scale bar: 50 µm. (**I**) $2^{-\Delta\Delta CT}$ values representing relative mRNA expression of *gfap* in the brains of CD (n = 15) vs. HFD (n = 14) groups. Data presented as group mean ± standard deviation. Statistical analysis by Mann–Whitney test, $p = 0.4472$. (**J**) Mean cell numbers of $GFAP^+$ cells/mm^2 in the cortex, hippocampus and hypothalamus of CD vs. HFD groups. Data presented as group mean ± standard deviation. Statistical analysis by repeated measures ANOVA with post hoc tests, without corrections for multiple comparisons; cortex: $p = 0.3384$, hippocampus: $p = 0.5936$, hypothalamus: $p = 0.1874$.

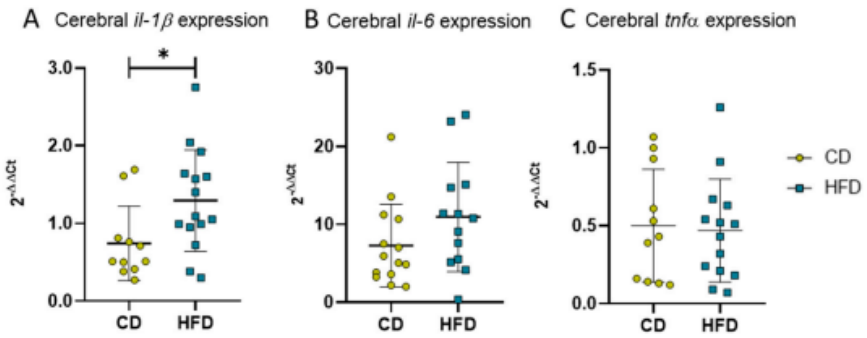

Figure 7. $2^{-\Delta\Delta CT}$ values representing relative mRNA expression of pro-inflammatory cytokines in brains of mice receiving control diet (CD) or high-fat diet (HFD) for 24 weeks. (**A**) Relative expression of *il-1β*. Statistical analysis by unpaired *t*-test, * $p < 0.05$. (**B**) Relative expression of *il-6*. Statistical analysis by Mann–Whitney test, $p = 0.0763$. (**C**) Relative expression of *tnfα*. Statistical analysis by unpaired *t*-test, $p = 0.8261$.

3.3. Spatial Memory Function Is Unaffected by Long-Term High-Fat Diet-Derived Changes in the Brain

After 24 weeks of the respective diet, the MWM test was performed as a measure for spatial reference memory. There was no difference in the time the mice spent in the target N zone of the maze (Figure 8A), number of platform crossings (Figure 8B) or latency to the first crossing of the platform area (Figure 8C). Only a difference in the mean velocity was observable between the two groups (Figure 8D, CD: 17.4 ± 1.5 cm/s vs. HFD: 15.5 ± 1.8 cm/s, $p = 0.0042$).

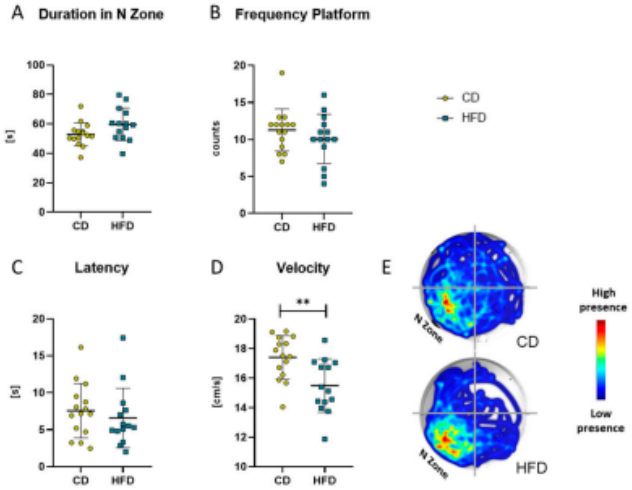

Figure 8. Results obtained with the Morris Water Maze test in the group receiving control diet (CD) and the group receiving the high-fat diet (HFD). (**A**) Time (in seconds (s)) spent in the N Zone, defined as quadrant containing the platform. (**B**) Frequency (counts) of platform crosses during 120 s. (**C**) Latency (s) to first platform crossing. (**D**) Velocity (cm/s) of the mice. Values are given as mean ± SD. Significance of differences between the groups was tested by unpaired Student's *t*-test (**A**,**D**) or Mann–Whitney test (**B**,**C**), ** $p < 0.005$. (**E**) Representative heat map of the performance of mice of CD and HFD groups.

4. Discussion

In the present study, we used in vivo PET imaging with the radiotracers [^{18}F]FDG and [^{18}F]GE-180, a TSPO ligand, to determine the effects of DIO in a long-term female HFD model on glucose metabolism and inflammatory processes in the brain, respectively. Complementarily, we performed histological and biochemical post mortem analyses of TSPO and further microglial (Iba1, TMEM119) as well as astroglial (GFAP) markers. Our main finding was a statistically significant elevation in pro-inflammatory *il-1β* mRNA expression without statistically significant changes in [^{18}F]GE-180 uptake and histological correlates of induced glial proliferation and activation.

In the present study, we used female mice receiving a 60% HFD for 24 weeks (long-term). This DIO model was chosen to reflect the development of overweight and obesity due to the high-caloric diets common in Western industrialized countries. Although a high caloric proportion of Western diets also consists of sucrose, which has been shown to induce neuroinflammatory processes even in non-obese rodents [38], a high caloric intake due to an elevated fat content and its described potential to induce neuroinflammatory processes is the focus of current research approaches [39,40]. Such DIO models are generally more representative of human obesity than genetic models of obesity [41,42]. However, it should be noted that currently there are several different experimental protocols published describing the establishment of DIO using a HFD. For example, some studies describe a HFD with ~20% fat content [43], while others use the term HFD for chow containing ~50% [44,45] or ~60% fat [46–48]. Furthermore, the administration of HFDs to study neuroinflammation in mice has ranged from a few days [47–49] to several weeks [46,47,50] or a few months [31,47,50]. This underlines the need for a clear definition and a higher standardization of the different compositions and lengths of HFD administration for better comparability and reproducibility of results, even if the present study cannot achieve this either. Moreover, there is a known sexual dimorphism in the development of concomitant morbidities [51] with differences in neuroinflammatory processes between female and male DIO mice [52,53]. As there is already abundant literature regarding the effects of DIO and the interplay between metabolic syndrome and neuronal function in male animals [54], we used female C57BL/6J mice to further investigate the effect of DIO on females. Despite the possible sexual dimorphism, in line with the above-mentioned studies in male mice, we were able to show a generalized HFD-derived obese phenotype after 24 weeks of a HFD in our female model. This obese phenotype was mainly characterized by increased body weight, visceral fat, free triglycerides and leptin in plasma, as well as increased fasted blood glucose levels. Furthermore, our in vivo approach using [^{18}F]FDG PET imaging showed cerebral glucose hypermetabolism in the female HFD mice compared to the CD mice. This pathological condition has already been described in male mice receiving HFD [55] and morbidly obese male and female patients [56].

In humans, obesity often has a slow onset, and the exact orchestration of the transition from an obesity-induced state of peripheral LGI to neuroinflammation is a process that is little understood and takes a long time, sometimes even decades [57]. Regarding the investigation into neuroinflammation, the literature provides plenty of insights on male mice receiving the same HFD that was used in this work with different experimental times of a few days up to a few weeks [47]. Findings from the current literature describe acute neuroinflammation after short-term HFD administration for a few days, which transiently subsides with prolonged HFD exposure; however, with chronic HFD exposure over 20 weeks (=long-term HFDs), renewed neuroinflammation becomes apparent [47]. In female mice, the available literature also describes a pro-inflammatory phenotype after 12 weeks of a HFD with ~60% fat content, albeit in a less severe manifestation compared to that of male mice [52]. In line with this, the working group of Lainez et al. suggests a protective role of ovarian hormones in this DIO model [52]. Though we cannot provide data on the estrus cycle of our mouse model, inconsistent estrogen levels might have impacted the current PET study.

Data on long-term HFDs (6 months and more), which would be a more valid representation of the long pathologic span in human obesity, and comorbidities in female mice are not yet available. This emphasizes the relevance of the present study. To observe neuroinflammation in our long-term HFD approach, we performed in vivo PET imaging with [^{18}F]GE-180, a well-established marker for microglial activation in preclinical studies [26–28]. In our model, the results suggest a tendency for the elevated uptake of [^{18}F]GE-180 in the HFD group compared to the CD group; however, these did not reach statistical significance. To further elucidate the [^{18}F]GE-180 PET imaging results of the mice after 24 weeks, their brains were analyzed post mortem using molecular biology as well as histological methods. Here, we measured relative *tspo* mRNA expression in the whole brain as well as TSPO-positive cells in our three main target regions: the cortex, hippocampus and hypothalamus. None of these analyses showed any difference between the HFD and CD groups.

In general, large differences in bodyweight are an obstacle to properly analyzing [^{18}F]GE-180 uptake. As we saw no relevant [^{18}F]GE-180 uptake into fat tissue, we reported our results as %ID/mL. This is in line with another working group that reported good agreement between in vivo TSPO signals and immunoreactivity and suggested the use of %ID/g for quantifying TSPO in living brains [31]. Interestingly, Barron et al. found similar results to our study when using %ID/g and immunoreactivity for TSPO [31]. Barron et al. used a 12-week HFD (60% fat) model and were able to show that obesity alone did not increase TSPO inflammatory signals [31]. A possible explanation for the PET findings could be the use of the semi-quantitative measure %ID/mL for the quantification of [^{18}F]GE-180. Kinetic modelling using dynamic PET data and metabolite-corrected plasma input functions are the gold standards for the quantification of radiotracers [58,59]. Nevertheless, in rodents, blood sampling can impact the physiological homeostasis [58]. The evaluation of time–activity curves in different brain regions, similar to previous work by Barron et al. [31] or Zatcepin et al. [60], can be more sensitive compared to the averaged data we used. We are aware that our averaged PET data contain perfusion and distribution phases that are not contributing to a TSPO-specific signal. However, we were not able to perform an additional dynamic reconstruction of the raw PET listmode data due to missing normalization and quantification files. Nevertheless, we obtained similar results compared to the dynamically and statically analyzed data from Barron et al. [31]. For future studies, dynamic PET data should be evaluated to increase the sensitivity of the outcome measure. A further approach for the analysis of TSPO tracer binding is the use of the cerebellum as a pseudo-reference region which has been successfully applied in humans [61]. For our model, we also applied this approach (Supplementary Material Figure S2); however, we obtained nearly the same insights that were already presented in the Section 3. A biological reason for the slightly elevated [^{18}F]GE-180 uptake in the HFD group without histological signs of neuroinflammation could be a blood–brain barrier (BBB) injury induced by the HFD [62] leading to increased BBB permeability and thus to the increased uptake of [^{18}F]GE-180, similar to results obtained in human multiple sclerosis patients [63,64].

To further evaluate HFD-induced neuroinflammation on a cellular level, we focused on TMEM119, a specific microglial marker [65] lacking sexual dimorphism [66], and GFAP, a marker for astroglia and reactive astrogliosis [67] that is generally more expressed in males than females [68]. Immunohistochemical reactions did not show an increase in the respective cell numbers in our HFD mice. Additionally, we observed Iba1, a marker for brain myeloid cells, with microglia as the most prominent cells [69,70]. We measured the relative *iba1* mRNA expression in the whole brain as well as Iba1-positive cells in our three main designated brain regions: the cortex, hippocampus and hypothalamus. In line with the other histological quantifications, we also found no significant differences between the CD and HFD groups. Additionally, we measured the mean ramification index of Iba1-positive microglial cells as an indicator for their activation [22] which also showed no difference between the HFD and CD groups. Nevertheless, the results in our female

model are in line with the current results in other female mice, showing no increase in microglial measures after the HFD [53].

In the context of neuroinflammation, we were not able to show a cognitive decline after 24 weeks of the HFD. This is contrary to findings of de Paula et al. [62] who showed cognitive changes in male mice after a few days of a HFD. However, recent findings from a rat model using a HFD point to a sex effect on spatial memory in the MWM test, for which only male and not female rats showed a HFD-derived cognitive decline [71]. Furthermore, it is possible that our long-term HFD of 24 weeks lead to a transient state of the mitigation of neuroinflammation in female mice, which has already been described for male mice by Thaler et al. [47]. This mitigation may be mediated by a transition of brain-resident immune cells from a pro-inflammatory (in macrophages, typically characterized as M1-like) state, lately reviewed by Yunna et al. [72], to a metabolically activated phenotype, as already described for peripheral macrophages [73,74]. This metabolically activated phenotype overexpresses pro-inflammatory cytokines via the signaling pathways typically observed in M1-like macrophages, but they cannot be identified using classical cell surface markers of activation [74]. As this is in line with the presented histological analyses, we further measured cerebral cytokine expression profiles. In the CNS, we observed no increase in tnfα or il-6 expression, as these cytokines seem to have a prominent role in the peripheral mediation of HFD-derived inflammation [37,75,76]. Interestingly, our analyses revealed a statistically significant increased expression of pro-inflammatory il-1β, which is described as a key feature of the metabolically activated phenotype of macrophages [77] and is reported as a key mediator in neuroinflammation [78,79]. Therefore, IL-1β could be an indicator for a chronic metabolically activated state of neuroinflammation derived from the long-term HFD in the present experiment.

5. Conclusions

From these results, we conclude that in our female DIO mouse model of a long-term (24-week) HFD, cytokine signaling via IL-1β is the predominant mediator of chronic neuroinflammation as there was no observable cellular inflammation using [^{18}F]GE-180 PET imaging or immunohistochemical reactions. Further experiments are needed to evaluate the exact orchestration of the phenotype changes in the brain-resident immune cells exposed to chronic long-term HFD-induced changes and possible adaption processes.

Supplementary Materials: The following supporting information can be downloaded at: https://www.mdpi.com/article/10.3390/biom13050769/s1, Figure S1: Corresponding negative controls of the immunohistochemical reactions of (A) TSPO, (B) Iba1, (C) TMEM119 and (D) GFAP. Scale bar representing 1000 µm; Figure S2: [^{18}F]GE-180 PET imaging. (A) Comparison of mean uptake (%ID/mL) cerebellum of control diet (CD, yellow, n = 12) or high-fat diet (HFD, blue, n = 12). Statistical analysis was performed by unpaired student-*t* test. (B) Ratios of cortex, hippocampus and hypothalamus to cerebellum as pseudo-reference region in CD (n = 12) or HFD (n = 12). Statistical analysis was performed by repeated measures ANOVA followed by post hoc tests with Sidak's correction for multiple comparisons.

Author Contributions: Conceptualization, A.K.; methodology, A.K., A.S., T.L., J.S., N.P.G., L.M., N.B., C.B. and T.A.; validation, N.P.G., L.M., A.S., S.T., A.K. and B.V.; formal analysis, L.M., N.P.G. and A.S.; investigation, N.P.G., L.M. and D.B.; resources, A.K., D.J., B.J.K., J.K. and B.V.; data curation, N.P.G., L.M. and A.K.; writing—original draft preparation, L.M. and N.P.G.; writing—review and editing, A.K., A.S., T.L., S.T., B.V., C.B. and J.K.; visualization, L.M. and N.P.G.; supervision, A.K., B.V. and D.J.; project administration, A.K. and D.J.; funding acquisition, A.K. and D.J. All authors have read and agreed to the published version of the manuscript.

Funding: This research was funded by grant from the Deutsche Forschungsgemeinschaft, Bonn, Germany (KU3280/1-2 and JA 2872/1-2).

Institutional Review Board Statement: The animal study protocol was approved by the local Animal Research Committee (Landesamt für Landwirtschaft, Lebensmittelsicherheit und Fischerei (LALLF)) of the state Mecklenburg-Western Pomerania (LALLF M-V/TSD/7221.3-2-001/18, approved on 1 March 2018) and all animals received human care according to the EU Directive 2010/63/EU.

Informed Consent Statement: Not applicable.

Data Availability Statement: The data presented in this study are available on request from the corresponding author.

Acknowledgments: We wholeheartedly thank all the animal attendants Mareike Degner, Ilona Klamfuß, Chantal von Hörsten, Karin Gerber, Petra Klafke, Petra Wolff, Andrea Wilhelm, Roland Gerber and Klaus-Dieter Russow for their excellent assistance in animal care. Furthermore, we would like to thank Berit Blendow, Maren Nerowski, Eva Lorbeer, Sabine Glaubitz, Dorothea Frenz, Christin Schlie, Joanna Förster, Anne Rupp and Daniel Wolter for their invaluable technical assistance in the laboratory.

Conflicts of Interest: The authors declare no conflict of interest.

References

1. WHO. Obesity and Overweight. 2021. Available online: https://www.who.int/news-room/fact-sheets/detail/obesity-and-overweight (accessed on 29 November 2021).
2. Blüher, M. Obesity: Global epidemiology and pathogenesis. *Nat. Rev. Endocrinol.* **2019**, *15*, 288–298. [CrossRef] [PubMed]
3. Gregor, M.F.; Hotamisligil, G.S. Inflammatory mechanisms in obesity. *Annu. Rev. Immunol.* **2011**, *29*, 415–445. [CrossRef] [PubMed]
4. Lumeng, C.N.; Saltiel, A.R. Inflammatory links between obesity and metabolic disease. *J. Clin. Investig.* **2011**, *121*, 2111–2117. [CrossRef] [PubMed]
5. Marchesini, G.; Moscatiello, S.; Di Domizio, S.; Forlani, G. Obesity-associated liver disease. *J. Clin. Endocrinol. Metab.* **2008**, *93* (Suppl. 1), S74–S80. [CrossRef] [PubMed]
6. Saltiel, A.R.; Olefsky, J.M. Inflammatory mechanisms linking obesity and metabolic disease. *J. Clin. Investig.* **2017**, *127*, 1–4. [CrossRef]
7. Alford, S.; Patel, D.; Perakakis, N.; Mantzoros, C.S. Obesity as a risk factor for Alzheimer's disease: Weighing the evidence. *Obes. Rev.* **2018**, *19*, 269–280. [CrossRef]
8. Olivo, G.; Gour, S.; Schiöth, H.B. Low neuroticism and cognitive performance are differently associated to overweight and obesity: A cross-sectional and longitudinal UK Biobank study. *Psychoneuroendocrinology* **2019**, *101*, 167–174. [CrossRef]
9. Singh-Manoux, A.; Czernichow, S.; Elbaz, A.; Dugravot, A.; Sabia, S.; Hagger-Johnson, G.; Kaffashian, S.; Zins, M.; Brunner, E.J.; Nabi, H.; et al. Obesity phenotypes in midlife and cognition in early old age: The Whitehall II cohort study. *Neurology* **2012**, *79*, 755–762. [CrossRef]
10. Chuang, Y.-F.; An, Y.; Bilgel, M.; Wong, D.F.; Troncoso, J.C.; O'Brien, R.J.; Breitner, J.C.; Ferruci, L.; Resnick, S.M.; Thambisetty, M. Midlife adiposity predicts earlier onset of Alzheimer's dementia, neuropathology and presymptomatic cerebral amyloid accumulation. *Mol. Psychiatry* **2016**, *21*, 910–915. [CrossRef]
11. Xu, W.L.; Atti, A.R.; Gatz, M.; Pedersen, N.L.; Johansson, B.; Fratiglioni, L. Midlife overweight and obesity increase late-life dementia risk: A population-based twin study. *Neurology* **2011**, *76*, 1568–1574. [CrossRef]
12. Yang, Y.; Shields, G.S.; Guo, C.; Liu, Y. Executive function performance in obesity and overweight individuals: A meta-analysis and review. *Neurosci. Biobehav. Rev.* **2018**, *84*, 225–244. [CrossRef] [PubMed]
13. de Bem, A.F.; Krolow, R.; Farias, H.R.; Linden de Rezende, V.; Pens Gelain, D.; Fonseca Moreira, J.C.; das Neves Duarte, J.M.; de Oliveira, J. Animal Models of Metabolic Disorders in the Study of Neurodegenerative Diseases: An Overview. *Front. Neurosci.* **2020**, *14*, 604150. [CrossRef] [PubMed]
14. Marques, C.G.; Dos Santos Quaresma, M.V.L.; Nakamoto, F.P.; Magalhães, A.C.O.; Lucin, G.A.; Thomatieli-Santos, R.V. Does Modern Lifestyle Favor Neuroimmunometabolic Changes? A Path to Obesity. *Front. Nutr.* **2021**, *8*, 705545. [CrossRef]
15. Thaler, J.P.; Guyenet, S.J.; Dorfman, M.D.; Wisse, B.E.; Schwartz, M.W. Hypothalamic inflammation: Marker or mechanism of obesity pathogenesis? *Diabetes* **2013**, *62*, 2629–2634. [CrossRef] [PubMed]
16. Guillemot-Legris, O.; Muccioli, G.G. Obesity-Induced Neuroinflammation: Beyond the Hypothalamus. *Trends Neurosci.* **2017**, *40*, 237–253. [CrossRef] [PubMed]
17. Prinz, M.; Erny, D.; Hagemeyer, N. Ontogeny and homeostasis of CNS myeloid cells. *Nat. Immunol.* **2017**, *18*, 385–392. [CrossRef]
18. Kälin, S.; Heppner, F.L.; Bechmann, I.; Prinz, M.; Tschöp, M.H.; Yi, C.-X. Hypothalamic innate immune reaction in obesity. *Nat. Rev. Endocrinol.* **2015**, *11*, 339–351. [CrossRef]
19. Bachiller, S.; Jiménez-Ferrer, I.; Paulus, A.; Yang, Y.; Swanberg, M.; Deierborg, T.; Boza-Serrano, A. Microglia in Neurological Diseases: A Road Map to Brain-Disease Dependent-Inflammatory Response. *Front. Cell. Neurosci.* **2018**, *12*, 488. [CrossRef]
20. Kwon, H.S.; Koh, S.-H. Neuroinflammation in neurodegenerative disorders: The roles of microglia and astrocytes. *Transl. Neurodegener.* **2020**, *9*, 42. [CrossRef]

21. Geloso, M.C.; Corvino, V.; Marchese, E.; Serrano, A.; Michetti, F.; D'Ambrosi, N. The Dual Role of Microglia in ALS: Mechanisms and Therapeutic Approaches. *Front. Aging Neurosci.* **2017**, *9*, 242. [CrossRef]
22. Zhan, J.; Mann, T.; Joost, S.; Behrangi, N.; Frank, M.; Kipp, M. The Cuprizone Model: Dos and Do Nots. *Cells* **2020**, *9*, 843. [CrossRef] [PubMed]
23. Betlazar, C.; Middleton, R.J.; Banati, R.; Liu, G.-J. The Translocator Protein (TSPO) in Mitochondrial Bioenergetics and Immune Processes. *Cells* **2020**, *9*, 512. [CrossRef]
24. Werry, E.L.; Bright, F.M.; Piguet, O.; Ittner, L.M.; Halliday, G.M.; Hodges, J.R.; Kiernan, M.C.; Loy, C.L.; Kril, J.J.; Kassiou, M. Recent Developments in TSPO PET Imaging as A Biomarker of Neuroinflammation in Neurodegenerative Disorders. *Int. J. Mol. Sci.* **2019**, *20*, 3161. [CrossRef] [PubMed]
25. Coenen, H.H.; Gee, A.D.; Adam, M.; Antoni, G.; Cutler, C.S.; Fujibayashi, Y.; Min Jeong, J.; Mach, R.H.; Mindt, T.L.; Pike, V.W.; et al. Consensus nomenclature rules for radiopharmaceutical chemistry—Setting the record straight. *Nucl. Med. Biol.* **2017**, *55*, v–xi. [CrossRef] [PubMed]
26. Chen, M.-K.; Guilarte, T.R. Translocator protein 18 kDa (TSPO): Molecular sensor of brain injury and repair. *Pharmacol. Ther.* **2008**, *118*, 1–17. [CrossRef]
27. Deussing, M.; Blume, T.; Vomacka, L.; Mahler, C.; Focke, C.; Todica, A.; Unterrainer, M.; Albert, N.L.; Lindner, S.; von Ungern-Sternberg, B.; et al. Coupling between physiological TSPO expression in brain and myocardium allows stabilization of late-phase cerebral 18FGE180 PET quantification. *Neuroimage* **2018**, *165*, 83–91. [CrossRef]
28. Rominger, A.; Brendel, M.; Burgold, S.; Keppler, K.; Baumann, K.; Xiong, G.; Mille, E.; Gildehaus, F.-J.; Carlsen, J.; Schlichtinger, J.; et al. Longitudinal assessment of cerebral β-amyloid deposition in mice overexpressing Swedish mutant β-amyloid precursor protein using 18F-florbetaben PET. *J. Nucl. Med.* **2013**, *54*, 1127–1134. [CrossRef]
29. Lee, Y.; Park, Y.; Nam, H.; Lee, J.-W.; Yu, S.-W. Translocator protein (TSPO): The new story of the old protein in neuroinflammation. *BMB Rep.* **2020**, *53*, 20–27. [CrossRef]
30. van Camp, N.; Lavisse, S.; Roost, P.; Gubinelli, F.; Hillmer, A.; Boutin, H. TSPO imaging in animal models of brain diseases. *Eur. J. Nucl. Med. Mol. Imaging* **2021**, *49*, 77–109. [CrossRef]
31. Barron, A.M.; Tokunaga, M.; Zhang, M.-R.; Ji, B.; Suhara, T.; Higuchi, M. Assessment of neuroinflammation in a mouse model of obesity and β-amyloidosis using PET. *J. Neuroinflamm.* **2016**, *13*, 221. [CrossRef]
32. Müller, L.; Power Guerra, N.; Stenzel, J.; Rühlmann, C.; Lindner, T.; Krause, B.J.; Vollmar, B.; Teipel, S.; Kuhla, A. Long-Term Caloric Restriction Attenuates β-Amyloid Neuropathology and Is Accompanied by Autophagy in APPswe/PS1delta9 Mice. *Nutrients* **2021**, *13*, 985. [CrossRef]
33. Rühlmann, C.; Dannehl, D.; Brodtrück, M.; Adams, A.C.; Stenzel, J.; Lindner, T.; Krause, B.J.; Vollmar, B.; Kuhla, A. Neuroprotective Effects of the FGF21 Analogue LY2405319. *J. Alzheimers Dis.* **2021**, *80*, 357–369. [CrossRef] [PubMed]
34. Mirrione, M.M.; Schiffer, W.K.; Fowler, J.S.; Alexoff, D.L.; Dewey, S.L.; Tsirka, S.E. A novel approach for imaging brain-behavior relationships in mice reveals unexpected metabolic patterns during seizures in the absence of tissue plasminogen activator. *Neuroimage* **2007**, *38*, 34–42. [CrossRef]
35. Kleiber, M. Body size and metabolic rate. *Physiol. Rev.* **1947**, *27*, 511–541. [CrossRef] [PubMed]
36. Kuhla, A.; Lange, S.; Holzmann, C.; Maass, F.; Petersen, J.; Vollmar, B.; Wree, A. Lifelong caloric restriction increases working memory in mice. *PLoS ONE* **2013**, *8*, e68778. [CrossRef] [PubMed]
37. Power Guerra, N.; Müller, L.; Pilz, K.; Glatzel, A.; Jenderny, D.; Janowitz, D.; Vollmar, B.; Kuhla, A. Dietary-Induced Low-Grade Inflammation in the Liver. *Biomedicines* **2020**, *8*, 587. [CrossRef]
38. Patkar, O.L.; Mohamed, A.Z.; Narayanan, A.; Mardon, K.; Cowin, G.; Bhalla, R.; Stimson, D.H.R.; Kassiou, M.; Beecher, K.; Belmer, A.; et al. A binge high sucrose diet provokes systemic and cerebral inflammation in rats without inducing obesity. *Sci. Rep.* **2021**, *11*, 11252. [CrossRef]
39. Cavaliere, G.; Trinchese, G.; Penna, E.; Cimmino, F.; Pirozzi, C.; Lama, A.; Annunziata, C.; Catapano, A.; Mattace Raso, G.; Meli, R.; et al. High-Fat Diet Induces Neuroinflammation and Mitochondrial Impairment in Mice Cerebral Cortex and Synaptic Fraction. *Front. Cell. Neurosci.* **2019**, *13*, 509. [CrossRef] [PubMed]
40. Dutheil, S.; Ota, K.T.; Wohleb, E.S.; Rasmussen, K.; Duman, R.S. High-Fat Diet Induced Anxiety and Anhedonia: Impact on Brain Homeostasis and Inflammation. *Neuropsychopharmacology* **2016**, *41*, 1874–1887. [CrossRef]
41. Kennedy, A.J.; Ellacott, K.L.J.; King, V.L.; Hasty, A.H. Mouse models of the metabolic syndrome. *Dis. Models Mech.* **2010**, *3*, 156–166. [CrossRef]
42. Tschöp, M.; Heiman, M.L. Rodent obesity models: An overview. *Exp. Clin. Endocrinol. Diabetes* **2001**, *109*, 307–319. [CrossRef]
43. Kim, M.S.; Choi, M.-S.; Han, S.N. High fat diet-induced obesity leads to proinflammatory response associated with higher expression of NOD2 protein. *Nutr. Res. Pract.* **2011**, *5*, 219–223. [CrossRef] [PubMed]
44. Kim, J.D.; Yoon, N.A.; Jin, S.; Diano, S. Microglial UCP2 Mediates Inflammation and Obesity Induced by High-Fat Feeding. *Cell Metab.* **2019**, *30*, 952–962.e5. [CrossRef] [PubMed]
45. Li, J.; Wu, H.; Liu, Y.; Yang, L. High fat diet induced obesity model using four strainsof mice: Kunming, C57BL/6, BALB/c and ICR. *Exp. Anim.* **2020**, *69*, 326–335. [CrossRef] [PubMed]
46. de Bona Schraiber, R.; de Mello, A.H.; Garcez, M.L.; de Bem Silveira, R.; Pereira Zacaron, R.; Pereira de Souza Goldim, M.; Budni, J.; Lock Silveira, P.C.; Petronilho, F.; Kozuchovski Ferreira, G.; et al. Diet-induced obesity causes hypothalamic neurochemistry alterations in Swiss mice. *Metab. Brain Dis.* **2019**, *34*, 565–573. [CrossRef] [PubMed]

47. Thaler, J.P.; Yi, C.-X.; Schur, E.A.; Guyenet, S.J.; Hwang, B.H.; Dietrich, M.O.; Zhao, X.; Sarruf, D.A.; Izgur, V.; Maravilla, K.R.; et al. Obesity is associated with hypothalamic injury in rodents and humans. *J. Clin. Investig.* **2012**, *122*, 153–162. [CrossRef]
48. Waise, T.M.Z.; Toshinai, K.; Naznin, F.; NamKoong, C.; Moin, A.S.M.; Sakoda, H.; Nakazato, M. One-day high-fat diet induces inflammation in the nodose ganglion and hypothalamus of mice. *Biochem. Biophys. Res. Commun.* **2015**, *464*, 1157–1162. [CrossRef] [PubMed]
49. Nakandakari, S.C.B.R.; Muñoz, V.R.; Kuga, G.K.; Calais Gaspar, R.; Ramos Sant'Ana, M.; Betim Pavan, I.C.; Salvino da Silva, L.G.; Morelli, A.P.; Moreira Simabuco, F.; Sanchez Ramos da Silva, A.; et al. Short-term high-fat diet modulates several inflammatory, ER stress, and apoptosis markers in the hippocampus of young mice. *Brain Behav. Immun.* **2019**, *79*, 284–293. [CrossRef] [PubMed]
50. Hao, S.; Dey, A.; Yu, X.; Stranahan, A.M. Dietary obesity reversibly induces synaptic stripping by microglia and impairs hippocampal plasticity. *Brain Behav. Immun.* **2016**, *51*, 230–239. [CrossRef]
51. Ávalos, Y.; Kerr, B.; Maliqueo, M.; Dorfman, M. Cell and molecular mechanisms behind diet-induced hypothalamic inflammation and obesity. *J. Neuroendocrinol.* **2018**, *30*, e12598. [CrossRef]
52. Lainez, N.M.; Jonak, C.R.; Nair, M.G.; Ethell, I.M.; Wilson, E.H.; Carson, M.J.; Coss, D. Diet-Induced Obesity Elicits Macrophage Infiltration and Reduction in Spine Density in the Hypothalami of Male but Not Female Mice. *Front. Immunol.* **2018**, *9*, 1992. [CrossRef]
53. Robison, L.S.; Albert, N.M.; Camargo, L.A.; Anderson, B.M.; Salinero, A.E.; Riccio, D.A.; Abi-Ghanem, C.; Gannon, O.J.; Zuloaga, K.L. High-Fat Diet-Induced Obesity Causes Sex-Specific Deficits in Adult Hippocampal Neurogenesis in Mice. *eNeuro* **2020**, *7*, ENEURO.0391-19.2019. [CrossRef]
54. Leonardi, B.F.; Gosmann, G.; Zimmer, A.R. Modeling Diet-Induced Metabolic Syndrome in Rodents. *Mol. Nutr. Food Res.* **2020**, *64*, e2000249. [CrossRef] [PubMed]
55. Sanguinetti, E.; Guzzardi, M.A.; Panetta, D.; Tripodi, M.; de Sena, V.; Quaglierini, M.; Burchielli, S.; Salvadori, P.A.; Iozzo, P. Combined Effect of Fatty Diet and Cognitive Decline on Brain Metabolism, Food Intake, Body Weight, and Counteraction by Intranasal Insulin Therapy in 3×Tg Mice. *Front. Cell. Neurosci.* **2019**, *13*, 188. [CrossRef] [PubMed]
56. Tuulari, J.J.; Karlsson, H.K.; Hirvonen, J.; Hannukainen, J.C.; Bucci, M.; Helmiö, M.; Ovaska, J.; Soinio, M.; Salminen, P.; Savisto, N.; et al. Weight loss after bariatric surgery reverses insulin-induced increases in brain glucose metabolism of the morbidly obese. *Diabetes* **2013**, *62*, 2747–2751. [CrossRef] [PubMed]
57. Miller, A.A.; Spencer, S.J. Obesity and neuroinflammation: A pathway to cognitive impairment. *Brain Behav. Immun.* **2014**, *42*, 10–21. [CrossRef]
58. Herfert, K.; Mannheim, J.G.; Kuebler, L.; Marciano, S.; Amend, M.; Parl, C.; Napieczynska, H.; Maier, F.M.; Castaneda Vega, S.; Pichler, B.J. Quantitative Rodent Brain Receptor Imaging. *Mol. Imaging Biol.* **2020**, *22*, 223–244. [CrossRef]
59. Lammertsma, A.A. Forward to the Past: The Case for Quantitative PET Imaging. *J. Nucl. Med.* **2017**, *58*, 1019–1024. [CrossRef]
60. Zatcepin, A.; Heindl, S.; Schillinger, U.; Kaiser, L.; Lindner, S.; Bartenstein, P.; Kopczak, A.; Liesz, A.; Brendel, M.; Ziegler, S.I. Reduced Acquisition Time 18FGE-180 PET Scanning Protocol Replaces Gold-Standard Dynamic Acquisition in a Mouse Ischemic Stroke Model. *Front. Med.* **2022**, *9*, 830020. [CrossRef]
61. Lyoo, C.H.; Ikawa, M.; Liow, J.-S.; Zoghbi, S.Z.; Morse, C.L.; Pike, V.W.; Fujita, M.; Innis, R.B.; Kreisl, W.C. Cerebellum Can Serve As a Pseudo-Reference Region in Alzheimer Disease to Detect Neuroinflammation Measured with PET Radioligand Binding to Translocator Protein. *J. Nucl. Med.* **2015**, *56*, 701–706. [CrossRef]
62. de Paula, G.C.; Brunetta, H.S.; Engel, D.F.; Gaspar, J.M.; Velloso, L.A.; Engblom, D.; de Oliveira, J.; de Bem, A.F. Hippocampal Function Is Impaired by a Short-Term High-Fat Diet in Mice: Increased Blood-Brain Barrier Permeability and Neuroinflammation as Triggering Events. *Front. Neurosci.* **2021**, *15*, 734158. [CrossRef] [PubMed]
63. Unterrainer, M.; Fleischmann, D.F.; Diekmann, C.; Vomacka, L.; Lindner, S.; Vettermann, F.; Brendel, M.; Wenter, V.; Ertl-Wagner, B.; Herms, J.; et al. Comparison of 18F-GE-180 and dynamic 18F-FET PET in high grade glioma: A double-tracer pilot study. *Eur. J. Nucl. Med. Mol. Imaging* **2019**, *46*, 580–590. [CrossRef]
64. Zanotti-Fregonara, P.; Veronese, M.; Pascual, B.; Rostomily, R.C.; Turkheimer, F.; Masdeu, J.C. The validity of 18F-GE180 as a TSPO imaging agent. *Eur. J. Nucl. Med. Mol. Imaging* **2019**, *46*, 1205–1207. [CrossRef] [PubMed]
65. Satoh, J.; Kino, Y.; Asahina, N.; Takitani, M.; Miyoshi, J.; Ishida, T.; Saito, Y. TMEM119 marks a subset of microglia in the human brain. *Neuropathology* **2016**, *36*, 39–49. [CrossRef]
66. Young, K.F.; Gardner, R.; Sariana, V.; Whitman, S.A.; Bartlett, M.J.; Falk, T.; Morrison, H.W. Can quantifying morphology and TMEM119 expression distinguish between microglia and infiltrating macrophages after ischemic stroke and reperfusion in male and female mice? *J. Neuroinflamm.* **2021**, *18*, 58. [CrossRef] [PubMed]
67. Hol, E.M.; Pekny, M. Glial fibrillary acidic protein (GFAP) and the astrocyte intermediate filament system in diseases of the central nervous system. *Curr. Opin. Cell Biol.* **2015**, *32*, 121–130. [CrossRef] [PubMed]
68. Boorman, D.C.; Keay, K.A. Sex differences in morphine sensitivity are associated with differential glial expression in the brainstem of rats with neuropathic pain. *J. Neurosci. Res.* **2022**, *100*, 1890–1907. [CrossRef]
69. Imai, Y.; Ibata, I.; Ito, D.; Ohsawa, K.; Kohsaka, S. A novel gene iba1 in the major histocompatibility complex class III region encoding an EF hand protein expressed in a monocytic lineage. *Biochem. Biophys. Res. Commun.* **1996**, *224*, 855–862. [CrossRef]
70. Ito, D.; Imai, Y.; Ohsawa, K.; Nakajima, K.; Fukuuchi, Y.; Kohsaka, S. Microglia-specific localisation of a novel calcium binding protein, Iba1. *Mol. Brain Res.* **1998**, *57*, 1–9. [CrossRef]

71. Abedi, A.; Foroutan, T.; Mohaghegh Shalmani, L.; Dargahi, L. Sex-specific effects of high-fat diet on rat brain glucose metabolism and early-onset dementia symptoms. *Mech. Ageing Dev.* **2023**, *211*, 111795. [CrossRef]
72. Yunna, C.; Mengru, H.; Lei, W.; Weidong, C. Macrophage M1/M2 polarization. *Eur. J. Pharmacol.* **2020**, *877*, 173090. [CrossRef] [PubMed]
73. Coats, B.R.; Schoenfelt, K.Q.; Barbosa-Lorenzi, V.C.; Peris, E.; Cui, C.; Hoffman, A.; Zhou, G.; Fernandez, S.; Zhai, L.; Hall, B.A.; et al. Metabolically Activated Adipose Tissue Macrophages Perform Detrimental and Beneficial Functions during Diet-Induced Obesity. *Cell Rep.* **2017**, *20*, 3149–3161. [CrossRef] [PubMed]
74. Kratz, M.; Coats, B.R.; Hisert, K.B.; Hagman, D.; Mutskov, V.; Peris, E.; Schoenfelt, K.Q.; Kuzma, J.N.; Larson, I.; Billing, P.S.; et al. Metabolic dysfunction drives a mechanistically distinct proinflammatory phenotype in adipose tissue macrophages. *Cell Metab.* **2014**, *20*, 614–625. [CrossRef] [PubMed]
75. Kim, K.-A.; Gu, W.; Lee, I.-A.; Joh, E.-H.; Kim, D.-H. High fat diet-induced gut microbiota exacerbates inflammation and obesity in mice via the TLR4 signaling pathway. *PLoS ONE* **2012**, *7*, e47713. [CrossRef] [PubMed]
76. van der Heijden, R.A.; Sheedfar, F.; Morrison, M.C.; Hommelberg, P.P.H.; Kor, D.; Kloosterhuis, N.J.; Gruben, N.; Youssef, S.A.; de Bruin, A.; Hofker, M.H.; et al. High-fat diet induced obesity primes inflammation in adipose tissue prior to liver in C57BL/6j mice. *Aging* **2015**, *7*, 256–268. [CrossRef] [PubMed]
77. Robblee, M.M.; Kim, C.C.; Porter Abate, J.; Valdearcos, M.; Sandlund, K.L.M.; Shenoy, M.K.; Volmer, R.; Iwawaki, T.; Koliwad, S.K. Saturated Fatty Acids Engage an IRE1α-Dependent Pathway to Activate the NLRP3 Inflammasome in Myeloid Cells. *Cell Rep.* **2016**, *14*, 2611–2623. [CrossRef]
78. Mendiola, A.S.; Cardona, A.E. The IL-1β phenomena in neuroinflammatory diseases. *J. Neural Transm.* **2017**, *125*, 781–795. [CrossRef]
79. Sobesky, J.L.; Barrientos, R.M.; de May, H.S.; Thompson, B.M.; Weber, M.D.; Watkins, L.R.; Maier, S.F. High-fat diet consumption disrupts memory and primes elevations in hippocampal IL-1β, an effect that can be prevented with dietary reversal or IL-1 receptor antagonism. *Brain Behav. Immun.* **2014**, *42*, 22–32. [CrossRef]

10.3 Studie 3

frontiers | Frontiers in Neuroscience

TYPE Original Research
PUBLISHED xx xx 2023
DOI 10.3389/fnins.2023.1052079

OPEN ACCESS

EDITED BY
David Mokler,
University of New England, United States

REVIEWED BY
Hideo Hagihara,
Fujita Health University, Japan
Anh Hai Tran,
Vietnam Military Medical University, Vietnam

*CORRESPONDENCE
Angela Kuhla
angela.kuhla@uni-rostock.de

†These authors have contributed equally to this work

SPECIALTY SECTION
This article was submitted to Neuroenergetics, Nutrition and Brain Health, a section of the journal Frontiers in Neuroscience

RECEIVED 23 September 2022
ACCEPTED 02 March 2023
PUBLISHED xx xx 2023

CITATION
Bühler D, Power Guerra N, Müller L, Wolkenhauer O, Düffer M, Vollmar B, Kuhla A and Wolfien M (2023) Leptin deficiency-caused behavioral change–A comparative analysis using EthoVision and DeepLabCut.
Front. Neurosci. 17:1052079.
doi: 10.3389/fnins.2023.1052079

Leptin deficiency-caused behavioral change–A comparative analysis using EthoVision and DeepLabCut

Daniel Bühler[1,2,3], Nicole Power Guerra[1,4], Luisa Müller[1,5,6], Olaf Wolkenhauer[3,7], Martin Düffer[1], Brigitte Vollmar[1,5], Angela Kuhla[1,5*†] and Markus Wolfien[3,8,9†]

[1]Rudolf-Zenker-Institute for Experimental Surgery, Rostock University Medical Center, Rostock, Germany, [2]Institute of Experimental Epileptology and Cognition Research, University Medical Center Bonn, Bonn, Germany, [3]Department of Systems Biology and Bioinformatics, University of Rostock, Rostock, Germany, [4]Clinic and Polyclinic for Otorhinolaryngology and Otolaryngology, Faculty of Medicine Carl Gustav Carus, Technische Universität Dresden, Dresden, Germany, [5]Centre for Transdisciplinary Neurosciences Rostock (CTNR), Rostock University Medical Center, Rostock, Germany, [6]Department of Psychosomatic Medicine and Psychotherapy, Rostock University Medical Center, Rostock, Germany, [7]Leibniz-Institute for Food Systems Biology, Technical University of Munich, Freising, Germany, [8]Institute for Medical Informatics and Biometry, Faculty of Medicine Carl Gustav Carus, Technische Universität Dresden, Dresden, Germany, [9]Center for Scalable Data Analytics and Artificial Intelligence (ScaDS.AI), Dresden, Germany

Introduction: Obese rodents e.g., the leptin-deficient (ob/ob) mouse exhibit remarkable behavioral changes and are therefore ideal models for evaluating mental disorders resulting from obesity. In doing so, female as well as male ob/ob mice at 8, 24, and 40 weeks of age underwent two common behavioral tests, namely the Open Field test and Elevated Plus Maze, to investigate behavioral alteration in a sex- and age dependent manner. The accuracy of these tests is often dependent on the observer that can subjectively influence the data.

Methods: To avoid this bias, mice were tracked with a video system. Video files were further analyzed by the compared use of two software, namely EthoVision (EV) and DeepLabCut (DLC). In DLC a Deep Learning application forms the basis for using artificial intelligence in behavioral research in the future, also with regard to the reduction of animal numbers.

Results: After no sex and partly also no age-related differences were found, comparison revealed that both software lead to almost identical results and are therefore similar in their basic outcomes, especially in the determination of velocity and total distance movement. Moreover, we observed additional benefits of DLC compared to EV as it enabled the interpretation of more complex behavior, such as rearing and leaning, in an automated manner.

Discussion: Based on the comparable results from both software, our study can serve as a starting point for investigating behavioral alterations in preclinical studies of obesity by using DLC to optimize and probably to predict behavioral observations in the future.

KEYWORDS
behavioral analysis, obesity, EthoVision, DeepLabCut, deep learning

Introduction

Abnormal and excessive accumulation of fat tissue associated with severe overweight and obesity is one of the most challenging diseases of the 21st century (World Health Organization [WHO], 2021). Obesity is a public health concern affecting both genders at all ages around the world and is an enormous burden on the global health system due to an increasingly high prevalence. Obesity-associated comorbidities are mostly diabetes type 2 (Drucker, 2021), cardiovascular diseases (Powell-Wiley et al., 2021), and vascular diseases that can affect function and quality of life and thus can cause mental disease (Sarma et al., 2021). The most common current psychiatric disorders in obese patients are depression and anxiety (Moradi et al., 2021). It is still largely unclear to what extent obesity affects mental health. Obese rodents remarkably exhibit behavioral alterations such as anxiety and are therefore effective models in behavioral research (Guma et al., 2022) to further address research questions on mental health. A transgene model for obesity research is the leptin deficient mouse (ob/ob) (Zhao et al., 2020). Animal behavior can be assessed by using different types of behavioral tests, such as the Open Field (OF) test and the Elevated Plus Maze (EPM). Both tests are among the most commonly used methods in behavioral laboratories to investigate changes in anxious-related behavior in rodents (Rodgers and Shepherd, 1993). For instance, reduced exploration (rearing/head dipping) indicates anxiety, and reduced locomotion has been linked to adaptive stress-related behaviors (Walf and Frye, 2007). To record such behavior, previously, this would be done live by a trained observer, scoring (i.e., classifying) the behavior of the animal live while the test was being conducted. Nowadays, the standard approach is to record the complete test session with high-speed cameras, which are positioned above the testing arenas as to capture all behavior of the animal. Subsequently, the behavior is being scored *post hoc* by analyzing the videos (CVPR 2019 Open Access Repository, 2019). Traditional approaches to analyze video data and score the animals behavior usually involved several researchers watching videos of behavioral test sessions and noting the times and locations of specific events of interest. Although previously seen as fold-standard, these investigations have been very time-consuming, needed professional knowledge of ethologists, and were prone to be influenced by potential observer bias (Datta et al., 2019). In order to produce behavioral data that is comparable across laboratories, it is important to develop standardized methods that are robust, reproducible and minimize the influence of biases. Therefore, semi-automated video analysis methods have been developed decades ago. However, only the latest developments in artificial intelligence (AI) and ever faster computing power enable it to evaluate videos automatically and reduce the bias by human observers even further (Valletta et al., 2017).

Advances in automatic video analysis make it possible to analyze animal behavior independently of an observer (Sturman et al., 2020). Commercial products, such as EthoVision (EV, Noldus, Wageningen, Netherlands), are available for semi-automated tracking of behavior in videos. However, these systems have some limitation, for example they depend on the ability to detect the subject based on differences of background color and cannot account for dynamic aspects of behavior. EV enables animal tracking in a wide range of animal testing batteries and is independent of visible or artificially applied markers, as it calculates the central point of the torso on the basis of the contour of the moving mouse (Sturman et al., 2020). To analyze the movement, this point is recalculated frame by frame. EV is widely used in behavioral analysis because it offers an easy-to-use interface and can be installed on common computers in almost any laboratory. Accordingly, Stringer et al. (2019) investigated spontaneous coding of visual signals and studied motion-related information in mouse visual cortex using such an approach. Moreover, Musall et al. (2019) analyzed cortical imaging data using multiple discrete measures of performance (e.g., stimulus type and reaction time) and video-based measures of movement from mice performing a decision-making task. While these approaches have led to novel insights into neural determinants of behavior, they are limited to categorize movements, measure transitions between different types of movements, or quantify the dynamics of movement sequences (Musall et al., 2019). Recent developments in the field of computer vision and machine learning (ML) offer a solution to measure these behavioral dynamics. As a result, first descriptions of unsupervised behavioral analyses revealed astonishing temporal and structural complexity of rodent behavior. However, these advanced analyses are not applicable for many behavioral research laboratories, as they usually lack necessary hardware and needed know-how. To overcome this issue, a growing number of research groups develop methods that enable an analysis of motion and associated-behavior more efficiently, and above all, automatically (Knutsen et al., 2005; Voigts et al., 2008; Perkon et al., 2011; Clack et al., 2012; Ohayon et al., 2013; Giovannucci et al., 2018; Dominiak et al., 2019; Vanzella et al., 2019; Betting et al., 2020; Petersen et al., 2020). Recently, Deep Learning (DL) applications have been used in behavior imaging data analysis. Most commonly used for this purpose are so-called convolutional neural networks (CNN), a class of deep neural networks. They consist of nodes ("neurons"), including with learnable weights and biases that have been trained from the input data ("edges"). In particular, the development of DeepLabCut (DLC), which is a markerless pose-estimation toolkit based on DL (Mathis et al., 2018), facilitates the generation of networks with very small training sets. Using DLC, it is now possible to score behavior completely independent of an observer and allows the tracking of animal movements of nearly any part of the body. In turn, it offers the possibility of uncovering new behavioral patterns with the help of unsupervised learning approaches. This could lead to the identification of causal mechanisms of various diseases that are reflected in behavioral changes.

Herein, this study was conducted to compare two common pose estimation methods, namely EV and DLC, to characterize obese-related behavioral changes in ob/ob mice. In addition, this preclinical research should help to clarify the extent to which behavioral changes can be covered just as well or even better with DLC in order to predict behavior with AI in the future.

Materials and methods

Animals

For the study, 45 (15 male and 30 female) leptin deficient mice (ob/ob) and 46 (13 male and 33 female) wild type (wt, C57BL6)

were used. The animals were littermates at the age of 8, 24, and 40 weeks. They were housed in standard cages with up to 5 animals per cage, in a temperature-controlled room (21 ± 3°C) with a 12/12 h day-night cycle (lights from 06:00 a.m. to 06:00 p.m.) containing a twilight period of 30 min. The exact number of the corresponding age groups is given in Table 1. Both wt and ob/ob mice were generated from our own breeding and were fed the same standard diet (ssniff R/M-H, ssniff® Spezialdiäten GmbH, Soest, Germany). All animal experimental work was carried out with permission of the local Animal Research Committee [Landesamt für Landwirtschaft, Lebensmittelsicherheit, und Fischerei (LALLF)] of the state Mecklenburg-Western Pomerania (LALLF M-V/TSD/7221.3-2-001/18, approved on 1 March 2018) and all animals received human care according to the EU Directive 2010/63/EU. The experimental design is illustrated in Figure 1.

Behavioral procedures

Behavioral analyses were performed on wt and ob/ob mice with no prior handling other than routine husbandry. Experiments were conducted between 07:00 a.m. and 03:00 p.m. under normal lighting conditions. The same operator (NPG for female mice; DB for male mice) assessed the mice aged 8, 24, and 40 weeks. All age groups and both sexes were used for the behavioral tests. Mice were brought into the testing room in their home cages 120 min prior to testing to allow adaptation. Each animal received a single trial, 5 min for both OF and EPM. Between both tests, breaks with a length of at least 1 day in the testing room were carried out. The behavior was recorded using a video camera system (Camera CCA1300-60 mg, Basler, and lens 15E, Computar, Japan) located 100 cm above the box and maze, and the EthoVision (EV) XT 11.5 software (Nodulus Information Technology). For more details please see Power Guerra et al. (2021).

Open field (OF)

Curiosity, exploratory, and locomotor activity of wt and ob/ob mice were assessed in a well illuminated, 50 cm × 50 cm squared plastic box, which was virtually divided into 16 zones by a 4 × 4 grid formation. Each zone was 12.5 cm × 12.5 cm. The walls were 40 cm high. For each trial the mice were placed into the center of the arena and were allowed to explore the field for 5 min. Next, each mouse was removed and placed back into the home cage. The total distance (cm), velocity (cm/s), visits in center (n) and periphery (n) were analyzed.

TABLE 1 Amount of animals.

Age of animals	Female (*n*)		Male (*n*)	
	wt	ob/ob	wt	ob/ob
8 weeks	10	10	3	5
24 weeks	10	10	5	5
40 weeks	13	10	5	5
	33	**30**	**13**	**15**

The groups were arranged based on age, sex, and genotype. wt, wild type; ob/ob, leptin deficient mice. The bold numbers indicate the respective sums of animals for the individual column.

Elevated plus maze (EPM)

The EPM is a behavioral test to investigate unconditioned anxiety-related behavior that involves a conflict between the desire to explore a novel environment and anxiogenic elements, such as elevation and a brightly illuminated arena. The EPM was made from gray poly vinyl chloride, according to the description of Komada et al. (2008). The 60 cm high elevated platform consists of two open arms measuring 37 cm × 6 cm (length × width) and perpendicular to the open arms were two closed arms of the same dimension, but with additional walls of 12.4 cm high. The cross at the center of the four arms consisted of a 6 cm × 6 cm square. The open arms contained a slight ledge (4 mm) to prevent mice from falling off the arms.

Each mouse was placed into the center square facing the open arm most distant to the experimenter and was allowed to freely move and explore the EPM for 5 min. Next, each mouse was removed and placed back into the home cage. Total distance (cm), velocity (cm/s), visits in open arm (n) and closed arms (n) were measured.

Video analysis with the EthoVision XT 11.5 software

In addition to analysis of videos, EV (EthoVision XT 11.5) was used to record all OF and EPM videos. The in-build "Automatic animal detection settings" of EV were used for all video analysis. Slight tuning of these settings was performed using the fine-tuning slider in the automated animal detection settings to ensure the animals could be tracked throughout the entire arena. We ensured there was a smooth tracking curve and that the center point of the animal remained stable before analysis took place. The automated tracker option of EV classified arm entries based on the nominal center of a mouse crossing into an arm. The rearing counts were collected manually by video analysis.

Video analysis with DeepLabCut

In addition to EV analysis, also DLC was used to evaluate the behavior of the animals in the OF and EPM. For this purpose, the same videos from the EV analysis were used. Data generated by DLC was processed using customized R Scripts that are available online.[1] The data acquisition workflow can be seen in the Supplementary Figure 1 [for more detailed information see Sturman et al. (2020)]. In brief, DLC was used to track 13 body points of interest (Supplementary Figure 2), and the corner points of the OF/EPM arena, since these are also recommended default parameters for subsequent analysis tools, e.g., SimBa (Nilson et al., 2020). To train the networks for both tests, 20 frames from multiple,

1 https://github.com/ETHZ-INS/DLCAnalyzer

randomly selected videos were selected and run for ~500.000 iterations. Subsequently, the coordinates obtained were analyzed with an adapted R GitHub script,[2] which was initially provided by ETH Zürich. Values of tracked points with low accuracy (<0.95) were removed. The velocity and distance of each point was determined by estimating the animal's position over 5 min.

Server specifications

The DLC computations have been utilized by a CentOS Linux compute node equipped with 8 × Nvidia Quadro RTX 2080 Ti, 2 × Intel Xeon Gold 6142 (16 Cores, 32 Threads), and 768 GB RAM.

Weight control and euthanasia

Body weight was measured (Kern PCB, Lübeck, Germany) prior to euthanasia. Under anesthesia (5 vol. % isoflurane; Baxter, Unterschleißheim, Germany) the mice were euthanized, laparotomized, and visceral and subcutaneous flanked fat deposits were harvested and weighed (Power Guerra et al., 2021).

Statistics

Statistical analysis was performed using GraphPad Prism 8.0.1 (GraphPad Software Inc., San Diego, CA, USA) or Excel. The ROUT method based on false discovery rate ($Q = 0.01$) was used to identify and re-move outliers if possible and necessary. Data were also excluded when mice did not perform behavioral tests. Data were tested for normal distribution and all comparisons between normally distributed datasets containing two independent groups were performed using unpaired Student's *t*-test, whereas all comparisons with more than two groups were performed using two- or three-way ANOVAs in order to identify group effects. Significant main effects were then followed up with *post-hoc* tests. Further information is given in respective Figure legends. The results are presented as box plots indicating the median, the 25th and 75th percentile in the form of a box with the confidence interval of 95%. To represent correlation between DLC and EV software (Figure 5 and Supplementary Figure 8) Spearman Correlation was performed by using confidence interval of 90% and measuring linear dependence of two parameters. Additionally, a Bland-Altman Plot analysis was performed to evaluate the agreement between the used methods (EV and DLC).

Results

Leptin deficiency affects massive body weight gain

Body weight (Figure 2A), visceral fat (Figure 2B), and subcutaneous fat (Figure 2C) were significantly increased in ob/ob mice compared to the control wt littermates by data showing a strong effect of genotype [A: $p < 0.0001$, $F_{(1,75)} = 508.6$; B: $p < 0.0001$, $F_{(1,74)} = 104.2$; C: $p < 0.0001$, $F_{(1,63)} = 148.7$]. In addition, the data also show a age effect [A: $p < 0.0001$, $F_{(2,75)} = 69.92$; B: $p = 0.0041$, $F_{(2,74)} = 5.940$; C: $p < 0.0001$, $F_{(2,63)} = 14.06$], but no sex effect (Figure 2).

Sex does not and age only partly impact behavioral alteration

Firstly, we examined the association of sex and age on behavioral alteration, analyzed in the OF (total distance movement, velocity, and counts in center and periphery) and EPM (total distance movement, velocity, and counts in open and closed arms). Statistical analysis including all correlating parameters of female and male ob/ob and wt mice at an age of 8, 24, and 40 weeks revealed that mainly the genotype was responsible for behavioral alteration in ob/ob mice, when compared to their wt littermates. Although statistical analysis revealed still partly an age effect, the obese genotype already showed significant changes at 8 weeks of age in comparison to wt mice, therefore age seems to play a minor role in obesity-related behavior alteration in the ob/ob mice. Concerning general locomotor activity, both female and male ob/ob as well as wt mice at age of 8, 24, and 40 weeks displayed no difference, neither in traveled distance nor in mean velocity in the OF, as can be seen in Supplementary Figure 3 (three-way ANOVA analysis revealed significant genotype and age, but no sex effect). Likewise, both sexes at all age groups spent approximately the same time in the center or peripheral zone in the OF (Supplementary Figure 4, three-way ANOVA analysis revealed significant genotype and partly age, but no sex effect). Correspondingly, both sexes at all age groups displayed the same behavior analyzed in the EPM (Supplementary Figures 5, 6, three-way ANOVA analysis revealed significant genotype and partly age and sex effect). Hence, for further *post hoc* analysis, both sex and age datasets were merged. In doing so, collected data in the OF test of total distance movement and velocity were significantly decreased for ob/ob mice when compared to wt mice (Figures 3A, B, $p < 0.0001$). Similarly, times spent in the center, as well as in peripheral zone, were significantly reduced for ob/ob vs. wt mice (Figures 3C, D, $p < 0.0001$). Correspondingly, in EPM significant differences in traveled distance and velocity (Figures 4A, B, $p < 0.0001$) were displayed between both mice strains. In addition, ob/ob mice visited significantly less open arms and closed arms in comparison to wt mice (Figures 4C, D, $p < 0.0001$).

DeepLabCut achieves comparable results to EthoVision

Precise animal tracking

In order to establish an alternative to the commercial tracking software EV, EV was compared with the more flexible and open source available software DLC. The developers of DLC have already demonstrated the robustness and precision of the tracking (Mathis et al., 2018). For this reason, we used DLC tracking in arenas compatible with commercial systems (such as EV) that we regularly

2 https://github.com/DaBue93/Deep-Behaviour-Master-Thesis

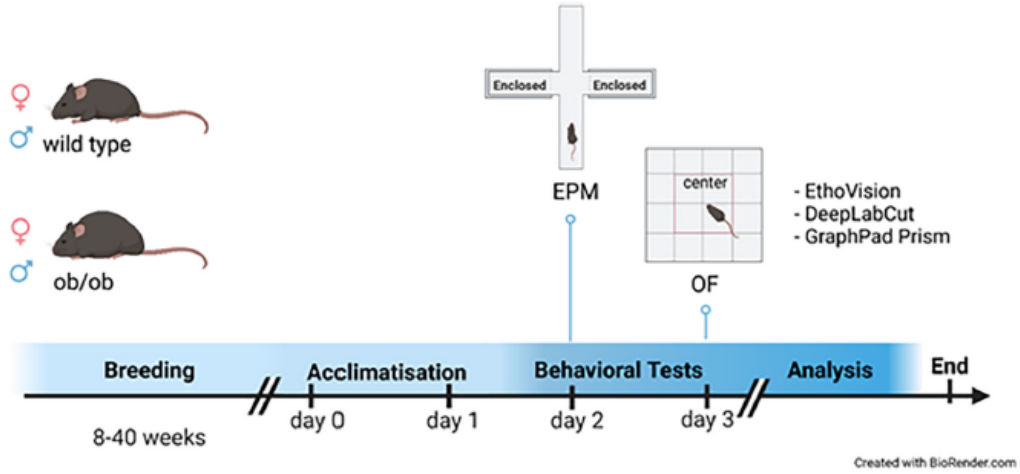

FIGURE 1
Experimental design. Graphical illustration of the experimental procedure; Male (♂ blue) and female (♀ red) leptin deficient (ob/ob) and wild type (wt) at the age of 8, 24, and 40 weeks were firstly habituated to the testing room on day 1 for 24 h; behavioral tests were conducted on day 2 [Elevated Plus Maze (EPM)] and 3 [Open Field (OF)]. After behavioral tests were conducted the animals were killed to obtain physiological data. All behavioral data were analyzed with both EthoVision (EV) and DeepLabCut (DLC), and statistically evaluated with GraphPad Prism and Excel. The graphic was created with BioRender.com.

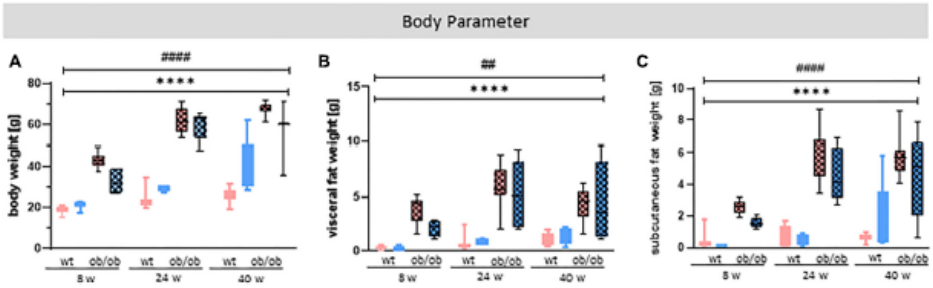

FIGURE 2
Statistical investigation of different body parameters to characterize obesity. **(A)** Body weight (g), **(B)** visceral, and **(C)** subcutaneous fat weight (g) of female (red) and male (blue) mice at age of 8, 24, and 40 weeks were analyzed at the end of the experiment. The group size was as follows: *n*(wt) = 45 **(A)**, 41 **(B)**, 33 **(C)**, *n*(ob/ob) = 42 **(A,C)**, 45 **(B)**. Significances of differences between the groups were tested by three-way ANOVA. The analysis revealed a genotype and age, but no sex effect for all three examined parameters. Statistical significance was set at $^{****}p < 0.0001$ for genotype effect and $^{\#\#}p < 0.01$ or $^{\#\#\#\#}p < 0.0001$ for age effect. ob/ob, leptin deficient mice; wt, wild type; w, weeks (these abbreviations will be consistently used in all following plots, unless stated otherwise).

use in our laboratory. To test for equivalent usability, data from the most commonly used tests in behavioral research, the OF and EPM, were used, and the results of the two different tools –EV and DLC- were cross-referenced.

Open field and elevated plus maze

To compare DLC-tracking performance with EV, data from OF and EPM behavioral tests that were collected with EV were included, and reused to create video files for training DLC models. Locomotor parameters of the OF and EPM analysis, such as total distance, mean velocity, and number of visits (counts) in predefined zones were comparable between DLC and EV (Figures 5A–D for OF; Supplementary Figure 8 for EPM). Both tools showed significant differences between ob/ob and wt mice (distance and velocity, $p < 0.0001$; counts in center and periphery, $p < 0.0001$) for OF and (distance and velocity, $p < 0.0001$; counts in open arm and closed arm, $p < 0.0001$) for EPM. Spearman correlation analysis of OF and EPM data-set further revealed that both software tools showed a high comparability, which was almost significant (Supplementary Figures 7, 9). Moreover, the descriptive analysis of Bland-Altman showed that both methods revealed a good agreement (Supplementary Figures 7, 9).

AI-supported video analysis with DLC enables advanced parameter assessment

Through the AI-supported video analysis by DLC, different behaviors could also be scored. These included rearing, leaning,

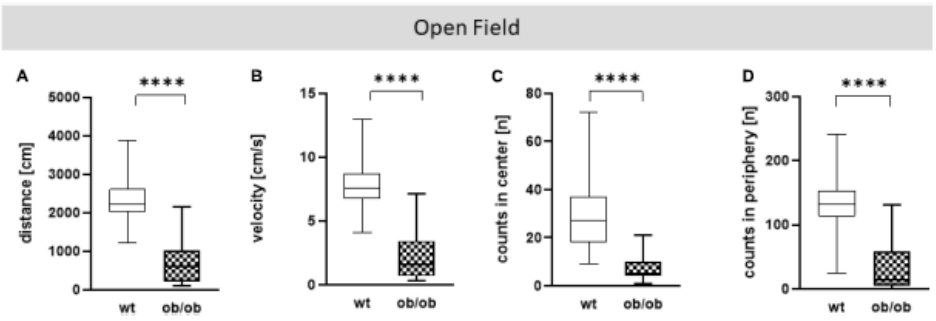

FIGURE 3
Open Field (OF) test analysis. **(A)** Moved distance (cm), **(B)** mean velocity (cm/s), **(C)** number of visits (counts) in center (n), **(D)** number of visits (counts) in periphery (n). Analyses were done with the EthoVision software. The group size was as follows: *n*(wt) = 36 **(A–D)**, *n*(ob/ob) = 40 **(A,B,D)** and 39 **(C)**. Significance of differences between the groups were tested by unpaired Student's *t*-test. Statistical significance was set at ****$p < 0.0001$.

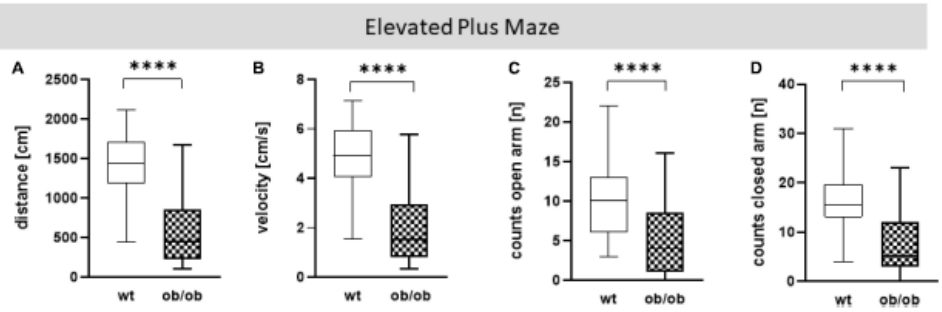

FIGURE 4
Elevated Plus Maze (EPM) analysis. **(A)** Moved distance (cm), **(B)** mean velocity (cm/s), **(C)** number of visits (counts) on open arm (n), **(D)** number of visits (counts) in closed arm (n). Analyses were done with the EthoVision software. The group size was as follows: *n*(wt) = 45 **(A–C)** and 44 **(D)**, *n*(ob/ob) = 45. Significance of differences between the groups were tested by unpaired Student's *t*-test. Statistical significance was set at ****$p < 0.0001$.

and head dipping, which were observed in both behavioral tests. A selection of EPM and OF recordings are accessible at the following link: OF and EPM (see text footnote 2). The above-mentioned parameters had to be recorded manually by direct observation, since the automated evaluation of the videos in EV software did not always detect rearing accurately. However, rearing and further leaning and head dipping could additional obtained automatically by DLC. In doing so, ob/ob vs. wt mice exhibited significantly less rearing-behavior (Figure 6A, $p < 0.001$ and Figure 6B, $p < 0.01$) whereby the manual and the automatical analyses showed equal results. Using pose estimation with DLC, we found in addition that ob/ob mice showed significantly less leaning (Figure 6C, $p < 0.01$) and dipping (Figure 6D, $p < 0.0001$) behavior when compared to wt mice.

Furthermore, DLC was used to create zone-visit-plots for individual animals. The plots show how much time one example wt (A) and ob/ob (B) mouse spend in areas of interest during the OF test (Figures 7A, B). In addition, Figure 7 shows representative heat maps of a wt (C) and an ob/ob (D) mouse. The wt mouse showed a normal movement pattern, while the ob/ob mouse hardly moved in the periphery after being placed more often in the corners, which is highlighted yellow.

Discussion

In the present study, we provided the cognizance that obesity-induced leptin deficiency was already present in early age and was the main cause in mediating anxiety-related behavior whereby the behavioral analyses with EV and DLC show comparable results.

Behavioral alterations in ob/ob mice are independent of sex and age

Adiposity–and the far worse stage obesity (defined as a BMI of over 30)–is not only a health risk itself, but is often associated with other concomitant and secondary diseases, including mood disorders and emotional diseases (Hamer and Stamatakis, 2012; McCrea et al., 2012). Aguilar-Valles et al. (2015) showed a possible correlation of obesity and neurodegeneration. Furthermore, it is suggested that obesity is associated with cognitive impairment and behavioral alterations (Buie et al., 2019). Therefore, behavioral experiments with animals are important approaches to obtain conclusions about the effect of obesity

10.3389/fnins.2023.1052079

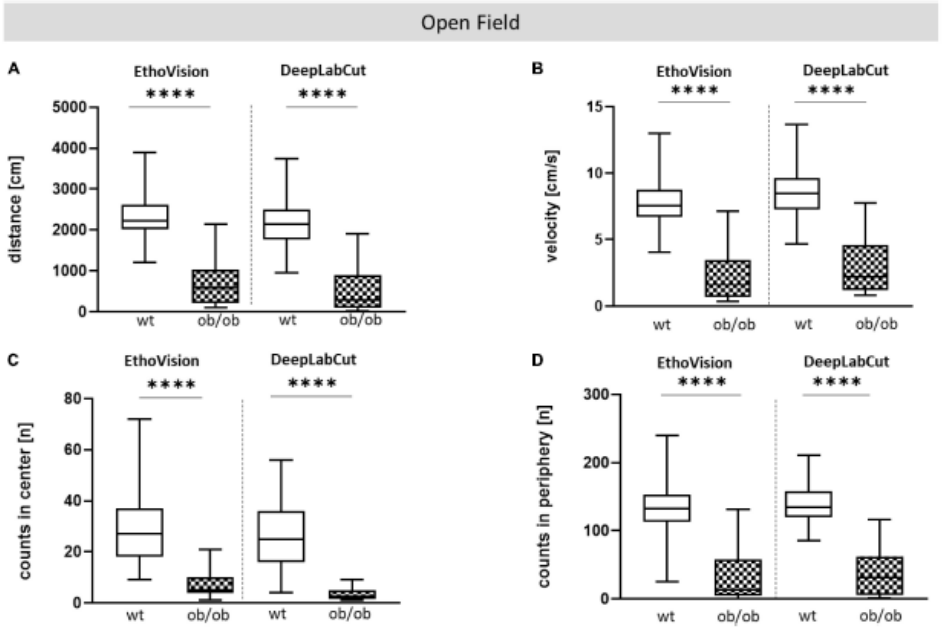

FIGURE 5
Comparative analysis with EV and DLC for OF test. OF analysis of wt and ob/ob mice. **(A)** Moved distance (cm), **(B)** mean velocity (cm/s), **(C)** number of visits (counts) in center (n), **(D)** number of visits (counts) in periphery (n). Significance of differences between the groups were tested by unpaired Student's *t*-test. Group size was as follows: *n*(wt) = 36(EV) or 35(DLC), *n*(ob/ob) = 40 [EV **(A,B,D)**] and 39 **(C)** or 38 [DLC **(A,B,D)**] and 34 **(C)**. Statistical significance was set at ****$p < 0.0001$. EV, EthoVision; DLC, DeepLabCut.

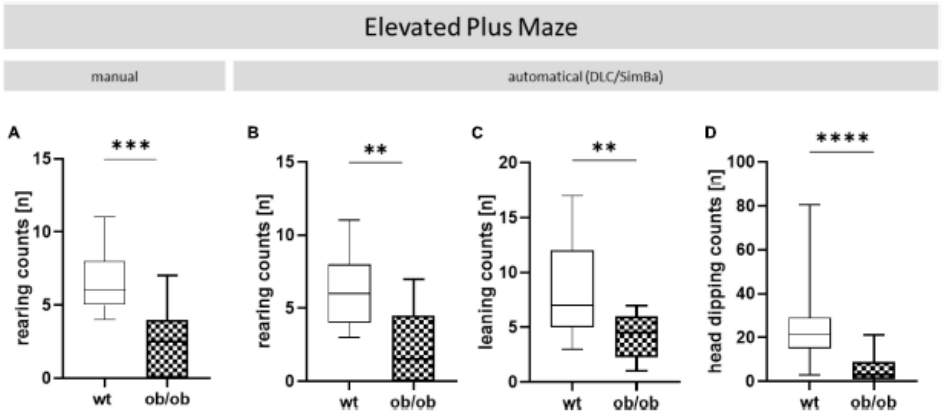

FIGURE 6
Additional parameters collected in the EPM. Wt and ob/ob mice were comparatively analyzed. **(A)** Rearing counts (n) manually scored by an observer *via* video analysis and **(B)** obtained automatically with DeepLabCut (DLC). Furthermore, **(C)** leaning (n), and **(D)** head dipping counts (n) were observed with DLC. Group size was as follows: *n*(wt) = 11 **(A–C)**, 46 **(D)** and, *n*(ob/ob) = 12 **(A)**, 10 **(B)**, 8 **(C)**, and 42 **(D)**. Significance of differences between the groups were tested by unpaired Student's *t*-test. Statistical significance was set at **$p < 0.01$, ***$p < 0.001$, and ****$p < 0.0001$.

on emotional states like anxious-related behavior or depression (McCrea et al., 2012).

The transgenic mouse model of leptin deficiency induced obesity (ob/ob mice) leads to a continuous sensation of hunger (Suliman et al., 2019), which causes the animals to continually search for food. Due to the increased food intake, excessive fat accumulation occurs at a young age (Hayakawa et al., 2018). In order to assess leptin deficiency-induced obesity, weight data of ob/ob and wt animals were analyzed first. As expected, ob/ob mice showed significantly increased body weights compared to wt mice. The values for both ob/ob mice and wt mice were within the age-, sex-, and genotype-specific, normal range (for more detailed

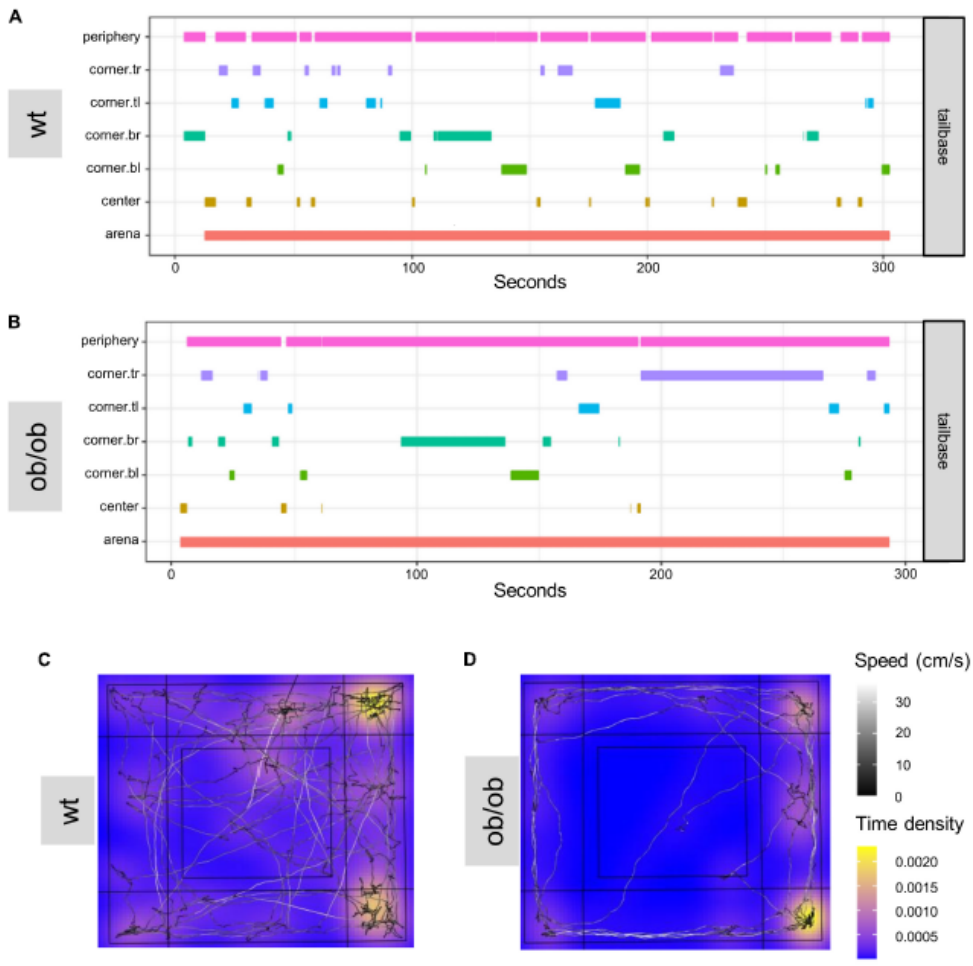

FIGURE 7
DeepLabCut (DLC) tracking results analyzed with customized R-script based on DLC-Analyzer. Example of a zone-visit-plot of a wild type [**(A)** wt] and an ob/ob **(B)** mouse in OF. The individual zones show how much time the body part of interest (**Supplementary Figure 2** for labeling of animals in DLC) was tracked in the predefined zones. Heat-maps of the OF test of wild type [wt **(C)**], and transgene leptin deficient [ob/ob **(D)**] mice. tl, top left; tr, top right; bl, bottom left, br, bottom right.

information see Jackson Laboratory). In the context of total body weight gain, a considerably higher proportion of subcutaneous fat was observed in the ob/ob mice, in addition to the increased visceral fat weight at dissection. Beside genetic-induced obesity, it is common to induce obesity also through different diets (Lutz and Woods, 2012). These include the high fat diet (HFD), western diet (WD), and cafeteria diet (CFD), which are also discussed to be responsible for the sharp increase in the obesity pandemic in humans (Sampey et al., 2011). These diets have a common feature: they lead to excess energy intake due to an unbalanced composition of fat and sugar, which in combination with reduced exercise facilitates obesity (Bracke et al., 2019a,b; Picone et al., 2020). However, applying these diets in wild type rodent models is time-consuming and takes several weeks and even months to take effect of an obese phenotype. To overcome this issue, we used the ob/ob mice knowing to reveal a significant weight gain already at young age as verifying in the present study. Therefore, this mouse model is ideal for studying obesity at a younger age. Due to this, it became apparent in the study that the time points of 24 and 40 weeks were not strictly necessary, since a pronounced adiposity was already present in 8-week-old mice, which ultimately reduces the stress of adiposity with increasing age.

Our study contributes to the overall assumption that obesity, in addition to the common comorbidities, causes behavioral alterations (Finger et al., 2011; Reverte et al., 2012; Alonso-Caraballo et al., 2019). Several related studies also show that in both the genetically induced obesity models and in diet-induced obesity models, particularly locomotion is altered (Collins et al., 2015; Zieba et al., 2019). This was demonstrated by López-Taboada et al. (2020) showing obesity-induced by a WD is associated with reduced locomotion. The same conclusion was reached by Yokoyama et al. (2020), who studied the effect of a

HFD, and by Teixeira et al. (2020), who linked the CFD diet to behavioral alteration. A similar situation can be observed in humans (Bracke et al., 2019a). However, it is not yet clear whether an increased weight *per se* leads to a reduction in locomotion, or whether there are other contributing factors on a neuronal or emotional level (Shafizadeh et al., 2021). Nevertheless, the present findings confirm that obesity is indeed associated with a behavioral alteration. Interestingly, our study showed that sex and partly age had no impact (even though statistical analysis revealed an age effect) on the behavior seen in ob/ob mice. Additionally, the finding that sex had no influence on the behavioral change means that both male and female mice can be included in the present and future studies. This reduces the number of animals needed to generate statistically sound results, as both sexes can be used equally. Moreover, it allows for more efficient use of breeding times, as less time is needed to generate a sufficient number of genetically identical mice (promoting the 3R-Principle of Reduction, Russell and Burch, 1959). Furthermore, independence of age means that experiments do not have to be carried out for an excessively long time, since at least in the ob/ob model a significant change in behavior is already visible at a very young age [promoting the 3R-Principle of Refinement, Russell and Burch (1959)].

Behavior analyses with EV and DLC have comparable results

The challenge that manual video analysis are prone to bias by the observer led to the development of easy-to-use, widely accessible semi-automated computer applications that can be deployed in almost any ethology laboratory, facilitating robustness and reproducibility of research findings. Previous studies have already investigated the benefits of AI-based evaluation methods compared to standard methods (Sturman et al., 2020). However, there has not yet been a study that used AI methods in a mouse model of leptin deficiency. Our work builds upon findings of other research groups to uncover the pathological accumulation of adipose tissue, the resulting and associated behavioral change in the mouse model using AI and could open up new approaches to study pathological conditions induced by malnutrition.

The collected data of the behavioral tests OF and EPM were evaluated both with conventional software, namely EV, which is used as a standard in many behavioral laboratories, and with a fairly new AI-based software, namely DLC (Mathis et al., 2020). To evaluate the new, open-source software DLC, the same animal recordings that were analyzed with EV were compared with the findings of DLC. Both methods yielded the same results, i.e., leptin deficiency but not sex or age caused behavioral alterations. From this perspective, DLC might contribute to fewer animals being used in the future, as these methods can predict behavior based on more complex parameters [promoting the 3R-Principle of Reduction, Russell and Burch (1959)]. These side observations show in addition to the fact that the DLC model is very robust with respect to different age groups, sex, and even mouse strains that DLC assures the implementation of the 3R principle (Russell and Burch, 1959). Alongside the advantages of modern methods already mentioned, which allow behavioral analysis to be replicable and almost with human accuracy, the open source software DLC has further advantages over EV (Mathis et al., 2018; Sturman et al., 2020). For instance, DLC is based on the open-source programming language Python, which makes the code more accessible, easier to understand and to adapt it to individual needs. This enables a collection and individualized analysis of more parameters in comparison to EV (where the code is not as accessible). In addition to the common parameters, such as speed, distance, rearing, and leaning, the DLC was also able to record head dipping (Sturman et al., 2020). Decreasing head dipping frequency is associated with increased anxiety, which makes it another important parameter for assessing the anxiety of animals. Previously, this parameter had to be laboriously recorded by hand. In summary, automatic video evaluation with DLC has made this data processing step much faster, however, this kind of behavioral assessment also requires necessary storage capacities and computing power that are not available to every ethological laboratory.

Future perspective of DLC

One of the greatest advantages of DLC is the broad and fast-growing DLC-community from all possible areas of science that make questions, data, and results publicly accessible (Mathis et al., 2018; Lauer et al., 2021). This facilitates data sharing, as well as the potential reuse of data other laboratories to train and improve ones own networks. DLC also allows multi-animal analyses to be performed in order to study the social behavior of animals (Lauer et al., 2021). This was hardly possible before, or would have required cost intense software updates for exciting commercial hardware. Further side-applications are emerging from collaborations, which use the DLC coordinates data for further analyses. For example, SimBA, a computer framework that enables users to use these pose-estimation approaches in combination with behavioral annotation and generation of supervised machine-learning behavioral predictive classifiers (Nilson et al., 2020). Accordingly, the pipeline was developed for the analysis of complex social behaviors, but also includes the flexibility for users to generate predictive classifiers across other behavioral modalities with minimal effort and no specialized computational background. Besides this huge advantage, it is already possible to explore new animal behavior patterns using unsupervised trained networks. One of the most widely used software programs for this purpose is B-SOiD (Hsu and Yttri, 2021). B-SOiD is an open-source tool to discover and extract behaviors and sub-actions from pose estimation data (Hsu and Yttri, 2021).

Summary and conclusion

In this investigation, we compared the accuracy of two pose estimation applications, namely EV and DLC in testing obesity-induced behavioral alterations in the ob/ob mice. The compared methods (both are based on the same algorithms) yielded almost identical results, whereby the more current AI-based application DLC allows more flexibility and enables the investigation of

additional parameters (e.g., head dipping and leaning). These findings provide new possibilities to analyze rodent behavior in a more consistent and repeatable way, which can be applied in almost every behavioral laboratory with no need of extensive professional computational knowledge. According to these findings, it is conceivable that data from this study will serve as a basis in further analyses to gain more insights into complex behavioral changes and to predict obesity-related behavioral alterations. In addition, the observation the independence of sex and age could also reduce the number of experimental animals needed to a certain degree, and possibly also replace some of them entirely, promoting the 3R-Principle. Taken together, this novel AI approach and the fact that this mouse model of leptin deficiency has been shown to be present obesity-associated behavioral change already in young age might significantly reduce the number of animals for preclinical research in the future.

Data availability statement

The datasets presented in this study can be found in online repositories. The names of the repository/repositories and accession number(s) can be found below: Full data table and all coding sections can be accessed under https://github.com/DaBue93/Deep-Behaviour-Master-Thesis.

Ethics statement

The animal study was reviewed and approved by the Animal Research Committee [Landesamt für Landwirtschaft, Lebensmittelsicherheit und Fischerei (LALLF)] of the state Mecklenburg-Western Pomerania.

Author contributions

AK: conceptualization, funding acquisition, and project administration. NPG: data curation, investigation, and validation. AK and LM: formal analysis. NPG, AK, LM, DB, and MD: methodology. OW and BV: resources. AK and MW: supervision. DB: visualization. DB, AK, and LM: roles/writing–original draft. DB, AK, MW, and LM: writing–review and editing. All authors contributed to the article and approved the submitted version.

Funding

This study was supported by a grant from the Deutsche Forschungsgemeinschaft, Bonn, Germany (KU 3280/1-2).

Acknowledgments

We cordially thank the technicians of the Institute for Experimental Surgery, the Central Animal Care Facility of the Rostock University Medical Center, and the support team of the Department of Systems Biology and Bioinformatics of the University of Rostock for their valuable assistance. We thank Dr. Valeska Stephan for final proofreading our manuscript.

Conflict of interest

The authors declare that the research was conducted in the absence of any commercial or financial relationships that could be construed as a potential conflict of interest.

Publisher's note

Supplementary material

The Supplementary Material for this article can be found online at: https://www.frontiersin.org/articles/10.3389/fnins.2023.1052079/full#supplementary-material

References

Aguilar-Valles, A., Inoue, W., Rummel, C., and Luheshi, G. (2015). Obesity, adipokines and neuroinflammation. *Neuropharmacology* 96(Pt A), 124–134.

Alonso-Caraballo, Y., Hodgson, K., Morgan, S., Ferrario, C., and Vollbrecht, P. (2019). Enhanced anxiety-like behavior emerges with weight gain in male and female obesity-susceptible rats. *Behav. Brain Res.* 360, 81–93. doi: 10.1016/j.bbr.2018.12.002

Betting, J., Romano, V., Al-Ars, Z., Bosman, L., Strydis, C., and De Zeeuw, C. (2020). WhiskEras: A new algorithm for accurate whisker tracking. *Front. Cell Neurosci.* 14:588445. doi: 10.3389/fncel.2020.588445

Bracke, A., Domanska, G., Bracke, K., Bracke, K., Harzsch, S., van den Brandt, J., et al. (2019a). Obesity alters mobility and adult neurogenesis, but not hippocampal dependent learning in ob/ob mice. *BioRxiv* [Preprint]. doi: 10.1101/537720

Bracke, A., Domanska, G., Bracke, K., Harzsch, S., van den Brandt, J., Bröker, B., et al. (2019b). Obesity impairs mobility and adult hippocampal neurogenesis. *J. Exp. Neurosci.* 13:1179069519883580. doi: 10.1177/1179069519883580

Buie, J., Watson, L., Smith, C., and Sims-Robinson, C. (2019). Obesity-related cognitive impairment: The role of endothelial dysfunction. *Neurobiol. Dis.* 132:104580. doi: 10.1016/j.nbd.2019.104580

Clack, N., O'Connor, D., Huber, D., Petreanu, L., Hires, A., Peron, S., et al. (2012). Automated tracking of whiskers in videos of head fixed rodents. *PLoS Comput. Biol.* 8:e1002591. doi: 10.1371/journal.pcbi.1002591

Collins, G., Chen, Y., Tschumi, C., Rush, E., Mensah, A., Koek, W., et al. (2015). Effects of consuming a diet high in fat and/or sugar on the locomotor effects of acute

and repeated cocaine in male and female C57BL/6J mice. *Exp. Clin. Psychopharmacol.* 23, 228–237. doi: 10.1037/pha0000019

CVPR 2019 Open Access Repository (2019). *RVOS: End-To-End Recurrent Network for Video Object Segmentation*. Available online at: https://openaccess.thecvf.com/content_CVPR_2019/html/Ventura_RVOS_End-To-End_Recurrent_Network_for_Video_Object_Segmentation_CVPR_2019_paper.html (accessed March 2, 2023).

Datta, S., Anderson, D., Branson, K., Perona, P., and Leifer, A. (2019). Computational neuroethology: A call to action. *Neuron* 104, 11–24. doi: 10.1016/j.neuron.2019.09.038

Dominiak, S., Nashaat, M., Sehara, K., Oraby, H., Larkum, M., and Sachdev, R. (2019). Whisking asymmetry signals motor preparation and the behavioral state of mice. *J. Neurosci.* 39, 9818–9830. doi: 10.1523/JNEUROSCI.1809-19.2019

Drucker, D. (2021). Diabetes, obesity, metabolism, and SARS-CoV-2 infection: The end of the beginning. *Cell Metab.* 33, 479–498. doi: 10.1016/j.cmet.2021.01.016

Finger, B., Dinan, T., and Cryan, J. (2011). High-fat diet selectively protects against the effects of chronic social stress in the mouse. *Neuroscience* 192, 351–360. doi: 10.1016/j.neuroscience.2011.06.072

Giovannucci, A., Pnevmatikakis, E., Deverett, B., Pereira, T., Fondriest, J., Brady, M., et al. (2018). Automated gesture tracking in head-fixed mice. *J. Neurosci. Methods* 300, 184–195. doi: 10.1016/j.jneumeth.2017.07.014

Guma, E., Bordeleau, M., González Ibáñez, F., Picard, K., Snook, E., Desrosiers-Grégoire, G., et al. (2022). Differential effects of early or late exposure to prenatal maternal immune activation on mouse embryonic neurodevelopment. *Proc. Natl. Acad. Sci. U.S.A.* 119:e2114545119. doi: 10.1073/pnas.2114545119

Hamer, M., and Stamatakis, E. (2012). Metabolically healthy obesity and risk of all-cause and cardiovascular disease mortality. *J. Clin. Endocrinol. Metab.* 97, 2482–2488. doi: 10.1210/jc.2011-3475

Hayakawa, J., Wang, M., Wang, C., Han, R., Jiang, Z., and Han, X. (2018). Lipidomic analysis reveals significant lipogenesis and accumulation of lipotoxic components in ob/ob mouse organs. *Prostaglandins Leukot Essent Fatty Acids* 136, 161–169. doi: 10.1016/j.plefa.2017.01.002

Hsu, A., and Yttri, E. A. (2021). B-SOiD, an open-source unsupervised algorithm for identification and fast prediction of behaviors. *Nat. Commun.* 12:5188. doi: 10.1038/s41467-021-25420-x

Knutsen, P., Derdikman, D., and Ahissar, E. (2005). Tracking whisker and head movements in unrestrained behaving rodents. *J. Neurophysiol.* 93, 2294–2301. doi: 10.1152/jn.00718.2004

Komada, M., Takao, K., and Miyakawa, T. (2008). Elevated plus maze for mice. *J. Vis. Exp.* 1088. doi: 10.3791/1088

Lauer, J., Zhou, M., Ye, S., Menegas, W., Schneider, S., Nath, T., et al. (2021). Multi-animal pose estimation and tracking with DeepLabCut. *BioRxiv* [Preprint]. doi: 10.1101/2021.04.30.442096

López-Taboada, I., González-Pardo, H., and Conejo, N. (2020). Western diet: Implications for brain function and behavior. *Front. Psychol.* 11:564413. doi: 10.3389/fpsyg.2020.564413

Lutz, T., and Woods, S. (2012). Overview of animal models of obesity. *Curr. Protoc. Pharmacol.* Chapter 5:Unit5.61. doi: 10.1002/0471141755.ph0561s58

Mathis, A., Mamidanna, P., Cury, K., Abe, T., Murthy, V., Mathis, M., et al. (2018). DeepLabCut: Markerless pose estimation of user-defined body parts with deep learning. *Nat. Neurosci.* 21, 1281–1289. doi: 10.1038/s41593-018-0209-y

Mathis, A., Schneider, S., Lauer, J., and Mathis, M. W. (2020). A primer on motion capture with deep learning: Principles, pitfalls, and perspectives. *Neuron* 108, 44–65. doi: 10.1016/j.neuron.2020.09.017

McCrea, R., Berger, Y., and King, M. (2012). Body mass index and common mental disorders: Exploring the shape of the association and its moderation by age, gender and education. *Int. J. Obes. (Lond.).* 36, 414–421. doi: 10.1038/ijo.2011.65

Moradi, Y., Albatineh, A., Mahmoodi, H., and Gheshlagh, R. (2021). The relationship between depression and risk of metabolic syndrome: A meta-analysis of observational studies. *Clin. Diabetes Endocrinol.* 7:4. doi: 10.1186/s40842-021-00117-8

Musall, S., Kaufman, M., Juavinett, A., Gluf, S., and Churchland, A. (2019). Single-trial neural dynamics are dominated by richly varied movements. *Nat. Neurosci.* 22, 1677–1686. doi: 10.1038/s41593-019-0502-4

Nilson, S. R., Goodwin, N. L., Choong, J. J., Hwang, S., Wright, H. R., Norville, Z. C., et al. (2020). Simple behavioral analysis (SimBA) – An open source toolkit for computer classification of complex social behaviors in experimental animals. *BioRxiv* [Preprint]. doi: 10.1101/2020.04.19.049452

Ohayon, S., Avni, O., Taylor, A., Perona, P., and Roian Egnor, S. (2013). Automated multi-day tracking of marked mice for the analysis of social behaviour. *J. Neurosci. Methods.* 219, 10–19. doi: 10.1016/j.jneumeth.2013.05.013

Perkon, I., Kosir, A., Itskov, P., Tasic, J., and Diamond, M. (2011). Unsupervised quantification of whisking and head movement in freely moving rodents. *J. Neurophysiol.* 105, 1950–1962. doi: 10.1152/jn.00764.2010

Petersen, R., Colins Rodriguez, A., Evans, M., Campagner, D., and Loft, M. (2020). A system for tracking whisker kinematics and whisker shape in three dimensions. *PLoS Comput. Biol.* 16:e1007402. doi: 10.1371/journal.pcbi.1007402

Picone, P., Di Carlo, M., and Nuzzo, D. (2020). Obesity and Alzheimer's disease: Molecular bases. *Eur. J. Neurosci.* 52, 3944–3950. doi: 10.1111/ejn.14758

Powell-Wiley, T., Poirier, P., Burke, L., Després, J., Gordon-Larsen, P., Lavie, C., et al. (2021). Obesity and cardiovascular disease: A scientific statement from the American heart association. *Circulation* 143, e984–e1010. doi: 10.1161/CIR.0000000000000973

Power Guerra, N., Parveen, A., Bühler, D., Brauer, D., Müller, L., Pilz, K., et al. (2021). Fibroblast growth factor 21 as a potential biomarker for improved locomotion and olfaction detection ability after weight reduction in obese mice. *Nutrients* 13:2916. doi: 10.3390/nu13092916

Reverte, I., Klein, A., Ratner, C., Domingo, J., and Colomina, M. (2012). Behavioral phenotype and BDNF differences related to apoE isoforms and sex in young transgenic mice. *Exp. Neurol.* 237, 116–125. doi: 10.1016/j.expneurol.2012.06.015

Rodgers, R., and Shepherd, J. (1993). Influence of prior maze experience on behaviour and response to diazepam in the elevated plus-maze and light/dark tests of anxiety in mice. *Psychopharmacology* 113, 237–242. doi: 10.1007/BF02245704

Russell, W. M. S., and Burch, R. L. (1959). *The principles of humane experimental technique*. Wheathampstead: Universities Federation for Animal Welfare.

Sampey, B., Vanhoose, A., Winfield, H., Freemerman, A., Muehlbauer, M., Fueger, P., et al. (2011). Cafeteria diet is a robust model of human metabolic syndrome with liver and adipose inflammation: Comparison to high-fat diet. *Obesity* 19, 1109–1117. doi: 10.1038/oby.2011.18

Sarma, S., Sockalingam, S., and Dash, S. (2021). Obesity as a multisystem disease: Trends in obesity rates and obesity-related complications. *Diabetes Obes. Metab.* 23(Suppl. 1), 3–16. doi: 10.1111/dom.14290

Shafizadeh, M., Parvinpour, S., Balali, M., Pazhuh, F., and Broom, D. (2021). Effects of locomotion task constraints on running in boys with overweight/obesity: The mediating role of developmental delays. *Gait Posture.* 86, 354–359. doi: 10.1016/j.gaitpost.2021.04.012

Stringer, C., Pachitariu, M., Steinmetz, N., Reddy, C., Carandini, M., and Harris, K. (2019). Spontaneous behaviors drive multidimensional, brainwide activity. *Science* 364:255. doi: 10.1126/science.aav7893

Sturman, O., von Ziegler, L., Schläppi, C., Akyol, F., Privitera, M., Slominski, D., et al. (2020). Deep learning-based behavioral analysis reaches human accuracy and is capable of outperforming commercial solutions. *Neuropsychopharmacology* 45, 1942–1952. doi: 10.1038/s41386-020-0776-y

Suliman, M., Buckley, A., Al Tikriti, A., Tan, T., le Roux, C., Lessan, N., et al. (2019). Routine clinical use of liraglutide 3 mg for the treatment of obesity: Outcomes in non-surgical and bariatric surgery patients. *Diabetes Obes. Metab.* 21, 1498–1501. doi: 10.1111/dom.13672

Teixeira, A., Rocha-Gomes, A., Pereira Dos Santos, T., Amaral, B., da Silva, A., Malagutti, A., et al. (2020). Cafeteria diet administered from lactation to adulthood promotes a change in risperidone sensitivity on anxiety, locomotion, memory, and social interaction of Wistar rats. *Physiol. Behav.* 220:112874. doi: 10.1016/j.physbeh.2020.112874

Valletta, J. J., Torney, C., Kings, M., Thornton, A., and Madden, J. (2017). Applications of machine learning in animal behaviour studies. *Anim. Behav.* 124, 203–220. doi: 10.1016/J.ANBEHAV.2016.12.005

Vanzella, W., Grion, N., Bertolini, D., Perissinotto, A., Gigante, M., and Zoccolan, D. (2019). A passive, camera-based head-tracking system for real-time, three-dimensional estimation of head position and orientation in rodents. *J. Neurophysiol.* 122, 2220–2242. doi: 10.1152/jn.00301.2019

Voigts, J., Sakmann, B., and Celikel, T. (2008). Unsupervised whisker tracking in unrestrained behaving animals. *J Neurophysiol.* 100, 504–515. doi: 10.1152/jn.00012.2008

Walf, A., and Frye, C. (2007). The use of the elevated plus maze as an assay of anxiety-related behavior in rodents. *Nat. Protoc.* 2, 322–328. doi: 10.1038/nprot.2007.44

World Health Organization [WHO] (2021). *Obesity and overweight*. Available online at: https://www.who.int/news-room/fact-sheets/detail/obesity-and-overweight (accessed March 2, 2023).

Yokoyama, Y., Nakamura, T., Yoshimoto, K., Ijyuin, H., Tachikawa, N., Oda, H., et al. (2020). A high-salt/high fat diet alters circadian locomotor activity and glucocorticoid synthesis in mice. *PLoS One* 15:e0233386. doi: 10.1371/journal.pone.0233386

Zhao, S., Li, N., Zhu, Y., Straub, L., Zhang, Z., Wang, M., et al. (2020). Partial leptin deficiency confers resistance to diet-induced obesity in mice. *Mol. Metab.* 37:100995. doi: 10.1016/j.molmet.2020.100995

Zieba, J., Uddin, G., Youngson, N., Karl, T., and Morris, M. (2019). Long-term behavioural effects of maternal obesity in C57BL/6J mice. *Physiol. Behav.* 199, 306–313. doi: 10.1016/j.physbeh.2018.11.004

10.4 Studie 4

frontiers | Frontiers in Nutrition

TYPE Original Research
PUBLISHED 10 August 2022
DOI 10.3389/fnut.2022.935805

OPEN ACCESS

EDITED BY
Olga Pivovarova-Ramich,
German Institute of Human Nutrition Potsdam-Rehbruecke (DIfE), Germany

REVIEWED BY
Xiaodong Chen,
Huazhong Agricultural University, China
Gerald Grandl,
Helmholtz Center München (HZ), Germany

*CORRESPONDENCE
Angela Kuhla
angela.kuhla@uni-rostock.de

SPECIALTY SECTION
This article was submitted to Nutrition and Metabolism, a section of the journal Frontiers in Nutrition

RECEIVED 04 May 2022
ACCEPTED 11 July 2022
PUBLISHED 10 August 2022

CITATION
Power Guerra N, Leyens K, Müller L, Brauer D, Janowitz D, Schlick S, Pilz K, Grabe HJ, Vollmar B and Kuhla A (2022) The effect of different weight loss strategies to treat non-alcoholic fatty liver disease focusing on fibroblast growth factor 21. *Front. Nutr.* 9:935805. doi: 10.3389/fnut.2022.935805

The effect of different weight loss strategies to treat non-alcoholic fatty liver disease focusing on fibroblast growth factor 21

Nicole Power Guerra[1,2], Katharina Leyens[1], Luisa Müller[1,3], David Brauer[4], Deborah Janowitz[5,6], Samin Schlick[5,6], Kristin Pilz[5], Hans J. Grabe[5], Brigitte Vollmar[1] and Angela Kuhla[1*]

[1]Institute for Experimental Surgery, Rostock University Medical Center, Rostock, Germany, [2]Institute of Anatomy, Rostock University Medical Center, Rostock, Germany, [3]Department of Psychosomatic Medicine, Rostock University Medical Center, Rostock, Germany, [4]Department of Systems Biology and Bioinformatics, University of Rostock, Rostock, Germany, [5]Department of Psychiatry, University Medicine Greifswald, Greifswald, Germany, [6]Clinic for Psychiatry and Psychotherapy, HELIOS Hanseklinikum Stralsund, Stralsund, Germany

Objective: Obesity, often associated with non-alcoholic fatty liver disease (NAFLD), is characterized by an imbalance between energy expenditure and food intake, which is also reflected by desensitization of fibroblast growth factor 21 (FGF21). FGF21 is strongly influenced, among others, by TNFα, which is known to be upregulated in obesity-induced inflammation. Successful long-term treatments of NAFLD might be dietary modification, exercise, or fasting.

Materials and methods: Whether succeeded NAFLD recovery is linked with improved FGF21 sensitivity and finally reverted FGF21 resistance was the focus of the present study. For this purpose, mice received a high-fat diet (HFD) for 6 months to establish obesity. Afterward, the mice were subjected to three different weight loss interventions, namely, dietary change to low-fat diet (LFD), treadmill training, and/or time-restricted feeding for additional 6 months, whereas one group remained on HFD.

Results: In addition to the expected decrease in NAFLD activity with dietary change, this was also observed in the HFD group with additional time-restricted feeding. There was also an associated decrease in hepatic TNFα and FGF21 expression and an increase in ß-klotho expression, demonstrated mainly by using principal component analysis. Pearson correlation analysis shows that independent of any intervention, TNFα expression decreased with improved NAFLD recovery. This was accompanied with higher FGF21 sensitivity, as expressed by an increase in β-klotho and FGFR1c expression and concomitantly decreased FGF21 levels.

Conclusion: In summary, we conclude that successful NAFLD therapy is associated with a reversion of the TNFα-triggered FGF21-resistant state or desensitization.

KEYWORDS

non-alcoholic fatty liver disease, high-fat diet, dietary change, treadmill exercise, time-restricted feeding, FGF21, TNFα, β-klotho

Introduction

Overall, 25% of people worldwide suffer from overweight or obesity, which has reached pandemic proportions. As early as 1989, Kaplan described the "deadly quartet" of abdominal obesity, hypertension, hyperglycemia, and hypertriglyceridemia (1), which is referred to as metabolic syndrome (2, 3). The metabolic syndrome is associated with non-alcoholic fatty liver disease (NAFLD), which is considered as hepatic manifestation of this disease (4–6). One potential reason for the prevalence of NAFLD and many other comorbidities and sequelae of obesity is the persistence of a systemic low-grade inflammation (LGI) (7, 8). In this context, white adipose tissue is capable of expressing both metabolic and immunological mediators (9), which act locally but may also have systemic effects affecting other organs, such as the liver. This is reflected by hepatic and also systemic upregulation of pro-inflammatory cytokines, such as interleukin (IL)-1β, IL-6, and tumor necrosis factor alpha (TNFα) (10–12). All these mediators are well coordinated and reciprocally regulated in signaling cascades. An imbalance of these mediators is likely responsible for an LGI-mediated interaction between obesity and NAFLD (13, 14).

In order to better understand the causality of obesity-related inflammatory processes, it is necessary to consider individual hormones, such as leptin, ghrelin, or orexin. They are involved in the regulation of food intake. A dysregulation of these hormones, also triggered by obesity-induced LGI, can further aggravate obesity. In addition, fibroblast growth factor 21 (FGF21), a hormone in addition to fatty acid oxidation, lipolysis, and increased energy dissipation, is also involved in the regulation of food uptake. FGF21 acts *via* its receptor complex of FGF21 receptor (FGFR)1c and β-klotho in an endocrine or paracrine manner (15–17).

Remarkably, on the one hand, FGF21 expression is increased in the liver during fasting states and caloric restriction (18, 19); on the other hand, exceptionally high circulating plasma FGF21 concentrations occur in obese humans and mice (20, 21). Termed the "FGF21 paradox" by Fisher et al. (21), this phenomenon describes, similar to leptin resistance (22), an FGF21-resistant state (21), although more recently, the term FGF21 desensitization has been used in this context (23). Thereby, increased FGF21 concentrations in obesity were associated with a concomitant reduction in the FGF21 receptor complex (21). A link between FGF21 and inflammation was demonstrated by Diaz-Delfin and coworkers in mouse adipocytes, where the application of TNFα inhibited β-klotho expression (24). Furthermore, a long-term study on the adipose tissue of obese mice demonstrated that expression of FGFR1c and β-klotho was markedly decreased and associated with a limited effect of exogenously applied FGF21, implying a decrease in FGF21 sensitivity.

To overcome the vicious cycle of obesity and hence obesity-induced LGI, intervention approaches, such as physical activity, dietary changes, or fasting are appropriate and commonly used methods (25–27). Therefore, the purpose of this study was to investigate to which extent obesity-associated NAFLD and accompanying inflammatory processes are reversible by treadmill training, dietary change, and/or time-restricted feeding, and whether this is associated with enhanced hepatic FGF21 sensitivity. Using principal component and correlation analyses, we tested the hypothesis that recovery from NAFLD is associated with a reversion of FGF21 resistance or desensitization.

Materials and methods

Animals

At the beginning, 90 4-week-old female mice (C57BL/6J) were purchased from Charles River (Sulzfeld, Germany). In compliance with our previous and ongoing investigations, female mice were used for comparability between different studies (28). All animal experimental work was carried out with permission of the local Animal Research Committee [Landesamt für Landwirtschaft, Lebensmittelsicherheit und Fischerei (LALLF) of the state Mecklenburg-Western Pomerania (LALLF M-V/TSD/7221.3-2-001/18, approved on March 1, 2018)] and by following the ARRIVE guidelines. All animals received human care according to the EU Directive 2010/63/EU. The mice were divided in a blinded manner into groups of five mice and were kept in standard cages. The room temperature was controlled (21 ± 3°C), and a 12-/12-h day/night cycle (lights on from 6:00 a.m.

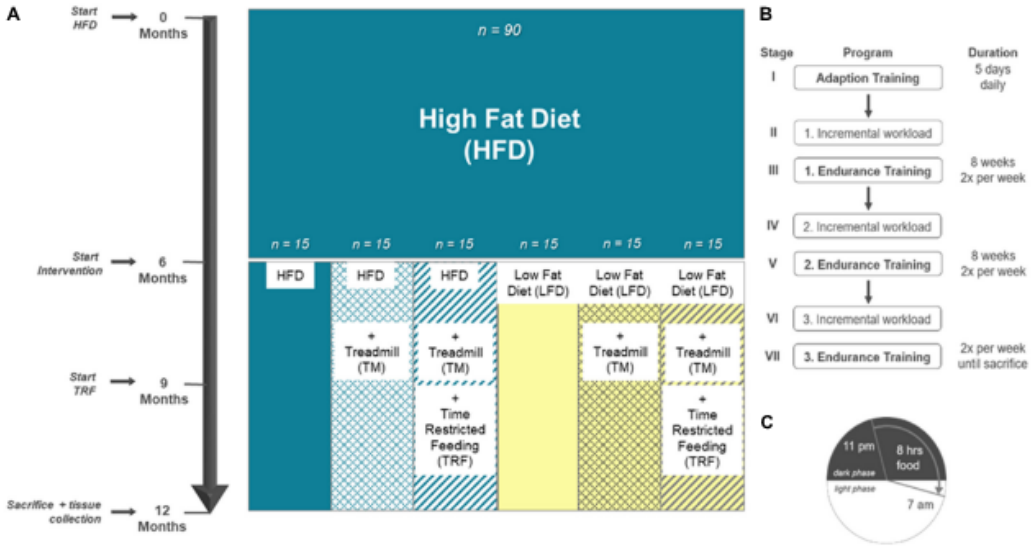

FIGURE 1
Experimental design adapted to Power Guerra et al. (28). **(A)** Female C57BL/6J mice (n = 90) were fed for 6 months with high-fat diet (HFD) to establish the model of diet-induced obesity. Thereafter, mice were divided into six groups. The first group remained on the HFD (n = 90). Groups 2–6 underwent an intervention. Second group: HFD plus treadmill exercise (TM; HFD/HFD + TM, n = 15); third group: HFD plus treadmill exercise and time-restricted feeding (TRF; HFD/HFD + TM + TRF, n = 15); fourth group: dietary change to a low-fat diet (LFD; HFD/LFD, n = 15); fifth group: dietary change plus treadmill exercise (HFD/LFD + TM, n = 15), and sixth group: dietary change, treadmill training, and time-restricted feeding (HFD/LFD + TM + TRF, n = 15). When dietary change was completed, treadmill training started. After 3 months of endurance exercise, time-restricted feeding was introduced. At the end, the mice were killed, and blood and liver tissue were collected. **(B)** Treadmill protocol consists of seven stages with three endurance sections. Prior to endurance training, an incremental workload test was performed to adjust the maximum velocity of the run. **(C)** Mice in the TRF group were restricted food from 7 a.m. to 11 p.m. (16 h). Food supply was provided in the nocturnal active phase for 8 h.

to 6:00 p.m.) was applied. All mice were handled equally for the first 6 months while establishing the model of diet-induced obesity. Therefore, all 90 mice received a high-fat diet (HFD; D12492; Research Diets, New Brunswick, NJ, United States) for 6 months *ad libitum*. According to randomization, the cages were divided into six groups. In the following 6 months, interventions were carried out as previously published by our group (28). The first group (n = 15) remained on an HFD, referred to as "HFD/HFD". In the second group, named "HFD/HFD + TM", treadmill (TM) exercise (TM 303401; TSE Systems Inc., Chesterfield, MO, United States) (n = 15) was added. The third group (n = 15) was trained on treadmills, and additionally, time-restricted food (TRF) intake was introduced after 3 months of intervention, designated as group "HFD/HFD + TM + TRF". The HFD was changed to a low-fat diet (LFD; D12450J; Research Diets, New Brunswick, NJ, United States) for (n = 15), building the fourth group "HFD/LFD". The fifth group (n = 15), called "HFD/LFD + TM", also changed diet to an LFD in addition to treadmill exercise for time of interventions. The last group (n = 15) underwent all given interventions, named "HFD/LFD + TM + TRF". Figure 1A illustrates the experimental design. Body weight was measured weekly and just before killing of the mice.

Interventions

Dietary change to low-fat diet

For the first intervention, 45 mice received an LFD, containing 10% fat, 20% protein, and 70% carbohydrates, matching the HFD in structure of lard and protein composition. Contrary to this, the HFD consists of 60% fat, 20% protein, and 20% carbohydrates.

Treadmill exercise

In addition to dietary change, TM exercise was established for n = 60 mice as the second intervention parameter. The exact TM protocol was previously described by our group (28). In brief, TM exercise was performed twice a week, running through a program, as shown in Figure 1B.

Time-restricted food

To treat obesity and metabolic disorders, time limited restriction of food is described as a beneficial method (29, 30),

which was the third intervention parameter, namely, TRF. After the third phase of TM exercise (Figure 1C), TRF was introduced to $n = 30$ mice using the same protocol, as previously described by our group (28). For the last 3 months, TRF was maintained. Food regulation was performed by using an autofeeder (EHEIM, Deizisau, Germany) with an enlarged opening. The food drop was controlled at 11 p.m. *via* a webcam with infrared light. The mice were transferred back to fresh cages at 7 a.m. with water supply and no enrichments.

In vitro experiment

The human hepatoma cell line HepG2 was used for *in vitro* experiments and was cultured as reported by Guy et al. (31). The cells were seeded in six-well plates. After reaching 95% confluence, cells were incubated with 20 µg/mL human TNFα (hTNFα; Sigma Aldrich, Taufkirchen, Germany) or Aqua Dest (B. Braun Melsungen AG, Melsungen, Germany) for 24 h. Afterward, the cells were harvested for analysis of β-klotho protein expression.

Sampling and assays

Under anesthesia (5 vol.% isoflurane; Baxter, Unterschleißheim, Germany), the mice were exsanguinated *via* retrobulbar puncture. Blood was collected and prepared according to Power et al. (31). Thereafter, a laparotomy was performed. The visceral and subcutaneous flanked fat deposits and liver tissue were harvested and weighted. Subsequently, the left lateral liver lobe was fixed in 4% paraformaldehyde (PFA, sc281692 Santa Cruz Biotechnology Inc., Dallas, TX, United States) for 5 days and embedded in paraffin (Carl Roth, Karlsruhe, Germany). The left medial lobe was embedded in Tissue-Tek® (Sakura Finetek Germany GmbH, Umkirch, Germany), snap-frozen in liquid nitrogen with the remaining tissue, and stored at −20°C. For the assessment of liver damage, plasma alanine aminotransferase (ALT), aspartate aminotransferase (AST), and albumin activities were spectrophotometrically determined (Cobas c111; Roche Diagnostics, Mannheim, Germany) using commercially available reaction kits (Roche Diagnostics, Mannheim, Germany). Measurements of the LDL/VLDL fraction, triglycerides, leptin, insulin, and FGF21 in plasma were performed using the LDL/VLDL cholesterol, leptin, insulin, and FGF21 assay kits according to the manufacturers' instructions (LDL/VLDL: Abcam, Cambridge, United Kingdom; leptin, insulin, FGF21: R&D System, Minneapolis, MN, United States; triglycerides: Cayman Chemical Company, Ann Arbor, MI, United States).

Histology, immunohistochemistry, and image analysis

Hematoxylin and eosin (H&E) staining (Merck, Darmstadt, Germany) was performed using standard protocols on 4 µm thin tissue sections. Images were recorded on a Carl Zeiss Axioskop 40 microscope (Carl Zeiss AG, Oberkochen, Germany) with a Zeiss AxioCamMRc5 camera (Carl Zeiss AG, Oberkochen, Germany) and corresponding Zeiss ZEN2 lite software (Carl Zeiss AG, Oberkochen, Germany).

From the H&E-stained specimen, the NAFLD Activity Score (NAS) was assessed in a blinded manner to characterize diet-induced liver damage. Following the description by Kleiner et al. (32) and our previous work (33), the parameters steatosis (scores 0–3), hepatocellular ballooning (scores 0–2), and lobular inflammation (scores 0–3) were used to calculate the NAS (total scores 0–8). Steatosis was assessed at 50× magnification and ballooning at 100× magnification. Inflammation was assessed by counting inflammatory foci from 10 representative low-power fields (LPF) (200× magnification), characterized as a grouping of at least five inflammatory cells in the tissue that are not arranged in a row (34). For Oil Red O staining of lipids, the frozen liver tissue was cut in 8 µm thick sections, air-dried, and fixed in paraformaldehyde. The staining was performed using Oil Red O (Sigma-Aldrich Corp., St. Louis, MO, United States) and counterstained with hematoxylin. In total, 10 images at 400× magnification were taken per sample. Quantitative analysis of the red-stained area was conducted using ImageJ (v 1.52, Wayne Rasband, National Institutes of Health, United States) (protocol provided in the supplements as ImageJ Code S1) analyzing the percentage of red pixels per image.

To substantiate inflammatory processes in the liver, naphthol-AS-C-chloracetate esterase (CAE) staining (Sigma Aldrich Corp., St. Louis, MO, United States) was used for characterizing granulocytes. After fixing in paraformaldehyde and embedding, sections were stained with CAE and counterstained with hematoxylin. The ratio of CAE-positive cells (CAE+) and the total number of hepatocytes in 10 consecutive high power fields (HPF) at 400× magnification were used to quantify granulocytes in a blinded manner. Macrophages were immunohistochemically stained for the indication of cellular hepatic LGI. Therefore, overnight incubation (4°C) with a rat anti-mouse-F4/80 (MCA497; Bio-Rad, Hercules, CA, United States) was followed by 1 h incubation at room temperature with the second antibody (goat anti-rat; abcam 97054; Abcam, Cambridge, United Kingdom). Afterward, the cells were stained with the chromogen Permanent Red (Ref. K0640, DAKO GmbH, Jena, Germany) and counterstained with hematoxylin. For quantification, the total number of F4/80-positive cells (F4/80+)

and the total number of hepatocytes were also counted in a blinded manner in 10 consecutive HPF at 400× magnification.

Western blot analysis

The harvested liver tissue and HepG2 cells incubated with TNFα were further processed for protein isolation. For this purpose, the liver tissue and cells were homogenized in lysis buffer (10 mM Tris pH 7.5, 10 mM NaCl, 0.1 mM EDTA, 0.5% Triton-X100, 0.02% NaN3, and 0.2 mM PMSF, protease inhibitor cocktail), incubated for 30 min on ice, and centrifuged for 10 min at 4°C and 10,000 × *g*. Protein contents were assayed by using the bicinchoninic acid method (Pierce Biotechnology Inc., Thermo Fisher Scientific, Waltham, MA, United States), with 2.5% BSA (Pierce Biotechnology Inc., Thermo Fisher Scientific, Waltham, MA, United States) as the standard. On an 8% SDS gel (FGFR1c and pFGFR1c) and a 10% Mini-PROTEAN® TGX Stain-FreeTM (Bio-Rad Laboratories, Munich, Germany) gel (β-klotho), 20 (liver tissue) or 10 (HepG2 cells) µg protein was separated. Mini-PROTEAN TGX gel was captured using the ChemiDoc XRS System (Bio-Rad Laboratories, Munich, Germany) before being transferred to a polyvinyldifluoride membrane (Immobilon-P; Millipore, Eschborn, Germany). After blockade with 2.5% BSA (Santa Cruz Biotechnology, Santa Cruz, CA, United States), membranes were incubated overnight at 4°C with a rabbit polyclonal anti-β-klotho (1:1.000, LSBioScience, Seattle, WA, United States), a rabbit polyclonal anti-pFGFR1c (Tyr653/654; 1:1.000, Cell Signaling Technology, Cambridge, United Kingdom), or a rabbit monoclonal anti-FGF21 [EPR8314(2), only HepG2 cells, 1:1.000, abcam, Cambridge, United Kingdom] antibody, respectively. Afterward, a secondary peroxidase-linked anti-rabbit antibody (β-klotho and pFGFR1c, 1:10.000; Cell Signaling Technology, Cambridge, United Kingdom) or only HepG2 cells (FGF21, 1:3.000) was applied. Protein expression was visualized by means of luminol-enhanced chemiluminescence (ECL plus; Amersham Pharmacia Biotech, Freiburg, Germany) and digitalized using the ChemiDoc™ XRS System (Bio-Rad Laboratories, Feldkirchen, Germany). Signals were densitometrically assessed (Quantity One; Bio-Rad Laboratories, Munich, Germany) and normalized either to the GAPDH signals (β-klotho and FGF21, HepG2 cells, and mouse monoclonal anti-β-GAPDH antibody; 1:20.000; Millipore, Eschborn, Germany, followed by secondary anti-mouse antibody, 1:40.000, Sigma Aldrich Corp., St. Louis, MO, United States) or to whole protein (β-klotho, liver tissue). To analyze the phosphorylation status of FGFR1c, signals of pFGFR1c were normalized to rabbit polyclonal anti-FGFR1c (clone D8E4, 1:1.000, Cell Signaling Technology, Cambridge, United Kingdom).

Quantitative real-time polymerase chain reaction

Ribonucleic acid (RNA) isolation and transcription into cDNA were performed as already published (28). mRNA expression analyses were performed *via* quantitative real-time polymerase chain reaction (PCR) in a BioRad iQ5 Multicolor Real Time PCR Detection System (Conquer Scientific, San Diego, CA, United States) with an iQ™ SYBR® Green Supermix (Bio-Rad Laboratories, Munich, Germany). Primer sequences are shown in Table 1. Measurement results are corrected against the housekeeping gene 40S ribosomal protein S18 (RPS18), and relative quantification was carried out *via* the $2^{-\Delta\Delta CT}$ method.

Statistics

Statistical analysis was performed using GraphPad Prism 8.0.1 (GraphPad Software Inc., San Diego, CA, United States) as previously described by our group (28). Data from animals that died during the experimental period or showed abnormalities during organ removal were excluded from all analysis. For expressional analyses of liver FGF21, IL-1β, IL-6, IL-10, and TNFα, each $n = 7$ samples and for HDL, LDL, and cholesterol assays, each $n = 5$ samples were measured. The ROUT method based on the false discovery rate ($Q = 0.01$) was applied to remove outliers. All results are presented as mean ± standard deviation (SD), and statistical significance was set at $p < 0.05$. For further details, see figure legends.

To represent correlation between all observational parameters, Pearson correlation was performed by measuring linear dependence of two parameters. Clustering between the six groups is represented as a dot plot of principal component analysis (PCA). For the parameters TNFα, FGF21, and β-klotho expressions in the liver, all data from $n = 84$ mice are included. Correlation between all 26 parameters (for AST, ALT, insulin, and leptin, see Supplementary Figure 1) is shown in a heatmap, indicating a strong positive correlation by red color (1.00–0.70), a strong negative correlation by blue color (−0.70 to −1.00),

TABLE 1 Primers used for quantitative real-time polymerase chain reaction (PCR).

Transcript	Forward primer (5′–3′)	Reverse primer (5′–3′)
fgf21	GCTGTCTTCCTGCTGGGG	CCTGGTTTGGGGAGTCCTTC
tnfα	ACATTCGAGGCTCCAGT GAATTCGG	GGCAGGTCTACTTTGGAGT CATTGC
il 1β	CCCAAGCAATACCCAAAGAA	TTGTGAGGTGCTGATGTACCA
il 6	TCTGACCACAGTGAGGA ATGTCCAC	TGGAGTCACAGAAGGAGT GGCTAAG
il 10	GCCTTGCAGAAAAGAGAGCT	AAAGAAAGTCTTCACCTGGC
rps18	AGGATGTGAAGGATGGGAAG	TTGGATACACCCACAGTTCG

10.3389/fnut.2022.935805

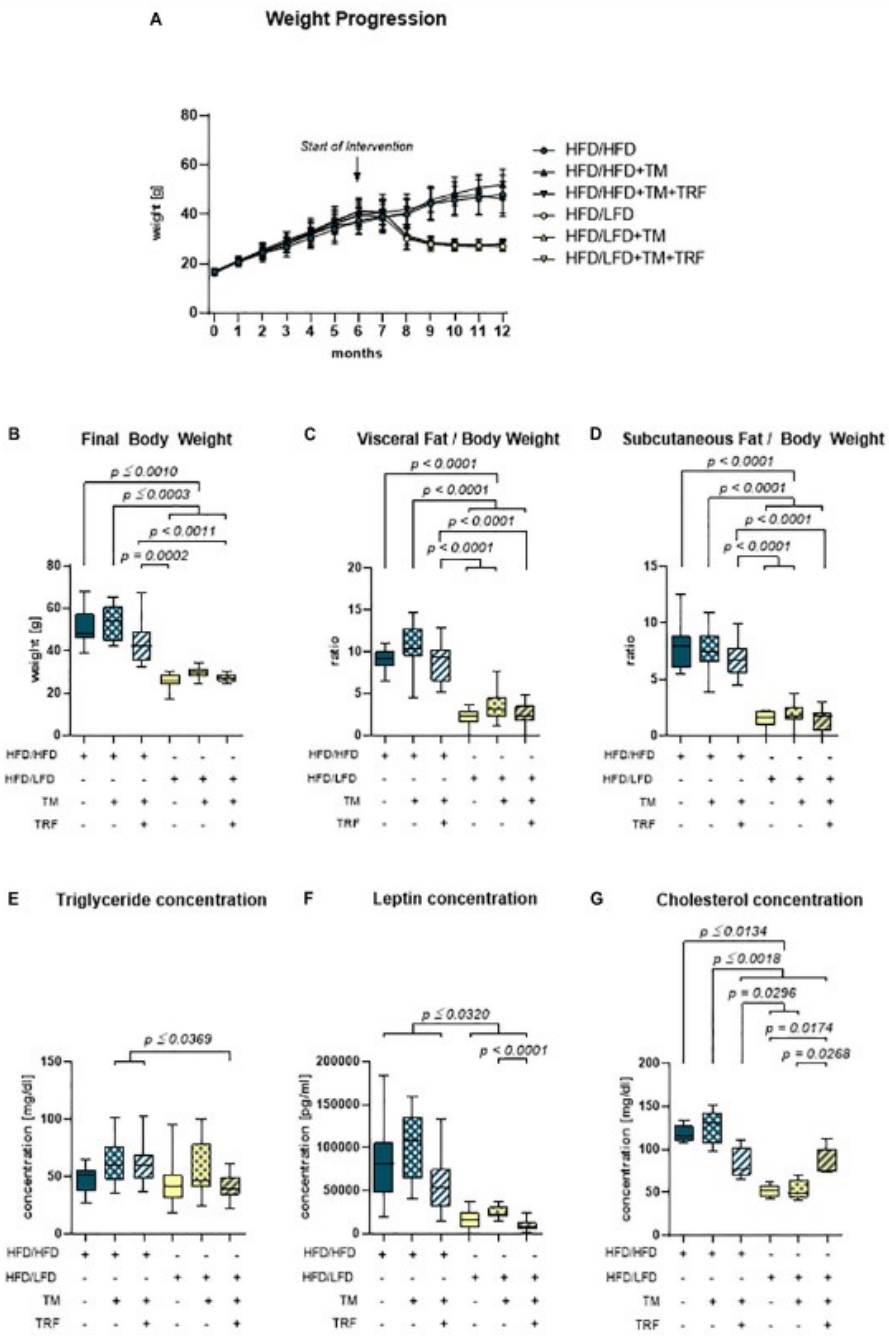

FIGURE 2
Body and fat composition. **(A)** Monthly weight progression with $n = 90$ mice at the beginning and $n = 84$ mice at the final time point. **(B)** Final body weights [g] before euthanasia (HFD/HFD: $n = 13$, HFD/HFD + TM: $n = 13$, HFD/HFD + TM + TRF: $n = 15$, HFD/LFD: $n = 14$, HFD/LFD + TM: $n = 15$, HFD/LFD + TM + TRF: $n = 13$; total $n = 83$). **(C)** Ratio of visceral body fat deposits to body weight. **(D)** Ratio of subcutaneous flanked fat deposits to body weight (**C,D** HFD/HFD: $n = 13$, HFD/HFD + TM: $n = 13$, HFD/HFD + TM + TRF: $n = 15$, HFD/LFD: $n = 14$, HFD/LFD + TM: $n = 15$, HFD/LFD + TM + TRF: $n = 14$; total $n = 84$). All HFD/LFD groups showed a significant fat loss with $p < 0.0001$ when compared to all three HFD/HFD groups, respectively [**A–D** from Power Guerra et al. (28)]. **(E)** Plasma triglyceride [mg/dL] (HFD/HFD: $n = 13$, HFD/HFD + TM: $n = 13$, HFD/HFD + TM + TRF: $n = 15$, HFD/LFD: $n = 14$, HFD/LFD + TM: $n = 15$, HFD/LFD + TM + TRF: $n = 14$; total $n = 84$). **(F)** Plasma leptin [pg/mL] (HFD/HFD: $n = 13$, HFD/HFD + TM: $n = 13$, HFD/HFD + TM + TRF: $n = 14$, HFD/LFD: $n = 14$, HFD/LFD + TM: $n = 15$, HFD/LFD + TM + TRF: $n = 13$; total $n = 82$) and **(G)** plasma cholesterol [mg/dL] (HFD/HFD: $n = 5$, HFD/HFD + TM: $n = 5$, HFD/HFD + TM + TRF: $n = 5$, HFD/LFD: $n = 5$,

(Continued)

FIGURE 2
HFD/LFD + TM: $n = 5$, HFD/LFD + TM + TRF: $n = 5$; total $n = 30$). Blue dots and box plots indicate HFD groups, and yellow dots and box plots indicate dietary change to LFD. Table displays the individual groups, respectively. Table is read from top to bottom; "+" denotes implementation of a given diet or intervention and "—" its absence. Significance of differences between groups was tested with either the Kruskal–Wallis test, followed by Dunn's *post hoc* test for multiple comparisons (**B**), the Brown–Forsythe test, and Welch's ANOVA with the Tamhane T2 *post hoc* test for multiple comparisons [**C**: *F* value (*F*) = 51.82, degree of freedom (DF) = 5; **D**: $F = 66.19$; DF = 5. F: $F = 22.68$, DF = 5], or by ordinary one-way ANOVA with Tukey's *post hoc* test for multiple comparisons (**E**). Data are presented as mean ± SD, and statistical significance was set at $p < 0.05$. HFD, high-fat diet; LFD, low-fat diet; TM, treadmill; TRF, time-restricted feeding.

and a moderate correlation by light colors (>0.40 or <-0.40) (35). The analysis was carried out in R (version 4.0.2, R studio, Boston, United States) *via* the prcomp method. Missing values were imputed ahead of analysis using the mean of the respective experimental group.

Results

Diet-induced obesity is attenuated by intervention strategies

Continuous administration of the HFD caused a large increase in body weight within the first 6 months (Figure 2A). After the introduction of the intervention approaches, such as LFD, TM training, and TRF, only the dietary change to LFD resulted in weight loss within a few weeks (Figure 2A, yellow vs. blue). Also, final body weight, and visceral and subcutaneous fat-to-body weight ratios were about 50% lower than those in all HFD/HFD groups (blue) (Figures 2B–D, yellow vs. blue). While in the HFD/LFD groups triglyceride concentrations were only decreased in tendency (Figure 2E), the concentrations of leptin and cholesterol were significantly reduced (yellow; Figures 2F,G).

High-fat diet-induced non-alcoholic fatty liver disease is treatable by intervention strategies leading to reduced pro-inflammatory tumor necrosis factor alpha expression

Accordingly, liver fat content, evaluated by Oil Red O staining, was found to be significantly diminished after dietary change (Figures 3A,B), which was also reflected by a significantly lower steatosis score (Figures 3C,D). Notably, livers of the HFD mice receiving TM and TRF displayed almost the same histological changes as observed in all LFD groups. In particular, Oil Red O staining showed a significant reduction in liver lipid in the HFD/HFD + TM + TRF group compared to the HFD/HFD group (Figure 3B). Although the parameters of hepatocellular ballooning and lobular inflammation were largely unchanged upon interventions, the NAFLD score was significantly decreased in all groups with dietary change, and in particular upon TM and TRF in the HFD group (Figure 3E). Despite the strong decrease in the lipid content after dietary change, there was no reduction in the number of resident macrophages and granulocytes in the liver, as indicated by no significant differences in the number of F4/80 (Figures 4A,B) and CAE (Figures 4C,D)-positive cells between the individual experimental groups. Consistent with this, mRNA expressions of the pro-inflammatory cytokines IL-1β and IL-6 were also nearly unchanged (Figures 5A,B), but the anti-inflammatory cytokine IL-10 showed tendencies to be increased mainly upon dietary change (Figure 5C). Noteworthy, the mRNA expression of TNFα was significantly decreased in all LFD vs. HFD groups (Figure 5D).

Reduced tumor necrosis factor alpha expression is accompanied by restoration of an fibroblast growth factor 21 sensitive state

Parallel to the reduction of TNFα, a significant decrease in the FGF21 concentration in plasma (Figure 5F) was observed. This was in line with the significant reduction of hepatic FGF21 mRNA expression (Figure 5E), whereby HFD mice receiving additional TM and TRF showed similar values, indicating that not only dietary change but also physical activity and intermittent fasting may trigger FGF21 levels. Of particular interest was the significant increase in hepatic β-klotho expression in all dietary change groups (Figure 5G), which was also associated with increased phosphorylation of FGFR1c, although this was only seen in the LFD groups with additional TM and TRF (Figure 5H). These results now suggest that especially with the dietary change, FGF21 sensitivity could be restored, that is, reduced FGF21 expression and increased expression of its receptors. The statistical results were confirmed by PCA (Figure 6). PCA showed for hepatic TNFα (A), FGF21 (B), and β-klotho (C) that the LFD groups clustered mainly on one side and the HFD groups on the other. In addition to this, the trained HFD group with additional intermittent fasting clustered more with the LFD groups. A further consideration of the correlation analysis (Figure 6D) showed that TNFα correlated with parameters, such as body weight, percentage of adipose tissue, and liver fat content (on average with $r = 0.6$;

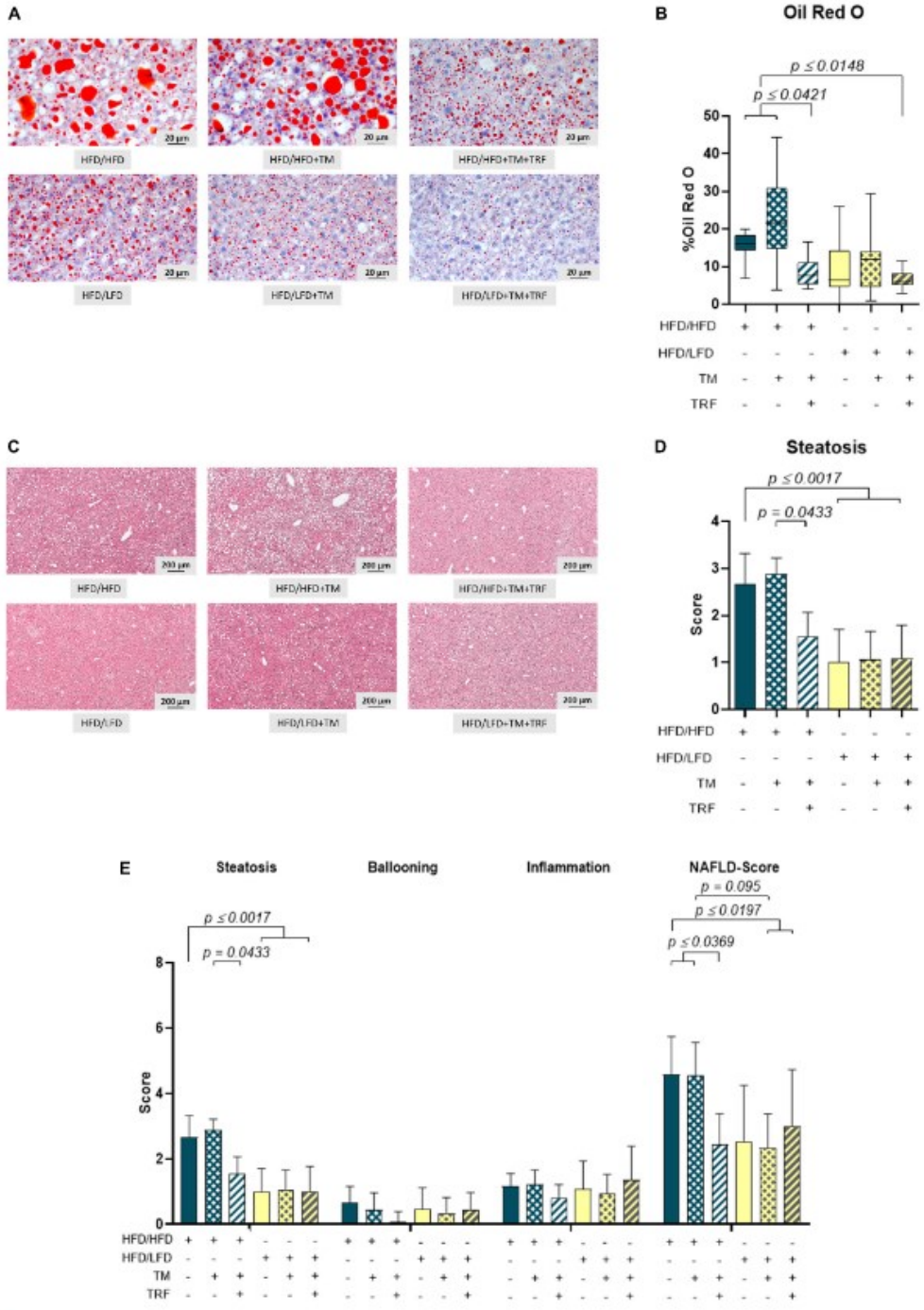

FIGURE 3

Representative images of Oil Red O **(A)** (400× magnification, scale bar represents 200 μm) and HE-stained liver specimen. **(C)** (50× magnification, scale bar represents 200 μm) and quantitative analysis of the Oil Red O-stained area in percentage **(B)** (HFD/HFD: $n = 11$, HFD/HFD + TM: $n = 11$, HFD/HFD + TM + TRF: $n = 12$, HFD/LFD: $n = 13$, HFD/LFD + TM: $n = 15$, HFD/LFD + TM + TRF: $n = 10$; total $n = 72$) and steatosis score **(D)** (HFD/HFD: $n = 12$, HFD/HFD + TM: $n = 9$, HFD/HFD + TM + TRF: $n = 11$, HFD/LFD: $n = 13$, HFD/LFD + TM: $n = 15$, HFD/LFD + TM + TRF: $n = 11$; total $n = 71$). Assessments of scores for steatosis, ballooning, and inflammation, as well as calculation of NAS for

(Continued)

FIGURE 3
the groups, are represented in panel E. Blue dots and box plots indicate HFD groups, and yellow dots and box plots indicate dietary change to LFD. Table displays the individual groups, respectively. Table is read from top to bottom; "+" denotes implementation of a given diet or intervention and "−" its absence. Significance of differences between groups was tested with either the Kruskal–Wallis test, followed by Dunn's *post hoc* test for multiple comparisons (**B**), the Brown–Forsythe test, and Welch's ANOVA with the Tamhane T2 *post hoc* test for multiple comparisons (**D**: F value (F) = 8.297, degree of freedom (DF) = 5, or by ordinary one-way ANOVA with Tukey's *post hoc* test for multiple comparisons (**E**: F = 9.765, DF = 5)]. Data are presented as mean ± SD, and statistical significance was set at $p < 0.05$. HFD, high-fat diet; LFD, low-fat diet; TM, treadmill; TRF, time-restricted feeding.

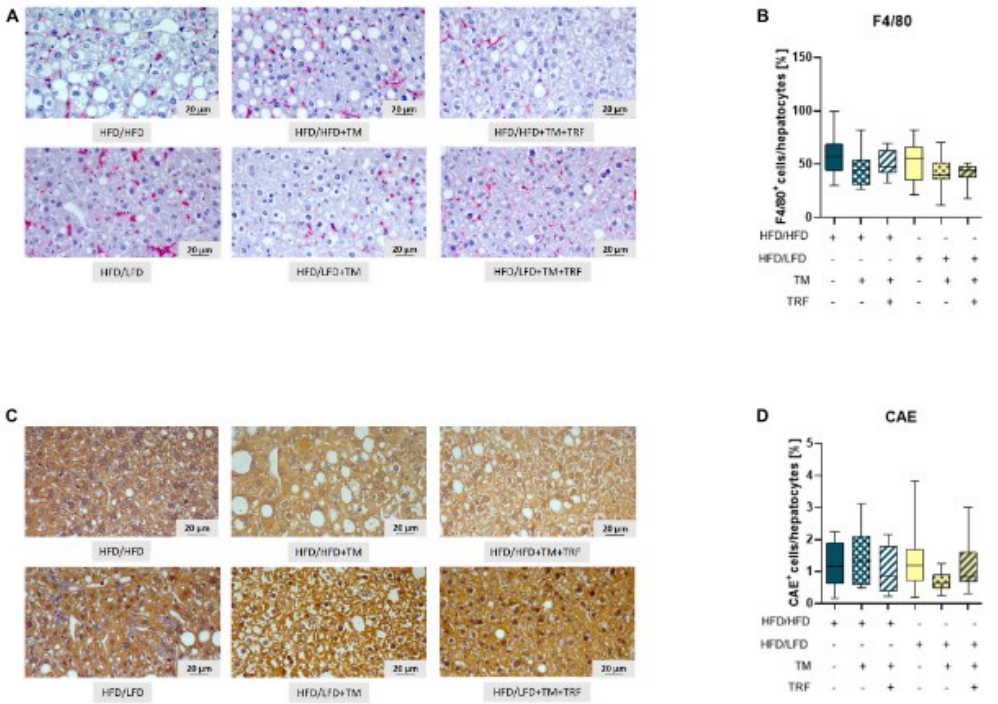

FIGURE 4
Representative images (both at 400× magnification, scale bar representing 20 μm) of F4/80 (**A**) as well as CAE-stained livers (**C**) and quantitative analysis of F4/80+ (**B**: HFD/HFD: n = 12, HFD/HFD + TM: n = 10, HFD/HFD + TM + TRF: n = 12, HFD/LFD: n = 13, HFD/LFD + TM: n = 15 or HFD/LFD + TM + TRF: n = 11; total n = 73) as well as CAE+ (**D**: HFD/HFD: n = 12, HFD/HFD + TM: n = 9, HFD/HFD + TM + TRF: n = 12, HFD/LFD: n = 13, HFD/LFD + TM: n = 13, HFD/LFD + TM + TRF: n = 11; total n = 70). Blue dots and box plots indicate HFD groups, and yellow dots and box plots indicate dietary change to LFD. Table displays the individual groups, respectively. Table is read from top to bottom; "+" denotes implementation of a given diet or intervention and "−" its absence. Significance of differences between groups was tested with either the Kruskal–Wallis test, followed by Dunn's *post hoc* test for multiple comparisons (**B**) or the Brown–Forsythe test, and Welch's ANOVA with the Tamhane T2 *post hoc* test for multiple comparisons (**D**) [F value (F) = 1.313, degree of freedom (DF) = 5]. Data are presented as mean ± SD, and statistical significance was set at $p < 0.05$. HFD, high-fat diet; LFD, low-fat diet; TM, treadmill; TRF, time-restricted feeding.

all $p \leq 0.05$). Of particular interest is that the NAFLD score positively correlated with hepatic TNFα ($r = 0.38$; $p \leq 0.05$), and particularly with systemic FGF21 ($r = 0.41$; $p \leq 0.05$).

Furthermore, the degree of dependency between TNFα and FGF21 sensitivity was investigated by correlation analysis (Figure 6D). We found that hepatic β-klotho correlated negatively with hepatic TNFα ($r = -0.38$; $p \leq 0.05$) and with hepatic FGF21 ($r = -0.32$; $p \leq 0.05$), while hepatic FGF21 correlated strongly positively with TNFα ($r = 0.82$; $p \leq 0.05$). This finding was partly supported by the *in vitro* analysis in HepG2 cells, showing that TNFα is indeed able to significantly reduce β-klotho expression (Figure 7A), whereas the phosphorylation of FGFR1c and protein expression of FGF21 was almost unchanged (Figures 7B,C).

Discussion and conclusion

The main finding of the study was that reversion of NAFLD is achieved not only by dietary change but also by continued

10.3389/fnut.2022.935805

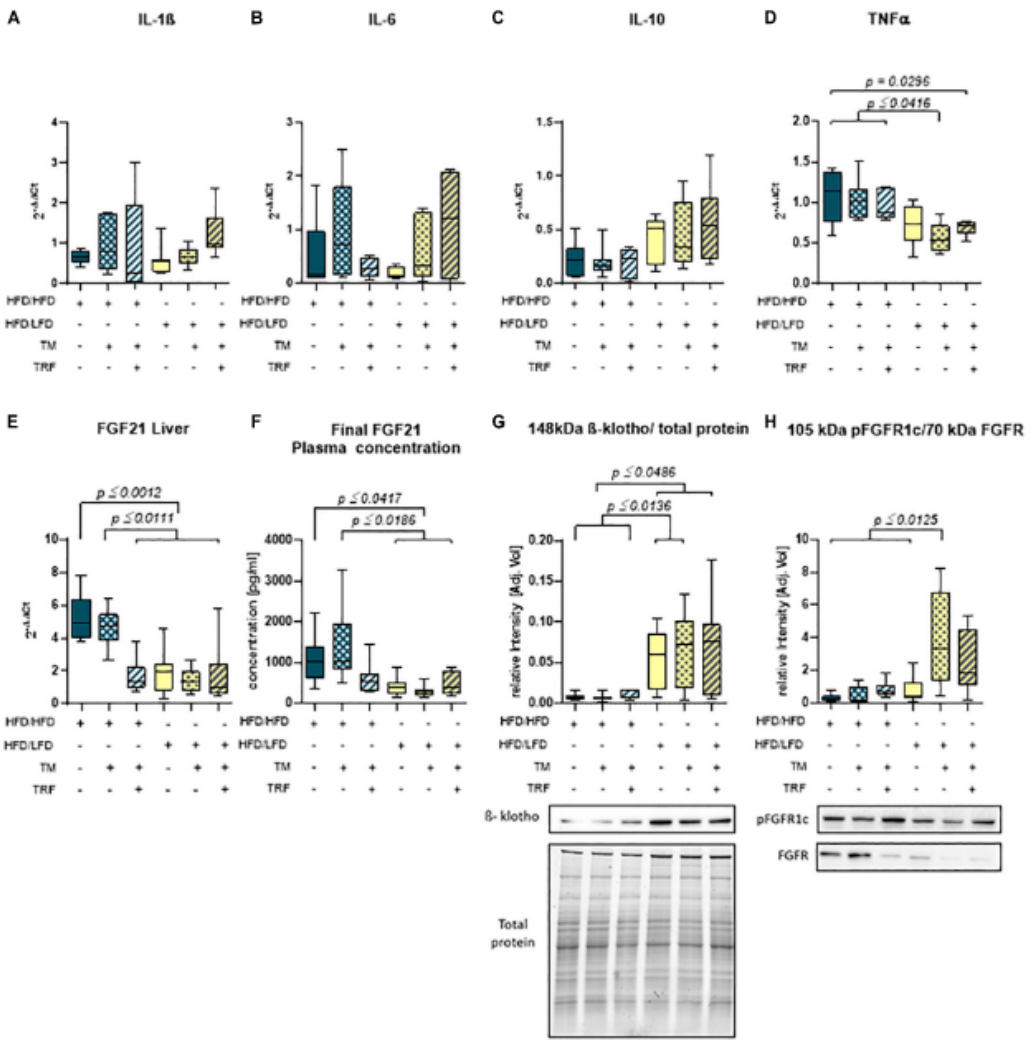

FIGURE 5
Hepatic mRNA expression of IL-1β **(A)** (HFD/HFD: $n = 6$, HFD/HFD + TM: $n = 7$, HFD/HFD + TM + TRF: $n = 7$, HFD/LFD: $n = 7$, HFD/LFD + TM: $n = 7$, HFD/LFD + TM + TRF: $n = 7$; total $n = 41$), IL-6 **(B)** (HFD/HFD: $n = 6$, HFD/HFD + TM: $n = 7$, HFD/HFD + TM + TRF: $n = 7$, HFD/LFD: $n = 6$, HFD/LFD + TM: $n = 7$, HFD/LFD + TM + TRF: $n = 7$; total $n = 40$), IL-10 **(C)** (HFD/HFD: $n = 7$, HFD/HFD + TM: $n = 7$, HFD/HFD + TM + TRF: $n = 6$, HFD/LFD: $n = 7$, HFD/LFD + TM: $n = 7$, HFD/LFD + TM + TRF: $n = 7$; total $n = 41$), TNFα **(D)** (HFD/HFD: $n = 6$, HFD/HFD + TM: $n = 7$, HFD/HFD + TM + TRF: $n = 7$, HFD/LFD: $n = 7$, HFD/LFD + TM: $n = 7$, HFD/LFD + TM + TRF: $n = 7$; total $n = 41$), plasma concentration **(E)** (HFD/HFD: $n = 13$, HFD/HFD + TM: $n = 13$, HFD/HFD + TM + TRF: $n = 15$, HFD/LFD: $n = 12$, HFD/LFD + TM: $n = 14$, HFD/LFD + TM + TRF: $n = 11$; total $n = 78$), and hepatic mRNA expression **(F)** (HFD/HFD: $n = 6$, HFD/HFD + TM: $n = 6$, HFD/HFD + TM + TRF: $n = 7$, HFD/LFD: $n = 7$, HFD/LFD + TM: $n = 7$, HFD/LFD + TM + TRF: $n = 7$; total $n = 40$) of FGF21. Data presented as $2^{-\Delta\Delta Ct}$ values determined by quantitative real-time PCR. Quantitative analysis of hepatic protein expression of β-klotho **(G)** (HFD/HFD: $n = 12$, HFD/HFD + TM: $n = 9$, HFD/HFD + TM + TRF: $n = 10$, HFD/LFD: $n = 12$, HFD/LFD + TM: $n = 15$, HFD/LFD + TM + TRF: $n = 11$; total $n = 69$) and phosphorylated form of the FGF receptor **(H)** (HFD/HFD: $n = 12$, HFD/HFD + TM: $n = 10$, HFD/HFD + TM + TRF: $n = 10$, HFD/LFD: $n = 9$, HFD/LFD + TM: $n = 10$, HFD/LFD + TM + TRF: $n = 8$; total $n = 59$) both with representative Western blots. Signals were normalized either to total protein (β-klotho) or to the non-phosphorylated FGF receptor. Blue dots and box plots indicate HFD groups, and yellow dots and box plots indicate dietary change to LFD. Table displays the individual groups, respectively. Table is read from top to bottom, and "+" denotes implementation of a given diet or intervention and "—" its absence. Significance of differences between groups was tested with either the Kruskal–Wallis test, followed by Dunn's *post hoc* test for multiple comparisons **(B)**, Brown–Forsythe, and Welch's ANOVA with the Tamhane T2 *post hoc* test for multiple comparisons [**A:** F value (F) = 1.165, degree of freedom (DF) = 5; **D:** $F = 5.742$, DF = 5. **E:** $F = 11.65$, DF = 5, **F:** $F = 9.902$, DF = 5 **G:** $F = 10.33$; DF = 5, **H:** $F = 9.214$; DF = 5], or by ordinary one-way ANOVA with Tukey's *post hoc* test for multiple comparisons **(C)**. Data are presented as mean ± SD, and statistical significance was set at $p < 0.05$. HFD, high-fat diet; LFD, low-fat diet; TM, treadmill; TRF, time-restricted feeding.

10.3389/fnut.2022.935805

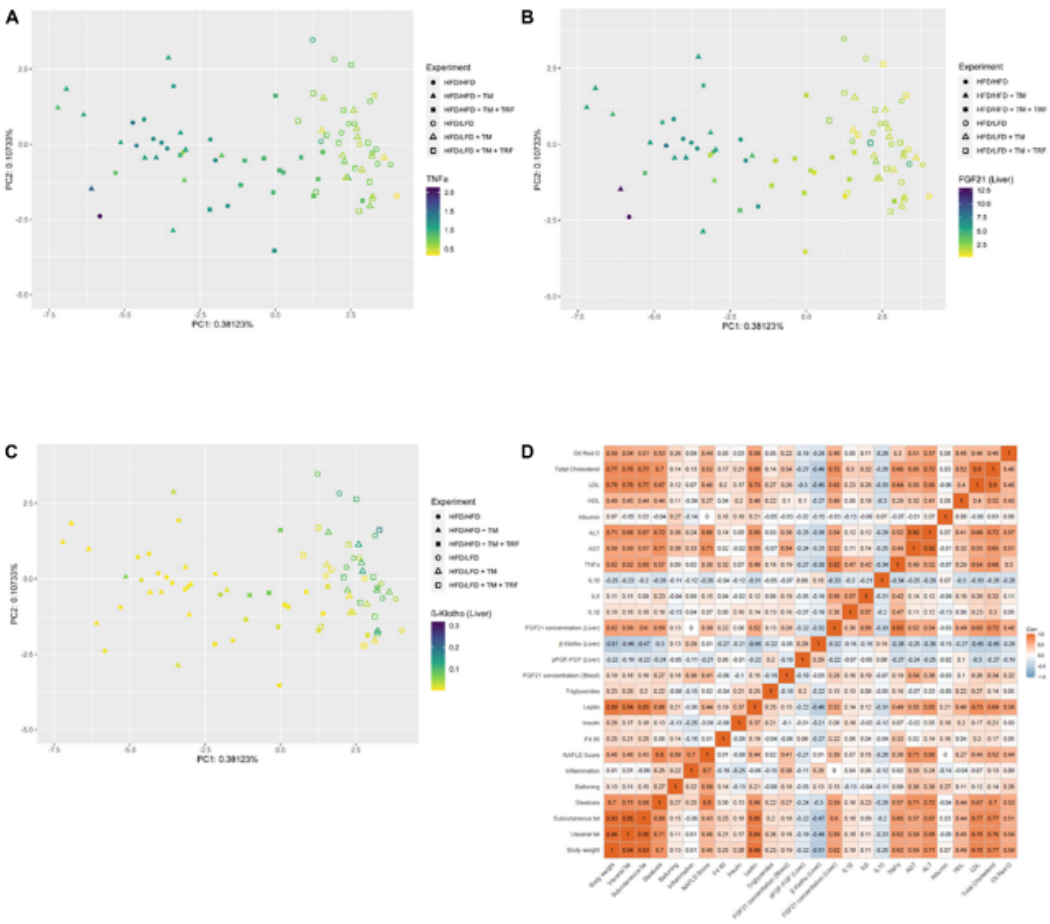

FIGURE 6

Dot plot of principal component analysis (PCA) for TNFα **(A)**, FGF21 in the liver **(B)**, and β-klotho in the liver **(C)** and correlation (Pearson, two-sided test, statistical significance was set at $p < 0.05$) represented as a multidimensional heatmap **(D)**. All parameters from previously acquired experiments were further used for PCA construction. TNFα (**A:** HFD/HFD $n = 13$, HFD/HFD + TM $n = 13$, HFD/HFD + TM + TRF $n = 15$, HFD/LFD $n = 14$, HFD/LFD + TM $n = 15$, HFD/LFD + TM + TRF $n = 14$; total $n = 84$), FGF21 liver (**B:** HFD/HFD $n = 13$, HFD/HFD + TM $n = 13$, HFD/HFD + TM + TRF $n = 15$, HFD/LFD $n = 14$, HFD/LFD + TM $n = 15$, HFD/LFD + TM + TRF $n = 14$; total $n = 84$), and β-klotho liver (**C:** HFD/HFD $n = 13$, HFD/HFD + TM $n = 13$, HFD/HFD + TM + TRF $n = 15$, HFD/LFD $n = 14$, HFD/LFD + TM $n = 15$, HFD/LFD + TM + TRF $n = 14$; total $n = 84$). In panels **A–C**, filled circles, triangles, and squares represent groups with HFD, and non-filled indicate dietary change to LFD. In panel **D**, red color indicates positive correlation, blue color indicates negative correlation, while white indicates no correlation. HFD, high-fat diet; LFD, low-fat diet; TM, treadmill; TRF, time-restricted feeding.

HFD combined with exercise and intermittent fasting. In addition, by observing decreased TNFα and FGF21 expression with concomitant increased β-klotho expression and a strong negative correlation between TNFα and β-klotho expression, we conclude that NAFLD recovery is associated with reversal of a TNFα-triggered FGF21-resistant state or desensitization.

For the treatment of NAFLD, next to bariatric surgery and pharmacological approaches, a less invasive method, namely, dietary change, is also feasible in some obese cases (36, 37). Thus, reduced calorie intake by lowering the fat content is recommended for sustainable weight loss (36) and thus for NAFLD recovery. As proof of principal, this was confirmed in the present study as indicated by the lowered liver fat content and steatosis score. Supporting this, our correlation analyses showed that a decrease in body weight and subcutaneous, as well as visceral fat, is associated with a reduced NAFLD score. In addition to dietary modification, physical activity is another modality for weight reduction in NAFLD therapy (38). However, in the present study, independent of LFD or HFD, no additional benefit was reached with treadmill exercise, as also shown by Ringseis et al. (39). This may be due to the frequency of training as daily training is recommended

10.3389/fnut.2022.935805

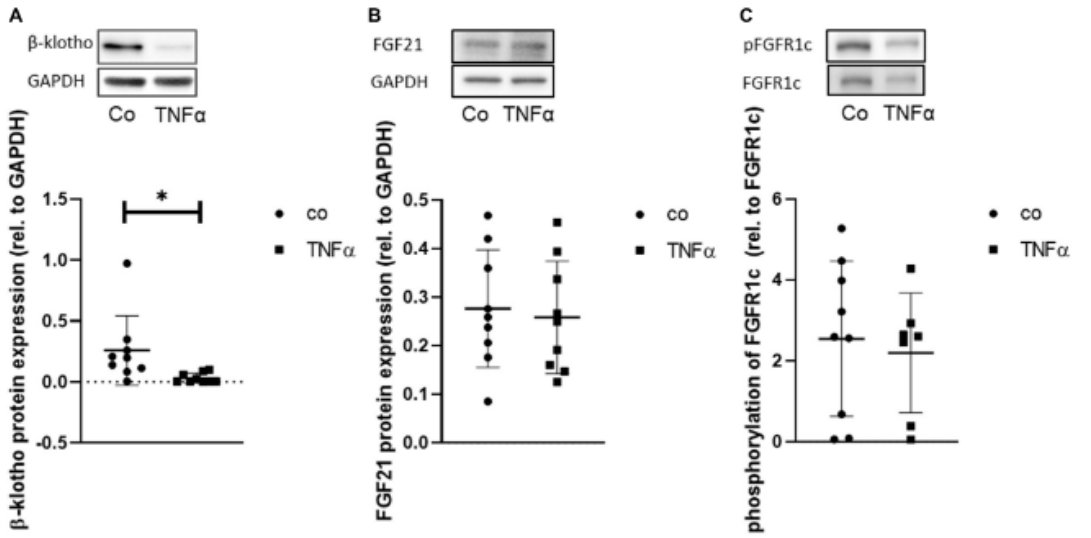

FIGURE 7
Representative Western blot and quantitative analysis of protein expression of β-klotho **(A)** and of FGF21, **(B)** and phosphorylation of FGFR1c **(C)** in HepG2 cells upon incubation of TNF for 24 h. Signals were normalized to GAPDH or FGFR1c, respectively. Data are presented as mean ± SD; $n = 9$ independent experiments; unpaired Student's t-test, $^*p < 0.05$ vs. control (Co).

for a reduction in body weight and thus for NAFLD therapy (37). Furthermore, the currently widespread intermittent fasting may have beneficial effects on NAFLD, especially since is knowing that this contributes to weight loss in obesity (40). Contrary to expectation, only the HFD mice receiving a time-restricted feeding additional to exercise revealed a reduced NAFLD score. As exercise alone did not benefit in NAFLD recovery, we conclude that in particular intermittent fasting in continued HFD is responsible for the observed effect. Similarly, cholesterol concentration was reduced only in the HFD group that received intermittent fasting in addition to exercise, which contradicts the study by Swift et al. (41), who showed that exercise alone reduced blood lipid levels. However, the extent to which the two interventions—treadmill training and intermittent feeding—influence each other in the context of a continued HFD and possibly overshadow any protective effect of training by intermittent fasting or vice versa can only be speculated. Nevertheless, the beneficial effect of time-restricted feeding is in line with the study of Chaix et al. (40) showing that body weight and body fat composition were markedly reduced in the HFD mice, which may be causative for recovery of NAFLD, as shown in the present study.

Obesity *per se* is often associated with increasing inflammatory mediators, such as TNFα (8). In turn, the reversion of NAFLD correlated positively with the reduction of TNFα expression, which persisted not only in dietary change but also in the HFD group receiving treadmill training and time-restricted feeding. TNFα has the ability to decrease the expression of β-klotho but not the phosphorylation of FGFR1c, as shown by Diaz-Delfin et al. (24) in adipocytes. This finding was underlined by the current study in hepatocytes, further highlighting the stronger role of β-klotho in FGF21 signaling. This statement is further supported when considering the groups with NAFLD recovery, where there was a stronger negative correlation of TNFα with β-klotho than with pFGFR1c, confirming the assumption that TNFα may alter FGF21 responsiveness, mainly *via* β-klotho. Although no increase in FGF21 expression could be detected after TNFα application *in vitro*, hepatic FGF21 expression, especially the circulating FGF21 plasma concentration, was decreased in mice that received dietary change in general. Interestingly, the exercising HFD group receiving additional time-restricted feeding also showed reduced FGF21 levels, suggesting that not only dietary change alone but also intermittent fasting may recover from obesity-induced FGF21 desensitization (20). This is also confirmed by the distribution of TNFα, FGF21, and β-klotho data points in the PCA plots, as indicated by clustering not only within the LFD groups but also within the treadmill training HFD group, which additionally underwent intermittent fasting. Accordingly, intermittent fasting has also been described to protect against consequences of obesity (27, 40), including the FGF21-resistant state (21). Since FGF21 has a circadian rhythm that is disrupted by a high-fat diet, intermittent fasting is thought to rebalance the oscillation of FGF21 by coupling food intake in a time-of-day-dependent manner (42, 43) and

thus counteracts obesity. Moreover, Geng et al. (26) showed that physical activity can decrease FGF21 expression and restore FGF21 sensitivity in obese mice and rebalance the metabolic interaction between the adipose tissue, liver, and skeletal muscle. However, this was not observed in the current study because exercise alone in the LFD as well as in the HFD group did not provide any additional benefit—neither in ameliorating NAFLD nor in reversing FGF21 sensitivity. Nevertheless, correlation analysis revealed, independent of any interventions, that with enhanced NAFLD recovery, TNFα expression was decreased, leading to increased FGF21 sensitivity expressed as an increase in β-klotho and FGFR1c expression with concomitantly reduced FGF21 levels. Thus, we conclude that hepatic FGF21 resistance or desensitization is most likely TNFα-dependent. Moreover, it was also observed that mainly circulating FGF21 correlates with the NAFLD score, suggesting a potential dependency between treated NAFLD and FGF21. This finding could provide a basis for considering non-invasive determination of plasma FGF21 as a possible marker to monitor NAFLD activity. This approach might have a high translational potential in treatment of NAFLD in obese patients.

Data availability statement

The datasets presented in this study can be found in online repositories. The names of the repository/repositories and accession number(s) can be found in the article/Supplementary material.

Ethics statement

This animal study was reviewed and approved by Landesamt für Landwirtschaft, Lebensmittelsicherheit und Fischerei (LALLF) of the state Mecklenburg-Western Pomerania (LALLF M-V/TSD/7221.3-2-001/18, approved on March 1, 2018).

Author contributions

AK: conceptualization, funding acquisition, and project administration. NPG: data curation, investigation, and validation. KL and LM: formal analysis. NPG, KL, LM, and DB: methodology. BV: resources. AK and BV: supervision. KL: visualization. AK, NPG, KL, and LM: roles and writing—original draft. DJ, SS, KP, BV, and HG: writing—review and editing. All authors contributed to the article and approved the submitted version.

Funding

This study was supported by a grant from the Deutsche Forschungsgemeinschaft, Bonn, Germany (KU 3280/1-2 and JA 2872/1-2).

Acknowledgments

We cordially thank the technicians of the Institute for Experimental Surgery and of the Central Animal Care Facility, Rostock University Medical Center, for their valuable assistance.

Conflict of interest

HG has received travel grants and speakers honoraria from Fresenius Medical Care, Neuraxpharm, Servier, and Janssen Cilag, as well as research funding from Fresenius Medical Care.

The remaining authors declare that the research was conducted in the absence of any commercial or financial relationships that could be construed as a potential conflict of interest.

Publisher's note

Supplementary material

The Supplementary Material for this article can be found online at: https://www.frontiersin.org/articles/10.3389/fnut.2022.935805/full#supplementary-material

References

1. Kaplan NM. The deadly quartet. Upper-body obesity, glucose intolerance, hypertriglyceridemia, and hypertension. *Arch Int Med.* (1989) 149:1514–20. doi: 10.1001/archinte.149.7.1514

2. Beilby J. Definition of metabolic syndrome: report of the national heart, lung, and blood institute/american heart association conference on scientific issues related to definition. *Clin Biochem Rev.* (2004) 25: 195–8.

3. Gogia A, Agarwal PK. Metabolic syndrome. *Indian J Med Sci.* (2006) 60: 72–81.

4. Marchesini G, Brizi M, Bianchi G, Tomassetti S, Bugianesi E, Lenzi M, et al. Nonalcoholic fatty liver disease: a feature of the metabolic syndrome. *Diabetes.* (2001) 50:1844–50. doi: 10.2337/diabetes.50.8.1844

5. Schattenberg JM, Schuppan D. Nonalcoholic steatohepatitis: the therapeutic challenge of a global epidemic. *Curr Opin Lipidol.* (2011) 22:479–88. doi: 10.1097/MOL.0b013e32834c7cfc

6. Hotamisligil GS. Inflammation and metabolic disorders. *Nature.* (2006) 444:860–7. doi: 10.1038/nature05485

7. Lumeng CN, Saltiel AR. Inflammatory links between obesity and metabolic disease. *J Clin Invest.* (2011) 121:2111–7. doi: 10.1172/JCI57132

8. Hotamisligil GS. Inflammation, metaflammation and immunometabolic disorders. *Nature.* (2017) 542:177–85. doi: 10.1038/nature21363

9. Juge-Aubry CE, Henrichot E, Meier CA. Adipose tissue: a regulator of inflammation. *Best Pract Res Clin Endocrinol Metab.* (2005) 19:547–66. doi: 10.1016/j.beem.2005.07.009

10. Wellen KE, Hotamisligil GS. Obesity-induced inflammatory changes in adipose tissue. *J Clin Invest.* (2003) 112:1785–8. doi: 10.1172/JCI20514

11. Kim KA, Gu W, Lee IA, Joh EH, Kim DH. High fat diet-induced gut microbiota exacerbates inflammation and obesity in mice via the TLR4 signaling pathway. *PLoS One.* (2012) 7:e47713. doi: 10.1371/journal.pone.0047713

12. Wu Z, Xu J, Tan J, Song Y, Liu L, Zhang F, et al. Mesenteric adipose tissue B lymphocytes promote local and hepatic inflammation in non-alcoholic fatty liver disease mice. *J Cell Mol Med.* (2019) 23:3375–85. doi: 10.1111/jcmm.14232

13. Koyama Y, Brenner DA. Liver inflammation and fibrosis. *J Clin Invest.* (2017) 127:55–64. doi: 10.1172/JCI88881

14. Saltiel AR, Olefsky JM. Inflammatory mechanisms linking obesity and metabolic disease. *J Clin Invest.* (2017) 127:1–4. doi: 10.1172/JCI92035

15. Kharitonenkov A, Shiyanova TL, Koester A, Ford AM, Micanovic R, Galbreath EJ, et al. FGF-21 as a novel metabolic regulator. *J Clin Invest.* (2005) 115:1627–35. doi: 10.1172/JCI23606

16. Coskun T, Bina HA, Schneider MA, Dunbar JD, Hu CC, Chen Y, et al. Fibroblast growth factor 21 corrects obesity in mice. *Endocrinology.* (2008) 149:6018–27. doi: 10.1210/en.2008-0816

17. Luo Y, Ye S, Li X, Lu W. Emerging structure-function paradigm of endocrine FGFs in metabolic diseases. *Trends Pharmacol Sci.* (2019) 40:142–53. doi: 10.1016/j.tips.2018.12.002

18. Domouzoglou EM, Maratos-Flier E. Fibroblast growth factor 21 is a metabolic regulator that plays a role in the adaptation to ketosis. *Am J Clin Nutr.* (2011) 93:901S–5S. doi: 10.3945/ajcn.110.001941

19. Zhang Y, Xie Y, Berglund ED, Coate KC, He TT, Katafuchi T, et al. The starvation hormone, fibroblast growth factor-21, extends lifespan in mice. *Elife.* (2015) 1:e00065. doi: 10.7554/eLife.00065

20. Gallego-Escuredo JM, Gómez-Ambrosi J, Catalan V, Domingo P, Giralt M, Frühbeck G, et al. Opposite alterations in FGF21 and FGF19 levels and disturbed expression of the receptor machinery for endocrine FGFs in obese patients. *Int J Obesity.* (2015) 39:121–9. doi: 10.1038/ijo.2014.76

21. Fisher FM, Chui PC, Antonellis PJ, Bina HA, Kharitonenkov A, Flier JS, et al. Obesity is a fibroblast growth factor 21 (FGF21)-resistant state. *Diabetes.* (2010) 59:2781–9. doi: 10.2337/db10-0193

22. Kälin S, Heppner FL, Bechmann I, Prinz M, Tschöp MH, Yi CX. Hypothalamic innate immune reaction in obesity. *Nat Rev Endocrinol.* (2015) 11:339–51. doi: 10.1038/nrendo.2015.48

23. Markan KR. Defining "FGF21 Resistance" during obesity: controversy, criteria and unresolved questions. *F1000Res.* (2018) 7:289. doi: 10.12688/f1000research.14117.1

24. Díaz-Delfín J, Hondares E, Iglesias R, Giralt M, Caelles C, Villarroya F. TNF-α represses β-Klotho expression and impairs FGF21 action in adipose cells: involvement of JNK1 in the FGF21 pathway. *Endocrinology.* (2012) 153:4238–45. doi: 10.1210/en.2012-1193

25. Kruse R, Vienberg SG, Vind BF, Andersen B, Højlund K. Effects of insulin and exercise training on FGF21, its receptors and target genes in obesity and type 2 diabetes. *Diabetologia.* (2017) 60:2042–51. doi: 10.1007/s00125-017-4373-5

26. Geng L, Liao B, Jin L, Huang Z, Triggle CR, Ding H, et al. Exercise alleviates obesity-induced metabolic dysfunction via enhancing FGF21 sensitivity in adipose tissues. *Cell Rep.* (2019) 26:2738–52.e4. doi: 10.1016/j.celrep.2019.02.014

27. Chaix A, Lin T, Le HD, Chang MW, Panda S. Time-restricted feeding prevents obesity and metabolic syndrome in mice lacking a circadian clock. *Cell Metab.* (2019) 29:303–19.e4. doi: 10.1016/j.cmet.2018.08.004

28. Power Guerra N, Parveen A, Bühler D, Brauer DL, Müller L, Pilz K, et al. Fibroblast growth factor 21 as a potential biomarker for improved locomotion and olfaction detection ability after weight reduction in obese mice. *Nutrients.* (2021) 13:2916. doi: 10.3390/nu13092916

29. Pietiläinen KH, Kaprio J, Borg P, Plasqui G, Yki-Järvinen H, Kujala UM, et al. Physical inactivity and obesity: a vicious circle. *Obesity.* (2008) 16:409–14. doi: 10.1038/oby.2007.72

30. Ferreira JC, Rolim NP, Bartholomeu JB, Gobatto CA, Kokubun E, Brum PC. Maximal lactate steady state in running mice: effect of exercise training. *Clin Exp Pharmacol Physiol.* (2007) 34:760–5. doi: 10.1111/j.1440-1681.2007.04635.x

31. Guy CS, Wang J, Michalak TI. Hepatocytes as cytotoxic effector cells can induce cell death by CD95 ligand-mediated pathway. *Hepatology.* (2006) 43:1231–40. doi: 10.1002/hep.21201

32. Kleiner DE, Brunt EM, Van Natta M, Behling C, Contos MJ, Cummings OW, et al. Nonalcoholic steatohepatitis clinical research network. Design and validation of a histological scoring system for nonalcoholic fatty liver disease. *Hepatology.* (2005) 41:1313–21. doi: 10.1002/hep.20701

33. Power Guerra N, Müller L, Pilz K, Glatzel A, Jenderny D, Janowitz D, et al. Dietary-induced low-grade inflammation in the liver. *Biomedicines.* (2020) 8:587. doi: 10.3390/biomedicines8120587

34. Liebig M, Hassanzada A, Kämmerling M, Genz B, Vollmar B, Abshagen K. Microcirculatory disturbances and cellular changes during progression of hepatic steatosis to liver tumors. *Exp Biol Med.* (2018) 243:1–12. doi: 10.1177/1535370217738730

35. Akoglu H. User's guide to correlation coefficients. *Turk J Emerg Med.* (2018) 18:91–3. doi: 10.1016/j.tjem.2018.08.001

36. Romero-Gómez M, Zelber-Sagi S, Trenell M. Treatment of NAFLD with diet, physical activity and exercise. *J Hepatol.* (2017) 67:829–46. doi: 10.1016/j.jhep.2017.05.016

37. Mantovani A, Dalbeni A. Treatments for NAFLD: state of Art. *Int J Mol Sci.* (2021) 22:2350. doi: 10.3390/ijms22052350

38. Nseir W, Hellou E, Assy N. Role of diet and lifestyle changes in nonalcoholic fatty liver disease. *World J Gastroenterol.* (2014) 20:9338–44. doi: 10.3748/wjg.v20.i28.9338

39. Ringseis R, Mooren FC, Keller J, Couturier A, Wen G, Hirche F, et al. Regular endurance exercise improves the diminished hepatic carnitine status in mice fed a high-fat diet. *Mol Nutr Food Res.* (2011) 55(Suppl. 2):S193–202. doi: 10.1002/mnfr.201100040

40. Chaix A, Zarrinpar A, Miu P, Panda S. Time-restricted feeding is a preventative and therapeutic intervention against diverse nutritional challenges. *Cell Metab.* (2014) 20:991–1005. doi: 10.1016/j.cmet.2014.11.001

41. Swift DL, Houmard JA, Slentz CA, Kraus WE. Effects of aerobic training with and without weight loss on insulin sensitivity and lipids. *PLoS One.* (2018) 13:e0196637. doi: 10.1371/journal.pone.0196637

42. Hatori M, Vollmers C, Zarrinpar A, DiTacchio L, Bushong EA, Gill S, et al. Time-restricted feeding without reducing caloric intake prevents metabolic diseases in mice fed a high-fat diet. *Cell Metab.* (2012) 15:848–60. doi: 10.1016/j.cmet.2012.04.019

43. Chapnik N, Genzer Y, Froy O. Relationship between FGF21 and UCP1 levels under time-restricted feeding and high-fat diet. *J Nutr Biochem.* (2017) 40:116–21. doi: 10.1016/j.jnutbio.2016.10.017

10.5 Studie 5

nutrients

MDPI

Article

Long-Term Caloric Restriction Attenuates β-Amyloid Neuropathology and Is Accompanied by Autophagy in APPswe/PS1delta9 Mice

Luisa Müller [1,2,3], Nicole Power Guerra [1], Jan Stenzel [4], Claire Rühlmann [1], Tobias Lindner [4], Bernd J. Krause [4,5], Brigitte Vollmar [1,4], Stefan Teipel [2,3,6] and Angela Kuhla [1,3,*]

1 Rudolf-Zenker-Institute for Experimental Surgery, Medical University Rostock, 18057 Rostock, Germany; luisa.mueller2@uni-rostock.de (L.M.); nicole.guerra@uni-rostock.de (N.P.G.); Claire_ruehlmann@web.de (C.R.); brigitte.vollmar@med.uni-rostock.de (B.V.)
2 Department of Psychosomatic Medicine and Psychotherapy, University of Rostock, 18147 Rostock, Germany; stefan.teipel@med.uni-rostock.de
3 Centre for Transdisciplinary Neurosciences Rostock (CTNR), University of Rostock, 18147 Rostock, Germany
4 Core Facility Multimodal Small Animal Imaging, Rostock University Medical Center, 18057 Rostock, Germany; jan2.stenzel@gmail.com (J.S.); tobias.lindner@med.uni-rostock.de (T.L.); bernd.krause@med.uni-rostock.de (B.J.K.)
5 Department of Nuclear Medicine, Rostock University Medical Center, 18057 Rostock, Germany
6 German Center for Neurodegenerative Diseases (DZNE)–Rostock/Greifswald, 18147 Rostock and 17489 Greifswald, Germany
* Correspondence: angela.kuhla@uni-rostock.de; Tel.: +49-381-494-2503

Citation: Müller, L.; Power Guerra, N.; Stenzel, J.; Rühlmann, C.; Lindner, T.; Krause, B.J.; Vollmar, B.; Teipel, S.; Kuhla, A. Long-Term Caloric Restriction Attenuates β-Amyloid Neuropathology and Is Accompanied by Autophagy in APPswe/PS1delta9 Mice. *Nutrients* **2021**, *13*, 985. https:// doi.org/10.3390/nu13030985

Academic Editors: Susanne Klaus and Takuya Chiba

Received: 4 February 2021
Accepted: 16 March 2021
Published: 18 March 2021

Abstract: Caloric restriction (CR) slows the aging process, extends lifespan, and exerts neuroprotective effects. It is widely accepted that CR attenuates β-amyloid (Aβ) neuropathology in models of Alzheimer's disease (AD) by so-far unknown mechanisms. One promising process induced by CR is autophagy, which is known to degrade aggregated proteins such as amyloids. In addition, autophagy positively regulates glucose uptake and may improve cerebral hypometabolism—a hallmark of AD—and, consequently, neural activity. To evaluate this hypothesis, APPswe/PS1delta9 (tg) mice and their littermates (wild-type, wt) underwent CR for either 16 or 68 weeks. Whereas short-term CR for 16 weeks revealed no noteworthy changes of AD phenotype in tg mice, long-term CR for 68 weeks showed beneficial effects. Thus, cerebral glucose metabolism and neuronal integrity were markedly increased upon 68 weeks CR in tg mice, indicated by an elevated hippocampal fluorodeoxyglucose [^{18}F] ([^{18}F]FDG) uptake and increased N-acetylaspartate-to-creatine ratio using positron emission tomography/computer tomography (PET/CT) imaging and magnet resonance spectroscopy (MRS). Improved neuronal activity and integrity resulted in a better cognitive performance within the Morris Water Maze. Moreover, CR for 68 weeks caused a significant increase of LC3BII and p62 protein expression, showing enhanced autophagy. Additionally, a significant decrease of Aβ plaques in tg mice in the hippocampus was observed, accompanied by reduced microgliosis as indicated by significantly decreased numbers of iba1-positive cells. In summary, long-term CR revealed an overall neuroprotective effect in tg mice. Further, this study shows, for the first time, that CR-induced autophagy in tg mice accompanies the observed attenuation of Aβ pathology.

Keywords: APPswe/PS1delta9; caloric restriction; [^{18}F]FDG-PET/CT; amyloid β; iba1; autophagy

1. Introduction

One hallmark of Alzheimer's disease (AD) is the accumulation of amyloid-β (Aβ), leading to formation of Aβ-plaques [1]. Transgenic animal models of Aβ pathology provide mechanistic insight into aspects of AD pathology related to Aβ accumulation and represent an important tool for translational AD research. Accordingly, APPswe/PS1delta9 mice, a well-established AD mouse model, display a variety of clinically relevant AD-like

symptoms, including increased parenchymal Aβ load, neuroinflammation, deficits in the cholinergic system, and cognitive impairment at an age of 4 months when developing first Aβ depositions [2]. Overall, neural activity in AD is linked with altered cerebral glucose metabolism. Accordingly, several clinical studies [3,4] have reported that hypometabolism is a well-described pathological hallmark of AD.

It is widely accepted that caloric intake may influence the relative risk for AD [5,6]. Most remarkably, while high caloric intake may promote AD neuropathology, experimental evidence strongly supports the hypothesis that caloric restriction (CR) prevents it. In this context, CR has attenuated Aβ deposition in several AD mouse models [7–10], whereby the duration of CR with 4 weeks [8] or 36 weeks [10] strongly differed. Moreover, Patel et al. and colleagues [8] showed reduced Aβ-associated astrocyte activation upon CR. Besides diminishing Aβ pathology, CR led to the reduction of neuronal loss in hippocampus [11] and to the improvement of cognitive deficits [12].

One process induced by CR is autophagy, a catabolic mechanism that degrades and recycles organelles and misfolded proteins such as Aβ. Therefore, autophagy is important in Aβ clearance from tissues [13]. Interestingly, AD-associated phenomena like neuroinflammation and glial activation can impair autophagy functionality, further amplifying neurodegeneration [14]. In this context, it has been reported that CR may induce glial autophagy, which is known to have a neuroprotective effect in AD [15]. In detail, autophagy is characterized by translocation of autophagy-gene-related (Atg) protein LC3BII together with sequestosom-1 (p62) to the autophagosome membrane, both commonly used as markers of autophagosome formation [16].

To date, no study has assessed whether CR-induced improvement in cognition is accompanied by autophagy. Moreover, the success of CR seems to be dependent on the duration of CR [17]. For example, our working group was able to show that only a lifelong CR for 74 weeks improved cognition performance in C57BL6 mice [18]. However, studies with AD mice have revealed an enhancement of cognition after 14 weeks CR [7,8]. To address this subject, we subjected APPswe/PS1delta9 mice to short-term (16 weeks) or long-term (68 weeks) CR and studied to what extent reduced amyloid pathology and improved cognition was accompanied with increased autophagy.

2. Materials and Methods

2.1. Animals

The study was performed in female APPswe/PS1delta9 (tg) mice co-expressing human amyloid-β precursor protein (APP) K594N and M595L mutation, as well as the human presenilin (PS) 1, L166P mutation under the control of the mouse prion protein promotor [19,20]. The APPswe/PS1delta9 mice were hemizygotes on B6xC3H and C57BL6 mouse backgrounds, and all mice were bred in-house. Female littermates of B6xC3H, as well as C57BL6 mice, were pooled and served as control group (wild-type; wt). Mice at the age of 4 weeks were fed either ad libitum (AL) or a caloric-restricted diet (CR, 60% of ad libitum chow) for 16 weeks (16 weeks or short-term, $n = 5–10$ for each group) or 68 weeks (68 weeks or long-term, $n = 5–10$ for each group). All mice were housed in standard cages in a temperature-controlled room (22 °C ± 2 °C) on a 12 h light/dark cycle (light on at 06:00 a.m.), with free access to water under specified pathogen-free conditions. At the beginning and end of the experiment, body weight was examined. Blood glucose was measured directly before sacrifice. The experimental protocol was approved by the local Animal Research Committee (Landesamt für Landwirtschaft, Lebensmittelsicherheit und Fischerei (LALLF) of the state Mecklenburg-Western Pomerania (LALLF M-V/TSD/7221.3-1.1-002/14)). All animals received care according to the German legislation on protection of animals and the Guide for the Care and Use of Laboratory Animals (European Directive 2010/63/EU).

2.2. Magnetic Resonance Imaging (MRI) and Spectroscopy (MRS)

In vivo imaging (representative Figure 1a), as well as single-voxel spectroscopy, was per-

formed according to the methodology described by Rühlmann et al. [21]. Spectra (exemplary in Figure 1b) were analyzed with jMRUI spectroscopy software (version 5.2) [22,23] and the jMRUI2XML package [24]. N-acetylaspartate/creatine ratios (NAA/Cr) were calculated. Therefore, the Hankel-Lanczos Singular Value Decomposition (HLSVD) method with 5 components was applied [25].

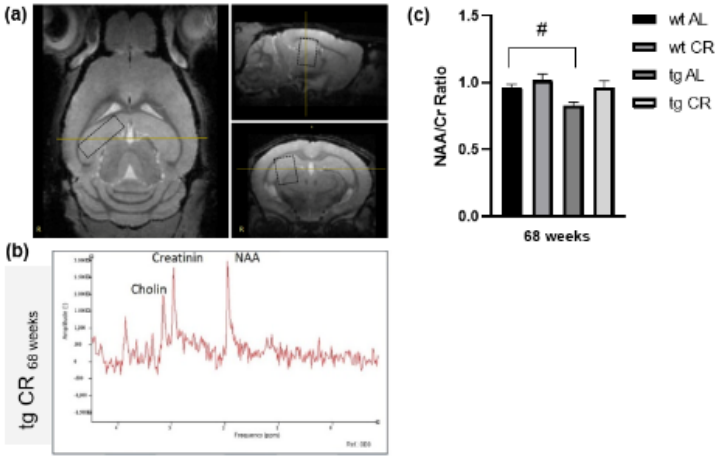

Figure 1. Representative magnetic resonance image including measured voxel (**a**). Example of magnetic resonance spectroscopy (MRS) with the prominent metabolites N-acetylaspartate (NAA resonates at 2.0 ppm) and creatine (Cr resonates at 3.0 ppm) from a transgenic APPswe/PS1delta9 (tg) mouse (**b**). Quantification of N-acetylaspartate/creatine (NAA/Cr) ratios in the brains of wild-type (wt) and tg mice fed either ad libitum (AL) or a caloric-restricted diet (CR, 60% of ad libitum) for 68 weeks (**c**). Values are given as mean ± SEM. Significance of differences between the groups was tested by one-way ANOVA on Ranks (Kruskal–Wallis) with Dunn's post hoc test for multiple comparisons: # $p < 0.05$ vs. wt.

2.3. Positron Emission Tomography/Computer Tomography (PET/CT) Imaging and PET/CT-Data Analysis

PET/CT imaging and data analysis were performed according to previous works of our group [21,26,27] using PMOD software (version 3.7; PMOD Technologies LLC, Zürich, Switzerland). The processed PET images were subsequently co-registered with the mouse brain volume-of-interest (VOI) template (Mouse Mirrione atlas), and the PMOD software and tracer uptake values were extracted for each delineated VOI. Due to the fact that mice differed in body weight, the injected dose percentage per gram (ID%/g) was chosen as unit of measurement and acquired for each VOI.

2.4. Morris Water Maze Test

The Morris Water Maze (MWM) was performed as measure for spatial reference memory according to previously published work [18]. The amount of platform crosses, latency to first platform crossing, time spent on platform, and north (N)-quadrant crosses were monitored in real time by a video camera (15E objective, Computar, CBC Europe, Düsseldorf, Germany with Camera CCA1300-60gm, Basler AG, Ahrensburg, Germany), with subsequent digital analysis (Ethovision XT II.5, Noldus Information Technology, Wageningen, The Netherlands).

2.5. Sampling

At the end of the experiment, all mice were anesthetized with a mixture of ketamine (98 mg/kg bodyweight, medistar, Ascheberg, Germany) and xylazine (6.5 mg/kg bodyweight, Bayer, Leverkusen, Germany), exsanguinated by puncture of the vena cava inferior for immediate separation of plasma, and harvested of brain tissue.

2.6. Immunohistochemistry

Brain tissue was fixed in 4% phosphate-buffered formalin, embedded in paraffin and sliced in 4 µm-thin sections. The sections were put on X-tra Adhesive Precleaned Micro Slides (Leica, Wetzlar, Germany) and exposed to mouse monoclonal anti-Aβ antibody (clone 6E10; 1:1000, BioLegend, San Diego, CA, USA, as described by the authors of [28]) and goat polyclonal anti-iba1 antibody (1:1000, Abcam, Berlin, Germany). DAB chromogen Universal LSAB® kits (System-HRP; DakoCytomation, Dako, Jena, Germany) were used for development according to the manufacturer's instructions. The sections were counterstained with hemalaun (Merck, Darmstadt, Germany), and images were acquired on microscope type BX51 with a Color View Soft Imaging System and the corresponding software cellSens Standard 1.14 (all from Olympus, Hamburg, Germany). Appropriate negative staining images are provided in Appendix A (Figure A1). Within the hippocampus (n = 5–10 of each mouse strain and feeding), the number and the area of anti-Aβ positive plaques, as well as the number of iba1-positive cells, were assessed and measured semiautomatically with ImageJ 1.47 v. in a high-power field (HPF) and are given in n/HPF and µm^2 for the area.

2.7. Western Blot Analysis of Brain Tissue

Harvested brain tissue was further processed for protein isolation. For this purpose, brain tissue was homogenized in lysis buffer (10 mM Tris pH 7.5, 10 mM NaCl, 0.1 mM EDTA, 0.5% Triton-X 100, 0.02% NaN_3 and 0.2 mM PMSF, protease inhibitor cocktail), incubated for 30 min on ice, and centrifuged for 10 min at 4 °C and 10,000× g. Protein contents were assayed by bicinchoninic acid method (Pierce Biotechnology, Rockford, IL, USA) with 2.5% BSA (Pierce Biotechnology, Rockford, IL, USA) as standard, as already described by the authors of [29]. On 14% (for LC3B) or 10% (for p62) SDS gels, 15 µg protein from brain tissue was separated and transferred to a polyvinyldifluoride membrane (Immobilon-P; Millipore, Burlington, MA, USA). After blockade with 2.5% BSA (Pierce Biotechnology, Rockford, IL, USA), membranes were incubated overnight at 4 °C with a rabbit polyclonal anti-p62 antibody (1:8000, Abcam, Berlin, Germany) and a rabbit polyclonal anti-LC3B antibody (1:1000, Sigma L7543, Sigma-Aldrich, Darmstadt, Germany). Exemplary raw images of western blot analysis of LC3B and p62 are shown in Appendix A (Figures A2 and A3). The anti-LC3B antibody is able to detect both isoforms, LC3BI (~18 kDa) and LC3BII (~16 kDa), which can be distinguished by their corresponding molecular weight, as seen in the original blots (Appendix A, Figure A2). Afterward, a secondary HRP-linked anti-rabbit antibody (1:10,000, cell signaling 7074, Cell Signaling Technology, Frankfurt am Main, Germany) was applied. Visualization of protein expression was performed by means of luminol-enhanced chemiluminescence (ECL plus; Amersham Pharmacia Biotech, Amersham, UK). After digitalization with the ChemiDoc™ XRS System (Bio-Rad Laboratories, Hercules, CA, USA), signals were densitometrically assessed (Quantity One; Bio-Rad Laboratories, Hercules, CA, USA) and normalized to the density of β-actin signal in the respective specimen (acquired with mouse monoclonal anti-β-actin antibody; 1:20,000; Sigma, A5441 and secondary HRP-linked anti-mouse antibody; 1:60,000; Sigma, A9044, Sigma-Aldrich, Darmstadt, Germany).

2.8. Statistical Analysis

Data were checked for normal distribution with the Shapiro–Wilk test and variances of standard deviations were verified by Bartlett's test. If standard deviations were not significantly different with $p > 0.05$, an ordinary one-way ANOVA was performed, followed by Sidak's multiple comparisons test or unpaired student t-test followed by Bonferroni correction with p threshold of 0.0166 was performed. Otherwise, Brown–Forsythe and Welch ANOVA were performed followed by Tamhane's T2 multiple comparisons test. If data were not normally distributed, the Kruskal–Wallis test with Dunn's post hoc test for multiple comparisons or Mann–Whitney test, followed by Bonferroni correction with p threshold of 0.0166, was conducted. All data are expressed as mean ± standard error of

mean (SEM). Statistical analysis was performed using the GraphPadPrism version 8.0.1 (GraphPad software, San Diego, CA, USA).

3. Results

3.1. Short-Term CR (16 Weeks) Showed No Effect in Glucose Uptake and Cognition Performance

CR vs. AL feeding for 16 weeks resulted in a significant decrease of bodyweight in wt and tg mice ($p \leq 0.0001$, student t-test followed by Bonferroni correction, Table 1). Of utmost interest, blood sugar concentrations were almost unaffected by CR in both mouse strains (Table 1). In our study, short-term CR did not change [^{18}F]FDG uptake (Table 2) nor cognitive performance (Table 3). Therefore, in the following evaluations, we only refer to the long-term CR.

Table 1. Blood glucose concentrations and body weight of short- (16 weeks) and long-term (68 weeks) ad libitum (AL) or caloric-restricted (CR, 60% of ad libitum) diet-fed wild-type (wt) and transgenic (tg) mice (all mice revealed starting weight of approximately 19 g). Values are given as mean ± SEM. Significance of differences between the groups was tested by unpaired student t-test or Mann–Whitney test, both followed by Bonferroni correction with p threshold of 0.0166: ** $p < 0.005$; *** $p \leq 0.0001$ vs. AL.

Genotype	wt		tg	
Feeding for 16 Weeks	**AL**	**CR**	**AL**	**CR**
Blood glucose (mmol/L)	7.94 ± 0.54	** 5.62 ± 0.27	7.15 ± 0.25	5.70 ± 0.27
Body weight (g)	28.90 ± 3.42	*** 20.26 ± 0.47	31.35 ± 0.95	*** 20.62 ± 0.44
Feeding for 68 Weeks	**AL**	**CR**	**AL**	**CR**
Blood glucose (mmol/L)	6.80 ± 0.27	6.78 ± 0.34	7.55 ± 0.05	6.15 ± 0.34
Body weight (g)	33.72 ± 2.29	*** 23.15 ± 0.55	28.88 ± 2.65	** 21.95 ± 0.71

Table 2. [^{18}F]FDG uptake (ID%/g) measurements of short-term (16 weeks) ad libitum (AL) or caloric restricted (CR, 60% of ad libitum) diet-fed wild-type (wt) and transgenic (tg) mice. Values are given as mean ± SEM. Significance of differences between the groups was tested by Brown–Forsythe and Welch ANOVA, followed by Tamhane's T2 multiple comparisons test (cortex) or ordinary one-way ANOVA and Sidak's multiple comparisons test (hippocampus).

Genotype	wt		tg	
Feeding for 16 Weeks	**AL**	**CR**	**AL**	**CR**
[^{18}F]FDG uptake (ID%/g)				
cortex	4.65 ± 0.25	4.90 ± 0.20	5.35 ± 0.25	5.18 ± 0.33
hippocampus	5.42 ± 0.28	5.46 ± 0.22	6.19 ± 0.31	5.94 ± 0.38

Table 3. Morris Water Maze parameters of short-term (16 weeks) ad libitum (AL) or caloric restricted (CR, 60% of ad libitum) diet-fed wild-type (wt) and transgenic (tg) mice. Values are given as mean ± SEM. Significance of differences between the groups was tested by unpaired student t-test, followed by Bonferroni correction with p threshold of 0.0166.

Genotype	wt		tg	
Feeding for 16 Weeks	**AL**	**CR**	**AL**	**CR**
Platform crosses (n)	6.0 ± 1.0	7.4 ± 1.5	5.0 ± 1.0	3.8 ± 0.9
Latency to first platform crossing (s)	10.1 ± 5.5	12.6 ± 4.2	37.7 ± 12.4	27.0 ± 7.1
Time spent on platform (s)	1.6 ± 0.5	2.9 ± 0.6	1.6 ± 0.6	1.5 ± 0.2
N-quadrant crosses (n)	18.3 ± 2.7	20.0 ± 2.3	19.5 ± 1.5	14.4 ± 1.2

3.2. Long-Term (68 Weeks) CR Significantly Increased [^{18}F]FDG Uptake

^{1}H-MRS demonstrated a significant reduction of the NAA/Cr ratio (p = 0.0272; Figure 1c) in tg vs. wt mice upon AL feeding. During CR feeding, the NAA/Cr ratio

of tg mice tended to be elevated in contrast to AL-fed tg mice ($p = 0.0523$) and reached similar values as wt mice (Figure 1c). Whereas CR for 68 weeks caused significant reductions of approximately 30% of bodyweight in wt ($p \leq 0.0001$, student t-test followed by Bonferroni correction) and tg mice ($p = 0.0027$, Mann–Whitney test followed by Bonferroni correction) vs. AL feeding, the blood sugar concentrations were almost unchanged (Table 1). Long-term CR vs. AL feeding in tg mice resulted in a significant increase of [^{18}F]FDG uptake in the cortex ($p = 0.0161$, student t-test followed by Bonferroni correction, Figure 2a) and hippocampus ($p = 0.0035$, student t-test followed by Bonferroni correction, Figure 2b) with representative PET-CT images (Figure 2c).

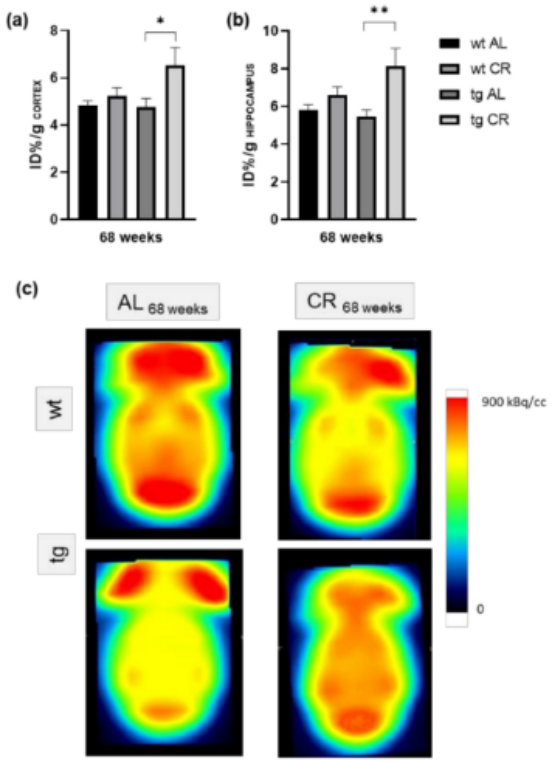

Figure 2. Quantification of [^{18}F]FDG uptake in the cortex (**a**) and hippocampus (**b**) given as ID%/g of wild-type (wt) and transgenic APPswe/PS1delta9 (tg) mice. Mice were fed either ad libitum (AL) or a caloric-restricted (CR, 60% of ad libitum) diet for 68 weeks. Values are given as mean ± SEM. Significance of differences between the groups was tested by unpaired student t-test followed by Bonferroni correction with p threshold of 0.0166: * $p < 0.05$ or ** $p < 0.005$ vs. AL. Visual comparison of representative Images of [^{18}F]FDG uptake in the brain of wt and tg mice (**c**).

3.3. Long-Term CR Increased Working Memory

Mice were tested in the spatial reference memory version of the MWM upon long-term CR. All mice were trained to find the platform (escape latencies were monitored, data not shown). In the trial, the platform was removed, and the number of platform crossings during 60 s was measured. The number of platform crosses measured in tg mice was almost half of those in wt mice upon AL feeding (Figure 3a). Long-term CR improved working memory performance as indicated by an almost two-fold increase of platform crosses in both mouse strains, whereas the increase was significant in tg mice ($p = 0.0161$, student t-test followed by Bonferroni correction Figure 3a). Moreover, latency to first platform crosses was found tendentially (up to three-fold) increased in tg mice when compared

to wt mice. CR shortened latency in wt and significantly shortened latency in tg mice ($p = 0.0069$, student t-test followed by Bonferroni correction, Figure 3b). Correspondingly, time spent on platform was reduced up to eight-fold in tg vs. wt mice and was increased up to 4-fold upon long-term CR vs. AL in tg mice (Figure 3c). Additionally, the number of N-quadrant crosses was found tendentially decreased in tg vs. wt mice ($p = 0.0200$, student t-test followed by Bonferroni correction), and again significantly increased upon CR when compared to AL feeding ($p = 0.0018$, student t-test followed by Bonferroni correction; Figure 3d).

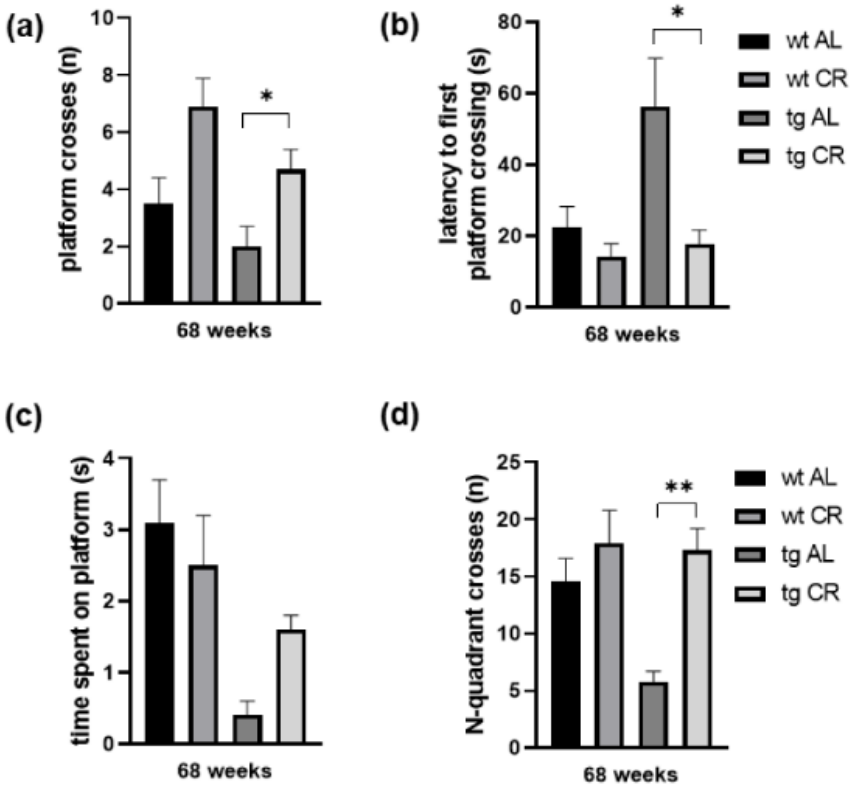

Figure 3. Number (*n*) of platform crosses during 60 s (**a**), latency (in s) to first platform crossing (**b**), time (in s) spent on platform (**c**), and n of north (N)-quadrant crosses (**d**) were measured for wild-type (wt) and transgenic APPswe/PS1delta9 (tg) mice. Mice were fed either ad libitum (AL) or a caloric-restricted diet (CR, 60% of ad libitum) for 68 weeks. Values are given as mean ± SEM. Significance of differences between the groups was tested by unpaired student *t*-test, followed by Bonferroni correction with *p* threshold of 0.0166: * $p < 0.05$ or ** $p < 0.005$ vs. AL.

3.4. Long-Term CR Increased Autophagy

The analysis of LC3BII protein expression revealed no difference between AL-fed wt and tg mice, while CR caused a marked increase of LC3BII expression which was significant in tg mice (Figure 4a; $p = 0.0392$). The analysis of p62 protein expression revealed a slight decrease in AL-fed tg vs. wt mice (Figure 4b). Protein expression of p62 was markedly increased upon CR in both mouse strains but was increased more significantly in tg mice ($p = 0.0176$) (Figure 4b).

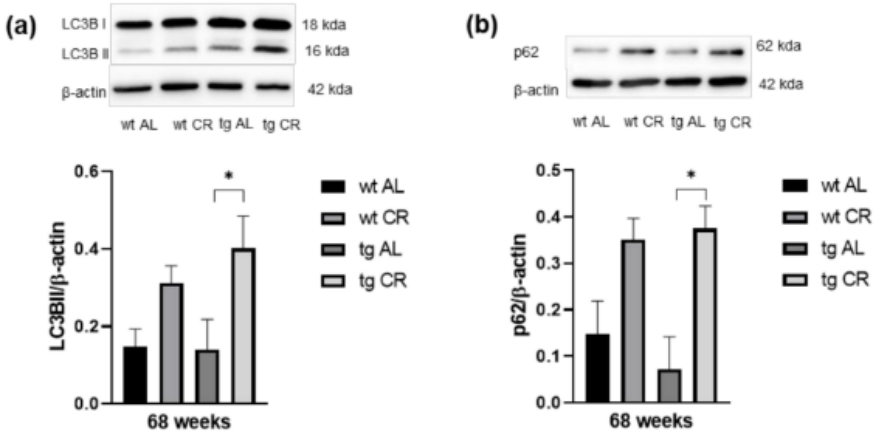

Figure 4. Representative Western blots, as well as densitometric analysis of (**a**) LC3BII and (**b**) p62 expression in brain of wild-type (wt) and transgenic APPswe/PS1delta9 (tg) mice. Mice were fed either ad libitum (AL) or a caloric-restricted diet (CR, 60% of ad libitum) for 68 weeks. Signals were corrected to that of β-actin. Values are given as mean ± SEM. Significance of differences between the groups was tested by one-way ANOVA on Ranks (Kruskal–Wallis) with Dunn's post hoc test for multiple comparisons: * $p < 0.05$ vs. AL.

3.5. Long-Term CR Reduced Aβ-Plaque Load and Size as Well as Accompanying Neuroinflammation

Analysis of Aβ-stained brain sections of tg mice (Figure 5a–f) revealed a mean plaque number of 39.5 ± 7.0 per HPF in the cortex (Figure 5a) and 59.1 ± 7.0 per HPF in the hippocampus (Figure 5d), and an average plaque size of 2.6 ± 0.2 µm2 in the cortex (Figure 5b) and 2.4 ± 0.2 μm^2 in the hippocampus (Figure 5e). In the wt samples, no Aβ plaque could be detected (not detected, n.d.). Nevertheless, the respective images are provided in Appendix A (Figure A4). Long-term CR significantly reduced the Aβ plaque number (21.3 ± 3.4; $p < 0.0001$; student t-test followed by Bonferroni correction; Figure 5d) and plaque area (1.3 ± 0.1 μm^2; $p < 0.0001$; student t-test followed by Bonferroni correction; Figure 5e) in the hippocampus.

The presence of plaque was accompanied by neuroinflammatory processes, displayed by a 40% increase of cortical (Figure 6a,b) and a significant increase of hippocampal ($p = 0.0009$; Figure 6c,d) iba1-positive cells in tg mice compared to wt mice. The reduction of plaque load and size in the hippocampus upon long-term CR in tg mice was accompanied by a significantly decreased number of iba1-positive hippocampal cells ($p = 0.0329$; Figure 6c).

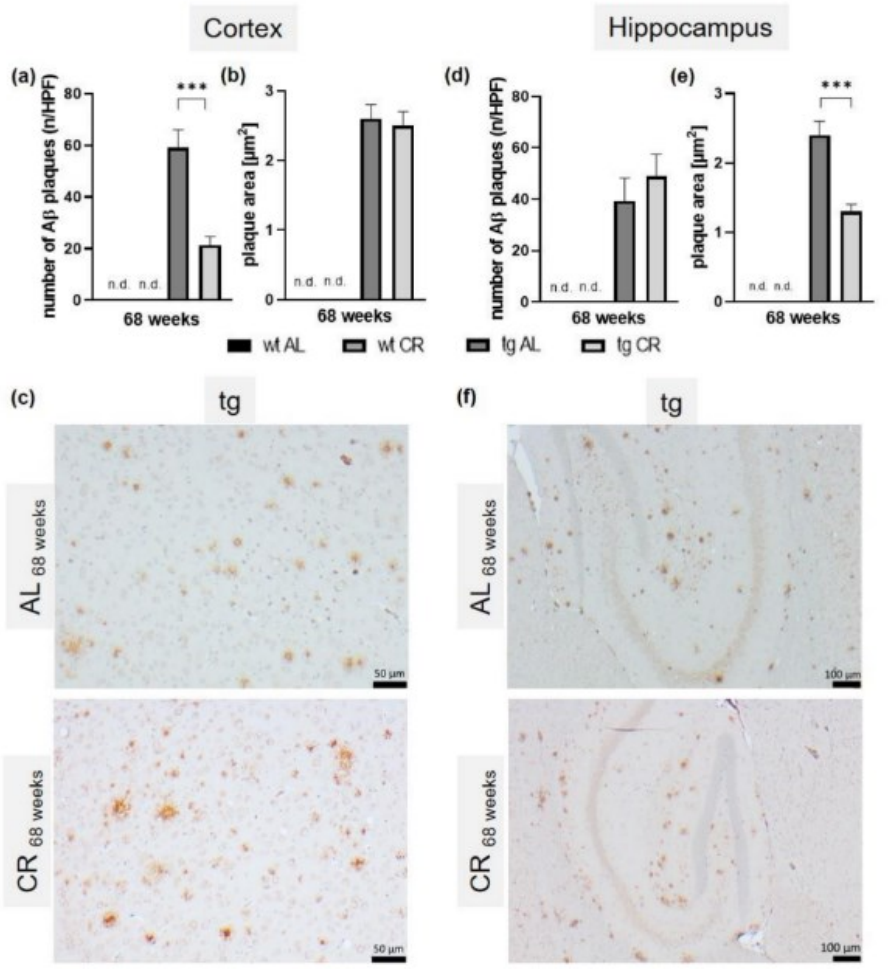

Figure 5. Quantitative analysis of the number of cortical (**a**) and hippocampal (**d**) amyloid-β (Aβ) plaques (*n*) per high-power field (HPF) and the cortical (**b**) and hippocampal (**e**) Aβ-plaque area (μm^2) of wild-type (wt; not detectable n.d.) and transgenic APPswe/PS1delta9 (tg) mice and representative immunohistochemical images of cortical (scale bar representing 50 µm (**c**)) and hippocampal (scale bar representing 100 µm (**f**)) Aβ-stained (6E10) brain sections of tg mice. Mice were fed either ad libitum (AL) or a caloric-restricted diet (CR, 60% of ad libitum) for 68 weeks. Significance of differences between the groups was tested by unpaired student t-test, followed by Bonferroni correction with *p* threshold of 0.0166: *** $p \leq 0.001$ vs. AL.

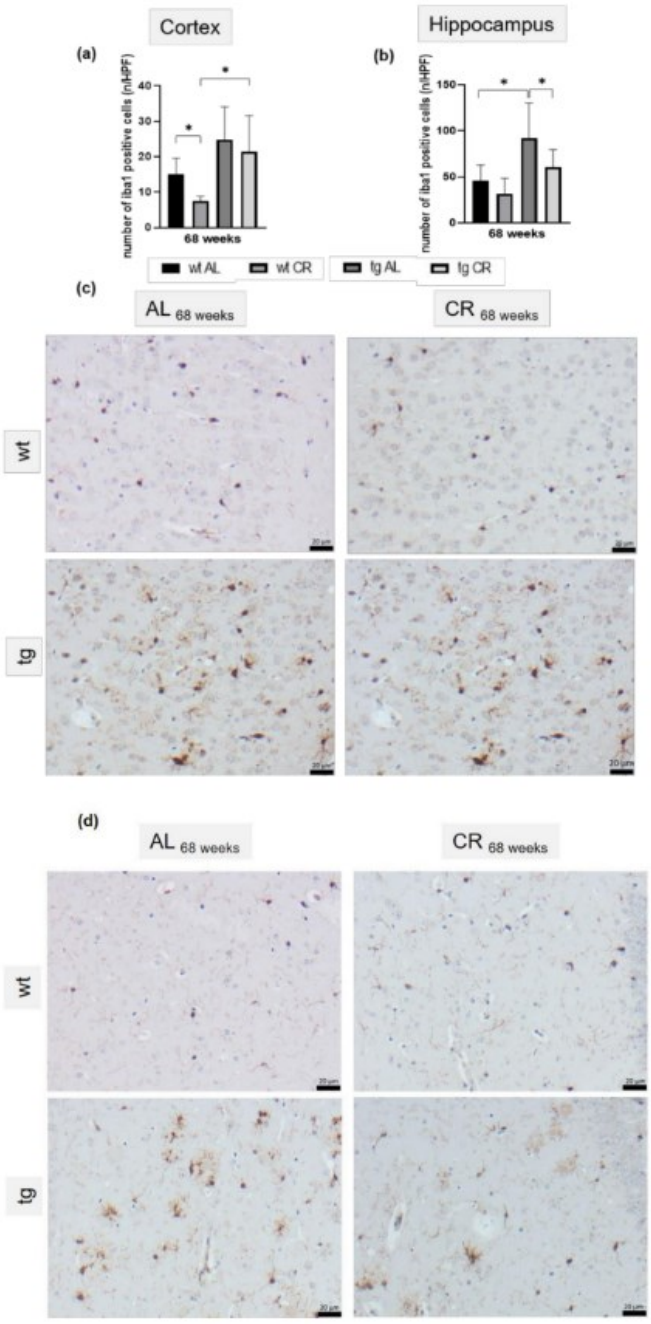

Figure 6. Quantitative analysis of the number of iba1-positive cortical (**a**) and hippocampal cells (**b**) per high-power field (*n*/HPF) of wild-type (wt) and transgenic APPswe/PS1delta9 (tg) mice and representative immunohistochemical images of cortical (**c**) and hippocampal (**d**) iba1-stained brain sections (scale bar representing 20 µm) of wt and tg mice. Mice were fed either ad libitum (AL) or a caloric-restricted diet (CR, 60% of ad libitum) for 68 weeks. Values are given as mean ± SEM; Significance of differences between the groups was tested by Brown–Forsythe and Welch ANOVA, followed by Tamhane's T2 multiple comparisons test (**a**) or ordinary one-way ANOVA and Sidak's multiple comparisons test (**b**): * $p < 0.05$.

4. Discussion

The main finding of the study was that CR ameliorates cognitive function by a measurable increase of glucose uptake, indicating a CR-induced increase in neuronal activity. This was accompanied by attenuated Aβ deposition and related microglia activation in the hippocampus. Overall, we speculate that this might be a result of CR-activated autophagy, but further investigation is needed to support this hypothesis.

CR-mediated attenuation of Aβ neuropathology in AD mouse studies has already been well described in literature. Mouton et al. [7] reported that CR reduced the total Aβ volume by about one-third in APP/PS1 mice. Moreover, Patel et al. [8] showed that, besides decreased plaque load and size, the immune-reactive area around Aβ plaques was markedly reduced upon CR in APP/PS1 mice as indicated by decreased numbers of astrocytes (GFAP-positive cells). Similarly, the current study demonstrates that the plaque load and size, as well as the number of activated microglia (iba1-positive cells), were significantly reduced in tg mice in the hippocampus. However, this could only be observed upon 68 weeks of CR. In contrast, 16-week ongoing CR showed no influence on Aβ pathology, although the study of Patel et al. [8] stated otherwise and was able to show an anti-amyloidogenic effect after 14 weeks of CR in double-transgenic APP/PS1 mice starting at 2 months of age. In contrast, longer CRs of 7 and 14 months were used by Halagappa et al. [12], showing that only CR of 14 months reduced Aβ levels and improved cognitive performance, as analyzed by MWM, in another transgenic mouse strain (3xTgAD) starting at 3 months of age. In this context, we are also able to show that only long-term CR attenuated the working memory of tg mice. Current literature has discussed whether better cognitive performance is mediated by CR-induced reduction of neuronal loss. Dong et al. [11] reported that CR significantly increased cell density in the CA3 region in the hippocampus. Moreover, CR has been described to prevent age-related disease or normal signs of age [30]. In this sense, the senescent (72-week-old) wt mice used in the current study benefited from low caloric intake, as indicated by better cognitive performance upon 68 weeks of CR. This anti-aging effect has been reported by several other groups [31–33]. In case of the AD mice, not only anti-aging processes are relevant for the neuroprotection, but anti-amyloidogenic mechanisms are also important [10]. Herein, it is shown that the mature form of ADAM10—an enzyme with α-secretase activity for the proteolytic processing of APP—was significantly upregulated in CR-fed Tg2576 mice [10], resulting in reduced Aβ plaque load. Since APPswe/PS1delta9 mice do not show any changes of ADAM10 expression in the hippocampus compared with their control littermates [34], we refrained from further investigating this pathway. Beside the anti-amyloidogenic process, CR is also able to induce autophagy, a well-documented catabolic mechanism which is known to degrade aggregated proteins [35], including Aβ. This processing pathway is characterized by translocation of Atg protein LC3BII, together with sequestosom-1 (p62) to the autophagosome membrane, which is commonly used as marker of autophagosome formation [16]. However, in AD animal models, autophagic activities have not yet been studied extensively as an underlying cause for the beneficial effects of CR [36]. Thus, it is still unclear if elevated autophagy has predominantly neuroprotective or neurodegenerative effects, as reported findings are partially contradictive. For example, CR-induced upregulation of SIRT-1 [37] may induce neuroprotective effects by upregulating autophagy through downstream signaling [36,38], whereas the neuroprotective effects of CR-upregulated BDNF [39] are due to autophagy suppression [40]. To complement the ambivalent data, the current study found that CR-fed tg mice exhibited a significant increase in autophagy. This was shown by elevated LC3BII and p62 levels, suggesting a neuroprotective mechanism of CR by restoration of cognitive function to wt levels through autophagy-induced Aβ degradation. Further experiments should be carried out in the future to clarify to what extend autophagy is the main driver of Aβ degradation.

Moreover, autophagy is also essential for accurate cellular and energy homeostasis. In this context, autophagy positively regulates glucose uptake via upregulation of GLUT-1 protein expression [41]. Therefore, it may be concluded that increased FDG uptake upon

CR in tg mice is a consequence of increased autophagic activity. However, it can also be assumed that CR-induced autophagy and the associated Aβ degradation lead to improved neuronal activity per se, indicated by increased FDG uptake. Restrictively, it is known that reduced blood glucose concentration may enhance FDG uptake [42]. However, due to the barely changed blood glucose concentration upon CR, this does not seem to be the reason for the increased FDG uptake in CR-fed tg mice. In general, measurement of the effect of CR by [^{18}F]FDG PET-CT opens the possibility to monitor CR-induced neuroprotection using a noninvasive method and, in particular, in a longitudinal manner. In addition to [^{18}F]FDG-PET/CT, 1H-MRS represents another in vivo technique which allows for the characterization of metabolic changes in AD brains [43,44]. NAA, as a representative metabolite of neuronal integrity, is found to be reduced in AD, indicating neuronal malfunction either due to diminished neuronal density, neuronal cell loss, or partially reversible neuronal dysfunction [45], and correlates with disease progression [46]. Further, APP/PS1 mice also show significantly decreased NAA to Cr ratio [28,45,47], which was also observed in the present study. Upon long-term CR, NAA/Cr ratios were increased, reaching the same values as those found in wt mice, indicating improved neuronal integrity. However, the transfer of findings from transgenic animal models to humans is limited [48]. Nevertheless, the use of quantitative neuroimaging methods possibly aids the improvement of translational potential of preclinical AD research regarding brain metabolism or morphology [49].

5. Conclusions

In summary, the present study showed, for the first time, that the known CR-induced Aβ degradation [7,8] is accompanied by increased autophagy and improved neuronal activity as well as integrity, resulting in a better cognitive performance. Further studies need to clarify to what extent the observed increased autophagy in CR tg mice (upon 68 weeks CR) is responsible for the attenuation of the Aβ pathology.

Author Contributions: Conceptualization: A.K.; Methodology: L.M., N.P.G., J.S., C.R., T.L., A.K.; Validation: L.M., B.V., A.K.; Formal Analysis: L.M., J.S., C.R., T.L., A.K.; Investigation: J.S., C.R., T.L.; Resources: B.J.K., B.V., S.T., A.K.; Data Curation: L.M., A.K.; Writing—Original Draft Preparation: L.M., A.K.; Writing—Review and Editing: B.V., S.T., A.K.; Visualization: L.M., T.L., A.K.; Supervision: B.J.K., B.V., S.T., A.K.; Project administration: A.K.; Funding acquisition: A.K.; Animal Care: N.P.G., C.R. All authors have read and agreed to the published version of the manuscript.

Funding: This study was supported by a grant from the Deutsche Forschungsgemeinschaft, Bonn, Germany (KU 3280/1-2).

Institutional Review Board Statement: The experimental protocol was approved by the local Animal Research Committee (Landesamt für Landwirtschaft, Lebensmittelsicherheit und Fischerei (LALLF) of the state Mecklenburg-Western Pomerania (LALLF M-V/TSD/7221.3-1.1-002/14)). All animals received care according to the German legislation on protection of animals and the Guide for the Care and Use of Laboratory Animals (European Directive 2010/63/EU).

Informed Consent Statement: Not applicable.

Data Availability Statement: The data presented in this study are available on request from the corresponding author.

Acknowledgments: The authors cordially thank the technicians of the Institute for Experimental Surgery, Central Animal Care Facility, Core Facility Multimodal Small Animal Imaging for their valuable assistance and the staff of the Department of Nuclear Medicine for the production of the radiotracer [^{18}F]FDG.

Conflicts of Interest: The other authors declare that they have no conflict of interest.

Appendix A

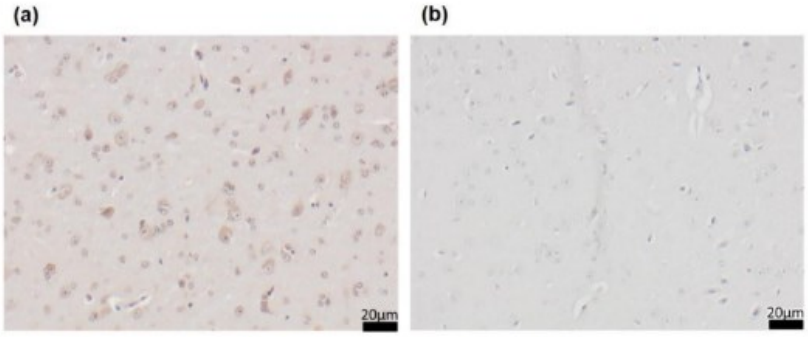

Figure A1. Negative controls of (**a**) 6E10 anti-Aβ staining and (**b**) iba1 staining.

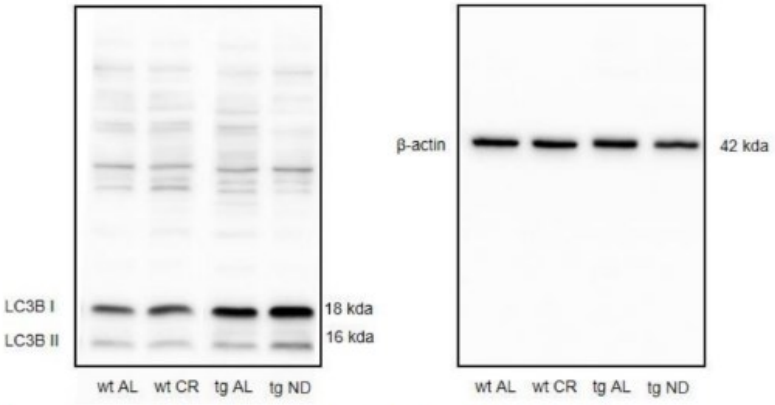

Figure A2. Raw Western blot:of LC3B and β-actin on 14% SDS gel.

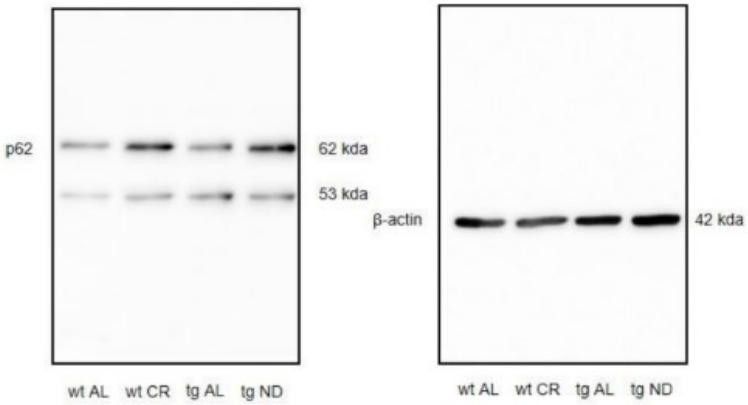

Figure A3. Raw Western blot of p62 and β-actin on 10% SDS gel.

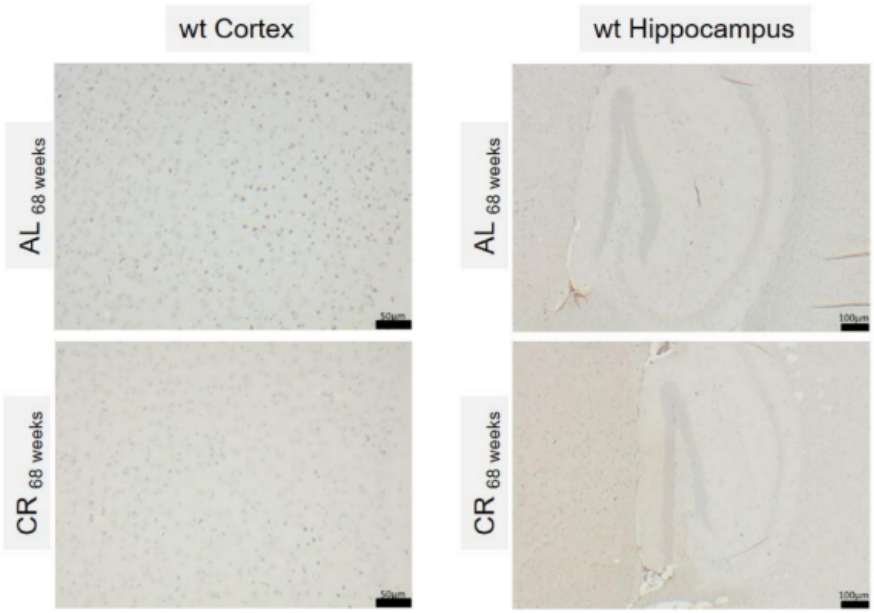

Figure A4. Representative immunohistochemical images of cortical (scale bar representing 50 µm) and hippocampal (scale bar representing 100 µm) Aβ-stained (6E10) brain sections of wt mice.

References

1. Hyman, B.T. The neuropathological diagnosis of Alzheimer's disease: Clinical-pathological studies. *Neurobiol. Aging* **1997**, *18* (Suppl. 4). [CrossRef]
2. Malm, T.; Koistinaho, J.; Kanninen, K. Utilization of APPswe/PS1dE9 Transgenic Mice in Research of Alzheimer's Disease: Focus on Gene Therapy and Cell-Based Therapy Applications. *Int. J. Alzheimer's Dis.* **2011**, *2011*, 517160. [CrossRef] [PubMed]
3. Del Sole, A.; Clerici, F.; Chiti, A.; Lecchi, M.; Mariani, C.; Maggiore, L.; Mosconi, L.; Lucignani, G. Individual cerebral metabolic deficits in Alzheimer's disease and amnestic mild cognitive impairment: An FDG PET study. *Eur. J. Nucl. Med. Mol. Imaging* **2008**, *35*, 1357–1366. [CrossRef]
4. Herholz, K.; Carter, S.F.; Jones, M. Positron emission tomography imaging in dementia. *Br. J. Radiol.* **2007**, *80*, S160–S167. [CrossRef]
5. Singh-Manoux, A.; Czernichow, S.; Elbaz, A.; Dugravot, A.; Sabia, S.; Hagger-Johnson, G.; Kaffashian, S.; Zins, M.; Brunner, E.J.; Nabi, H.; et al. Obesity phenotypes in midlife and cognition in early old age: The Whitehall II cohort study. *Neurology* **2012**, *79*, 755–762. [CrossRef] [PubMed]
6. Xu, W.L.; Atti, A.R.; Gatz, M.; Pedersen, N.L.; Johansson, B.; Fratiglioni, L. Midlife overweight and obesity increase late-life dementia risk: A population-based twin study. *Neurology* **2011**, *76*, 1568–1574. [CrossRef]
7. Mouton, P.R.; Chachich, M.E.; Quigley, C.; Spangler, E.; Ingram, D.K. Caloric restriction attenuates amyloid deposition in middle-aged dtg APP/PS1 mice. *Neurosci. Lett.* **2009**, *464*, 184–187. [CrossRef] [PubMed]
8. Patel, N.V.; Gordon, M.N.; Connor, K.E.; Good, R.A.; Engelman, R.W.; Mason, J.; Morgan, D.G.; Morgan, T.E.; Finch, C.E. Caloric restriction attenuates Abeta-deposition in Alzheimer transgenic models. *Neurobiol. Aging* **2005**, *26*, 995–1000. [CrossRef]
9. Schafer, M.J.; Alldred, M.J.; Lee, S.H.; Calhoun, M.E.; Petkova, E.; Mathews, P.M.; Ginsberg, S.D. Reduction of β-amyloid and γ-secretase by calorie restriction in female Tg2576 mice. *Neurobiol. Aging* **2015**, *36*, 1293–1302. [CrossRef]
10. Wang, J.; Ho, L.; Qin, W.; Rocher, A.B.; Seror, I.; Humala, N.; Maniar, K.; Dolios, G.; Wang, R.; Hof, P.R.; et al. Caloric restriction attenuates beta-amyloid neuropathology in a mouse model of Alzheimer's disease. *FASEB J.* **2005**, *19*, 659–661. [CrossRef]
11. Dong, W.; Wang, R.; Ma, L.-N.; Xu, B.-L.; Zhang, J.-S.; Zhao, Z.-W.; Wang, Y.-L.; Zhang, X. Influence of age-related learning and memory capacity of mice: Different effects of a high and low caloric diet. *Aging Clin. Exp. Res.* **2016**, *28*, 303–311. [CrossRef] [PubMed]
12. Halagappa, V.K.M.; Guo, Z.; Pearson, M.; Matsuoka, Y.; Cutler, R.G.; LaFerla, F.M.; Mattson, M.P. Intermittent fasting and caloric restriction ameliorate age-related behavioral deficits in the triple-transgenic mouse model of Alzheimer's disease. *Neurobiol. Dis.* **2007**, *26*, 212–220. [CrossRef] [PubMed]
13. Nilsson, P.; Loganathan, K.; Sekiguchi, M.; Matsuba, Y.; Hui, K.; Tsubuki, S.; Tanaka, M.; Iwata, N.; Saito, T.; Saido, T.C. Aβ secretion and plaque formation depend on autophagy. *Cell Rep.* **2013**, *5*, 61–69. [CrossRef] [PubMed]

14. Alirezaei, M.; Kemball, C.C.; Whitton, J.L. Autophagy, inflammation and neurodegenerative disease. *Eur. J. Neurosci.* **2011**, *33*, 197–204. [CrossRef]
15. Gregosa, A.; Vinuesa, Á.; Todero, M.F.; Pomilio, C.; Rossi, S.P.; Bentivegna, M.; Presa, J.; Wenker, S.; Saravia, F.; Beauquis, J. Periodic dietary restriction ameliorates amyloid pathology and cognitive impairment in PDAPP-J20 mice: Potential implication of glial autophagy. *Neurobiol. Dis.* **2019**, *132*, 104542. [CrossRef]
16. Moreira, P.I.; Santos, R.X.; Zhu, X.; Lee, H.-G.; A Smith, M.; Casadesus, G.; Perry, G. Autophagy in Alzheimer's disease. *Expert Rev. Neurother.* **2010**, *10*, 1209–1218. [CrossRef]
17. Hashimoto, T.; Watanabe, S. Chronic food restriction enhances memory in mice–analysis with matched drive levels. *Neuroreport* **2005**, *16*, 1129–1133. [CrossRef]
18. Kuhla, A.; Lange, S.; Holzmann, C.; Maass, F.; Petersen, J.; Vollmar, B.; Wree, A. Lifelong caloric restriction increases working memory in mice. *PLoS ONE* **2013**, *8*, e68778. [CrossRef]
19. Jankowsky, J.L.; Younkin, L.H.; Gonzales, V.; Fadale, D.J.; Slunt, H.H.; Lester, H.A.; Younkin, S.G.; Borchelt, D.R. Rodent A beta modulates the solubility and distribution of amyloid deposits in transgenic mice. *J. Biol. Chem.* **2007**, *282*, 22707–22720. [CrossRef]
20. Xiong, H.; Callaghan, D.; Wodzinska, J.; Xu, J.; Premyslova, M.; Liu, Q.-Y.; Connelly, J.; Zhang, W. Biochemical and behavioral characterization of the double transgenic mouse model (APPswe/PS1dE9) of Alzheimer's disease. *Neurosci. Bull.* **2011**, *27*, 221–232. [CrossRef]
21. Rühlmann, C.; Dannehl, D.; Brodtrück, M.; Adams, A.C.; Stenzel, J.; Lindner, T.; Krause, B.J.; Vollmar, B.; Kuhla, A. Neuroprotective Effects of the FGF21 Analogue LY2405319. *J. Alzheimer's Dis.* **2021**. [CrossRef]
22. Naressi, A.; Couturier, C.; Castang, I.; de Beer, R.; Graveron-Demilly, D. Java-based graphical user interface for MRUI, a software package for quantitation of in vivo/medical magnetic resonance spectroscopy signals. *Comput. Biol. Med.* **2001**. [CrossRef]
23. Stefan, D.; Di Cesare, F.; Andrasescu, A.; Popa, E.; Lazariev, A.; Vescovo, E.; Strbak, O.; Williams, S.; Starcuk, Z.; Cabanas, M.; et al. Quantitation of magnetic resonance spectroscopy signals: The jMRUI software package. *Meas. Sci. Technol.* **2009**. [CrossRef]
24. Mocioiu, V.; Ortega-Martorell, S.; Olier, I.; Jablonski, M.; Starčuková, J.; Lisboa, P.; Arús, C.; Julià-Sapé, M. From raw data to data-analysis for magnetic resonance spectroscopy—The missing link: jMRUI2XML. *BMC Bioinform.* **2015**, *16*, 378. [CrossRef] [PubMed]
25. Pijnappel, W.; Boogaart, A.V.D.; De Beer, R.; Van Ormondt, D. SVD-based quantification of magnetic resonance signals. *J. Magn. Reson.* **1992**. [CrossRef]
26. Kuhla, A.; Meuth, L.; Stenzel, J.; Lindner, T.; Lappe, C.; Kurth, J.; Krause, B.J.; Teipel, S.; Glass, Ä.; Kundt, G.; et al. Longitudinal 18FFDG-PET/CT analysis of the glucose metabolism in ApoE-deficient mice. *EJNMMI Res.* **2020**, *10*, 119. [CrossRef]
27. Stenzel, J.; Rühlmann, C.; Lindner, T.; Polei, S.; Teipel, S.; Kurth, J.; Rominger, A.; Krause, B.; Vollmar, B.; Kuhla, A. 18F-florbetaben PET/CT Imaging in the Alzheimer's Disease Mouse Model APPswe/PS1dE9. *Curr. Alzheimer Res.* **2019**, *16*, 49–55. [CrossRef] [PubMed]
28. Kuhla, A.; Rühlmann, C.; Lindner, T.; Polei, S.; Hadlich, S.; Krause, B.J.; Vollmar, B.; Teipel, S.J. APPswe/PS1dE9 mice with cortical amyloid pathology show a reduced NAA/Cr ratio without apparent brain atrophy: A MRS and MRI study. *Neuroimage Clin.* **2017**, *15*, 581–586. [CrossRef]
29. Kuhla, A.; Ludwig, S.C.; Kuhla, B.; Münch, G.; Vollmar, B. Advanced glycation end products are mitogenic signals and trigger cell cycle reentry of neurons in Alzheimer's disease brain. *Neurobiol. Aging* **2015**, *36*, 753–761. [CrossRef] [PubMed]
30. Liang, Y.; Liu, C.; Lu, M.; Dong, Q.; Wang, Z.; Wang, Z.; Xiong, W.; Zhang, N.; Zhou, J.; Liu, Q.; et al. Calorie restriction is the most reasonable anti-ageing intervention: A meta-analysis of survival curves. *Sci. Rep.* **2018**, *8*, 5779. [CrossRef] [PubMed]
31. Al-Regaiey, K.A. The effects of calorie restriction on aging: A brief review. *Eur. Rev. Med. Pharmacol. Sci.* **2016**, *20*, 2468–2473. [PubMed]
32. Speakman, J.R.; Mitchell, S.E. Caloric restriction. *Mol. Asp. Med.* **2011**, *32*, 159–221. [CrossRef] [PubMed]
33. Valdez, G.; Tapia, J.C.; Kang, H.; Clemenson, G.D.; Gage, F.H.; Lichtman, J.W.; Sanes, J.R. Attenuation of age-related changes in mouse neuromuscular synapses by caloric restriction and exercise. *Proc. Natl. Acad. Sci. USA* **2010**, *107*, 14863–14868. [CrossRef] [PubMed]
34. Huang, H.; Nie, S.; Cao, M.; Marshall, C.; Gao, J.; Xiao, N.; Hu, G.; Xiao, M. Characterization of AD-like phenotype in aged APPSwe/PS1dE9 mice. *AGE* **2016**, *38*, 303–322. [CrossRef]
35. Lilienbaum, A. Relationship between the proteasomal system and autophagy. *Int. J. Biochem. Mol. Biol.* **2013**, *4*, 1–26. [PubMed]
36. Yang, Y.; Zhang, L. The effects of caloric restriction and its mimetics in Alzheimer's disease through autophagy pathways. *Food Funct.* **2020**, *11*, 1211–1224. [CrossRef]
37. Quintas, A.; de Solís, A.J.; Díez-Guerra, F.J.; Carrascosa, J.M.; Bogónez, E. Age-associated decrease of SIRT1 expression in rat hippocampus: Prevention by late onset caloric restriction. *Exp. Gerontol.* **2012**, *47*, 198–201. [CrossRef] [PubMed]
38. Braidy, N.; Jayasena, T.; Poljak, A.; Sachdev, P.S. Sirtuins in cognitive ageing and Alzheimer's disease. *Curr. Opin. Psychiatry* **2012**, *25*, 226–230. [CrossRef]
39. Duan, W.; Lee, J.; Guo, Z.; Mattson, M.P. Dietary restriction stimulates BDNF production in the brain and thereby protects neurons against excitotoxic injury. *J. Mol. Neurosci.* **2001**, *16*, 1–12. [CrossRef]
40. Nikoletopoulou, V.; Sidiropoulou, K.; Kallergi, E.; Dalezios, Y.; Tavernarakis, N. Modulation of Autophagy by BDNF Underlies Synaptic Plasticity. *Cell Metab.* **2017**, *26*, 230–242.e5. [CrossRef]

41. Lee, Y.-R.; Wu, S.-Y.; Chen, R.-Y.; Lin, Y.-S.; Yeh, T.-M.; Liu, H.-S. Regulation of autophagy, glucose uptake, and glycolysis under dengue virus infection. *Kaohsiung J. Med. Sci.* **2020**. [CrossRef] [PubMed]
42. Coleman, R.A.; Liang, C.; Patel, R.; Ali, S.; Mukherjee, J. Brain and Brown Adipose Tissue Metabolism in Transgenic Tg2576 Mice Models of Alzheimer Disease Assessed Using 18F-FDG PET Imaging. *Mol. Imaging* **2017**, *16*, 1536012117704557. [CrossRef]
43. Arora, A.; Bhagat, N. Insight into the Molecular Imaging of Alzheimer's Disease. *Int. J. Biomed. Imaging* **2016**, *2016*, 7462014. [CrossRef]
44. Mlynárik, V.; Cacquevel, M.; Sun-Reimer, L.; Janssens, S.; Cudalbu, C.; Lei, H.; Schneider, B.L.; Aebischer, P.; Gruetter, R. Proton and phosphorus magnetic resonance spectroscopy of a mouse model of Alzheimer's disease. *J. Alzheimer's Dis.* **2012**, *31* (Suppl. 3), S87–S99. [CrossRef] [PubMed]
45. Clark, J.B. N-acetyl aspartate: A marker for neuronal loss or mitochondrial dysfunction. *Dev. Neurosci.* **1998**, *20*, 271–276. [CrossRef] [PubMed]
46. Ross, B.D.; Bluml, S.; Cowan, R.; Danielsen, E.; Farrow, N.; Tan, J. In vivo MR spectroscopy of human dementia. *Neuroimaging Clin. N. Am.* **1998**, *8*, 809–822.
47. Chen, S.-Q.; Cai, Q.; Shen, Y.-Y.; Wang, P.-J.; Teng, G.-J.; Zhang, W.; Zang, F.-C. Age-related changes in brain metabolites and cognitive function in APP/PS1 transgenic mice. *Behav. Brain Res.* **2012**, *235*, 1–6. [CrossRef] [PubMed]
48. Foley, A.M.; Ammar, Z.M.; Lee, R.H.; Mitchell, C.S. Systematic review of the relationship between amyloid-β levels and measures of transgenic mouse cognitive deficit in Alzheimer's disease. *J. Alzheimer's Dis.* **2015**, *44*, 787–795. [CrossRef]
49. Teipel, S.J.; Buchert, R.; Thome, J.; Hampel, H.; Pahnke, J. Development of Alzheimer-disease neuroimaging-biomarkers using mouse models with amyloid-precursor protein-transgene expression. *Prog. Neurobiol.* **2011**, *95*, 547–556. [CrossRef]

11. Anhang: Selbstständigkeitserklärung

Hiermit versichere ich, dass ich die vorliegende Arbeit selbstständig und ohne fremde Hilfe verfasst, keine anderen als die von mir angegebenen Quellen und Hilfsmittel benutzt habe und die den benutzten Quellen wörtlich oder inhaltlich entnommenen Stellen als solche kenntlich gemacht habe.

Greifswald, 07.06.2024	Luisa Müller
Ort, Datum	Unterschrift

12. Anhang: Lebenslauf

Angaben zur Person

Name:	Luisa Müller
Anschrift:	Gützkower Str. 26, 17489 Greifswald
Geburtsdatum und -ort:	10.04.1994, Schlema
E-Mail Adresse:	lulu.mueller94@web.de
Telefonnummer:	017678726625

Praktische Erfahrungen:

2023 – jetzt	**Wissenschaftliche Mitarbeiterin** am Institut für Transfusionsmedizin der Universitätsmedizin Greifswald
2021 – 2023	**Medical Scientist** am Centre for Transdisciplinary Neurosciences Rostock (CTNR) mit dem Forschungsschwerpunkt: *„Zusammenspiel neuronaler Übererregbarkeit, zirkadianer Rhythmik und Hirn-Clearance in einem Alzheimer-Mausmodell“*
2019 – 2021	**Wissenschaftliche Mitarbeiterin** an der Klinik für Psychosomatische Medizin und Psychotherapie, Sektion Gerontopsychosomatik und demenzielle Erkrankungen und an dem Institut für Experimentelle Chirurgie der Universitätsmedizin Rostock im Projekt: *„EXCITE – Cerebral HyperEXCITability as trans-disciplinary targEt for pathogenetic modelling, target identification, and intervention in neurodegenerative diseases”*
2018 – 2019	**Studentische Hilfskraft** bei Centogene AG Rostock, Abteilung: Klinische Studien
2017 – 2018	**Studentische Hilfskraft** am Albrecht-Kossel-Institut für Neuroregeneration der Universitätsmedizin Rostock, Abteilung: Klinische Studien
2014 – 2019	Methodenpraktika und Wahlmodule im Rahmen des Studiums zu den Themen: histologische Techniken, experimentelle Neurologie, Transfusionsmedizin, Immunhämatologie

Ausbildung

2019 – 2023	Promotionsstudium an der Universität Rostock
2017 – 2019	Studium: Medizinische Biotechnologie an der Universität Rostock, Abschluss: Master of Science (Abschluss mit „sehr gut“), Thema der Abschlussarbeit: *„Charakterisierung einer ‚Low-grade‘-Inflammation in der High-Fat-Diet-Maus“*
2014 – 2017	Studium: Medizinische Biotechnologie an der Universität Rostock, Abschluss: Bachelor of Science (Abschluss mit „gut“), Thema der Abschlussarbeit: *„Untersuchung der Effekte von Sauerstoff auf die kortikale, embryonale Neurogenese der Maus“*
2012 – 2014	Berufsfachschule für Technik der Bildungsinstitut Pscherer gGmbH in Lengenfeld: Schulische Ausbildung zur chemisch-technischen Assistentin, Fachrichtung Biotechnologie (Abschluss mit „sehr gut“)

Publikationen:

Müller L, Kirschstein T, Köhling R, Kuhla A, Teipel S. Neuronal Hyperexcitability in APPSWE/PS1dE9 Mouse Models of Alzheimer's Disease. J Alzheimers Dis. 2021 Apr 5. doi: 10.3233/JAD-201540

Müller L*, Power Guerra N*, Schildt A, Lindner T, Stenzel J, Behrangi N, Bergner C, Alberts T, Bühler D, Kurth J, Krause BJ, Janowitz D, Teipel S, Vollmar B, Kuhla A. (*equal contribution) [18F]GE-180-PET and Post Mortem Marker Characteristics of Long-Term High-Fat-Diet-Induced Chronic Neuroinflammation in Mice. Biomolecules 2023, 13, 769. https://doi.org/10.3390/biom13050769

Müller L, Power Guerra N, Stenzel J, Rühlmann C, Lindner T, Krause BJ, Vollmar B, Teipel S, Kuhla A. Long-Term Caloric Restriction Attenuates β-Amyloid Neuropathology and Is Accompanied by Autophagy in APPswe/PS1delta9 Mice. Nutrients. 2021 Mar 18;13(3):985. doi: 10.3390/nu13030985

Bühler D, Power Guerra N, **Müller L**, Wolkenhauer O, Düffer M, Vollmar B, Kuhla A* and Wolfien M* (*equal contributions) Leptin deficiency-caused behavioral change–A comparative analysis using EthoVision and DeepLabCut. Front. Neurosci. 2023 17:1052079. doi: 10.3389/fnins.2023.1052079

Power Guerra N, Leyens K, **Müller L**, Brauer D, Janowitz D, Schlick S, Pilz K, Grabe HJ, Vollmar B, Kuhla A. The effect of different weight loss strategies to treat non-alcoholic fatty liver disease focusing on fibroblast growth factor 21. Front Nutr. 2022 Aug 10;9:935805. doi: 10.3389/fnut.2022.935805

Power Guerra N, Parveen A, Bühler D, Brauer DL, **Müller L**, Pilz K, Witt M, Glass Ä, Bajorat R, Janowitz D, Wolkenhauer O, Vollmar B, Kuhla A. Fibroblast Growth Factor 21 as a Potential Biomarker for Improved Locomotion and Olfaction Detection Ability after Weight Reduction in Obese Mice. Nutrients. 2021 Aug 24;13(9):2916. doi: 10.3390/nu13092916

Power Guerra N, **Müller L**, Pilz K, Glatzel A, Jenderny D, Janowitz D, Vollmar B, Kuhla A. Dietary-Induced Low-Grade Inflammation in the Liver. Biomedicines. 2020 Dec 9;8(12):587. doi: 10.3390/biomedicines8120587

Markert F, **Müller L**, Badstübner-Meeske K, Storch A. Early Chronic Intermittent Maternal Hyperoxygenation Impairs Cortical Development by Inhibition of Pax6-Positive Apical Progenitor Cell Proliferation. J Neuropathol Exp Neurol. 2020 Nov 1;79(11):1223-1232. doi: 10.1093/jnen/nlaa072

Konferenzbeiträge:

Müller L, Kirschstein T, Köhling R, Deike-Hofmann K, Radbruch A, Kuhla A, Teipel S. Excitability and glymphatic function in an animal model of Alzheimer's disease. (Poster presentation Alzheimer's Association International Conference 2022)

Müller L, Power Guerra N, Engel N, Vollmar B, Kuhla A, Teipel S. Measurement of brain clearance and its daytime-dependent efficacy in mice. (Poster presentation Alzheimer's Association International Conference 2021)

Weitere Kenntnisse:

Zertifikate und Weiterbildungen:

- Versuchstierkunde der GV-SOLAS (FELASA B äquivalent)
- Kursteilnahme: „Scientific Writing“ und „Effective Scientific Communication”
- Kursteilnahme: „Project Management for Academics”, „Führungskompetenzen für Akademiker*innen” und „Konfliktmanagement”
- Reviewer-Tätigkeit für Obesity Facts - The European Journal of Obesity (Karger) und Neurobiology of Aging (Elsevier)

Fremdsprachen:

- Englisch: sehr gut in Wort und Schrift, UNIcert Stufe 3
- Spanisch: Grundkenntnisse

EDV-Kenntnisse:

- Sehr gute Kenntnisse im Umgang mit den Microsoft-Office-Anwendungen
- Sehr gute Kenntnisse in (semi-)quantitativer und (semi-)automatisierter Bildauswertung mit ImageJ/Fiji und QuPath
- Umfassende Erfahrungen im Umgang mit den Zitierprogrammen Citavi und Endnote
- Gute Kenntnisse im Umgang mit GraphPad Prism
- Basiswissen Python for Datascience

13. Danksagungen

An dieser Stelle bleibt mir nur noch, ein riesengroßes DANKE an all meine Begleiter auf dem Weg zur fertigen Dissertation auszusprechen.

Starten möchte ich mit einem Dank an Herrn Prof. Stefan Teipel als themenvergebenden Betreuer, der mir eine Bearbeitung dieses innovativen Themas ermöglichte und mich trotz einiger Höhen und Tiefen des Projektes auf wissenschaftlicher Ebene mit viel konstruktiver Kritik auf Kurs gehalten hat.

Danach gilt mein Dank dem gesamten Rudolf-Zenker-Institut für Experimentelle Chirurgie (IEC), an welchem ich für die praktische Durchführung meiner Arbeiten auf das Herzlichste aufgenommen wurde. Allen voran gilt dafür der Dank Frau Prof. Brigitte Vollmar für die Möglichkeit, am IEC zu arbeiten und ihrer unvergleichbaren Art, mich in meiner fachlichen wie persönlichen Entwicklung zu unterstützen.

Direkt danach möchte ich meinen Dank an Frau Prof. Angela Kuhla („Angie“) richten. Danke, dass ich mich mit Dir an meiner Seite nie allein gelassen gefühlt habe. Du hast mir auch in den stressigsten Situationen ein offenes Ohr entgegengebracht, mir mit viel Verständnis so manche dunkle Stunde aufgehellt und mit Deiner unkomplizierten Art auch für den ein oder anderen Lacher im Büro gesorgt. Ich danke Dir dafür, dass Du mir gezeigt hast, was alles zu einer guten Wissenschaftlerin gehört und ich danke Dir für Dein Vertrauen in den letzten Jahren, durch das ich oftmals über mich selbst hinausgewachsen bin.

Danken möchte ich außerdem einer weiteren Kollegin, die im Laufe der Jahre zu einer echten Freundin geworden ist. Auch wenn Du, Nicole (mittlerweile ja Frau Dr. Power), mittlerweile nicht mehr am IEC arbeitest, hältst Du mich auch aus Dresden mit Deiner positiven Art immer bei Laune und ermöglichst mir immer wieder optimistische Blickwinkel. Danke, dass ich seit der Masterarbeit so viel von Deinem Projekt mitbegleiten durfte und wir als wissenschaftliches Dream-Team auch bereits so erfolgreich zusammen publizieren konnten.

Außerdem haben mich am IEC viele weitere (ehemalige) Doktoranden wie Wissenschaftler durch unseren gemeinsamen Diskurs geprägt. Hier geht mein Dank vor allem an Dr. Simone Kumstel, Prof. Dietmar Zechner, Dr. Susanne Reuter, Marcel Kordt, Wiebke Nierath, Benjamin Schulz, Tim Schreiber, Emily Leitner, Jakob Brandstetter und speziell in Angies Arbeitsgruppe an Katharina Leyens, Franziska Eyo, Charlotte Köhler und Sidney Szilleweit.

Meine experimentelle Arbeit wäre aber ohne die vielen weiteren helfenden Hände am IEC undenkbar gewesen. Deshalb geht auch ein großer Dank an Anja Gellert und Henrike Seydel für die gesamte administrative Unterstützung. Außerdem geht ein großer Dank an Berit Blendow, Maren Nerowski, Eva Lorbeer, Dr. Sabine Glaubitz, Dorothea Frenz und Christin Schlie, die mir bei allen Laborarbeiten exzellent weitergeholfen haben und ein weiterer großer Dank richtet sich an Mareike Degner, Ilona Klamfuß, Chantal von Hörsten, Karin Gerber, Petra Klaffke, Petra Wolff, Andrea Wilhelm, Roland Gerber und Klaus-Dieter Russow für Eure unentbehrliche Hilfe bei allen Tierversuchen.

Daneben habe ich auch an viele Wegbegleiter und Wegbegleiterinnen anderer Einrichtungen positive Erinnerungen. Hier möchte ich mich zunächst bei Yvonne Fehr, Katharina Schweder und Henrike Pfaff vom DZNE/der KPM in Gehlsdorf für die Hilfe bei allen administrativen Belangen bedanken. Außerdem bedanke ich mich bei dem gesamten Team der Core Facility Multimodale Kleintierbildgebung unter der Leitung von Prof. Brigitte Vollmar, Prof. Bernd J. Krause und Prof. Marc-André Weber. Danken möchte ich insbesondere Dr. Tobias Lindner und Anna Schildt, PhD für ihre unschätzbare Hilfe in der Planung und Durchführung der

Experimente und Joanna Förster und Anne Rupp für die Hilfe bei der Durchführung. Auch wenn Kleintierbildung ein hochkomplexes Thema ist, ist es Euch gelungen, mir durch Eure Erklärungen die Methodik zugänglich zu machen. Zu dieser Thematik geht deshalb auch ein großer Dank an Dr. Stefan Polei vom Institut für Diagnostische und Interventionelle Radiologie, Kinder- und Neuroradiologie der Universitätsmedizin Rostock. Danke, dass Du Dir so viel Zeit genommen hast und mir mit dem Blickwinkel eines Medizinphysikers auch noch einige neue Denkanstöße gegeben hast. Bedanken möchte ich mich des Weiteren bei Prof. Alexander Radbruch und Dr. Katerina Deike-Hofmann von der Uniklinik in Bonn für die konstruktive Zusammenarbeit in der Gadoliniumkontrastmittel-basierten Bildgebung. Für die Zusammenarbeit zum Thema Hyperexzitabilität gilt auch dem Institut für Physiologie der Universitätsmedizin Rostock mein Dank, vor allem Prof. Rüdiger Köhling, Prof. Timo Kirschstein, Valentin Neubert und Katrin Porath. Für die Unterstützung am Mikroskop möchte ich Daniel Wolter aus der Klinik und Poliklinik für Mund-, Kiefer- und Plastische Gesichtschirurgie der Universitätsmedizin Rostock meinen herzlichsten Dank aussprechen.

Zum Schluss wäre diese Arbeit aber auch ohne die vielen lieben Menschen aus meinem privaten Umfeld undenkbar gewesen. Hier gilt deshalb der größte Dank zunächst meiner Familie: meinen Eltern, meiner Tante Marlies und am meisten meiner Oma. Danke, dass Ihr immer Verständnis für mich hattet, auch wenn Euch mein wissenschaftliches Thema manchmal unverständlich erschien und danke, dass ich immer darauf zählen kann, dass Ihr für mich da seid, auch wenn mal nicht alles wie geplant läuft.

Der zweite große Dank im privaten Umfeld geht an meine ganzen Freunde, die mir immer wieder aufgezeigt haben, dass es auch noch andere schöne Seiten neben der Arbeit gibt. Insbesondere an Paula, David, Moritz, Torge, Züli, Adi, Mozi, Freddy und Eva, Eric und Jule, Janine und Georg sowie Maik, Phil und unseren Bekannten Dome geht ein riesiges Dankeschön für die schönen Erinnerungen, die ich während der Promotionszeit mit Euch sammeln durfte. Und ein weiterer Dank geht an Meli und Franz (mit Lina und Kurt) und Jessy und Felix, mit denen ich seit der Grundschule befreundet bin und die auch immer wieder mein Ankerpunkt in der alten Heimat sind.

Am Ende geht noch ein riesiges Dankeschön an Christopher, den wichtigsten Menschen, der mich die letzten Jahre begleitet hat, auf den ich immer zählen kann, der mich jeden Tag froh macht und mit mir durch alle Höhen und Tiefen des Alltags gemeinsam geht.